

# TRANSIENT THERMAL STRESSES AND FATIGUE IN PRESSURE VESSEL NOZZLES

---

CONSTANTINE NICHOLAS OIKONOMIDES  
B.Sc(Eng)., M.Sc(Lon)., DIC., AMemASME.

A THESIS SUBMITTED FOR THE DEGREE OF  
DOCTOR OF PHILOSOPHY IN THE FACULTY  
OF ENGINEERING OF THE UNIVERSITY OF  
LONDON.

DEPARTMENT OF MECHANICAL ENGINEERING,  
IMPERIAL COLLEGE OF SCIENCE AND TECHNOLOGY,  
EXHIBITION ROAD,  
LONDON SW 7.

FEBRUARY 1977

## ABSTRACT

---

The present work, which incorporates a theoretical and an experimental part, deals with the determination of thermal stresses and their influence on the fatigue life of pressure vessel nozzles. Numerical and computational methods are developed for the calculation of transient thermal stress distribution, in radial nozzles of various geometries and under specific heating conditions. A literature review is made of recent developments in pressure vessel technology and investigations relating to pressure vessel nozzles.

The heat transfer analysis makes use of the finite difference and finite element methods. The elastic thermal stress analysis is dealt with exclusively by the finite element method. The methods can be used to achieve more accurate design in nozzles and other parts of the vessel. The thermostructural computer programs developed in this work are flexible and can be applied to complex geometries.

The experimental part sets out to measure the thermal stresses for a particular nozzle configuration. When theoretical predictions and experimental results are compared the former are shown to be in more than adequate agreement for design purposes. The accuracy of the numerical methods in the measurements of stresses are also analysed.

With fatigue being an aspect of vital importance for safe and reliable design of pressure vessels and their components, a

theoretical investigation, dealing with crack initiation and propagation is made in Chapter 7 based on the boundary collocation analysis. The analysis determines the values of the stress intensity factor  $K$  along the axis of a hypothetical crack introduced in the structure and subsequently compares it with experimental values of the critical stress intensity factor  $K_c$ . This will determine if the applied level of thermal stress will be large enough to initiate a crack or, in case of an already existing one, cause it to propagate. The nozzle specimen was subjected to a thermal fatigue test of alternating heating and cooling cycles for a period of four months to investigate possible crack initiation and/or propagation.

## ACKNOWLEDGMENTS

---

The author wishes to express his sincere thanks to Dr. Cyril Laming for supervising this research and for his continuous interest, encouragement and advice throughout the whole period of this work.

The author also wishes to express his appreciation to the following persons and organisations who have contributed to the completion of this work:

- (i) The Science Research Council for their financial support through a Research Contract.
- (ii) CTA Co.Ltd. for financing part of the project.
- (iii) The technical staff of the Mechanical Engineering Department, especially Mr. Ken Walker, Mr. Fred Seabury, and Mr. Jack Pooley who have helped during the experimental part of the project and the assembly of the rig.
- (iv) The Library Staff and especially the librarian Miss Edna Archer for supplying necessary literature, often from quite remote sources.

Finally thanks are due to Mrs. E. Noel for typing this thesis.

C.N. OIKONOMIDES



**CONTENTS****PAGE**

---

TITLE	1
ABSTRACT	2
ACKNOWLEDGEMENTS	4
GENERAL NOTATION	10
LIST OF TABLES	13
LIST OF FIGURES	14
INTRODUCTION	18
1. <u>DEVELOPMENTS IN PRESSURE VESSEL TECHNOLOGY</u>	20
1.1 Pressure Vessels	20
1.2 Criteria for Design Analysis	23
1.2.1 Strength Theories	29
2. <u>REVIEW OF RECENT INVESTIGATIONS IN PRESSURE VESSEL NOZZLES</u>	36
2.1 Nozzle and Openings	36
2.2 Theoretical Investigations of Nozzles	38
2.2.1 Limit Pressure and Loads	40
2.2.2 Elastic Analysis	43
2.2.3 Reinforcement of Nozzle Openings	44
2.2.3.1 Spherical Shells	45
2.2.3.2 Cylindrical Shells	46
2.3 Experimental Investigations of Nozzles	47

3.	<u>THE NATURE OF THE PRESENT PROBLEM OF THERMAL STRESSES</u>	50
3.1	The Geometry of the Pressure Vessel Nozzles	52
3.2	Nozzle-Vessel Cases Examined Theoretically	53
3.3	Thermal Stresses and How They Develop	55
3.3.1	Thermal Shock of Ductile Material	56
4.	<u>THEORETICAL DETERMINATION OF TRANSIENT THERMAL DISTRIBUTIONS FOR THE NOZZLE-VESSEL CASES</u>	59
4.1	Flow in Nozzle-Vessel and Forced Convection Heat Transfer Coefficient	60
4.2	Evaluation of Heat Transfer Coefficient for CASES A, B and C	62
4.2.1	CASE A. Forced Convection across Nozzle and Vessel Walls	62
4.2.2	CASE B. Forced Convection across Nozzle only	65
4.2.3	CASE C. Radiation Heat Transfer in Nozzle	65
4.3	Two-Dimensional Transient Heat Flow in Nozzle-Vessel and Finite Difference Analysis	70
4.3.1	Finite Difference Analysis	71
4.4	Solution and Results of Thermal Distributions for CASE A	73
4.5	Solution and Results of Thermal Distributions for CASE B	79
4.6	Solution and Results of Thermal Distributions for CASE C	81
5.	<u>THEORETICAL DETERMINATION OF THERMAL STRESSES</u>	84
5.1	Computer Program STREN	
5.2	Thermal Stress Results for CASE A and B	87
5.3	Thermal Stress Results. CASE C	93

6.	<u>EXPERIMENTAL DETERMINATION OF THERMAL STRESSES</u>	95
6.1	Geometry and Characteristics of the Specimen	95
6.2	The Design and Construction of the Rig	97
6.3	Strain Gauge Measurements of Thermal Stresses	102
6.4	Experimental Results and Comparisons with Theoretical Analysis	106
7.	<u>BASIC CONSIDERATIONS OF THERMAL FATIGUE EXPERIENCED BY VESSEL AND NOZZLE</u>	116
7.1	Thermal Fatigue and Fracture Mechanics	116
7.2	Mechanics of Fracture and Crack Propagation	117
7.2.1	Crack Propagation	120
7.3	A Theoretical Investigation of Crack Growth for CASE C	122
7.3.1	Regions of High Stress Concentration for CASE C	123
7.3.2	Determination of Stress Intensity Factor K by Boundary Collocation Theory	124
7.4	Experimental Thermal Cycling of Specimen	131
8.	<u>CONCLUSIONS</u>	133
8.1	General Conclusions	133
8.2	Conclusions to Chapter 7	135
9.	<u>DISCUSSION OF NUMERICAL METHODS</u>	137
APPENDIX 1.	<u>TRANSIENT HEAT CONDUCTION AND CONVECTION</u>	138
A1.1	Transient Heat Conduction Finite Difference Equations inside the Walls	138
A1.2	Difference Equations for Convective Boundary Condition	141
A1.3	Natural Convection to Air for CASE C	143

APPENDIX 2.	<u>TRANSIENT THERMAL ANALYSIS FOR SPHERICAL</u>	
	<u>VESSELS</u>	146
A2.1	Introduction	146
A2.2	Theoretical Formulation of the Finite Element Method	147
A2.3	Rectangular Prism (x,y,z). Element Shape Functions	151
A2.4	Three Dimensional Element. Rectangular Prism	152
A2.5	Numerical Solution of the Thermal Distribution	153
A2.6	Boundary Conditions	154
A2.7	Computer Program TEFEL	157
A2.8	Thermal Distribution Results	162
APPENDIX 3.	<u>DATA DESIGNATIONS AND LISTINGS FOR</u>	
	<u>COMPUTER PROGRAMS TRAN1, TRAN2, TRAN3,</u>	
	<u>SUBROUTINE PLOT</u>	169
A3.1	Data Designations for Programs TRAN1, TRAN2, TRAN3, Subroutine PLOT	169
A3.2	Listing of Program TRAN1 and Subroutine PLOT	171
A3.3	Listing of Program TRAN2	175
A3.4	Listing of Program TRAN3	178
APPENDIX 4.	<u>STRESS ANALYSIS BY FINITE ELEMENTS</u>	182
A4.1	Finite Elements	182
A4.2	Equations	182
APPENDIX 5.	<u>DATA DESIGNATIONS AND LISTINGS FOR COMPUTER</u>	
	<u>PROGRAMS STREN1, STREN2, STREN3</u>	188
A5.1	Data Designations	188
A5.2	Listing of Program STREN1	195
A5.3	Listing of Program STREN2	201
A5.4	Listing of Program STREN3	207

APPENDIX 6.	<u>EXPERIMENTAL DETERMINATION OF STRESSES</u>	213
A6.1	Determination of Apparent Strain for Temperatures above 180°C	213
A6.2	Determination of Direct Stresses and Strains. Principal Strains and Stresses, Direction Angles and Maximum Shear Stresses. Program EXPER2	215
APPENDIX 7.	<u>BOUNDARY COLLOCATION ANALYSIS</u>	222
A7.1	Boundary Collocation Analysis. Derivation of Boundary Conditions	222
A7.2	Program STREN4	224
A7.3	Program FUNSTR and Subroutine DMATRX	231
APPENDIX 8.	<u>REFERENCES</u>	236
APPENDIX 9.	<u>COMPARISON OF TEMPERATURE DISTRIBUTION</u>	244-1
A9.1	Finite Difference Equation in a Cylindrical System	244-1
A9.2	Determination of Temperature Distribution	244-2
A9.3	Comparison of Temperature Results	244-3
TABLES		244
FIGURES		268

---

## GENERAL NOTATION

Symbol	Definition
a	crack length
$C_s$	specific heat of steel
c	depth of crack
$c_p$	specific heat of air at atmospheric pressure
$d_1$	first matrix coefficient
$D_i$	inside diameter of vessel
$d_i$	inside diameter of nozzle
E	modulus of elasticity
g	acceleration due to gravity
h	crack height
$h_{av}$	average heat transfer coefficient
$h_c$	convection heat transfer coefficient for nozzle
$h_{COND}$	conduction heat transfer coefficient for nozzle
$h_N$	heat transfer coefficient for nozzle
$h_r$	radiation heat transfer coefficient for nozzle
$h_v$	heat transfer coefficient for vessel
M	moment
Nu	Nusselt number

Symbol	Definition
k	thermal conductivity of steel
$k_a$	thermal conductivity of air
K	stress concentration factor
$l_v$	characteristic length of vessel
Pr	Prandtl number
p	pressure
$q_{rad}$	heat transfer rate due to radiation
Re	Reynolds number
r	crack co-ordinate
S	allowable stress (code)
$S_y$	shear stress at the yield point
$S_m$	average tensile stress
$S_b$	bending stress
$T_f$	temperature of fluid
$T_w$	wall temperature
$T_m$	mean temperature
$t_v$	wall thickness vessel
$t_n$	nozzle thickness
$U_f$	velocity of fluid flow

GREEK SYMBOLS

$\alpha$	thermal expansion coefficient
$\alpha'$	thermal diffusivity, $\alpha' = \frac{k}{\rho c}$
$\beta$	volume coefficient of expansion
$\epsilon$	emissivity
$\epsilon$	true strain
$\epsilon_1, \epsilon_2, \epsilon_3$	principal strains
$\theta$	crack co-ordinate
$\mu$	dynamic viscosity
$\nu$	Poisson's ratio
$\nu$	Kinematic viscosity
$\rho$	density
$\sigma'$	Stefan-Boltzman constant
$\sigma_1, \sigma_2, \sigma_3$	principal stress
$\sigma_x, \sigma_y, \sigma_z, \sigma_L, \sigma_R$	direct stresses
$\sigma_{maxp}$	maximum principal stress
$\tau$	time
$\tau_{max(12)}$	maximum shear stress in xy plane
$\tau_{max(23)}$	maximum shear stress in yz plane
$\tau_{max(31)}$	maximum shear stress in zx plane
$\chi$	stress function
$\Delta x$	space increment in x direction
$\Delta y$	space increment in y direction
$\Delta t$	time increment

NOTE: Numbers in parentheses as (R.1-6) indicate references in Appendix 8.



## LIST OF TABLES

---

### TABLE

- 4.4.1 CASE A. Thermal results sample for time = 9 min.30 secs.
- 4.5.1 CASE B. Thermal results sample for time = 10 minutes.
- 4.6.1 CASE C. Thermal results sample for time = 11 minutes.
- 5.2.1(a) CASE A. Stresses for outside boundary.
- 5.2.1(b) CASE A. Maximum shear stresses for outside boundary.
- 5.2.2 CASE A. Stresses for inside boundary.
- 5.2.3 CASE B. Stresses for outside boundary.
- 5.2.4 CASE B. Stress for inside boundary.
- 5.3.1 CASE C. Stresses at various time intervals for  
outside boundary.
- 5.3.2 CASE C. Maximum principal and maximum shear stresses  
at various time intervals for outside  
boundary.
- 6.4.1(a) Experimental stress results sample.
- 6.4.1(b) Experimental principal stresses results.
- 6.4.2 Experimental results. Direct stresses for  
time = 12 minutes.
- 6.4.3 Experimental results. Maximum principal stresses and  
maximum shear stresses for time = 12 minutes.
- 6.4.4 Experimental stresses in vessel node 12 during  
heating-up and cooling-down.
- 6.4.5 Experimental stresses in nozzle node 43 during  
heating-up and cooling-down.
- 7.3.2.1 Theoretical values of stress intensity factor K

# LIST OF FIGURES

---

## FIGURES

- 3.1.1 Pressure vessel nozzle configurations
- 3.1.2 Section of pressure vessel
- 3.1.3 Section of spherical vessel
- 3.2.1 Nozzle section for CASE A
- 3.2.2 Nozzle section for CASE B
- 3.2.3 Nozzle section for CASE C
- 4.4.1 Temperature grid for CASE A
- 4.4.2(a) Temperature profiles for time = 9 min 30 secs for CASE A
- 4.4.2(b) Temperature profiles for time = 54 minutes for CASE A
- 4.4.3 Junction boundary determination
- 4.4.4(a) Temperature profiles for CASE A
- 4.4.4(b) Temperature profiles for CASE A
- 4.4.4(c) Temperature profiles for CASE A
- 4.4.5 Mean temperature variation  $\Delta T_m$  between nozzle and vessel for CASE A
- 4.5.1 Temperature grid for CASE B
- 4.5.2(a) Temperature profiles for time = 10 minutes. CASE B
- 4.5.2(b) Temperature profiles for time = 54 minutes. CASE B
- 4.5.3(a) Temperature profiles for CASE B
- 4.5.3(b) Temperature profiles for CASE B
- 4.5.4 Mean temperature variation  $\Delta T_m$
- 4.6.1 Temperature grid for CASE C

- 4.6.2(a) Thermal profiles for CASE C
- 4.6.2(b) Thermal profiles for CASE C
- 4.6.2(c) Thermal profiles for CASE C
- 4.6.3 Mean temperature variation  $\Delta T_m$  between nozzle and vessel. CASE C
  
- 5.1.1 Modulus of elasticity versus temperature
- 5.1.2 Coefficient of thermal expansion versus temperature
- 5.1.3 Poisson's ratio versus temperature
- 5.1.4 Direction of stresses
  
- 5.2.1 CASE A. Finite element mesh
- 5.2.2 CASE A. Direct stresses for outside boundary
- 5.2.3 CASE A. Maximum principal and maximum shear stress for outside boundary
- 5.2.4 CASE A. Direct stresses for inside boundary
- 5.2.5 CASE A. Maximum principal and maximum shear stress for inside boundary
- 5.2.6 CASE B. Finite element mesh
- 5.2.7 CASE B. Direct stresses for outside boundary
- 5.2.8 CASE B. Maximum principal and maximum shear stress for outside boundary
- 5.2.9 CASE B. Maximum principal and maximum shear stress for inside boundary
  
- 5.3.1 CASE C. Finite element mesh
- 5.3.2 CASE C. Stress  $\sigma_L$  at time intervals for the outside boundary
- 5.3.3 CASE C. Stress  $\sigma_R$  at time intervals for the outside boundary
- 5.3.4 CASE C. Stress  $\sigma_z$  at time intervals for the outside boundary

- 5.3.5 CASE C. Maximum principal stress  $\sigma_{\max p}$  at time intervals for outside boundary
- 5.3.6 CASE C. Maximum shear stress  $\tau_{\max(12)}$  at time intervals for outside boundary
- 6.1.1 Experimental specimen
- 6.1.2 Section of the specimen
- 6.1.3 Photograph of the specimen with strain gauges, heating and cooling arrangements
- 6.1.4 Photographs of the rig showing control panel and automatic strain recorder
- 6.2.1 Photograph of control devices
- 6.2.2 Electrical circuit diagram of control panel
- 6.3.1(a) Positions of strain gauge rosettes on the nozzle and junction
- 6.3.1(b) Positions of strain gauge rosettes on the vessel
- 6.4.1 Stress  $\sigma_L$  at time = 12 minutes. Experimental and theoretical results
- 6.4.2 Stress  $\sigma_z$  at time = 12 minutes. Experimental and theoretical results
- 6.4.3 Maximum principal stress  $\sigma_{\max p}$  at time = 12 minutes. Experimental and theoretical results
- 6.4.4 Maximum shear stress  $\tau_{\max(12)}$  at time = 12 minutes. Experimental and theoretical results
- 6.4.5 Stress  $\sigma_y$  at vessel node 12 during heating-up and cooling-down. Experimental and theoretical results
- 6.4.6 Stress  $\sigma_z$  at vessel node 12 during heating-up and cooling-down. Experimental and theoretical results
- 6.4.7 Maximum principal stress  $\sigma_{\max p}$  at vessel node 12. Experimental and theoretical results

- 6.4.8 Stress  $\sigma_x$  at nozzle node 43 during heating-up and cooling-down. Experimental and theoretical results
- 6.4.9 Stress  $\sigma_z$  at nozzle node 43 during heating-up and cooling-down. Experimental and theoretical results
- 6.4.10 Maximum principal stress  $\sigma_{maxp}$  during heating-up and cooling-down. Experimental and theoretical results
- 7.2.1 Co-ordinate system for crack
- 7.2.2 Idealised variation of fatigue crack growth rate ( $da/dN$ ) with alternating stress intensity  $\Delta K$
- 7.3.1.1 Maximum principal stresses in Area A of CASE C
- 7.3.2.1 Area A where crack is considered in CASE C
- 7.3.2.2 Finite element mesh for Area A of CASE C
- 7.3.2.3 Grid for determination of stress function .  
Cell for finite difference solution of  $\nabla^4 \chi = 0$
- 7.4.1 Photograph of a section through the longitudinal plane of the specimen

# INTRODUCTION

---

The design and analysis of modern pressure vessels and their components constitute two very important tasks which often require a broad understanding of a number of fields. Subjects like pressure vessel design criteria, fatigue fracture, elastic and plastic analysis, as well as the influence of high temperatures and external loads are of vital importance. As the design requirements become more and more strict the need for understanding of the above mentioned subjects grows stronger.

In recent years basic changes have taken place in the design of pressure vessels and pressure vessel components. With the introduction of high speed computers, analysis of localised stresses and strains is possible and more accurate results can be obtained. Present design criteria are based on a design which accounts for all possible modes of failure such as fatigue, brittle fracture, plasticity, shakedown, mechanical and thermal ratcheting. As a result of all these considerations today's design criteria are safer and more reliable.

Fatigue, both mechanical and thermal, continues to be a field of major concern in pressure vessels and components, especially nozzles. Nevertheless, as a result of major advances and studies which have been made in the atomic, microscopic and macroscopic aspects of various materials, fatigue can be considered as a problem for which sound theoretical and experimental analyses have been achieved, and results have been obtained which provide the ground for safer design.

The risk of fracture of components, like nozzles, increases as the characteristic length of the member increases. This is because there are always hidden flaws in the metal due to manufacturing or welding. It is impossible that any structural component of a pressure vessel including the vessel shell can be completely free of flaws. It is even more speculative to assume such a thing for welded regions. Of course there is always an attempt to keep the number of such flaws at a minimum through careful fabrication but this is an ideal rather than a practical target.

The advancement of the digital computer and computational techniques has made elastic-plastic analysis possible, although plastic analysis does tend to depend on plastic theories concerning the behaviour of the material after yielding. Computing has also made the consideration of more complicated geometries possible both in 2- and 3-dimensional cases.

# 1. DEVELOPMENTS IN PRESSURE VESSEL TECHNOLOGY

---

## 1.1 Pressure Vessels

The main characteristic of a pressure vessel is the pressure it can hold. This however makes the vessel a potential source of danger if it fails, leading to uncontrolled release of the pressure. Therefore the study of the failure and of the general behaviour of pressure vessels has been of great value in preventing failures. This also leads of course to better design, which is not only safer, but also more economical. During the years of pressure vessel research and development attention was concentrated in various areas of the design and construction. In early steam and chemical vessels, rivet joints were the weakest link and were the subject of much investigation. The development of the welding process and its adoption switched attention to other areas, one of which was the improvement made possible by better shapes and reinforcements for the vessel. When the design of a particular vessel included the attachment of nozzles, attention had to be paid to the possibility of failure of such branches and also the way of welding these components on to the main body of the vessel.

Most vessels are built as cylinders due to ease of fabrication. Nevertheless their actual configuration may vary according to purpose, and spherical vessels for example are often used for storage purposes. Great attention is generally



attached to vessel heads enclosing the ends of cylindrical vessels, and to nozzles. The nozzle and in particular the area of attachment to the vessel is the area of study of the present work.

In recent years the development of nuclear power has been an important factor in the improvement of pressure vessel design. Since safety was of significant concern and protection against radiation hazards very important the structural analysis of pressure vessels was crucial. A second equally important factor was the desire to upgrade all the pressure vessel codes to take advantage of the many advances that had been made in the understanding of pressure vessel behaviour, thereby eliminating potential weaknesses of existing codes and permitting safe, and in some cases more economical, construction.

Also new criteria concerning the design of pressure vessels were formulated in the 1950's. It was during this period that a reasonable understanding of brittle fracture and low-cycle fatigue was reached, the principles of limit design were established, and the mechanics of thermal ratcheting, shakedown, elastic-plastic action, and constrained plasticity were explained. Of equal importance to the understanding of physical processes were the advances made in computational methods. The electronic computer made the routine solution of complex problems first possible and then economical.

Since 1960 new criteria have been accepted and are based on fundamental considerations of analysis and material behaviour. An attempt has also been made to understand all possible modes of failure and provide rational margins of safety against each type of failure in a manner consistent with the consequences of what type. As a result of this quest for fundamental understanding

several basic concepts have emerged. Thermal stresses have been the subject of a more detailed analysis and vessels built to the new criteria have a balanced design to better carry thermal and mechanical stresses. It is well known that stresses resulting from a given thermal gradient increase with section thickness, whereas for a given diameter, pressure stresses decrease with shell thickness.

The basis for design stress limits and structural evaluation has also been shifted from the maximum principal stress theory to the more accurate maximum shear stress theory. This is a fundamental change and is very important in regions where one principal stress is tensile and the other is compressive. Equally significant is the recognition that pressure vessels may be subject to changing thermal stresses, and specific procedures and criteria were introduced for evaluation of thermal fatigue damage. Incorporation of these methods was made possible by the understanding gained of low-cycle fatigue failure mechanisms in the 1950's. Equipment made of ductile material will normally fail only after some plastic action. In structural evaluation of equipment, in general, only elastic analysis is required, nevertheless, many concepts from plasticity theory have proved exceedingly useful in the development of design stress limits. The use of plastic theory is a result of the attempt to understand fundamental mechanical behaviour and is only possible because of major advances in applied mechanics theory and computational ability.

The most important feature of the change in normal design procedure is the concept of design by analysis. A complete and detailed analysis of the vessel is required and the calculated stresses must be compared to various allowable values. The

allowable values are established by consideration of the possible modes of vessel failure. Thus, average membrane stresses are set up by consideration of gross distortion and bursting, local stresses are permitted to exceed yield but must "shake down" to elastic action. Peak stresses are considered in conjunction with specified cyclic service to ensure suitable fatigue life.

So far general considerations of vessel design and developments have been reviewed for the last two decades. But the effort for future advance in the field of pressure vessels is continuing. One of the more significant developments at present is the preparation of new design criteria for use in the temperature range above 800<sup>o</sup>F (427<sup>o</sup>C). High temperature design criteria under development are expected to follow the "design by analysis" philosophy, namely, consideration of all possible modes of failure, and design criteria associated with each mode.

It is certain that methods and criteria will continue to evolve and computer programs will be used extensively to calculate and analyse cyclic, non-linear and time-dependent deformations. The development of rational design criteria against which to evaluate local and general creep and stress relaxation, fatigue in the creep range, and other time-dependent structural behaviour is already under development. As criteria are developed, structures designed and built, and experience is gained the understanding of 'in-service' behaviour will become clearer and the fitness for purpose of any pressure vessel be more assured.

## 1.2 Criteria for Design Analysis

The determination of stresses in pressure vessels is the primary objective of the investigator, but a calculated, or even measured value of stress or strain means rather little until it

is associated with its location and distribution in the structure and with the type of loading which produced it. This can be illustrated by comparing the average stress and strain in the wall of a pressure vessel with the stress and strain at the root of a sharp notch in the wall. When the internal pressure reaches a value which produces an average hoop stress in excess of the yield strength, the wall becomes thinner, the diameter becomes larger, and if it were not for strain hardening of the material, the vessel would burst. Therefore the average stress produced by internal pressure must be kept below the yield strength. On the other hand, the material at the root of the notch yields even before the working pressure is reached, but no failure occurs. At the notch the local strain can be several times the yield strain but this condition is perfectly safe as long as the material is ductile and the load is not cycled often enough to start a fatigue crack. There are also other stresses whose calculated values can be safely allowed to exceed the yield strength of a ductile material. A well known example is a thermal stress, which is self equilibrating within the structure. There is no fixed external load which must be balanced and yielding helps the material to accommodate the imposed distortion pattern. Another example is the discontinuity stress near the junction of a head and shell which is produced by internal pressure. In this case the head and the shell want to expand by different amounts and distortion is required to keep them together at the junction. Usually stresses can be grouped in three distinct categories. These can be designated as primary stresses, secondary stresses and local or peak stresses. Primary stresses are stresses developed by the imposed loading which is necessary to satisfy the laws of equilibrium of external and

internal forces and moments. The basic characteristic of primary stresses is that they are not self-limiting. If a primary stress exceeds the yield strength of the material, the prevention of failure is entirely dependent on the strain hardening properties. Secondary stresses are developed by the self constraint of the structure. The basic characteristic of secondary stresses is that they are self-limiting since minor distortions can satisfy the discontinuity conditions which cause the stresses to occur. The local or peak stresses are the highest stresses in the region under consideration. Both primary and secondary stresses, as well as stress concentration effects, are considered. The basic characteristic of local stresses is that they cause no significant distortion and are objectionable only as a possible source of fatigue failure, brittle fracture or stress corrosion cracking. Nevertheless it can also be said that membrane stresses, the average value across a section, and bending stresses (linearly variable across the section) are stresses that can be included within the above three groups of stresses.

If assessment has to be made of how close a given calculated stress is to the danger point, it is helpful to consider the various possible modes of failure. According to the International Institute of Welding (R.1-1) these modes can be grouped as follows:

1. Excessive plastic deformation, including plastic instability.
2. High strain fatigue.
3. Corrosion fatigue.
4. Stress corrosion.
5. Brittle fracture.
6. Excessive elastic deformation, including elastic instability.

The specification of allowable stresses is in fact a function of the code writing bodies rather than of research. Nevertheless the researcher must be able to produce concrete answers on what conditions will or will not produce failure so that designers can have a basis for choosing their margin of safety.

The analysis of stresses and strains must be sufficiently detailed to include multiaxiality. It is not sufficient to know only the magnitude of the largest principal stress at a given point. All three of the principal stresses should be known in both magnitude and direction, since it is well established that the distortion energy theory (also known as the Mises criterion and the octahedral shear theory) is a much better criterion of yielding and fatigue failure in ductile metals than is the maximum stress theory. The maximum shear stress theory is often used as a close and conservative approximation to the distortion energy theory, but this also requires knowledge of all three principal stresses. Knowledge of the stress distribution, as distinguished from knowledge of only the peak stress at a single point, is important. A stress which is uniform across the thickness of a section has a different significance from one which varies across the thickness because if the uniform stress exceeds the yield strength, the load must be transferred to other sections in other parts of the structure if collapse is to be avoided, and this may involve large distortions. On the other hand, if a member is subjected to a bending load which puts only the outer fibres of a section into a yielded condition the load is transferred to the inner fibres and a great load is required to produce collapse. Knowledge of stress distribution is also important in the study of fatigue phenomena. It is well

known that theoretical stress concentration factors frequently give an exaggerated picture of the real fatigue strength reduction in a member and one of the most important quantities is the stress gradient at the notch as well as the value of the peak stress.

In order to prevent failure of the pressure vessel by any of the failure modes that have already been mentioned certain limits have to be imposed on the value of stresses. The lowest of the allowable values must be assigned to primary stresses, which are the stresses required to satisfy the laws of equilibrium of internal and external forces. These stresses are not self-limiting and if the average value across a solid section exceeds the strain hardened yield strength, failure will occur. Consideration should also be given to the distribution of the primary stress across the thickness of a section, since the sum of membrane and bending components may be allowed to attain a higher value than the membrane component itself. The chosen allowable stress values must keep the imposed mechanical loading safely below the collapse load of the structure. Considerably higher values may be assigned to the calculated values of primary-plus-secondary stresses. If these stresses are calculated on an elastic basis, they do not need to be kept below yield strength, but must be kept low enough to insure that the elastic analysis is a valid measure of the strains in the structure. The primary-plus-secondary stresses must be limited to values which will prevent both cyclic and incremental collapse. Additionally, the sum of the primary and secondary stresses must be kept below the value which might produce brittle fracture, considering the temperature of operation and the size of the

possible defects. Finally a third set of allowable values must be assigned to the peak stresses in the structure, since they may form the nuclei for fatigue or stress corrosion cracking. The allowable value to prevent fatigue depends on the threshold stress for this phenomenon determined from tests. The establishment of allowable stresses is based on the assumption that the material being used has sufficient ductility to accommodate the required plastic flow. Most of the materials commonly used for pressure vessels do have enough ductility to accommodate secondary and localised stresses as described above. When, however, higher strength steels are used what degree of reduced ductility can be accepted? When analysis assumes the idealised stress-strain curve it is assumed that there is no limit to the amount of plastic strain which can occur. Sharp corners and defects such as might be found in many vessels can produce theoretical stress concentration factors as high as 10 or even more, even though the fatigue strength reduction factor is much lower. Secondary stresses can produce strains as high as twice the yield strain in relatively large volumes of material without causing failure. Nevertheless sometimes loadings and stresses do not affect the failure criteria directly. For instance, the burst pressure is significant because it indicates how much safety margin exists as protection against gross over-pressure, but for protection against fatigue failure the burst pressure has no significance at all. The true fatigue margin in the design is the ratio between the highest strain range found at any point and the strain range which the material can tolerate for the required number of cycles. In establishing this true safety margin for fatigue, the notch sensitivity of the material is important, since the fatigue strength reduction factor, as



differentiated from the theoretical stress concentration factor, depends on both the notch sensitivity of the material and the stress gradient at the notch. For higher temperature when creep is significant, the differentiation between primary and secondary stresses is particularly important. Creep, like plastic flow, aggravates primary stresses but reduces secondary stresses. Therefore in the absence of notches, it is probably feasible to select values of allowable primary stress for use at high temperature which are controlled by the creep strength. Allowable values of secondary stress might still be based on the yield strength at the operating temperature. When notches are present, additional precautions are required to control the concentrated values of primary stresses, since the stress rupture strength at high temperature may be reduced by notches, whereas the yield strength at room temperature is not.

### 1.2.1 Strength Theories

The stress state at any point in a structure may be completely defined by giving the magnitudes and directions of the three principal stresses. When two or three of these stresses are different from zero, the proximity to yielding must be determined by means of a strength theory. The theories most commonly used are the maximum stress theory, the maximum shear stress theory (also known as the Tresca criterion), and the distortion energy theory (also known as the octahedral shear theory and the Mises criterion). It has been known for many years that the maximum shear stress theory and the distortion energy theory are both much better than the maximum stress theory for predicting yielding and fatigue failure in ductile metals. Most experiments show that the distortion energy theory is even more

accurate than the shear theory, but the shear theory is a little more conservative, it is easier to apply, and it offers some advantages in some applications of the fatigue analysis.

The maximum shear stress at a point is defined as one-half of the algebraic difference between the largest and the smallest of the three principal stresses. Thus, if the principal stresses are  $\sigma_1$ ,  $\sigma_2$  and  $\sigma_3$ , and  $\sigma_1 > \sigma_2 > \sigma_3$ , the maximum shear stress is  $\frac{1}{2}(\sigma_1 - \sigma_3)$ . The maximum shear stress theory of failure states that yielding in a component occurs when the maximum shear stress reaches a value equal to the maximum shear stress at the yield point in a tensile test. In the tensile test, at yield,  $\sigma_1 = S_y$ ,  $\sigma_2 = 0$  and  $\sigma_3 = 0$ .  $S_y$  is the shear stress at the yield point. The maximum shear stress is  $S_y/2$ . Therefore yielding in the component occurs when

$$\frac{1}{2}(\sigma_1 - \sigma_3) = \frac{1}{2} S_y \quad (1.2.1.1)$$

In order to avoid dividing both the calculated and the allowable stresses by two before comparing them, a new term called "equivalent intensity of combined stress" or "stress intensity" is used. The stress intensity is defined as twice the maximum shear stress and is equal to the largest algebraic difference between any two of the three principal stresses. Thus the stress intensity is directly comparable to strength values found from tensile tests. For simple analysis of low pressure vessel stresses, it makes little difference whether the maximum stress theory or the maximum shear stress theory is used. For example, in the wall of a thin-walled cylindrical pressure vessel, remote from any discontinuities, the hoop stress is twice the axial stress and the radial stress on the inside is compressive and equal to the internal pressure,  $p$ . If the hoop stress is  $\sigma$ , the

principal stresses are:  $\sigma_1 = \sigma$ ,  $\sigma_2 = \sigma/2$  and  $\sigma_3 = -p$ . According to the maximum shear stress theory, the controlling stress is the stress intensity, which is  $(\sigma + p)$ . Since  $p$  is small in comparison with  $\sigma$  for a thin-walled vessel, there is little difference between the two theories. In more complex stress situations, however, the difference between the two theories often becomes important.

Stress intensity limits are one of the major considerations in the design of pressure vessels. It has already been mentioned that stresses can be grouped in three basic categories of primary stresses, secondary stresses, and peak stresses. Limit design theory is based on certain assumptions and the choice of the stress intensity limits for the stress categories mentioned above is accomplished by the application of the limit design theory. The basic assumption which is made is that there is perfect plasticity with no strain-hardening. In a structure as simple as a straight bar in tension, a load producing yield stress,  $S_y$ , results in collapse. If the bar is loaded in bending, collapse does not occur until the load has been increased by a factor known as the shape factor of the cross section, at that time a plastic hinge is formed. The shape factor for a rectangular section, for instance, in bending is 1.5. When the primary stress in a rectangular section consists of a combination of bending and axial tension, the value of the limit load depends on the ratio between the tensile and bending loads. Fig.1.2.1.1 shows the value of the maximum calculated stress at the outer fibre of a rectangular section which would be required to produce a plastic hinge plotted against the average tensile stress across the section, both values expressed as multiples of the yield stress,  $S_y$ . When the average tensile stress,  $S_m$ , is zero,

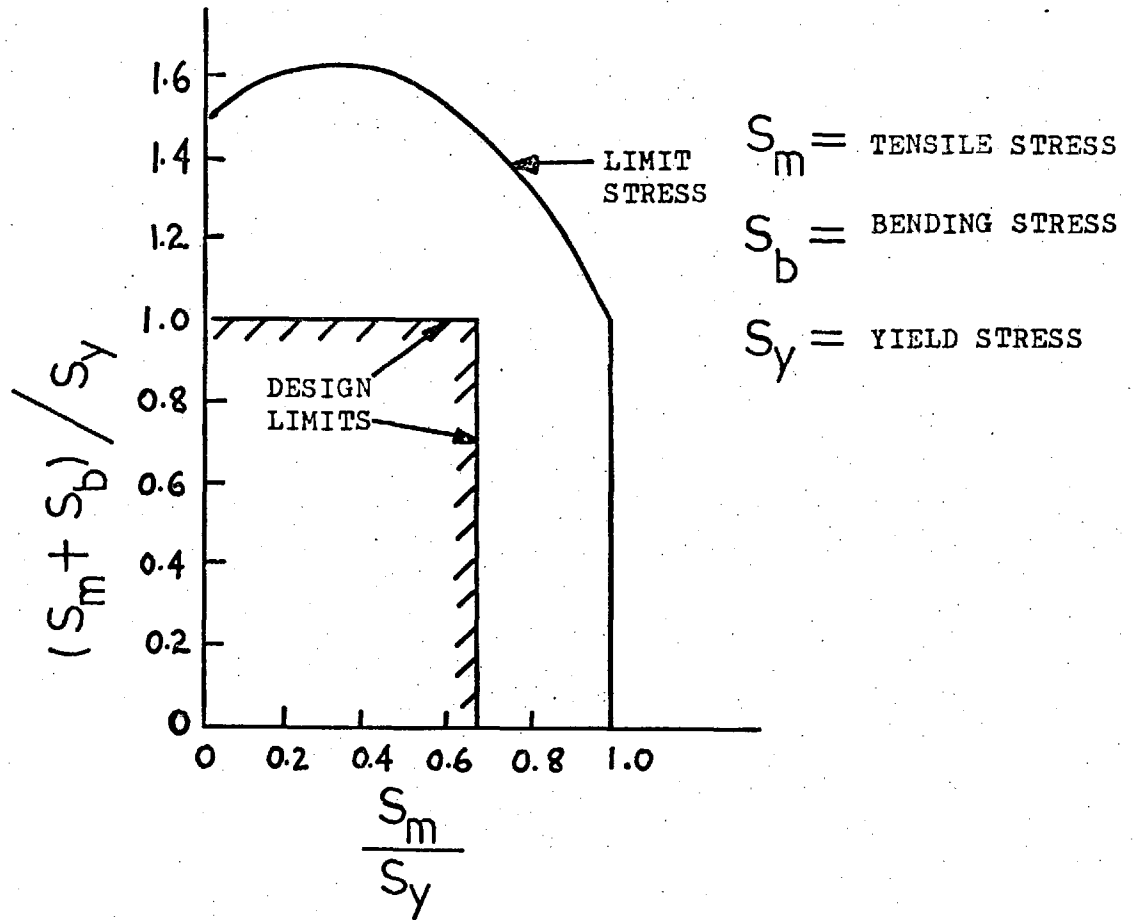


FIG. 1.2.1.1. Limit stress for combined tension and bending for rectangular section.

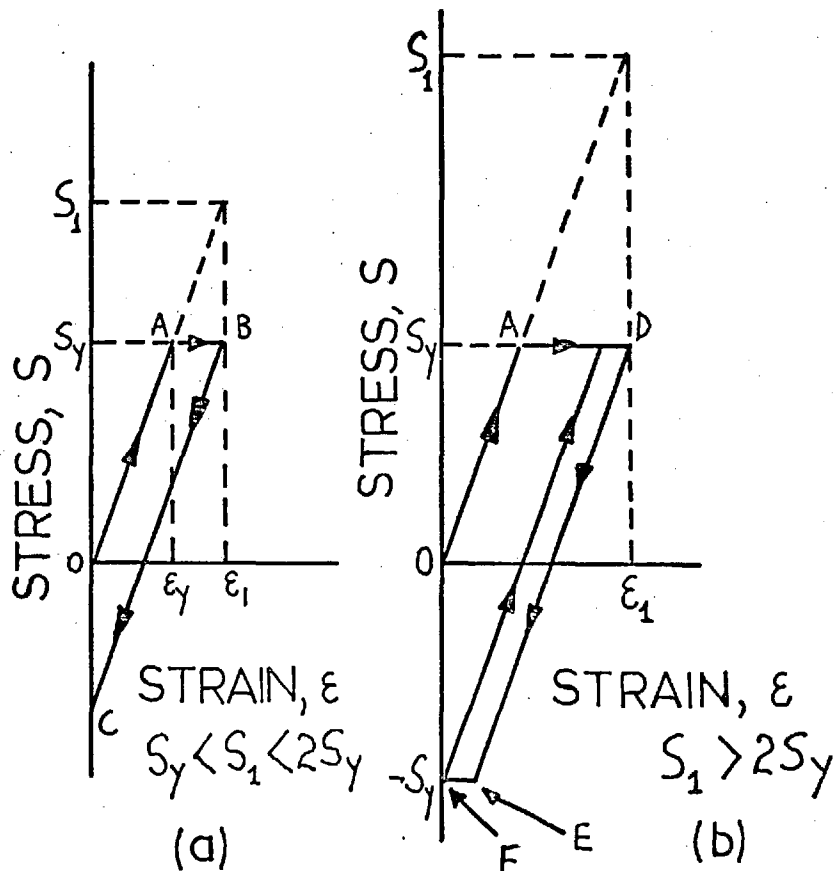


FIG. 1.2.1.2. Strain beyond yield.

the failure stress for bending is  $1.5S_y$ . When the average tensile stress is  $S_y$ , no additional bending stress,  $S_b$ , may be applied. Fig.1.2.1.1 can provide allowable values, in terms of the yield stress, for general primary membrane stress,  $S_m$ , and primary membrane plus bending stress,  $S_m + S_b$ . It may be seen that limiting  $S_m$  to  $(2/3)S_y$  and  $S_m + S_b$  to  $S_y$  provides adequate safety. Nevertheless the safety factor is not constant for all combinations of tension and bending, but a design rule to provide a uniform safety factor would be unnecessary complicated.

In the study of allowable secondary stresses, a calculated elastic stress range equal to twice the yield stress has a very special significance. It determines the borderline between loads which, when repetitively applied, allow the structure to "shake down" to elastic action and loads which produce plastic action each time they are applied. The theory of limit design provides rigorous proof of this statement, but the validity of the concept can easily be visualised. If, for example, the outer fibre of a beam is considered which is strained in tension to a strain value  $\epsilon_1$ , somewhat beyond the yield strain as shown in Fig.1.2.1.2(a) by the path OAB. The calculated elastic stress would be  $S = S_1 = E \epsilon_1$ . Since the case of secondary stress is considered it will be assumed that the nature of the loading is such as to cycle the strain from zero to  $\epsilon_1$  and back to zero, rather than cycling the stress from zero to  $S_1$ , and back to zero. When the beam is returned to its undeflected position, O, the outer fibre has a residual compressive stress of magnitude  $S_1 - S_y$ . On any subsequent loading, this residual compression must be removed before the stress goes into tension and thus the elastic range has been increased by the quantity  $S_1 - S_y$ . If  $S_1 = 2S_y$ , the elastic range becomes  $2S_y$ , but if  $S_1 > 2S_y$ , the fibre yields in

compression, as shown by EF in Fig.1.2.1.1(b) and all subsequent cycles produce plastic strain. Therefore,  $2S_y$  is the maximum value of calculated secondary elastic stress which will "shake down" to purely elastic action.

The allowable stress intensity for austenitic steels and some non-ferrous materials, at temperatures above  $100^{\circ}\text{F}$ , may exceed  $(2/3)S_y$  and may reach  $0.9S_y$  at temperature. Nevertheless if Fig.1.2.1.1 is considered it will be seen that loads in excess of the limit load are permitted. This is because these materials have different stress strain diagram. Austenitic steels that are usually employed for the construction of pressure vessels have no well-defined yield point but have strong strain-hardening capabilities so that their yield strength is effectively raised as they are highly loaded. This is equivalent to choosing a different definition of the "design yield strength" for those materials which have no sharply defined yield point and which have strong strain hardening characteristics. It can be concluded that the primary criterion of the structural adequacy of a design, is that the stresses, as determined by calculation or experimental stress analysis, shall not exceed the specified allowable limits. The third category of stresses, peak stresses, are related only to fatigue and they will be discussed in Chapter 7. In the case of fatigue analysis, plastic action can actually persist throughout the life of the vessel and plastic zones within the structure are responsible for initiation and propagation of cracks. Repetitive plastic action occurs only as the result of peak stresses in relatively localised regions and these regions are intimately connected to larger regions of the vessel which behave elastically. Typical examples of peak stresses are those at the root of a notch in a fillet, at the

edge of a small hole, or at the junction of nozzle and vessel. The material in these small regions is strain-cycled rather than stress-cycled and the elastic calculations give numbers which have the dimensions of stress but are really proportional to the strain.

## 2. REVIEW OF RECENT INVESTIGATIONS IN PRESSURE VESSEL NOZZLES

---

### 2.1 Nozzle and Openings

It has generally been accepted that the design of nozzles and openings in pressure vessels is guided by the "replacement of area" rules. The rules stipulate that the area cut out of the vessel by the opening must be replaced within a prescribed zone around the opening. The area replacement rule may be considered as a crude limit pressure design. The nozzles and openings so designed are not likely to rupture due to a few applications of pressure up to the yield pressure of the unperforated vessel. This statement is made on the assumption that fabrication does not introduce cracks in the material and that brittle fracture does not occur. Nevertheless it is found that during fabrication, cracks are introduced and rupture of the component occurs below the expected limit of yield pressure. Additionally the area replacement rule does not give any assurance that performance will be satisfactory for cyclic pressure loading, for static or cyclic external loads such as piping systems which may impose forces and moments on the nozzles, for cyclic thermal gradients, or for combinations of those loads. Therefore, while design rules exist for nozzles and openings, a significant amount of research effort has been and is being directed toward improvement in their design and analysis. Elastic stresses in isolated, radial nozzles and circular openings in spherical shells can be analysed by means of axisymmetric shell theory. Waters



(R.2-1) developed a theory specifically for a uniform wall nozzle in a uniform wall sphere for internal pressure loading. Leckie and Penny (R.2-2) developed a similar theory, but more general in that it also covers moment, thrust, and shear loads applied to the nozzle. Calculated data on stresses at nozzles in spherical shells are given in reference (2-3). These data are for both internal pressure and external loads on the nozzle and cover a wide range of dimensional parameters, and they are useful for design at the design code level.

Computer programs have also been developed for various loading conditions but only a limited number of them will be referred to here. An axisymmetric shell computer program applicable to nozzles in spherical shells with variable wall thickness and for internal pressure, external loads on the nozzle and thermal gradients was developed by Kalnins (R.2-4). Axisymmetric finite element computer programs, such as that developed by Wilson (R.2-5), are also applicable to the same geometries and loadings as the shell computer programs but can be used to establish stresses in greater detail and with more accuracy than possible with shell programs.

Nozzles in cylindrical shells present a more difficult theoretical problem. Until a few years ago, analytical estimates of elastic stresses at small nozzles or openings were often obtained by reducing the problem to that of an opening or nozzle in a flat plate with edge loads. Papers by Beskin (R.2-6) and Waters (R.2-7) are examples of this sort of approximation. Solutions to the problem of a cylindrical shell with a circular opening are given in (R.2-8 and 2-9). Solutions to the problem of two normally intersecting cylindrical shells, with internal pressure loading is treated by A.C. Eringen (R.2-10). He solves

the boundary value problem by solving the differential equations of the two shells for a ratio of radii smaller than 0.3 and subjected to edge conditions along the intersection curve and at the ends of the cylinders. Bijlaard, Dohrman and Wang (R.2-11) formulated the problem for  $d_i = D_i$  and indicated the form of the solution. Pan and Beckett (R.2-12) developed a theory for  $d_i/D_i$  up to unity and give a numerical example for  $d_i = 0.5 D_i$ .

Several papers related to the subject of non-radial nozzles and non-circular holes are published in the Welding Research Council Bulletin No.153.

The overall problem of nozzles and openings in pressure vessels is quite complex because of the many dimensional parameters involved and because of the variety of loadings. The advances in the field of pressure vessel nozzles will now be examined from the theoretical and experimental sides. As will be seen, although a considerable amount of work has been done on calculating stresses in nozzles due to internal and/or external pressure and loadings the field of thermal stresses has been neglected and there are hardly any works that are directly concerned with thermal stresses exclusively. The behaviour of nozzles and openings at elevated temperatures, where creep and/or relaxation occurs, also needs further work in order to develop reliable design methods.

## 2.2 Theoretical Investigations of Nozzles

The theoretical work which has been done the last twenty years is concerned with elastic theory applied to nozzles, limit analysis of pressure and loads. Considerations on external loads have been met with difficulty and the work by Bijlaard (R.2-13, 2-14 and 2-15) estimates external loads on the nozzle

for distributed loads on the surface of cylindrical shells. Bijlaard's theory has been completed with empirical modifications but is essentially limited to small values of  $d_i/D_i$  (up to  $1/3$  or at most  $1/2$ ). Pressure vessel nozzles can have a variety of shapes and arrangements. Considerable amount of effort must be spent to adapt straightforward solutions of the shell theory to the mathematical idealisation of the local geometry. First Beskin (R.2-6) studied the subject of reinforcement. He represented the reinforcement by a pair of pads on both sides of the vessel wall, or a rim at the edge of the hole, or a combination of both. He considered the vessel wall to be an infinite flat-plate and therefore the results were thus strictly applicable only to small openings. With larger opening-diameter to vessel-diameter ratio, the effect of curvature increases the stress concentration. Nevertheless it was found that the high predicted stresses at the junction were sometimes much greater than that observed. Agreement may be good along the nozzle and the vessel wall, but the theoretical meridional bending-stress at the junction does not represent adequately the actual load stress at the junction and is, in many cases, much too high when the nozzle is of the protruding type or when the nozzle is finished with no sharp stress-raiser. This inaccuracy is due to the limitations of the thin-shell theory which represents the shell as being located at its mid-wall position, and thus cannot picture accurately the local stresses at a shell discontinuity unless additional correction is made there to a direct application of the thin-shell theory.

Theoretical solutions of non-symmetric shells are harder to achieve than shells of revolution. Nevertheless, recently, finite

element analysis and computer programs are used and can calculate elastic and plastic stresses for nozzles in cylindrical shells. The geometry of the configuration can be non-symmetric since finite element analysis employs basic elements into which the structure is broken down. Therefore finite element methods are of course, applicable to variable wall thickness and many possible nozzle or opening configurations. The significance of the calculated elastic stresses in pressure vessel nozzles must be assessed in terms of performance criteria such as excessive deformation or rupture, due to either single loads applications, or many load applications leading to fatigue failure, which is the more normal operational condition.

#### 2.2.1 Limit Pressure and Loads

Theoretical analysis of limit pressure for various types of nozzles has attracted the attention of a great number of researchers and S.S. Gill (R.2-16) gives an account of a theoretical analysis for flush cylindrical nozzle in a spherical pressure vessel. Membran forces in circumferential and meridional directions in the shell and longitudinal membrane force in nozzle are used to define a yield surface and the limit pressure was calculated for a flush nozzle for a range of parameter ratios of nozzle radius to sphere radius, and thickness ratios. The analysis considers plastic behaviour and the method uses upper and lower bound theorems. The nozzle is subjected to internal pressure, shear force and moment at the junction. Using similar methods Dinno and Gill (R.2-17) calculated the limit pressure for the case of a spherical and cylindrical vessel with hemispherical ends intersected by a nozzle. Various mechanisms of failure were considered and the collapse pressure for the vessel was studied. It was

assumed that the effect of strain hardening and the effect of fillet welds at the junction are neglected. The junction hinge is assumed to form at the intersection of the centre lines of the plate thickness of the cylinder and sphere. Upper and lower bounds to the collapse pressure are calculated and these are for the assumed interaction surface which circumscribes the true interaction surface for a material which obeys the Tresca yield criterion. The effect of changes of geometry on the collapse pressure is also neglected. Cloud (R.2-18) has calculated limit pressure in a spherical shell intersected by a cylindrical nozzle and also for a pad reinforced shell. The analysis assumes a perfectly plastic material and the equations for equilibrium for the axisymmetric shell of revolution were used. Graphs of radial deflection of shell at nozzle junction for various internal pressures were provided. The theory was completed with deformation tests made on three steel models of cylindrical nozzles in hemispherical heads.

Coon, Gill and Kitching (R.2-19) obtained a lower bound of the limit pressure in a cylindrical pressure vessel with an unreinforced hole. The stress distribution was restricted to one in which the principal stress directions were in the circumferential and longitudinal directions of the cylinder. The results of the theoretical analysis were compared with experimental work on the limit pressure of cylindrical pressure vessels with branches. It was evident from the analysis that as the ratio  $t/T$  of the thickness of the branch ( $t$ ) to the thickness of the cylinder ( $T$ ) decreased a rapid fall of the limit pressure was observed. An approximate analysis of the plastic limit pressures of nozzles in cylindrical vessels was made by Cloud and Rodabaugh (R.2-20) who estimated the limit

pressure from an upper bound analysis. The analysis was restricted to nozzle/shell diameter ratios of  $\frac{1}{2}$  or less. They also compared the theoretical analysis with other theoretical approaches and the results of a single experiment. Design graphs based on the analysis were prepared to indicate the amount of nozzle or shell thickness required to make the limit pressure of the nozzle-cylinder structure approximately equal to the yield pressure of the unperforated cylinder. Calladine and Goodall (R.2-21) studied the plastic behaviour of thin cylindrical pressure vessels with circular openings and radial branches.

Shakedown pressures for cylinder-sphere shell intersections were studied by Leckie (R.2-22). Lower bound estimates were found of the shakedown pressure. This was achieved by applying Melan's theorem and making use of elastic solutions already in existence. The stress concentration and shakedown factors were presented in graphical form for various ratios of nozzle/shell thickness from 0.25 to 1.0. The same author together with Penny (R.2-23) obtained further theoretical estimates of shakedown values for pressure and thrust and moment loadings applied through a radial nozzle in a spherical vessel. Again Melan's theorem was used and by using available elastic solutions. The results were obtained by using linear programming techniques and have been presented in a useful graphical form. Elastic-plastic behaviour of flush nozzles in spherical pressure vessels were studied by Marcal and Turner (R.2-24) by developing a computer program for the elasto-plastic analysis of axially symmetrical shells of revolution. The program was modified appropriately to allow interaction loads at nozzle junctions to be distributed over bands of finite width, rather than the conventional concentrated lines of loading at the intersection of the shell centre

lines. They compared the results with previously published test results for displacements, yield and collapse loads of flush nozzles and showed that the above modification in the approach improves the predictions from those of conventional shell theory. Deflections of nozzle junctions were plotted against pressure and meridional strain (maximum) were also plotted for various values of pressure. This was done for nozzles with and without fillet weld. It was found that the results were in broad agreement with experiment.

### 2.2.2 Elastic Analysis

Stresses due to internal pressure loadings have been studied on the basis of elastic theory as well as experimentally.

Bijlaard (R.2-25) developed a method where the stresses in a juncture of a nozzle to cylindrical pressure vessel for equal diameters can be determined. The application of the proposed method included pipe lines, header nozzle junctures, process reactors, etc. In the derivation of the methods utilised to compute the stresses, the proposed shell theory takes into account in fact that the shells are thick. This fact is neglected in conventional thin shell theory. As part of the development in the paper the shell shear deformation and the resulting stresses are considered in addition to the thick shell stress distributions caused by internal pressure loadings. The solution of the three coupled partial differential shell equations is obtained through the use of a series solution that satisfies the differential equations as well as the continuity conditions at the juncture of the two shells. In addition to the theoretical development, a proposed method for the numerical solution of the equation is given. Hasberry and Jones (R.2-26) made a theoretical study

into the elastic behaviour of a joint formed by the normal intersection of a right circular cylindrical shell with another of larger diameter. The wall of the larger cylinder was assumed to remain open inside the joint in order to give an arrangement which is encountered frequently in pressure vessels or pipeline intersections. An external bending moment which acts in the plane of the joint was applied to the nozzle cylinder and is equilibrated by moments of half this magnitude applied to either end of the parent cylinder. A solution for this loading has been obtained by assuming antisymmetric distributions of certain stresses across a plane transverse to the joint. The analysis presented is believed to be valid for nozzle to cylinder diameter ratios of less than  $1/3$ . Numerical results are given by a number of cases having radius ratios of  $1/10$  and  $1/4$ .

The problem of two normally intersecting cylindrical shells subjected to internal pressure was considered by Pan and Beckett (R.2-27). They solved the differential equations of shells subject to the boundary conditions imposed along the intersection between the two cylinders. Numerical results for a radius ratio of  $1/2$  are also given. They also discuss problems concerned with the numerical computations and there is certain comparison with some experimental results. Most of the analyses of elastic stresses due to external loads are experimental and they are discussed in Section 2.3.

### 2.2.3 Reinforcement of Nozzle Openings

Reinforcement of nozzle openings has so long been served by the "area replacement rule". This has been proved to be a satisfactory method. Although failure of pressure vessels is relatively rare, many of the failures occur in the vicinity of



the openings due either to brittle fracture or fatigue (even though the nature of the operation may not be cyclic in the normal sense of the term). Although inadequate welding and inspection are often factors in such failures, there is no doubt that the high stress level existing in the vicinity of the openings is a basic factor in the problem. Theoretical and experimental procedures are quite difficult to be formulated and this is mainly due to the large number of variables involved. Nevertheless theoretical analyses have been made and an account of some of them is given below.

#### 2.2.3.1 Spherical Shells

A relatively rigorous analysis of the stresses in nozzle connections in spherical shells have been made by Professor E.O. Waters (R.2-28). The work indicated that there were some significant differences under certain circumstances between theoretical and experimental work. It has been found that the outside fillet radius at the nozzle shell junction can have a major influence on the resulting stress level. This is rather apparent due to the fact that even a small fillet radius can constitute an appreciable increase in effective nozzle wall thickness at the most critical location, and is particularly important at small  $d_1/D_1$  ratios where the fillet radii used for the experimental modes were sometimes relatively large in relation to nozzle wall thickness.

Professor N.C. Lind (R.2-29) provided another more simplified analysis which gives only the hoop stress at the intersection. Comparison of the results from Water's and Lind's solutions with those of Penny and Leckie (R.2-30) indicated that there is reasonable agreement for  $d_1/D_1$  ratios in the range

of 0.25-0.50, for  $D_m/t_v$  ratio of 100. However, for the same range of diameter ratio and a materially greater  $D_i/t_v$ , the Penny and Leckie results are low, and for a materially smaller  $D_i/t_v$  ratio, the results are high. Rose and Thompson (R.2-31) provided values of stress concentration and for small diameter ratios they tend to agree with Penny's and Leckie's results but both give results higher than Water's solution.

### 2.2.3.2 Cylindrical Shells

Theoretical investigations of stresses around holes in cylindrical shells have been made by A.C. Eringen. Two solutions were developed, the first is reported in reference (2-32) and employs a perturbation technique. The second reference (2-33) employs an exact solution of thin shell theory and satisfies the boundary conditions in a collocation sense, that is in a definite number of points along the boundary. The later work was later programmed for a digital computer, and extensive data calculated for the case of a circular hole with membrane closure ( $t_n/t_v = 0$ ), the results of which are reported in references (2-34) and (2-35). The limitations of the presently available data are as follows:

$$d_i/D_i \leq 0.35$$

$$D_i/t_v \leq 20.0$$

$$(d_i/D_i) \sqrt{(D_i/t_v)} - \text{between } 0.155 \text{ and } 3.90$$

The works give graphs of diameter and thickness ratios against stresses tangential to the edge of the opening on the longitudinal and transverse axes of the cylinder. The distribution of the tangential membrane stress around the edge of the hole is also given and it is possible to locate points of maximum membrane stress. Work is being done to extend the study to larger diameter ratios.

### 2.3 Experimental Investigations of Nozzles

Experimental measurements of stresses due to various loads and internal pressure have been obtained using the strain gauge. Recent research on the experimental side of the stresses in pressure vessel nozzles has produced test data for various cases and an account of this research is given herein. The strain gauge is laid on and usually adhered on to the surface of the vessel. Any straining of the surface in the direction of the gauge causes a small change in the electrical resistance of the gauge wire, which is detected and quantitatively measured by a sensitive amplifying instrument.

The other commonly used method for analysing stresses at a pressure vessel is photoelastic analysis. Stress freezing is used and it is a very convenient way for three-dimensional geometries. Vessel components forming shells of revolution simplify the analysis and reduce the work because of symmetry, but stress freezing is still required. The great advantage of stress freezing photoelastic analysis is that stress changes through the shell wall can also be measured. A complete picture can thus be made of the stresses if required. This is especially useful for thick-walled vessels, thin vessels are known to have a linear distribution of stresses through the thickness. Nevertheless there is always an unknown factor in the use of photoelastic results, this being the effect to the stress values caused by differences in the Poisson's ratio  $\nu$ . Steel and other common pressure vessel materials have a value  $\nu$  of about 0.3 while photoelastic plastics undergoing stress freezing have a value of 0.5. Studies on the nature of this effect have been made in references (2-36) and (2-37). The observations were

found to apply only to specific problems and could not be generalised, even extensions of observations to other similar geometries and loadings have to be treated with care.

Elastic stresses due to internal pressure have been investigated by a large number of researchers and Everett and McCutcham (R.2-38) have investigated the stress conditions in full-size branch connections under internal pressure. William, Morgan and Bizon (R.2-39) investigated the elastic stress distributions of two shell junctions and obtained measurements of the stresses. The junctions were incorporated in a single type of structure, a cylinder with a toriconical head. The data obtained from the tests were compared with theoretical curves determined by previously published analyses. It was established that one of the principal sources of experimental error was the variation in geometry from the dimensional values assumed for purposes of analysis.

In reference (2-40) experimental data were obtained by Hardenbergh and Zamrik to show the general state of stress in nozzles. This is one of the most complete works and includes studies of five hot-formed contoured nozzles, four insert nozzles, and one juncture reinforced by an annular pad. The nozzles vary in size, and in the amount and distribution of the reinforcing material around the outlets. The tests were conducted under internal pressure and various external loads to the branch pipe. Bending moments and effects of internal pressure on the elastic stress distributions in the vicinity of two transition rings used to connect cylindrical ducts with large spherical pressure vessel have been studied by Kitching and Jones (R.2-41). Experimental values of stresses were obtained near the weld where it was found that stresses attained

their maximum value. Riley measured stress distributions in thin walled cylindrical and spherical vessels with circular nozzles. Stress distributions were determined in a series of vessels for internal pressure, axial thrust on the nozzle, and also external moment forms of loading (R.2-41). Stresses due to axial loads and internal pressure on forged nozzles in spherical pressure vessels were studied by Kitching and Duffield for two different type forging rings which provide different degrees of reinforcement. It was found that there was a marginal reduction in maximum stress for the heavier specimen. Stress concentration factors due to pressure were also determined (R.2-43). Experimental investigations of plastic behaviour of nozzles were made by Dinno and Gill (R.2-44) and Cottam and Gill (R.2-45).

### 3. THE NATURE OF THE PRESENT PROBLEM OF THERMAL STRESSES

---

A great deal of research and investigation has been done in the field of pressure vessel nozzles, as described in the previous sections; but the research has been exclusively concentrated on evaluating stresses due to internal pressure and external loads. Thermal stresses, although very important to the design, have been treated rather qualitatively than quantitatively. Allowances for thermal stresses in design tend to take the form of an increase of the value of the safety factor based on predictions of thermal stresses at regions where they can be quite high and calculations have been far from detailed and precise. Temperatures across the thickness of nozzle and vessel walls were represented by mean values and thermal transients were treated by various analytical methods which were limited to simple geometries and boundary conditions and could not be applied easily to complex cases. Whenever the wall thickness is small the approximation of a mean temperature can be accepted and the error involved is comparatively small too, but this is not true when the vessel or nozzle wall is thick. Additionally, since the design of pressure vessel is greatly influenced by economic factors the precise and detailed determination of thermal stresses has become a desirable goal.

The theoretical part of this work deals with the following three main areas:-

- (i) The determination of time dependent temperature distributions within the nozzle and vessel walls during warm-up for radial nozzles of various thicknesses attached to the vessel by different junction configurations.
- (ii) The calculation of transient thermal stresses due to the effect of the thermal transients during warm-up and cool-down and the determination of the areas of high thermal stress concentrations.
- (iii) The determination of stress intensity factors  $K$  at areas of high stress concentration in order to make predictions about fatigue life and possible crack growth and propagation which could lead to fracture under certain conditions.

Initially, the methods by which the above quantities have to be evaluated are formulated. The equations describing the various physical conditions are obtained and solved numerically by writing the appropriate computer program and using the College CDC6400 and the London University CDC6600 computers. Numerical methods have the great advantage that they are immensely flexible thus permitting them to be used over a wide range of various geometries and boundary conditions. They are also fast and accurate. Nevertheless it must be noted that whenever computational methods are employed attention must be paid to the evaluation of the errors involved in the numerical procedures. This in turn will permit the necessary steps to be taken to ensure that these, such as convergence and round-off errors, do not affect the values of the quantities under investigation.

### 3.1 The Geometry of the Pressure Vessel Nozzle

There are various types of nozzles attached to pressure vessels but here only the radial type is considered. Radial nozzles are the most common ones and sections of a radial nozzle are shown in Fig.3.1.1. Nozzles can be of the protruding type or flush type. Protruding nozzles penetrate the vessel wall and are continued within the vessel. Alternatively, nozzles can be welded directly on to the vessel wall. In Fig.3.1.1 a radial nozzle of the protruding type and a flush nozzle are shown, together with a nozzle directly welded on the vessel. Variations of type (c) are the ones that are examined herein. The sections of the nozzles are through the longitudinal plane of the vessel as shown in Fig.3.1.2.

When a nozzle is directly welded on the vessel the junction can have different configurations. The form of the welding connection can also vary. The geometry of the junction affects the stresses directly and therefore is an area that requires investigation. The accurate determination of the stress levels near the junction on both nozzle and vessel sides inevitably leads to the designer being able to reinforce the area without having to speculate on the amount and type of reinforcement. The area replacement method as it has already been explained is rather a crude way of applying reinforcement. This is due to the fact that up to now stresses around the junction, as well as peak stresses at the junction, could not be evaluated accurately.

The configuration of Fig.3.1.1(c) is studied theoretically and experimentally. The advantage of this configuration is that the junction is now part of the main shell and the weld is further away from the junction. Therefore this contributes to



a higher strength since there are no discontinuities due to welding connections. Nevertheless the above design is more expensive because the vessel wall has to be machined down and this is costly. It is also limited to rather small pressure vessels and when the number of nozzles, inlet or outlet, is not large. The different cases of nozzle configurations which are investigated theoretically are described in the next section. Cases are not only distinguished for their particular geometry but also for the particular physical conditions which prevail with respect to heat transfer conditions across the nozzle-vessel boundaries.

The present analysis of thermal distributions and stresses applies not only to cylindrical vessels but to spherical vessels too under a main assumption: in Fig.3.1.3 a spherical vessel is shown; when the diameter of the vessel is large the curvature of the shell wall is small and can be neglected. In most practical cases spherical vessels do have large  $D_i/d_i$  ratios and therefore the analysis can be used to determine stresses with the present methods. Appendix 2 of this work deals with a spherical vessel nozzle where the curvature is larger and is taken into account.

### 3.2 Nozzle-Vessel Cases Examined Theoretically

The cases examined theoretically are shown in Figs.3.2.1, 3.2.2, 3.2.3. Case A (Fig.3.2.1) represents a radial nozzle attached to the vessel and the geometry of the junction is as indicated, where the radius  $R$  and the rest of the dimensions can vary to any specified values. For all three cases the dimensions studied are shown in the figures. Case B (Fig.3.2.2) differs in the geometry of the junction and also in that heat is conducted only across the boundary of the nozzle while in

Case A heat is transferred across the vessel boundary as well. Case C (Fig.3.2.3) is quite different from the other two. It is the theoretical model of the experimental specimen. There is no insulation on the outside and heat is conducted only across the inside surface of the nozzle. The dimensions are shown in the figure and the geometry of the junction is similar to Case B. Heat conduction takes place when hot fluid passes through the nozzle and enters the vessel. At an inlet nozzle during the heating-up period stresses occur at the nozzle and junction. The stresses are produced by thermal expansion in the nozzle and by relative strain between nozzle and main vessel shell, due to a difference in temperatures between the two components. Inlet nozzles are subjected to higher thermal stresses than outlet nozzles because of the higher thermal gradients set up. In Case A and B the structure is thermally insulated on the outside and the direct effect of this is that temperature inside the wall increases more rapidly than in Case C where there is no insulation.

The stresses produced are the combination of two effects:

(a) Thermal stresses developed due to variation of temperature across the thickness of the nozzle and vessel walls. Thermal stresses of this nature decrease as the thickness of the wall decreases. In practical problems they can be neglected completely if the thickness becomes very small, although their values can still be estimated theoretically.

(b) Thermal discontinuity stresses which are produced due to the difference in temperature between vessel and nozzle. These stresses will be manifested immediately around the junction because of the discontinuity of the structure in that area. The combination of the stresses above produces an overall effect which is studied in this work.

In certain pressure vessels inlet nozzles are thermally sealed on the inside and thermal stresses (a) above do not develop or are rendered minimal.

Wherever there is a discontinuity in a structure, such as the transition from nozzle to vessel, the variation in thickness of the corresponding walls will produce a differential strain. It is therefore desirable to make such discontinuities as smooth as possible in order to reduce the stresses. Thermal stresses develop along the outside surface of the nozzle and vessel as well as along the inside. The stresses reach maximum values at different areas, these areas being designated as high stress concentration areas. With the present theoretical analysis the stresses are calculated not only along the inside and outside surfaces of the structure, but also across the full thickness of the walls. This provides a complete picture of the stress field and decisions about reinforcement at the junction and position of the weld can be made for safer design.

### 3.3 Thermal Stresses and How They Develop

Often it is necessary to distinguish between thermal stress and thermal shock by saying that in thermal shock the thermal stresses are produced by transient temperature gradients, resulting from step changes in boundary temperature. For instance, if a body originally at a uniform temperature is suddenly immersed in a medium of different temperature, a condition of thermal shock is then introduced. At any instant the stresses are determined by the temperature distribution, and they are the same as they would be if this temperature distribution could be obtained in the steady-state condition. But the temperature gradient that can be established in the

'step change' initiated state are generally much higher than those that occur in the steady state. Hence, thermal shock is important relative to ordinary thermal stress because of the higher stress that can be induced. Another distinction between thermal stress due to finite rate transients and thermal shock is that the rate of application of stress is very rapid, and many materials are affected by the rate at which load is applied. Some materials are embrittled by rapid application of stress and therefore may not be able to withstand a stress in thermal shock which, if applied slowly, could readily be absorbed.

In dealing with thermal stresses it is thus desirable to distinguish between brittle and ductile materials. Brittle materials allow only a very small amount of strain prior to rupture. Ductile materials can undergo appreciable strain without rupture. Since thermal shock behaviour depends mainly on the ability of the material to absorb the induced strains necessary to maintain a continuous body upon the application of thermal strains, brittle materials generally exhibit inability to withstand these superimposed strains without rupture.

Ductile materials, on the other hand, can withstand these strains for many cycles, and in the absence of mechanical loads, ultimate fracture must involve exhaustion of the ductility through cyclic loading.

### 3.3.1 Thermal Shock of Ductile Material

It is the rapid step-change of heat that distinguishes thermal shock from ordinary conditions of time-dependent thermal stress. Such properties as specific heat and conductivity, which do not enter directly into consideration for thermal stresses under known conditions of temperature, become important in thermal shock applications because these properties determine the temperature, the temperature gradients, and the rate of

change of the gradients, which, in turn, govern strains and strain rates. Some materials are more sensitive than others to stress gradients or to strain rate, and therefore thermal shock may rate various materials differently than would slowly applied thermal stress.

Ductile materials cannot fail in one thermal cycle as brittle materials can. Therefore it is to be expected that considerations of failure will be limited to the mechanisms of distortion and fatigue rather than to fracture upon the application of a single cycle. The thermal fatigue aspects of such failure are examined later in this work. The thermal shock resistance of a material depends on several parameters. These include conductivity, thermal expansion coefficient and Poisson's Ratio. Thus for example the temperature distribution is governed to a considerable extent by the conductivity. Therefore good conductors will have an advantage over poor conductors. In a severe thermal shock, on the other hand, the induced strain is governed mainly by the parameter  $\alpha\Delta T$  where  $\alpha$  is the thermal expansion coefficient and  $\Delta T$  the change in temperature of the structure, and is almost independent of the material conductivity. When the  $\alpha\Delta T$  parameter is large and thus plastic strain is large, the ductile material will tend to have the highest cyclic life. When  $\alpha\Delta T$  is small, on the other hand, the strain may be absorbed largely elastically and the material with the highest endurance limit will show a life advantage.

Thus when considering different materials it must be realised that their relative merits may interchange depending on the conditions. In addition, it is important to consider that the metallurgy of a material may change as its temperature increased. The properties of some materials deteriorate rapidly

as the temperature is raised, hence it is important to use the properties at the temperatures at which the strains are imposed in order to arrive at valid conclusions regarding relative resistance to high temperature transients.

## 4. THEORETICAL DETERMINATION OF TRANSIENT THERMAL DISTRIBUTIONS FOR THE NOZZLE-VESSEL CASES

---

Here the three cases of nozzle-vessel configurations mentioned in Section 3.2 are examined, and the thermal distributions are determined at different times during the heating-up period. Fluid enters and leaves the vessel through the nozzles; in most cases the fluid is at a relatively high temperature and the value of this temperature for the present investigations is considered to be  $T_f = 450^\circ\text{F}$ . This temperature value is used for both the theoretical and experimental parts. In order to proceed to the evaluation of the temperature inside the material in any practical problem involving fluid flow in nozzle and vessel, the heat transfer coefficient must be determined. The heat transfer coefficient affects the rate of heat flow across the fluid/metal boundary and when the flow is low the heat transfer coefficient is also low (see Section 4.1). In the case of low flow there is a large convection boundary film thickness and the rate of heat transfer from fluid to metal is decreased proportionally. Therefore whenever the flow rate is small thermal stresses are also small. Nevertheless in here a high flow rate is considered for cases A and B which can be encountered in practical problems. For Case C there is no flow of fluid. This is because Case C is the theoretical model of the experimentally examined specimen, where the fluid is simulated by a resistance coil inserted in the nozzle. The resistance provides heat at a rate necessary to maintain the inside surface of the

nozzle at  $T_f = 450^\circ\text{F}$ . Hence in the theoretical analysis of Case C the temperature on the inside surface of the nozzle is taken as  $T_f = 450^\circ\text{F}$ . As has already been said, there is no heating along the vessel inside surface for Case C; thus the theoretical model is equivalent to high flow in the nozzle, and very low at the vessel wall.

#### 4.1 Flow in Nozzle-Vessel and Forced Convection Heat Transfer Coefficients

The problem of forced convection heat transfer for a number of physical problems can be solved analytically. In such cases the principles of the convection processes and their relation to fluid dynamics are employed to obtain an analytical solution. However this is not always possible and experimental methods are used to obtain empirical formulas or graphical charts, so that they may be used with a maximum of generality.

The relationships used herein to obtain the values of heat transfer coefficients for the vessel and nozzle are empirical and the physical conditions are as follows:-

The flow within the nozzle and vessel is turbulent and this is a realistic situation encountered in almost all cases of fluid flow within pressure vessels. For the vessel the relationship is approximated to that of turbulent forced convection past a flat plate. This assumption is true when the diameter of the vessel is large and therefore the curvature of the shell small. The properties of the flow are evaluated at the mean film temperature. This is the arithmetic mean of the temperature of the surface of the wall,  $T_w$  and the fluid temperature  $T_f$ . Using  $T_m$  to denote the mean temperature,

$$T_m = \frac{T_w + T_f}{2} \quad (4.1.1)$$



Sometimes in the case of internal flow a mean film temperature which is the average of the surface temperature and the bulk temperature is used in place of the mean temperature. The analysis of the basic differential equations of motion, continuity, and energy of fluid mechanics (R.4-1) shows that forced convection problems can be represented by a relation of the form

$$\text{Nu} = f(\text{Re}, \text{Pr}) \quad (4.1.2)$$

On the basis of this relation, experimental forced convection data can be correlated to yield an empirical equation for a certain set of conditions. The formulation above is based on the assumption that the fluid properties involved in the dimensionless parameters of Reynolds and Prandtl numbers are constant. This assumption is not always true. For instance the evaluation of all the properties at a mean temperature does not produce a satisfactory correlation of the experimental data, because, for example, of one strongly temperature-dependent property (usually viscosity). In cases like this the introduction of another dimensionless parameter which allows for a description of the temperature dependence of one or more of the properties will permit a satisfactory correlation of experimental data. In general the experimental forced convection data correlations can deviate up to  $\pm 20\%$ , and consequently even this order of accuracy has to be considered quite satisfactory in the absence of specific data on the configuration being considered.

Nusselt (R.4-2) has calculated the average heat transfer coefficient  $h_{av}$  for a plate of length  $L$  as,

$$h_{av} = \frac{1}{L} \left[ 0.0292(\text{Pr})^{1/2} \left(\frac{U}{v}\right)^{0.8} k \int_0^L x^{-0.2} dx \right] \quad (4.1.3)$$

where  $x$  is the distance of any point on the plate from the leading edge. A Nusselt average number can be evaluated by integration of the above equation.

$$\bar{h}_{av} = \frac{1}{L} \left[ \frac{5}{4} 0.0292 (\text{Pr})^{1/3} \left( \frac{U}{\nu} \right)^{0.8} k L^{4/5} \right] \quad (4.1.4)$$

hence

$$\text{Nu} = \frac{hL}{k} = 0.036 (\text{Re})^{0.8} (\text{Pr})^{1/3} \quad (4.1.5)$$

where  $k$  is the thermal conductivity and  $\nu$  the viscosity of the fluid. The relation of 4.1.5 assumes that the boundary layer is fully turbulent from the leading edge of the plate.

For fully developed turbulent flow in tubes Dittus and Boelter (R.4-3) have proposed the following relation:

$$\text{Nu} = \frac{hd}{k} = 0.023 (\text{Re})^{0.8} (\text{Pr})^{0.4} \quad (4.1.6)$$

Again the properties in the equation are evaluated at the fluid mean temperature. The mean temperature  $T_m$  is normally used when the wall temperature  $T_w$  is different from the fluid free stream or bulk temperatures.

## 4.2 Evaluation of Heat Transfer Coefficient for Cases A,B and C

### 4.2.1 CASE A. Forced Convection across Nozzle and Vessel Walls

Referring to Fig.3.2.1 it can be seen that for Case A there is heat transfer by forced convection across the nozzle and vessel walls. Fluid of temperature  $T_f = 450^\circ\text{F}$  flows through the nozzle and along the inside wall of the main shell. The fluid is assumed to have velocity  $U_f = 2.00 \text{ ft/sec}$ . This is a common velocity order of magnitude for pressure vessels where transient thermal stresses become important. The velocity of the fluid in the vessel and/or nozzle, and consequently the vessel and nozzle heat transfer coefficients, can take any

value, but the computer program developed in here is able to determine the thermal transients for the various cases by simply taking the predetermined values of velocities. The nozzle and vessel inside surfaces are exposed to a convection boundary condition and the temperature of the wall does not automatically attain the temperature of the fluid. Nevertheless during warm-up the wall temperature increases fast due to the relatively high Reynold's number due to turbulent flow and the small film thickness. The effect of the convection boundary on the surface of the nozzle and vessel is determined later on by considering the heat transfer coefficients of nozzle and vessel sides which are calculated herein. The properties of the fluid are obtained at the initial mean temperature which is given by

$$T_m = \frac{T_f + T_w}{2} = \frac{450 + 60}{2} = 255^\circ\text{F}$$

Fluid Properties for water at mean temperature  $T_m = 255^\circ\text{F}$ .

$$k = 0.306 \text{ btu/ft.h.}^\circ\text{F}$$

$$\text{Pr} = 1.405$$

$$\mu = 0.543 \text{ lb/ft.h}$$

$$\rho = 62.428 \text{ lb/ft}^3$$

Also the relation between dynamic and kinematic viscosities is:

$$\nu = \frac{\mu}{\rho} \quad (4.2.1.1)$$

(i) Heat transfer coefficient  $h_v$  for the vessel

Characteristic length  $\ell_v$  for the vessel = 7.00 in = 0.583 ft.

The characteristic length is considered for half of the vessel-nozzle configuration above the centre line since the configuration is symmetrical about the xx' axis (see Fig.3.2.1).

Fluid velocity  $U_f = 2.00 \text{ ft/sec} = 7200 \text{ ft/h}$ .

$$Re = \frac{U_f \ell_v}{\nu} = \frac{U_f \ell_v \rho}{\mu} \quad (4.2.1.2)$$

and by substituting the values for the above quantities the Reynolds number is obtained.

$$Re = 0.4826 \times 10^6$$

Now using Equation (4.1.5) and substituting for length  $\ell_v$  we have,

$$Nu = \frac{h_v \ell_v}{k} = 0.036 (Re)^{0.8} (Pr)^{1/3}$$

hence

$$h_v = \frac{k}{\ell_v} 0.036 (Re)^{0.8} (Pr)^{1/3}$$

By substituting the values for  $k$ ,  $\ell_v$ ,  $Re$  and  $Pr$  the heat transfer coefficient for the vessel is obtained  $h_v$  964.8 Btu/ft<sup>2</sup>.h.<sup>o</sup>F.

(ii) Heat transfer coefficient  $h_N$  for the nozzle

The same fluid properties hold for the flow through the nozzle at fluid temperature of 450<sup>o</sup>F and fluid velocity 2.00 ft/sec. The characteristic length is now the diameter of the nozzle  $d_i = 1.00$  in = 0.083 ft.

Reynolds number is,

$$Re = \frac{U_f d_i \rho}{\mu} \text{ and by substituting the values for } U_f, d_i, \rho, \text{ and } \mu$$

$$Re = 0.06871 \times 10^6$$

The heat transfer coefficient is then given by Equation (4.1.6) for forced convection within pipes

$$Nu = \frac{h_N d_i}{k} = 0.023 (Re)^{0.08} (Pr)^{0.4}$$

hence,

$$h_N = \frac{k}{d_i} 0.023 (Re)^{0.08} (Pr)^{0.4}$$

Substituting the appropriate values above for  $k$ ,  $d_i$ ,  $Re$  and  $Pr$  the coefficient is obtained.

$$h_N = \underline{906.1 \text{ Btu/ft}^2 \cdot \text{h.}^{\circ}\text{F}}$$

#### 4.2.2 CASE B. Forced Convection across Nozzle Only

In this case there is no heat transfer across the vessel surface but only across the nozzle surface. The case is shown in Fig.3.2.2. The condition of heat transfer only across the nozzle is studied here because it is believed that the differential stresses developed are higher than those produced when heat transfer takes place across both the nozzle and vessel surfaces. This is because the thermal differential stresses set up between nozzle and vessel are higher due to larger difference in relative expansion between vessel and nozzle parts. In practice Case B can be considered as the one where fluid flows towards the vessel through a relatively long nozzle or pipe setting up differential stresses between nozzle and vessel while the fluid is not actually coming in contact with the inside surface of the vessel. This is particularly true when power plants involving pressure vessels are started-up, and hot 'slugs' of liquid enter vessels. It can also be said that Case B can be encountered in inlet nozzles while Case A corresponds more to outlet nozzles when there is a flow down the shell and out through the nozzle.

The flow conditions are the same as in Case A. The temperature of the fluid is  $T_f = 450^{\circ}\text{F}$  and its velocity 2.00 ft/sec. Therefore all the other properties of the fluid are similar to the ones in Case A and the coefficient  $h_N$  is the same and equal to  $906.1 \text{ Btu/ft}^2\text{h.}^{\circ}\text{F}$ . It must be noted that this is true because the nozzle inside diameter has the same value of  $d_i = 1.00\text{in} = 0.083 \text{ ft}$ .

#### 4.2.3 CASE C. Radiation Heat Transfer in Nozzle

The configuration of this case, shown in Fig.3.2.3, is similar to the specimen which is tested experimentally and which

is shown in Fig.6.1.2. The fluid flow is simulated experimentally by a heating cartridge element of 5/8in diameter which is placed inside the nozzle and fixed so that it is concentric with the nozzle as shown in the figure. More details of the arrangement are given later on in the experimental part of this work.

The heating cartridge heats the inside of the nozzle by radiation and by means of a thermocouple attached on the inside of the nozzle the surface temperature is maintained at 450°F. The temperature of the sheath of the heater is allowed to reach the value of 600°C (1112°F) which is less than the maximum of 700°C (1293°F) which can be obtained with clearances between 0.005in and 0.010in. Since the clearance between nozzle and heater is 0.187in ( $\frac{d_i - d_{el}}{2}$ ), the watt density is reduced by means of an adjustable Variac which controls the voltage to the heater and therefore the sheath temperature is limited to 1112°F (600°C).

It is desirable in this case to obtain theoretically the heat transfer coefficient as in the previous two cases. In this case heat is transferred by three modes; radiation, convection and conduction. It is found that the conduction heat transfer coefficient is the dominant one followed by the radiation heat transfer coefficient. Since the clearance between the nozzle and the heater is small (0.187in) and the air is almost stagnant around the heater, the convection term is small compared to the other two. Nevertheless, the convective heat transfer coefficient is also obtained in order to determine the overall coefficient.

The radiation problem is limited to that of determining the radiation heat transfer coefficient between two concentric cylinders of different surface temperatures.

When two concentric cylinders as shown in Fig.4.2.3.1 exchange heat by radiation the equation of heat transfer can be written in terms of certain parameters characteristic of the two cylinders. This is given by

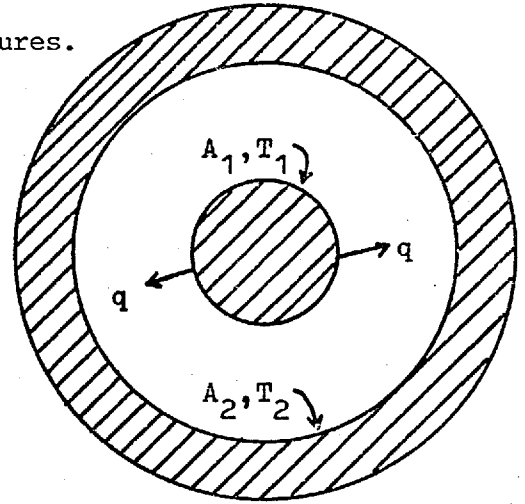


FIG.4.2.3.1

$$q_{\text{rad}} = \frac{\sigma' A_1 (T_1^4 - T_2^4)}{1/\epsilon_1 + (A_1/A_2)(1/\epsilon_2 - 1)} \quad (4.2.3.1)$$

where the suffixes 1 and 2 refer to inner and outer cylinders respectively.

$\epsilon_1$  and  $\epsilon_2$  = emissivities

$A_1$  and  $A_2$  = total surface areas

$T_1$  and  $T_2$  = temperature of the surfaces

$\sigma'$  = Stefan-Boltzmann constant.

The derivation of the above relation is given in Ref.4-4. The ratio of areas  $A_1/A_2$  can be replaced by the diameter ratio  $d_1/d_2$ .

It is now possible to evaluate the radiation heat transfer coefficient  $h_r$  for the nozzle of Case C as follows. From Equation (4.2.3.1)

$$\frac{q}{A_1} = \frac{\sigma' (T_1^4 - T_2^4)}{1/\epsilon_1 + (A_1/A_2)(1/\epsilon_2 - 1)} = h_r (T_1 - T_2)$$

and hence,

$$h_r = \frac{\sigma'(T_1^2 + T_2^2)(T_1 + T_2)}{1/\epsilon_1 + (A_1/A_2)(1/\epsilon_2 - 1)} \quad (4.2.3.2)$$

and by putting  $A_1/A_2 = d_1/d_2$

$$h_r = \frac{\sigma'(T_1^2 + T_2^2)(T_1 + T_2)}{1/\epsilon_1 + (d_1/d_2)(1/\epsilon_2 - 1)} \quad (4.2.3.3)$$

Now the quantities in Equation (4.2.3.3) can be given the appropriate values in the case of nozzle heating.

#### Cartridge heater

The heater is the inner cylinder at a sheath temperature  $T_1 = 1112^\circ\text{F}$ . The diameter  $d_1 = 5/8\text{in} = 0.052\text{ft}$  and is manufactured of stainless steel. The emissivity  $\epsilon_1$  of stainless steel at the temperature of  $T_1 = 1112^\circ\text{F}$  is obtained from Ref.(4-4) as 0.586.

#### Nozzle

The nozzle is the outer cylinder of Fig.4.2.3.1. The temperature  $T_2$  is  $450^\circ\text{F}$  and this is recorded by a thermocouple attached on the inside surface of the nozzle (shown in Fig.6.1.2). The inside diameter of the nozzle is  $d_2 = 1.00\text{in} = 0.083\text{ft}$ . The emissivity  $\epsilon_2$  is that of stainless steel at temperature  $T_2 = 450^\circ\text{F}$  and is equal to 0.540 (R.4-4).

The above values are now substituted in Equation (4.2.3.3) where the Stefan-Boltzmann constant  $\sigma'$  is  $0.171 \times 10^{-8}$  Btu ft<sup>2</sup>h.<sup>o</sup>R<sup>4</sup> and the radiation heat transfer coefficient obtained as

$$h_r = 6.24 \text{ Btu/ft}^2\text{h.}^\circ\text{F.}$$

The convection heat transfer coefficient is determined by considering a relation for free convection from a heated horizontal cylinder given in Ref.(R.4-4). The relation is for



laminar flows and in the present case the air in the space between the cartridge heater and the nozzle can be considered still. The convective heat transfer coefficient  $h_c$  is given by

$$h_c = 0.27 \frac{\Delta T}{d}^{1/4} \quad (4.2.3.4)$$

where  $\Delta T = T_1 - T_2$ ;  $T_1$  is the temperature at the surface of the cartridge heater,  $T_2$  the temperature at the surface of the nozzle, and  $d$  the diameter of the heater in feet. For this problem:

$$T_1 = 1112^\circ\text{F}$$

$$T_2 = 450^\circ\text{F}$$

$$d = 5/8\text{in} = 0.052\text{ft.}$$

$$\text{Therefore } h_c = 2.87 \text{ Btu/ft}^2\text{h.}^\circ\text{F.}$$

Heat is transferred by conduction through the air between the inside cylinder (cartridge heater) and outside cylinder (nozzle). The conduction heat transfer coefficient is given by:

(R.4-4)

$$h_{\text{cond}} = \frac{2\pi k(T_1 - T_2)}{\ln(r_2/r_1)} \quad (4.2.3.5)$$

where

$$k = \text{thermal conductivity of air (at } \frac{450^\circ\text{F} + 1112^\circ\text{F}}{2} = 781^\circ\text{F)}$$

$$= 0.0340 \text{ Btu/ft.h.}^\circ\text{F}$$

$$T_2 = 450^\circ\text{F (see Fig.4.2.3.1)}$$

$$T_1 = 1112^\circ\text{F}$$

$$r_1 = 0.026\text{ft}$$

$$r_2 = 0.0415\text{ft}$$

Hence the conduction heat transfer coefficient is found as

$$h_{\text{cond}} = 302.44 \text{ Btu/ft}^2\text{h.}^\circ\text{F}$$

Therefore the overall heat transfer coefficient due to the combined effects of radiation, convection and conduction is now equal to:

$$\begin{aligned}
 h_{\text{TOTAL}} &= h_{\text{RADIATION}} + h_{\text{CONVECTION}} + h_{\text{CONDUCTION}} \\
 &= 311.55 \text{ Btu/ft}^2\text{h.}^{\circ}\text{F}
 \end{aligned}$$

#### 4.3 Two-Dimensional Transient Heat Flow in Nozzle-Vessel and Finite Difference Analysis

In all three cases heat is transferred inside the nozzle-vessel walls by conduction. The problem of heat conduction is a two-dimensional one, the heat being transferred in x and y directions across the section of the nozzle-vessel configuration in the xy plane.

The objective is to determine the temperature distribution within the walls at any particular time during warm-up. The thermal stresses can then be calculated at any time using the values of the obtained temperatures. The temperature of the fluid is considered steady with respect to time. In Cases A and B, where the outside of the nozzle and vessel is insulated, theoretically the temperature of the structure becomes everywhere the same and equal to that of the fluid. This happens after a period of prolonged exposure and under the assumption that the insulation is perfect and therefore there are no heat losses at the outside surface of the nozzle and vessel.

For all cases there are the following four basic heating-up phases.

- (a) The nozzle-vessel section is initially at uniform room temperature  $T_R = 60^{\circ}\text{F}$  and in thermal equilibrium with the surroundings. At this state the surface heat flux  $q'$  (heat rate per unit surface area) across the vessel and/or nozzle is zero.
- (b) As fluids enters the nozzle the inside surface boundaries of the section are exposed at time  $t = 0$  to the fluid

temperature  $T_f = 450^\circ\text{F}$ . There is now a surface heat flux  $q' > 0$  across the convection boundary film and the temperature at the wall is proportional to the heat transfer coefficient. The rest of the section is still at room temperature.

- (c) Heat is transferred by conduction and the temperature distribution within the nozzle-vessel walls is now a time-dependent quantity.
- (d) In Cases A and B where the outside of the nozzle-vessel section is insulated and there is no heat flow across the insulated boundary, the temperature of the structure reaches everywhere the temperature of the fluid after a certain prolonged exposure period. In Case C where there is no insulation the thermal distribution within the section becomes steady and the heat fluxes across the inside and outside surfaces become steady too.

The problem of heat conduction through the nozzle-vessel section is solved using the numerical method of finite differences. The method is analysed in the following section and in detail in Appendix 1.

#### 4.3.1 Finite Difference Analysis\*

The differential equation which governs the heat flow within a solid body in two dimensional unsteady-state conduction is given by

$$k\left(\frac{\partial^2 T}{\partial x^2} + \frac{\partial^2 T}{\partial y^2}\right) = \rho c \frac{\partial T}{\partial \tau} \quad (4.3.1.1) \quad 2$$

where  $T$  is the temperature at any point defined by  $(x,y)$  coordinates at a particular time  $\tau$ ,  $\rho$  the density of the body,  $k$  the thermal conductivity and  $c$  the thermal capacity.

---

\*See note on this paragraph and equation 4.3.1.1 in page 83-N1 at the end of this chapter.

The solution to Equation (4.3.1.1) will give the temperature in a two-dimensional section of the solid as a function of two independent space coordinates  $x$  and  $y$ . The equation of heat flow can be solved analytically but only for certain specific boundary conditions and geometries.

Nevertheless the development of high speed digital computers enables us to obtain numerical solutions to many problems which cannot be solved by analytical methods.

In order to apply the finite difference method to solve the problem, the section is divided into equal increments in both the  $x$  and  $y$  directions. The grid thus produced has a number of nodal points as shown in Fig.4.4.1. Finite differences are then used to approximate differential increments in the temperature and space co-ordinates. The smaller the chosen finite increments the more closely the true temperature distribution is approximated.

The temperature gradients  $\frac{\partial T}{\partial x}$  and  $\frac{\partial T}{\partial y}$  at each nodal point are expressed by finite difference equations as is explained in detail in Appendix 1. Then the temperature at each nodal point after a time increment  $\Delta t$  is calculated using the values of the temperatures of the nodes at the end of the previous time interval. The same procedure is repeated to obtain the temperature distribution after any desired number of time increments. This is done by computational methods described in the next sections.

The difference equations which are used to determine the conduction of heat through the solid cannot be used to calculate the temperature at the inside walls of nozzle and vessel. At the boundary of the section a convection resistance to heat flow exists which is a function of the heat transfer coefficients

already obtained. The equations governing the temperature change on the wall are also obtained in Appendix 1. Each convection boundary condition must be handled separately, depending on the particular geometric shape under consideration.

#### 4.4 Solution and Results of Thermal Distributions for CASE A

The temperatures at the various time increments are determined by solving the equations obtained in Appendix 1. This is done by computer program TRAN1 which solves the transient thermal distributions for CASE A. The construction and operation of the program is described in this section. The program data designations and the listing is given in Appendix 3.

First the nozzle-vessel section of Case A is divided into the grid shown in Fig.4.4.1. The grid space increment  $\Delta x$  is equal to  $\Delta y$  and equal to 0.1in. This division produces a total of 3533 nodal points for the dimensions in Case A. Temperatures are determined for all the nodal points at selected time intervals. In the program the dimensions of the section are designated with variables I1, I2, I3, J1, J2 and J3 which can be given any values so that the dimensions of the section can be changed accordingly. This makes the program flexible for the study of different cases. There is heat flow across the inside boundaries of the nozzle and vessel but there is zero heat gradient  $\frac{\partial q}{\partial t}$  on the outside insulated boundary. The nozzle and vessel heat transfer coefficients are the ones already determined in Section 4.2.

#### COMPUTER PROGRAM TRAN1 - CASE A

The program solves the difference equations of heat flow across the boundaries for all the boundary nodal points and for all the nodes inside the section for specified time intervals

during the transient heating-up period. It then prints the numerical results of the temperatures for all the nodes for each time interval as shown in Table 4.4.1. A subroutine named PLOT is incorporated in the main program and plots the temperature profiles for the corresponding times as shown in Figs.4.4.2(a) and 4.4.2(b).

The main program and the subroutine were constructed by the author in order to solve the case problems of nozzle-vessel transients presented hereby. The plotting of the profiles provides a more comprehensive picture than the numerical results but the exact values of the temperatures are used later to obtain the thermal stresses. The series of the main operations of the program and the subroutine are given below and an attempt is made to present the sequence of operations as comprehensively as possible. This is as follows:

- The total number of nodal point temperatures is defined.
- The maximum number of time increment iterations is defined as well as the maximum number of iterations for the convergence of the temperature equations.
- The dimensions of the section are given including the radius RA of the junction, nozzle and vessel heat transfer coefficients, coefficient of thermal conductivity, initial temperature of the section and fluid temperature.
- The initial temperature of the section is defined by scanning all 3533 nodal points. This is set to 60<sup>o</sup>F.
- The temperature of the fluid is set and the temperature of the boundary nodal points on the vessel and nozzle walls are determined for the first time increment using Equations (A1.12) and (A1.13) respectively (Appendix 1). These are

$$T_{i,j}^{n+1} = \frac{\alpha' \Delta\tau}{(\Delta x)^2} \left\{ 2 \frac{h_v \Delta x}{k} T_f + 2T_{i,j+1}^n + T_{i+1,j}^n + T_{i-1,j}^n \right. \\ \left. + \left[ \frac{(\Delta x)^2}{\alpha' \Delta\tau} - 2 \frac{h_v \Delta x}{k} - 4 \right] T_{i,j}^n \right\}$$

for the vessel, where  $h_v$  is the vessel heat transfer coefficient.

And

$$T_{i,j}^{n+1} = \frac{\alpha' \Delta\tau}{(\Delta x)^2} \left\{ 2 \frac{h_N \Delta x}{k} T_f + 2T_{i+1,j}^n + T_{i,j+1}^n + T_{i,j-1}^n \right. \\ \left. + \left[ \frac{(\Delta x)^2}{\alpha' \Delta\tau} - 2 \frac{h_N \Delta x}{k} - 4 \right] T_{i,j}^n \right\}$$

for the nozzle, where  $h_N$  is the heat transfer coefficient for the nozzle.

- The nodal temperatures are calculated for the first time increment  $\Delta\tau$  inside the section for all nodal points using Equation (A1.7) in Appendix 1 and temperatures in the insulated boundaries of vessel junction and nozzle using Equations (A1.8), (A1.10) and (A1.9) respectively.
- For the second time increment the boundary values of the nodal temperatures are determined using the values of the temperatures at the end of the previous time increment. The temperatures of the inside of the section are also determined using the same equations described above and the temperatures at the end of the first time increment.

The procedure is the same for subsequent time increments until the temperature of the section is uniform.

- The values of the temperatures are printed every 0.5 minutes (30 seconds) and calculated for every 0.3 minutes for the first 12 minutes and <sup>printed for</sup> every 3 minutes thereafter.

The printing time can be changed to any value desired.

In Table 4.4.1 the printing of the temperature for selected value of the index I at the time interval of 9 min 30 secs is shown. Each nodal point is identified by two indices I and J. The value of I changes at the top of the page and the value of J across. Every temperature is then identified as  $T_{ij}$ .

The temperatures for every time increment printed are plotted by subroutine PLOT in a comprehensive way as it is explained below.

#### SUBROUTINE PLOT-CASE A

The thermal profiles for the section at the time intervals of 9 min 30 secs and 54 min are shown in Figs.4.4.2(a) and 4.4.2(b) as they are plotted by the subroutine. Every letter represents a band of 10 degrees F. Each temperature is translated into a blank or a letter according to the table provided with the figure. The subroutine incorporates the following steps.

- Define the temperature bands by designating a letter to each band of 10 degrees  $^{\circ}$ F.
- Put index I = I1 and plot the temperatures for every value of the index J along the row.
- The junction boundary is determined as follows.

The junction is a quarter circle. In the Fig.4.4.3 the co-ordinates of the quarter circle at points A and B are I2, J2-R and I2-R, J2.

The equation will then be:

$$I = ( - \sqrt{R^2 - (J - J2)^2} ) + I2 \quad (4.4.1)$$

and

$$J = ( - \sqrt{R^2 - (I - I2)^2} ) + J2 \quad (4.4.2)$$



where  $R = RA/\Delta x$  and  $RA$  the radius of the junction. These two equations give the corresponding values of  $i$  and  $j$  for any values of the radius of the junction. Since the grid elements are finite, the nodal points on the quarter circle are rounded by computation according to the decimal part of their value to give a smooth curve through the points.

- When the plotting of the temperatures for the entire nozzle-vessel section is completed for the first time interval, the operation is repeated for the subsequent time intervals.

Data designations and listing of the subroutine are given in Appendix 3.

#### Thermal Results - CASE A

The temperatures for each time interval of 30 seconds for the first 12.0 minutes, and each time interval of 1 minute thereafter of the heating-up period were obtained by the main program and plotted by the subroutine in order to study the behaviour of thermal distributions in the section. The exact values of the temperatures are subsequently used to determine the thermal stresses. This is done for only one time interval when the developed stresses are maximum, and it is explained below. In Fig.4.4.4(a) to Fig.4.4.4(c) the thermal distributions are shown for the time intervals  $\tau = 3$  min, 9 min 30 secs, 18 min, 27 min, 36 min, 45, 63, 81, 126, 144, 162, 200 minutes. It can be seen that the temperature rises faster in the nozzle because the thickness of the wall is smaller than that of the vessel. At early time intervals the temperature variation across the walls is larger. Later the heat flow becomes steadier and it can be noticed that the profiles become more distinct. In Fig.4.4.4(c) it is quite clear that temperature

variation across the section is decreasing appreciably. The bounds of  $10^{\circ}\text{F}$  isothermals are getting wider and heat flow is now more steady. As there is no heat flow across the insulated boundary the temperature of the nozzle first becomes uniform at time  $\tau = 2 \text{ hr } 06 \text{ min}$  (Fig.4.4.4(c)). The temperature of the entire vessel-nozzle configuration becomes uniform after 3 hours and 20 minutes (Fig.4.4.4(c)). Thermal differential stresses are present during the whole period of the transient heating-up as the mean temperature of the nozzle is always higher than the mean temperature of the vessel wall. The thermal differential stresses are due to different expansion rates of nozzle and vessel and are the most important ones but not the only ones as has already been pointed out. Thermal stresses also develop across the thickness of the vessel and nozzle walls due to the variation in temperature. These are complementary to the differential stresses and they contribute to the increase of the overall value of the thermal stress field.

At time  $\tau = 9 \text{ min } 30 \text{ secs}$  the variation of mean temperature between nozzle and vessel  $\Delta T_m = T_{m(\text{nozzle})}^* - T_{m(\text{vessel})}^*$  is maximum. In Fig.4.4.5 the value of  $\Delta T_m$  is plotted against time. The value of  $\Delta T_m$  increases continuously until the time of 9 min 30 secs, when it attains its maximum value of  $193.1^{\circ}\text{F}$  and then decreases steadily to zero at the time of 3 hours 20 min when the temperature of the section becomes uniform. It is evident that maximum thermal stresses will develop after 9 min 30 secs of the heating-up period. It is these maximum thermal stresses that are examined later on in Section 5.

---

\*  $T_{m(\text{nozzle})}$  is the mean temperature in the nozzle calculated as the average of all the nodal temperatures in the nozzle. The same holds for the vessel  $T_{m(\text{vessel})}$ .

#### 4.5 Solution and Results of Thermal Distributions for CASE B

In Case B heat flows only across the boundary of the nozzle. The variation of temperature between nozzle and vessel will therefore be higher and differential expansion between nozzle and vessel will produce higher differential stresses.

The temperatures are determined using the same method of finite differences and program TRAN2. The nozzle-vessel section is divided into the grid shown in Fig.4.5.1. The physical conditions are also shown. There is a rate of heat flow  $\partial q/\partial t$  across the inside boundary of the nozzle and there is no heat flow at the outside insulated boundary. The temperature of the fluid is  $T_f = 450^\circ\text{F}$  and the heat transfer coefficient of the nozzle is  $h_v = 906.1 \text{ Btu/ft}^2\text{hr.}^\circ\text{F}$ . This was calculated in Section 4.2.1. The temperature grid comprises of a total of 3712 nodal points with a grid spacing  $\Delta x = \Delta y = 0.1\text{in.}$  The data designations for TRAN2 are the same as for TRAN1 and are given in Appendix 3 together with the listing of TRAN2. The steps in program TRAN2 are the same as in Case A with the following differences.

##### PROGRAM TRAN2 - CASE B

- The temperature of the fluid is set and the temperature of the boundary nodal points on the nozzle walls are determined for the first time interval using Equation A1.13 (Appendix 1). This is

$$T_{ij}^{n+1} = \frac{\alpha' \Delta \tau}{(\Delta x)^2} \left\{ 2 \frac{h_N \Delta x}{k} T_f + 2 T_{i+1,j}^n + T_{i,j+1}^n + T_{i,j-1}^n + \left[ \frac{(\Delta x)^2}{\alpha' \Delta \tau} - 2 \frac{h_N \Delta x}{k} - 4 \right] T_{i,j}^n \right\}$$

- There is no heating across the vessel inside boundary.
- For the second time interval the boundary values along the nozzle are determined using the temperatures at the end of

the first interval. The interior nodal temperatures are then determined using the Equations (A1.1), (A1.8), (A1.9), and (A1.10) of Appendix 1. Equation (A1.10) for the junction is valid for the geometry of this case.

- Temperatures are determined for subsequent time intervals using the values at the end of the previous times.

The temperatures profiles are plotted by subroutine PLOT.

The junction geometry is a straight line inclined at  $45^\circ$  in respect of the vessel and nozzle. (See Fig.3.2.2.)

#### Thermal Results - CASE B

The temperatures of the section are calculated by the program and plotted by the subroutine for time increments of 30 seconds for the first 15 minutes and 1 minute thereafter. The time increments at which the temperatures are printed can be changed to any desirable value of 18 seconds or more. The minimum value of 0.18 seconds is limited by the value of the parameter  $\frac{(\Delta x)^2}{\alpha \Delta T}$  which must be equal to 4 so that it can be eliminated from Equation A1.7 (Appendix 1). Table 4.5.1 gives the values of the nodal temperatures of the entire section for time  $\tau = 10$  min. In Figs.4.5.2(a) and 4.5.2(b) the thermal profiles are shown as they are plotted by the subroutine for times  $\tau = 10$  min and  $\tau = 54$  min. In Figs. 4.5.3(a) and 4.5.3(b) the thermal distributions are shown for time  $\tau = 0.0$  to  $\tau = 54$  minutes.

The isothermal lines obtained in this case are different to the ones obtained in the previous one. It can be seen that heat flows across the nozzle inside surface, changing the nozzle wall temperature first and then as time proceeds the temperature of the vessel wall. The nozzle is heated to a considerable higher temperature than the vessel. This will introduce differential stresses between nozzle and vessel. Generally it can be seen

that in Case B the section is heated-up slower than in Case A, and the variation temperature between nozzle and vessel is higher. This makes the differential stresses in Case B generally higher than in Case A but the overall stresses are higher in Case A due to higher temperatures. The variation in mean temperature between nozzle and vessel  $\Delta T_m$  is shown in Fig.4.5.4. The maximum value is 302.4<sup>o</sup>F and it is attained after 10 minutes.

As there is no heating across the vessel boundary in Case B and the vessel wall is insulated, comparison of the two curves for  $\Delta T_m$  for Case A and B indicates that maximum temperature variation for Case B contributes to higher differential stresses than in Case A, where the maximum value of  $\Delta T_m$  is considerably lower (see Fig.4.5.4).

#### 4.6 Solution and Results of Thermal Distributions for CASE C

Case C examines theoretically the thermal distributions and thermal stresses of the nozzle-vessel geometry of the specimen tested experimentally. This makes possible the comparison of theoretical and experimental results and provides a criterion of how accurately the theory can approximate experimentation. The correlations of stress results between the theoretical Case C and the experiments are described in Chapter 6. In here only the thermal distributions are obtained, as for the two previous cases, and these distributions are used in Section 5 to obtain the thermal stresses.

Case C has the dimensions shown in Fig.3.2.3. The nozzle-vessel section is a section in the xy plane (longitudinal plane) of the specimen which is shown in Figs.6.1.1 and 6.1.2. The section is heated by a cartridge heater which is inserted inside the nozzle. This simulates the fluid of the previous cases.

Heat flow across the nozzle boundary is now a combined result of radiation, natural convection and conduction. This mode of heat transfer is different from the forced convection in the two previous CASES A and B. The combined radiation, convection and conduction heat transfer coefficient was obtained in Section 4.2.3 and its value is  $h_{\text{TOTAL}} = 311.55 \text{ Btu/ft}^2 \cdot \text{hr} \cdot ^\circ\text{F}$ . The heat transfer coefficient  $h_{\text{TOT}}$  can be used to obtain the temperature of the wall when it is not known. In this case the cartridge heater provides the necessary amount of heat to maintain the inside surface of the nozzle at a temperature of  $450^\circ\text{F}$ . There is no insulation on the outside and therefore there is a heat loss  $dq/dt$  by natural convection from the outside walls to the surrounding air. The heat flow inside the wall by conduction and the heat loss to the air by natural convection are described in Appendix 1. Program TRAN3 (Appendix 3) determines the temperature distributions for CASE C.

#### PROGRAM TRAN3

- Temperatures of nodal points inside the wall are calculated by Equation (A1.7):

$$T_{i,j}^{n+1} = \frac{1}{4} (T_{i,j}^n + T_{i-1,j}^n + T_{i,j+1}^n + T_{i,j-1}^n) \quad (\text{A1.7})$$

- The heat transfer coefficient for the vessel outside wall and the junction outside wall are determined by Equation (A1.14):

$$\frac{hL}{k_a} = 0.13 \left[ \frac{L^3 g \beta (T_w - T_\infty)}{v^2} (\text{Pr}) \right]^{0.33}$$

- The heat transfer coefficient for the nozzle outside wall is determined by Equation (A1.15):

$$\frac{hL}{k_a} = 0.54 \left[ \frac{L^3 g \beta (T_w - T_\infty)}{\nu^2} (Pr) \right]^{0.25}$$

- The temperature grid comprises a total of 1387 nodal points and is shown in Fig.4.6.1.

Temperatures are obtained at 1 minute intervals for up to 18 minutes. In Figs.4.6.2(a) to 4.6.2(c) the thermal profiles are shown for times = 0,4,6,10,12,14 minutes during heating-up. In Table 4.6.1 the values of temperatures are shown for time  $\tau = 11$  min. The mean temperature variation  $\Delta T_m$  between nozzle and vessel attains its maximum value of  $236.9^\circ\text{F}$  at time  $\tau = 11$  min. In Fig.4.6.3  $\Delta T_m$  is plotted against time. After the eleventh minute the value of  $\Delta T_m$  decreases with time. Nevertheless the value of  $\Delta T_m$  will never be zero since there is no insulation on the outside and heat flows across the boundaries.

Note on paragraph 4.3.1 (page 71)

The differential equation of heat conduction which governs the heat flow within a solid body in three-dimensional time-dependent conduction in cylindrical coordinates, specified as  $r$  (radial),  $z$  (axial)  $\theta$  (circumferential), is given by

$$k \left[ \frac{\partial^2 T}{\partial r^2} + \frac{1}{r} \frac{\partial T}{\partial r} + \frac{1}{r^2} \frac{\partial^2 T}{\partial \theta^2} + \frac{\partial^2 T}{\partial z^2} \right] = \rho c \frac{\partial T}{\partial \tau} \quad (N.1)$$

If a cylinder (Fig.N.1) whose axis coincides with the axis of  $z$  is heated and the initial and boundary conditions are independent of the coordinates

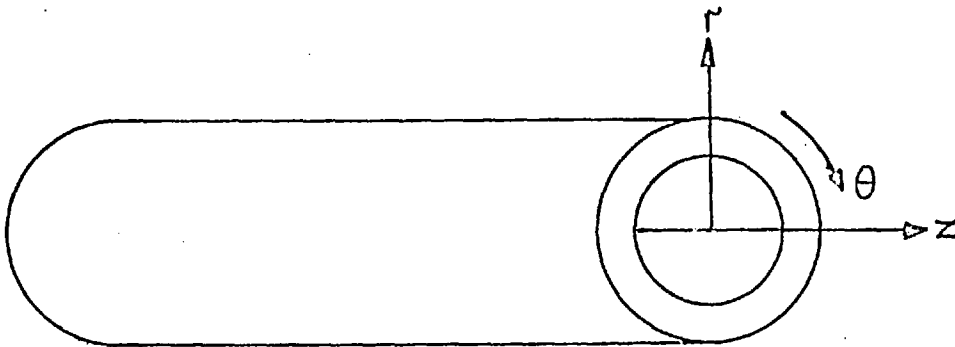


Figure N.1

$\theta$  and  $z$  the temperature will be a function of  $r$  and time only and the equation reduces to:

$$k \left[ \frac{\partial^2 T}{\partial r^2} + \frac{1}{r} \frac{\partial T}{\partial r} \right] = \rho c \frac{\partial T}{\partial \tau} \quad (N.2)$$

In this case the flow of heat takes place in planes perpendicular to the axis and the lines of flow are radial.

When the initial and boundary conditions do not contain  $\theta$ , the flow of heat takes place in planes through the axis and the equation of conduction becomes



$$k \left[ \frac{\partial^2 T}{\partial r^2} + \frac{1}{r} \frac{\partial T}{\partial r} + \frac{\partial^2 T}{\partial z^2} \right] = \rho c \frac{\partial T}{\partial \tau} \quad (\text{N.3})$$

Nevertheless, when two axially symmetric bodies intersect as in the problem of this work the above equation N.3 cannot be used to analyse the transient temperature distribution in both cylinders and especially around the junction area due to lack of symmetry of the cylinders.

Therefore an approximation is made in order to overcome this difficulty which results in using Equation 4.3.1.1.

$$k \left( \frac{\partial^2 T}{\partial x^2} + \frac{\partial^2 T}{\partial y^2} \right) = \rho c \frac{\partial T}{\partial \tau}$$

whose solution still involves three independent variables, but it treats the problem in two-dimensional plane wall cartesian coordinates. This is an approximation which works accurately (the error is between 1% and 2% for a vessel of thick wall and large diameter  $D_i/t \approx 20$ ) and quite accurately for the nozzle. The plane wall approximation for the nozzle of the present problem produces results where the error averages at about 11.5%.

In Appendix 9 (page 244) the temperature distributions which were obtained in the nozzle by using the two-dimensional time dependent plane wall equation

$$k \left( \frac{\partial^2 T}{\partial x^2} + \frac{\partial^2 T}{\partial y^2} \right) = \rho c \frac{\partial T}{\partial \tau} \quad (4.3.1.1, \text{ p. 71})$$

away from the junction for Case C are compared to the temperature distribution obtained in the same nozzle configuration using Equation N.2.

It has not been possible to compare the results with analytical solution data for the cylinder time-dependent equation with the above boundary conditions or with insulated outside boundary due to lack of any such data. However comparisons are made to the results of

temperature distribution for the cylinder obtained by solving the Equation N.2. numerically as is shown in Appendix 9 (p.244). The plane wall approximation for the nozzle of the present problem produces results in which the differences average at about 11.5%.

## 5. THEORETICAL DETERMINATION OF THERMAL STRESSES

---

Elastic thermal stresses are calculated for all three cases by computational analysis using the temperatures obtained in the previous section. Maximum thermal stresses develop at times when  $\Delta T_m$  is maximum. It has been shown that for Case A,  $\Delta T_m$  becomes maximum at time  $\tau = 9$  min 30 secs, for Case B at  $\tau = 10$  min and for Case C at  $\tau = 11$  min. Only maximum thermal stresses are determined for Cases A and B. For Case C stresses are determined for time intervals of very two minutes up to 18 minutes. This makes possible the comparison between theoretical values of stresses and experimental results.

The analysis and solution of the stress problem is based on the method of finite elements. An account of the method is given in Appendix 4. The finite element method does provide a tool for solution of problem with complex geometries but it also has its limitations. The analysis of the present problem for example assumes a linear displacement field across each of the triangular elements into which the nozzle-vessel section is divided. This assumption tends to be true for small area triangles. The concept of imaginary forces at nodal points representing the distributed stresses actually acting on the element boundaries is also another assumption. This is acceptable to a certain extent when the stress field is more or less uniform. But in places where stresses change abruptly the

elements must be small to allow for the possible variation of stress field within the elements. The combination of triangular elements is called a MESH. Fine meshes are required at places where peak stresses are expected, or where the stress concentrations are high.

### 5.1 Computer Program STREN

The analysis given in Appendix 4 presents the mathematical procedure used for the determination of stresses. The equations are solved by computer program STREN which analyses the displacements in the structure due to thermal expansion. The programme calculates the direct stresses  $\sigma_x$ ,  $\sigma_y$ ,  $\sigma_z$ , where  $\sigma_x$  and  $\sigma_y$  are in the xy plane of the section (Fig.5.1.4) and  $\sigma_z$  is in a direction perpendicular to the plane. (See Fig.5.1.4 for stress notation)

The two principal stresses  $\sigma_1$  and  $\sigma_2$  in the x-y plane are also determined as well as the shear stress  $\tau_{xy}$ . The angle of the principal stress  $\sigma_1$  is determined in respect to the x axis. Stresses are calculated for every element and node of the mesh and they are printed in such a way that they can be read for each node and element.

The general analysis and the computational procedure consists of the following steps.

(i) Initially the physical data of the material are defined. The material used is Austenitic stainless steel of the EN58J type. The values of Young's modulus E, the coefficient of thermal expansion  $\alpha$  and Poisson's ratio  $\nu$  are all temperature dependent. A relation is therefore established for each of the above quantities with respect to the temperature. Values are obtained from reference (R.5-1) and are plotted against temperature. In Fig.5.1.1 the modulus of elasticity is shown for the

temperature range  $0^{\circ}\text{C}$  ( $32^{\circ}\text{F}$ ) to  $800^{\circ}\text{C}$  ( $1472^{\circ}\text{F}$ ). In Fig.5.1.2 the coefficient of thermal expansion  $\alpha$  is plotted against the temperature. The coefficient behaves linearly up to about  $500^{\circ}\text{C}$  ( $932^{\circ}\text{F}$ ). Finally in Fig.5.1.3 Poisson's ratio  $\nu$  is shown for a temperature range of  $400^{\circ}\text{C}$  ( $720^{\circ}\text{F}$ ). The temperature of the nozzle-vessel section at the various time intervals is not the same everywhere. Most of the elements and nodes are at a temperature generally different to that of other elements or nodes. It would be extremely difficult, even with computational techniques, to use different values of the above quantities for each element and node according to their temperature. This would of course be theoretically an ideal situation but practically it involves an unnecessary amount of calculations which is not justified by the degree of accuracy obtained. Therefore the mean temperature of the section at each time interval concerned is that at which the quantities above are obtained.

(ii) The number of elements and nodes of the mesh is defined together with the x and y co-ordinates for every node. The initial displacements of each node in x and y directions are set to zero and the boundary conditions are defined as unrestrained. The temperatures of all elements are given for the particular time interval. The temperatures of the elements is the average value of the <sup>three</sup>temperatures of the three surrounding nodes, and are fed as data into the program.

(iii) The program calculates the areas of the elements and takes into account any forces present at the nodes. These forces are zero in the present problem since no external reactions are considered. The stiffness coefficients for the nodes are summed and the stiffness matrices for each element are subsequently formed. The displacement of each node is calculated due to

internal thermal forces set up by thermal expansion and by inversion of the main diagonal stiffness submatrix the flexibility submatrix at each node is formed.

A Gauss-Seidel iteration on the stiffness matrix for the entire section is performed and a test for convergence is used to check if a predetermined tolerance has been achieved. The stress components for each element are then calculated from the equations shown in Appendix 4. The stresses are also calculated for all nodes. Finally the direct stresses  $\sigma_x$ ,  $\sigma_y$  and  $\sigma_z$  are printed for each node and element together with the principal stresses  $\sigma_1$  and  $\sigma_2$  in the xy (longitudinal) plane, the shear stress  $\tau_{xy}$ , and the angle  $\theta$  (in degrees) that  $\sigma_1$  forms with respect to the x-axis. The displacements u and v of each node in x and y directions are also determined.

## 5.2 Thermal Stress Results for Case A and B

The finite element mesh for Case A is shown in Fig.5.2.1. The mesh has 377 elements and 221 nodes and it is finer at the junction where stress concentration is high. The stress results for the mesh are obtained by program STREN1 which is given in Appendix 5. Stresses are obtained for the time interval  $\tau = 9 \text{ min } 30 \text{ secs}$  during heating-up when their values are maximum. For each element and node three direct stresses  $\sigma_x$ ,  $\sigma_y$  and  $\sigma_z$  are determined. The two principal stresses  $\sigma_1$  and  $\sigma_2$  are also determined and the maximum principal stress is selected and plotted for the outside boundary of the structure. In Fig.5.2.2 the three direct stresses are plotted for time  $\tau = 9 \text{ min } 30 \text{ sec}$ . Stress  $\sigma_L$  is compressive for the vessel and its value increases as the junction is approached. At node 7 it attains its maximum value of  $-21371 \text{ lb/in}^2$  and then gradually decreases to  $-2638 \text{ lb/in}^2$  at node 18. Then the  $\sigma_L$  becomes tensile for the rest of the

junction reaching a peak value at node 23 of +11.089 lb/in<sup>2</sup>. It then decreases along the outside of the nozzle but its value remains tensile for the nozzle. The transition from compression to tension for the  $\sigma_L$  stress occurs between nodes 17 and 18 in the junction region. The two peak values also occur at the junction, with the compressive maximum being on the vessel side of the junction (node 7) and the tensile highest value on the nozzle side of the junction (node 23). The exact values of the stresses for the nodes along the outside of the structure are given in Table 5.2.1

The physical explanation of thermal stress results and their interpretation for complicated sections like the one under investigation, are not always as straightforward as for instance the results obtained under internal pressure loads. This is because thermal loads affect the structure in more ways than one. For example expansion of one part of the structure sets up tensile stresses in the fibres of the metal. At the same time this same part is under compression by the rest of the structure surrounding it as its expansion is restricted by the cooler metal around it. Again, during cooling compressive forces are set up in the metal due to the drop in temperature but since contraction is restricted by the rest of the structure which is at a higher temperature tension is also applied on it. Therefore the net effect eventually will be determined by the magnitude of the different stresses, compressive and/or tensile, that are present as the result of the specified thermal loads.

It can be seen from Fig.5.2.2 that the other two direct stresses  $\sigma_z$  follow almost the same pattern as the stress  $\sigma_L$ . It has a compressive maximum at the junction node (7) and (8) respectively and a tensile maximum at junction

node (23). Their values are compressive for the vessel, increasing gradually as the junction is approached, then they decrease along the junction and they become tensile between nodes (17) and (18). Along the nozzle part of the section they are tensile and they decrease as we move away from the junction. It can also be seen that the value of the stress  $\sigma_L$  is higher throughout the structure than that of stress  $\sigma_z$ .

This clearly indicates that higher direct stresses are set up in the longitudinal plane of the section than in the transverse plane.

The compressive values of  $\sigma_L$ ,  $\sigma_R$  and  $\sigma_z$  for the vessel from node (1) to node (17) are due to the expansion of the inner part of the vessel section which is at a higher temperature than the outer part, therefore setting up compressive forces on the outside boundary. These compressive stresses become higher as the junction is approached due to the discontinuity at node (7). For the vessel and part of the nozzle, up to node (17), the compressive stresses are higher than the tensile therefore producing an overall compressive result. Compressive forces for this part of the vessel and junction are also increased due to the effect of the expansion of the nozzle which as it expands compresses the vessel and the area around the junction.

The maximum principal stress for every node on the outside is plotted in Fig.5.2.3. The shear stress  $\tau_{xy}$  is determined by the program but from the design point of view the maximum shear stress  $\tau_{\max}^{(12)} = \left| \frac{1}{2}(\sigma_1 - \sigma_2) \right|$ , where  $\sigma_1$  and  $\sigma_2$  are the principal stresses in the xy plane, is more important. The maximum value of  $\tau_{\max}^{(12)}$  depends of course on the magnitude of the principal stresses and also their signs. When  $\sigma_1$  and  $\sigma_2$



are of the same sign,  $\tau_{\max}^{(12)}$  is equal to their difference and when  $\sigma_1$  and  $\sigma_2$  are of opposite signs  $\tau_{\max}^{(12)}$  is equal to their sum. Additionally the other two maximum principal shear stresses  $\tau_{\max}^{(23)}$  and  $\tau_{\max}^{(31)}$  are equal to  $\frac{1}{2} |\sigma_2 - \sigma_3|$  and  $\frac{1}{2} |\sigma_3 - \sigma_1|$  respectively. It is found (Fig.5.2.3) that  $\tau_{\max}^{(12)}$  (acting in the xy plane) is considerably larger than the other two maximum shear stresses. From Fig.5.2.3 it can also be seen that the maximum principal stress graph is similar to the graphs of the three direct stresses but with considerably higher stress values. There is a maximum compressive stress at node (8) of the junction of  $-23,665 \text{ lb/in}^2$  and a tensile maximum at node (23) of the junction of  $+11,091 \text{ lb/in}^2$ . The maximum shear stress  $\tau_{\max}^{(12)}$  graph also has a maximum value at node (8) of  $10579 \text{ lb/in}^2$  and at node (23) of  $5104 \text{ lb/in}^2$ . It is clear that high stress concentrations at the junction points (7), (8) and (23) are present and it is at these regions where failure is possible. The smooth geometry of the junction decreases the magnitude of the peak stresses around that area, but maximum peak stresses still develop at the points where the vessel and nozzle join up with the junction (points (7)-(8), and (23)). This leads to the conclusion that the welding of nozzles on vessels has to be undertaken with great care to avoid sharp transitions from one point to another. Even if the overall transition appear to be smooth it is possible to have small discontinuities and corners within the weld which will unavoidably produce peak stresses at these areas. Nevertheless by providing a smooth overall junction high stress concentrations can be avoided and discontinuities within the junction region can be prevented from acting as nuclei for very high peak stresses which could lead to crack initiation. A method of machining down the

vessel wall and making the area of the junction part of the vessel is thought to be more effective in combating failure at the junction. The nozzle is then welded on further away from the junction. This method of construction places the weld away from the region where stresses are high and at the same time it renders the junction region stronger since the junction is now part of the vessel. This method is used in the experimental part of this project.

Stresses are equally important on the inside surface of the nozzle and vessel which is in contact with the fluid (Fig.5.2.1 nodes (206) to (75)). It is found that direct stresses  $\sigma_x$ , and  $\sigma_z$  are compressive with a maximum compressive value at nodes (156) for  $\sigma_x$  and (157) for  $\sigma_z$  (Fig.5.2.4). Again stress  $\sigma_x$  is greater than  $\sigma_z$  especially between nodes (192) to (126) but both stresses have approximately the same values for nodes further along the nozzle. The thermal stresses for the inside surface are also given in Table 5.2.2.

The maximum principal stress graph for the inside surface is shown in Fig.5.2.5 and it can be seen that a maximum compressive value is obtained at node (157). The maximum shear stress also attains its maximum value of 5173 lb/in<sup>2</sup> at node (156). The stresses at this part of the vessel are partly the result of a bending moment produced by the relative expansion of the nozzle. As the expansion of the nozzle is restricted a bending moment is set up with a direct effect on the stresses developed on the vessel side.

The finite element mesh for Case B is shown in Fig.5.2.6. The three direct stresses are again plotted for the outside surface and are shown in Fig.5.2.7. Table 5.2.3 gives the

values of the computed stresses. Both stress components are compressive for the vessel and they increase to a maximum at node (5) and then decrease gradually to become tensile at node (9). There is a tensile maximum for the stresses at node (11). The maximum principal stress and the maximum shear stress are shown in Fig.5.2.8. The highest compressive value for the principal stress is again at node (5) and the highest tensile stress at node (11). For the shear stress a maximum of 15,245 lb/in<sup>2</sup> occurs at node (5) and at node (11) a value of 1354 lb/in<sup>2</sup> is obtained which is relatively higher than the rest of the values along the nozzle. These high values of the stresses at the points where the junction forms sharp corners with the vessel and nozzle shows how discontinuities of this kind affect stress concentrations.

Stresses developed in Case A are generally higher than those in Case B. Comparison of the temperatures in the structure at time  $\tau = 9$  min 30 sec for Case A and at time  $\tau = 10$  min for Case B indicates that the temperatures are higher for Case A. This is because heat flows across both the vessel and nozzle inside surfaces thus producing a greater overall thermal load in Case A. Nevertheless it has been explained that the difference between the mean temperature of the nozzle and vessel is greater in Case B and therefore thermal differential stresses will generally be higher than in Case A. The net effect of the thermal expansion stresses and the thermal differential stresses eventually determines the magnitude of the resulting stresses.

The situation on the inside surface in Case B (Fig.5.2.9 and Table 5.2.4) is similar to that in Case A. The maximum principal stress is compressive at the vessel, junction and

nozzle and its value increases from  $-1362 \text{ lb/in}^2$  at node (149) to  $-10,442 \text{ lb/in}^2$  at node (102). It then decreases along the nozzle. The maximum shear stress develops a similar pattern with the highest value of  $4924 \text{ lb/in}^2$  at node (102).

Wherever the maximum shear stress develops peak values, a crack can be initiated or an existing crack can propagate under certain conditions of stress level. This could lead to failure of the structure when cyclic loading is applied, as for instance under continuous heating and cooling. The thermal fatigue problem is considered later on when crack propagation is also investigated.

### 5.3 Thermal Stress Results. Case C

The finite element mesh is shown in Fig.5.3.1. The mesh is geometrically identical to the experimental specimen. The theoretical results obtained are then compared to the experimental results. This is done in the next chapter. The stresses for Case C are presented for the time intervals of  $\tau = 4, 8$  and 11 minutes of the heating up period. At time 11 minutes the maximum thermal stresses are developed. Temperatures for each of the 549 elements and for each of the 340 nodes are taken from the temperature results obtained by program TRAN3 for each of the three time intervals. The temperatures are fed as data in the program STREN3 which calculates the stresses at the respective time intervals. Program STREN3 is similar to the previous two programs which are used for Cases A and B. The listing is given in Appendix 5.

The overall stress results obtained in this case indicate that the magnitude of the stresses is lower than that of Case A or B. This is partly due to a lower  $\Delta T_m$  between nozzle and

vessel and partly due to the smaller dimensions of the section which makes the thermal transients across the thickness of the vessel and nozzle considerably lower in magnitude. The stress  $\sigma_L$  is shown in Fig.5.3.2 and Table 5.3.1 gives the exact values for the three time intervals. Stress  $\sigma_L$  is plotted for the outside boundary of the section from node (1) to node (77). The stress is comparable for the vessel with a maximum at node (21). It becomes positive at the middle of the junction and remains positive along the nozzle with a maximum value at node (43) of the nozzle. Graphs are plotted for the three time intervals of the heating-up period. In Fig.5.3.3 and Fig.5.3.4 the other two direct stresses  $\sigma_R^*$  and  $\sigma_z$  are plotted respectively and their values are also given in Table 5.3.1. Generally the pattern of the graphs is similar. Both  $\sigma_R$  and  $\sigma_z$  have a maximum compressive value at node (21) for all the three time intervals, and a tensile maximum value at node (43) of the nozzle. Stresses reduce considerably near the ends of the nozzle and vessel. Again Figs.5.3.5 and 5.3.6 show the maximum principal stress  $\sigma_{\max}$  and the maximum shear stress  $\tau_{\max}$  (12). Their values are given in Table 5.3.2. A maximum compressive principal stress of  $-8247 \text{ lb/in}^2$  is recorded at time 11 minutes at node (21) compared to  $-14897 \text{ lb/in}^2$  for Case B and  $-23665 \text{ lb/in}^2$  in Case A. The shear stress  $\tau_{\max}$  (12) has a maximum of  $7872 \text{ lb/in}^2$  at node (21) and time 11 min compared to  $15245 \text{ lb/in}^2$  for Case B and  $10579 \text{ lb/in}^2$  for Case A.

Stresses are calculated for every element and node within the section and the results are used to determine the stress field which is used in the fatigue section of this project.

---

\* Values of  $\sigma_R$  are at the centroids of the elements near the boundary. The values of  $\sigma_R$  is zero at the boundary.

## 6. EXPERIMENTAL DETERMINATION OF THERMAL STRESSES

---

In this experimental part of the project an attempt is made to determine the thermal stresses developed at the vessel, nozzle and junction areas using a specimen which was constructed to specifications described (Section 6.1). By determining the stresses experimentally, it is possible to determine how accurately we can predict the stresses by finite element analysis, and also by approximate theoretical analyses.

Strain gauges are used to measure the stresses. It has been found that thermal stress measurements pose considerable difficulties and special strain gauges are used. The situation is made more difficult by the strain gauges having to operate at relatively high temperatures.

The second objective of the experimental part is to discover whether, under continuous heating and cooling cycles,

it is possible to initiate any cracks at regions of high stress concentration or make existing cracks propagate to the extent of causing failure of the structure. This second aim is considered in Chapter 7 together with a theoretical analysis on crack propagation and fatigue.

### 6.1 Geometry and Characteristics of the Specimen

The specimen used for the experimental part of the project simulates the part of the vessel where the nozzle is attached and the curvature in the tangential (hoop) direction is

neglected. This assumption is quite realistic, as has already been explained, since when the diameter of the vessel is large curvature is small compared to nozzle wall curvature and it can be neglected over a small arc of the vessel wall. A stereogram of the specimen is shown in Fig.6.1.1 and a section of it through the longitudinal plane is shown in Fig.6.1.2 with the exact dimensions. The specimen is constructed of austenitic stainless steel of the EN58J type and its physical characteristics are obtained from the graphs plotted for Young's modulus  $E$ , thermal coefficient  $\alpha$ , thermal conductivity  $k$ , and Poisson's ratio  $\nu$ .

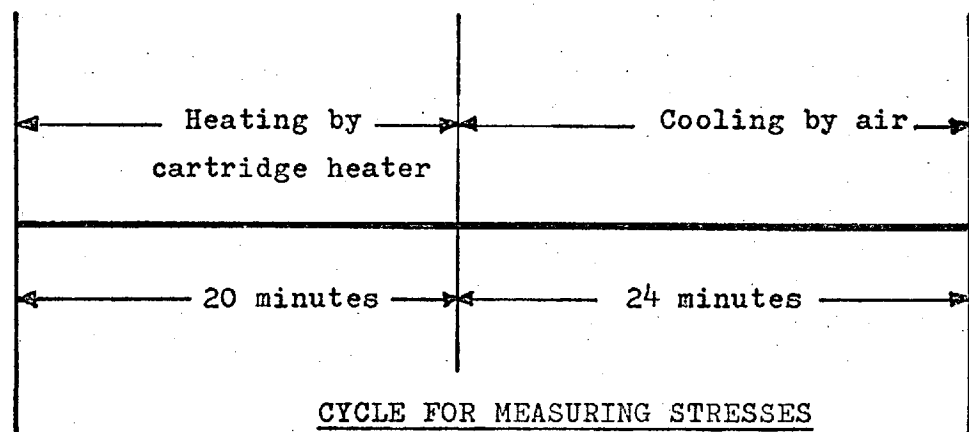
The specimen was machined down from an original block of 4.5" x 8" x 8" to produce the result shown in Figs.6.1.1 and 6.1.2 where the junction is part of the vessel. The nozzle is then electrically welded on the vessel and the weld is well away from the junction where stress concentrations are high. This procedure is more expensive than welding the nozzle straight on to the vessel wall but it is generally considered stronger. The nozzle is made of the same steel EN58J and therefore has the same physical characteristics. In theory the weld is a region of discontinuity but if its dimensions are not large and if it is made of the same material as the specimen its effect can be neglected. This is not strictly correct since welding processes may change the properties of the material and thus produce discontinuities between the weld and the structure material which eventually influences the stress pattern. Nevertheless this aspect is not the object of the investigation. The specimen is shown in the picture of Fig.6.1.3.

## 6.2 The Design and Construction of the Rig

The general mode of operation of the rig consists of a number of alternative heating and cooling cycles. There are two objectives:

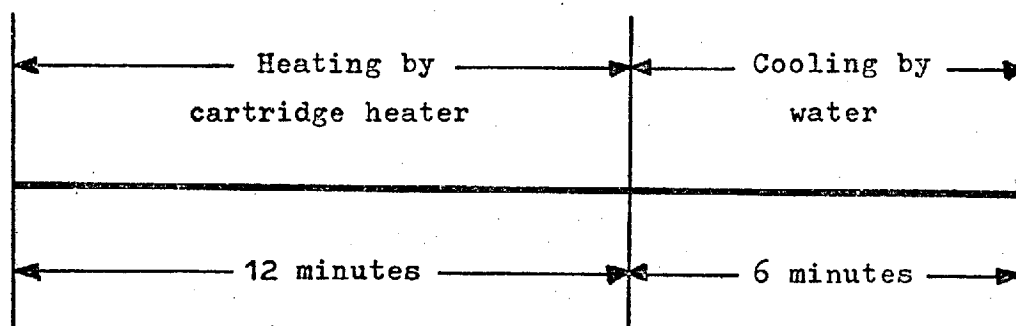
- (a) To record the stresses on the outside of the specimen during heating and cooling.
- (b) To subject the specimen to a continuous thermal cycling for fatigue investigations.

When measurements of thermal stresses are recorded, the specimen is heated for 20 minutes by means of a cartridge heater inserted into the nozzle as described below, and subsequently cooled by air for another 24 minutes (see figure below).



For the fatigue experiment the cycle consists of 12 minutes heating (enough for the maximum stresses to develop) by means of the cartridge and 6 minutes cooling by water (see figure in next page).





CYCLE FOR FATIGUE EXPERIMENT

Details of the heating and cooling cycles are described in this section and Section 7.4.

In order to record the thermal stresses on the outside surface of the specimen, the specimen is heated by means of a cartridge heater inserted within the nozzle as shown in Fig.6.1.2. The diameter of the heater is  $\frac{5}{8}$ " and is mounted concentrically within the nozzle with a clearance of 0.187". The element consists of fine gauge resistance wire which is wound around a refractory former and then inserted in a stainless steel sheath. The total length of the heater is 12" with a cold length at one end of  $\frac{3}{4}$ " which allows the heater to be clamped in the horizontal position. The maximum sheath temperature is  $700^{\circ}\text{C}$  and the maximum watt density 100 watts/sq.in (or 960 watts total). The inside surface of the nozzle/vessel is maintained at  $450^{\circ}\text{F}$  ( $233^{\circ}\text{C}$ ) by means of a thermocouple which is spot welded at one end of the nozzle as shown in Fig.6.1.2. An alternative way of positioning the thermocouple is to drill a hole through the nozzle or vessel and insert the thermocouple through the hole. This arrangement has basically two disadvantages: a hole would introduce stress concentration on the outside surface where the stress field is recorded and it would be difficult in determining the influence of this stress concentration on the overall stress field. Second the thermocouple lead would be subjected to a considerable temperature gradient as it passed through the nozzle or vessel and thus could affect the controlling temperature.

In welding the thermocouple on the inside surface of the nozzle care is taken to place the tip of the thermocouple within a small groove and cover it with a thin layer of high thermal resistance solder. This ensures that the thermocouple is recording the temperature of the surface without being affected by direct radiation from the cartridge heater. The voltage to the heater was reduced to 190 volts (maximum operating voltage 220 volts) by means of an adjustable transformer. This reduces the sheath temperature of the heater to  $1112^{\circ}\text{F}$  ( $600^{\circ}\text{C}$ ) since the maximum sheath temperature of  $1292^{\circ}\text{F}$  ( $700^{\circ}\text{C}$ ) can only be applied for clearance between 0.005" and 0.010". The reduction of the voltage, and consequently of the watt density and sheath temperature, prevents the heater from burning out. The cartridge heater is shown in Fig.6.2.1(a).

The heating-up and cooling-down processes of the specimens are controlled by a series of devices which are mounted on an instrument panel shown in the photograph of Fig.6.1.4. The instrument panel has dimensions 4'11" x 2' x 1'4" and is constructed of wood with metal legs. The sides are protected with expanding wire mesh. The following switches, fuse holders and instruments are mounted on the panel:

1. Main power switch (13A rating) and "orange" power indicating light.
2. Relay (AC 220/250 volts, 10A rating) with eleven contact points.
3. A cycle counter.
4. Electronic timer and timer switch (13A).
5. High temperature controller and switch (13A).
6. Low temperature controller and switch (13A).

7. Reset switch to isolate the high temperature controller from the lower temperature controller.
8. Cooling cycle switch (13A) and "green" cooling indicating light.
9. Heating cycle switch (13A) and "orange" indicating light.

On the panel the following fuses are mounted:

- (a) low temperature controller fuse (5A)
- (b) timer fuse (5A)
- (c) high temperature controller fuse (15A)
- (d) water valve fuse (5A)
- (e) compressed air valve fuse (5A).

The operational procedures for the heating and cooling process are as follows: initially the high temperature controller is set at the desired maximum temperature at which the inside surface of the nozzle/vessel is to be maintained. This is  $450^{\circ}\text{F}$  ( $233^{\circ}\text{C}$ ) for the present experiments. The temperature is sensed by the Nickel Chromium/Nickel Aluminium thermocouple which is thermally insulated and it is connected to the high temperature controller. The controller is a thermic solid state one with a temperature range  $0^{\circ}\text{C}$  to  $450^{\circ}\text{C}$  ( $842^{\circ}\text{F}$ ). It is provided with a temperature deviation meter calibrated in degrees centigrade. It is also fitted with an over or under temperature alarm output (Fig.6.2.1 (e)) which is adjustable within the range of  $\pm 15^{\circ}\text{C}$  from set point. The alarm circuit provides a changeover output contact rated at 5A and 240 V AC. The high temperature controller is shown in Fig.6.2.1(e).

The cartridge heater is switched on through the high temperature controller and by means of the thermocouple the temperature of the inside surface of the nozzle/vessel is maintained at  $450^{\circ}\text{F}$  ( $233^{\circ}\text{C}$ ) for 20 minutes by means of the

timer (Fig.6.2.1(c)). The timer provides two time ranges of 1 to 120 seconds and 2 to 30 minutes by changing the range sliding knob from position x1 to x20. At the end of the specified time interval the timer, through the relay, switches off the high temperature controller and consequently the heating cartridge and at the same time it turns on the low temperature controller and the cooling system. The low temperature controller is similar to the high temperature controller. It has a range from  $0^{\circ}\text{C}$  to  $150^{\circ}\text{C}$  ( $302^{\circ}\text{F}$ ). The controller is used to control the cooling temperature of the specimen. This is done with the same thermocouple which senses the high temperature. The low temperature controller is connected to the high temperature controller by Nickel Chromium/Nickel Aluminium compensation leads. The connections are fitted with electronic cold junction compensation to reduce the thermoelectric effects in the thermocouple circuit. There are two cooling systems. Compressed air is used to cool the specimen when strain gauge readings are taken and water, which is more effective, is used for the fatigue experiment. The compressed air is switched on at the end of the heating-up period by the timer. This is done by a two way spool valve which is connected to the relay. The water cooling circuit operates by means of a pressure operated solenoid valve shown in Fig.6.2.1(b). A series of pipes shown in the picture of Fig.6.1.3 cool the nozzle and block. The cooling temperature is set at  $60^{\circ}\text{F}$  ( $15.6^{\circ}\text{C}$ ) which is also the value used for the theoretical analysis. The complete electrical circuit diagram is shown in Fig.6.2.2.

### 6.3 Strain Gauge Measurements of Thermal Stresses

As the temperature on the outside of the nozzle reaches an average of  $380^{\circ}\text{F}$  ( $193.3^{\circ}\text{C}$ ), special high thermal resistance strain gauges are used to record changes in strain. The gauges used are the  $45^{\circ}$  degree rosettes manufactured by the Tokyo Sokki Ltd. The dimensions of the rosette is  $7.5 \times 7.5\text{mm}$  with a gauge resistance of  $120 \pm 0.5 \Omega$ . The rosette is a polyamide backing foil and it has a special grid configuration with good performance, especially in sensitivity, and creep characteristics at high temperature. The gauges are specially constructed for temperature up to  $572^{\circ}\text{F}$  ( $300^{\circ}\text{C}$ ) and for locations of stress concentration. The maximum admissible current is 25mA and they have a fatigue life of  $10^6$  for a strain level of  $1500 \times 10^{-6}$ .

The strain gauge rosettes are bonded on the metal using a special adhesive made by the same manufacturer. The adhesive, NP-50, is a polyester with two components. The mixing ratio of the components is 2 ~ 4 in weight. The surface of the metal is first smoothed with emery cloth and subsequently cleaned with acetone. Adhesive is applied to the surface of the metal and the back of the rosette foil and the rosette is then placed on the metal. A very fine line is grooved along the longitudinal and transverse planes so that rosettes are bonded with gauge number 1 in line with the planes. The accurate positioning of the gauges is very important since even small angles will affect the results. In order to be able to bond the rosettes with accuracy the rosettes are placed on a piece of cellotape and subsequently placed on the metal and held in position for one hour. The maximum operating temperature for the adhesive is the same as the maximum temperature for the gauges of  $572^{\circ}\text{F}$  ( $300^{\circ}\text{C}$ ). The adhesive does not require any curing and has a

very good resistance to humidity. When the rosette is placed on the metal, care must be taken to avoid any bubbles trapped underneath the foil. Existing air bubbles are forced to escape by pressing the rosette onto the metal working gradually from the centre towards the edges taking care not to destroy the gauges. Bubbles can produce false readings since the gauge is not touching the surface of the metal, apart from the destructive effect of the bubble expansion on heating.

Fifteen rosettes are placed on the specimen (Figs.6.3.1(a) and (b)). Eleven of them are placed in the direction of the longitudinal plane. Of these eleven three are on the vessel, one on the junction and seven on the nozzle. The other four are positioned in the transverse plane of the vessel as shown in the figure. Due to symmetry it is expected that the gauges in the transverse plane will indicate the same amounts of strain as the corresponding ones in the longitudinal plane. Therefore no gauges are placed in the transverse plane along the nozzle.

The centre of each rosette, that is the point where the centre line of each of its three gauges meet which is near the top right hand corner of the rectangular foil, is placed so that it corresponds to the following nodes of the finite element mesh of Fig.5.3.1.

Rosette	Gauge	Node
1	1,2,3	75 (Nozzle)
2	4,5,6	67 (Nozzle)
3	7,8,9	59 (Nozzle)
4	10,11,12	51 (Nozzle)
5	13,14,15	43 (Nozzle)
6	16,17,18	35 (Nozzle)
7	19,20,21	27 (Nozzle)
8	22,23,24	23 (Junction)
9	25,26,27	19 (Vessel)
10	28,29,30	12 (Vessel)
11	31,32,33	5 (Vessel)

For each of the forty five gauges a pair of connection terminals is used as junction point to connect the gauges to the instrumentation leads. This prevents the gauges being destroyed in the case of an accidental pull. An intermediate junction box is also used for the instrumentation leads before they are connected to the strain recorder. The intermediate box is held rigidly in position as shown in the photograph of Fig.6.1.3(b) to ensure that any pulling of the leads will not damage the gauges.

The strains are recorded using a multi-channel automatic strain recorder (Data-Log). The basic bridge-circuit is a direct current Whetstone bridge circuit with the electric potential drawn from a constant voltage electronic power pack. A digital voltmeter reads the out-of-balance voltage. Fifty bridges are provided in the recorder unit, each with its own

balancing unit, thus giving 50 available channels. A commutator unit selects the channels, either repeatedly or in turn, and the voltage reading is displaced each time on the digital voltmeter and printed on to paper tape through a fast printer for permanent record. The maximum selection speed of the unit is 10 channels per second. It is thus possible for a set of 50 readings to be recorded within 5 seconds from the moment of trigger. A slower speed of 4 channels per second was used throughout this series of experiments giving a time of 11.2 seconds for recording all 45 gauges.

The bridges in the recorder are separated from each other and each active gauge must be provided with a corresponding dummy gauge. However since thermal stresses are recorded and the gauges are temperature self compensating up to  $356^{\circ}\text{F}$  ( $180^{\circ}\text{C}$ ) the dummy gauges are replaced by 0.5 watts metal oxide resistors of the same resistance ( $120\ \Omega$ ) as the active gauges. Attention is paid when selecting the resistors as an alternative to dummy gauges to ensure that their resistance does not change very much with temperature.

Voltage readings are taken every minute during the heating-up period for twenty minutes; this covers the necessary time for the maximum stresses to develop. Since transient heating is not a static but a dynamic process the time needed for the strain recorder to scan all 45 gauges has to be taken into account when comparison with theoretical results is made. It takes 11.2 seconds to record and print voltage changes for all 45 gauges at a scanning speed of 4 channels per second. Although the Data-Log maximum recording speed is 10 channels per second this cannot be used as the automatic printer can only record accurately at a maximum speed of 4 channels per second.



Therefore readings for every minute are actually recorded from approximately 6 seconds before the minute to 6 seconds after the minute. At the end of the twentieth minute the compressed air is switched on and cooling measurements are obtained again for every minute for 25 minutes of cooling.

A total of fourteen sets of readings are obtained under identical heating and cooling conditions. It is observed that a maximum of  $\pm 0.27\%$  variation in voltage occurs between different sets of readings, which in turn produces a variation of direct and principal strains and stresses of  $\pm 0.27\%$ . The maximum variation occurs for strain gauges 1-21 along the nozzle where the temperature on the outside averages  $380^{\circ}\text{F}$  ( $193.3^{\circ}\text{C}$ ). At the beginning of the thirteenth test it was found that gauges 16, 18 and 19 were not working due to failure of the adhesive material. Careful examination indicated that the adhesive was cracked under the rosette foil and there was no proper contact between the gauges and the metal.

Special care is taken for the instrumentation leads to be kept away from the hot metal to prevent melting. The experimental results and comparisons with the theoretical analysis are presented and discussed in the next section.

#### 6.4 Experimental Results and Comparisons with Theoretical Analysis

During heating-up measurements of stresses the strain gauges would under normal circumstances record changes in voltage due to strains set up in the structure plus a voltage change due to the expansion of each gauge. The apparent increase of the voltage due to the thermal expansion of the gauge is avoided by using temperature-compensating gauges. The gauge

exhibits a negative apparent strain due to heating (see Appendix 6) up to a certain temperature and therefore the indicated change in voltage is exclusively the result of the stresses occurring in the material. However the strain gauges used are temperature compensating only up to  $180^{\circ}\text{C}$  ( $356^{\circ}\text{F}$ ) and therefore any strains recorded at points where the temperature is higher than  $180^{\circ}\text{C}$  are apparent strains.

In the experiments conducted only the outside surface of the nozzle at the time interval of 12 minutes is at temperatures higher than  $180^{\circ}\text{C}$ . Adjustments of the values of the voltage, and consequently strain and stresses, are performed for the strain gauges of the following rosettes at the temperatures indicated:

Rosette	Gauges	Temperature $^{\circ}\text{C}$	Apparent Strain
1 (Nozzle)	1,2,3	198.0	$40 \times 10^{-6}$
2 (Nozzle)	4,5,6	197.9	$33 \times 10^{-6}$
3 (Nozzle)	7,8,9	197.9	$33 \times 10^{-6}$
4 (Nozzle)	10,11,12	197.8	$28 \times 10^{-6}$
5 (Nozzle)	13,14,15	189.4	$10 \times 10^{-6}$
6 (Nozzle)	16,17,18	188.4	$7 \times 10^{-6}$
7 (Nozzle)	19,20,21	186.3	$5 \times 10^{-6}$

The detail calculations are shown in Appendix 6. The value of the voltage indicated is reduced by the determined value of the observed strain which will give an adjusted value of strain, and therefore stress, free from the apparent strain due to the expansion of the gauge.

Measurements are obtained during the heating-up process for every one minute for all the fifteen rosettes (forty five gauges) up to twenty minutes. Cooling-down measurements are then recorded for another 24 minutes for every minute. The Data-Log records changes in voltage which are printed on a tape by the printer and are identified by the number of the gauge. The observed values of the voltage are then converted into strain using the relationship

$$\epsilon_{\text{indicated}} (\text{in/in}) = \frac{1}{250(F)} \times \frac{\Delta V}{V} \quad (6.4.1)$$

where : F = the gauge factor

$\Delta V$  = voltage indicated in mV ( $10^{-3}$  volts)

V = voltage across the bridge in volts (this is set to 6 volts)

The calculated strain from the above relationship is directly expressed in in/in and therefore is dimensionless. When it is used in relationships to calculate stresses, the units of stresses obtained will thus be unaffected. The above relationship is derived by considering the bridge circuits of the Data-Log strain recorder (R.A2-8).

The voltage readings are converted into strain and then stress by using Equation 6.4.1 and computer program EXPER2. The mathematical analysis of the equations and the program details are given in Appendix 6.

Basically the program performs the following calculations for each time interval of one minute during heating-up and cooling-down processes.

1. Converts voltage readings into strain for each gauge by using Equation (6.4.1).

2. Determines the three direct strains for each of the three gauges of each rosette and subsequently calculates the three direct stresses.
3. It then calculates the principal strains for each rosette, the principal stresses and the angle of the principal strain  $\epsilon_I$  with respect to the longitudinal plane.
4. It then prints all the strain and stress results in a comprehensive form as shown in Table 6.4.1(a) and 6.4.1(b).

The results obtained by the program are the indicated or observed results. The corrections for the apparent strains at time = 12 minutes during heating up for the rosettes along the nozzle are made separately.

First experimental results of stresses are plotted for the time interval  $\tau = 12$  minutes when the stresses are maximum.

These are presented in the following graphs and tables:

Fig.6.4.1 and Table 6.4.2. Stress  $\sigma_L$ .

It is observed that for the vessel and junction gauges the observed values of stress are also real values. This is because the temperature at the corresponding positions of the rosettes is below  $180^\circ\text{C}$  and the gauges are self-compensating. Along the nozzle the observed values are higher due to the apparent strains for temperatures over  $180^\circ\text{C}$  as has already been explained. The difference between observed and real values of stresses increases along the nozzle as the apparent strain increases due to higher temperatures away from the junction.

The theoretical graph is shown by the continuous line. Generally there is good agreement at the vessel and the part of the nozzle from nodes 35 to 75 with the experimental values higher than the theoretical by an average of 16%. The possible factors which account for the difference between the experimental

results are analysed at the end of this section. In the figure there are two experimental values that deviate appreciably from theory, at gauges (22) and (19). Gauge (22) is on the junction and gauge (19) near the junction. Stress discontinuities at this region produce this high amount of difference in value between theory and experiment and it can be concluded that prediction or measurement of stresses at or near the junction is subject to a considerable degree of uncertainty. Nevertheless the average between theoretical and experimental results at that region can be considered as a realistic prediction.

Fig.6.4.2 and Table 6.4.2. Stress  $\sigma_z$

Generally the situation for the  $\sigma_z$  stress is similar to the previous figure with the theoretical values again higher than the experimental. The observed values due to apparent strain are also higher along the nozzle where the temperature on the outside surface is higher than  $180^\circ\text{C}$ . There are two positions along the nozzle (gauges 18 and 15) where the theoretical predictions are higher than the experimental.

Fig.6.4.3 and Table 6.4.3. MAXIMUM PRINCIPAL STRESS  $\sigma_{\text{maxp}}$

The experimental readings for the maximum principal stress at time  $\tau = 12$  minutes during heating-up are calculated by program EXPER2 from the direct stresses at each rosette. The values presented are the real principal stresses after the corrections for apparent strains. There is again generally good agreement with theory. Experimental values are higher than theoretical at the vessel and junction but for most of the rosettes along the nozzle theoretical values are higher than experimental with the exception of rosettes (2) and (1).

Fig.6.4.4 and Table 6.4.3. MAXIMUM SHEAR STRESS  $\tau_{\max(12)}$

Maximum shear stress values are calculated using the values of principal stresses obtained by program EXPER2 which analyses the experimental readings of the direct stresses. Experimental values are again in reasonable agreement with theory within  $\pm 12\%$  to  $\pm 16\%$ , with maximum differences again near the junction.

Figs.6.4.5, 6.4.6, 6.4.7. Table 6.4.4. STRESSES AT THE VESSEL

In the figures above the stress  $\sigma_y$ , the stress  $\sigma_z$  and the maximum principal stress  $\sigma_{\max p}$  are plotted for the vessel for every two minutes during heating-up and cooling down. Both theoretical and experimental results are shown for node 12 on the vessel where strain gauge rosette number 10 is positioned. The strain gauge readings are the real ones since the temperature on the outside of the vessel is below  $180^\circ\text{C}$  and therefore there are no apparent strains for the gauges placed on the block. It can be observed that experimental readings are again higher than the theoretical values. Maximum experimental stresses occur at time  $\tau = 12$  minutes during the heating-up and after 10 minutes from the beginning of the cooling-down process. Theoretically the maximum stresses occur at time  $\tau = 11$  minutes and therefore there is a difference of one minute between theory and experiment. Variation of the actual value of  $k$  from that listed (Ref.R.5-1) for this material could account for this. Heat loss at the outside surface of the vessel and nozzle can be higher than the theoretically estimated value and this also delays the development of the maximum stresses in the structure.

Experimental stresses developed during cooling-down are relatively higher than the equivalent stresses during heating-up. Since cooling-down is performed by blowing a compressed air stream of  $55^\circ\text{F}$  through the nozzle and around the specimen; no

theoretical predictions of stresses are made for the cooling-down process. In real situations, pressure vessels are usually cooled by natural convection which is a long process and therefore the stresses developed are generally lower than the ones set up during the heating phase.

Figs.6.4.8, 6.4.9, 6.4.10, Table 6.4.5. STRESSES AT THE NOZZLE

Stresses at node 43 (rosette number 5) on the nozzle are shown in the figures and values are recorded in Table 6.4.5. Tensile stresses for this particular point on the nozzle increase rapidly with time during the heating-up process to reach a maximum of 5541 lb/in<sup>2</sup> for  $\sigma_x$ , 1890 lb/in<sup>2</sup> for  $\sigma_z$  and 5545 lb/in<sup>2</sup> for  $\sigma_{maxp}$  after 12 minutes. These are strain gauge readings of voltage converted to stress and again they represent real values. At time 12 minutes the observed values have to be adjusted for the effect of apparent strain as the temperature at that time is over 180°C. The observed values are indicated on the graphs.

Theoretical values are lower than the experimentally recorded ones by an average of 17% and theoretically the maximum stresses develop one minute earlier at 11 minutes. Stresses during cooling-down are compressive for the nozzle reaching a maximum of -6240 lb/in<sup>2</sup> for  $\sigma_x$ , -2086 lb/in<sup>2</sup> for  $\sigma_z$  and -6377 lb/in<sup>2</sup> for  $\sigma_{maxp}$ , after 10 minutes of cooling.

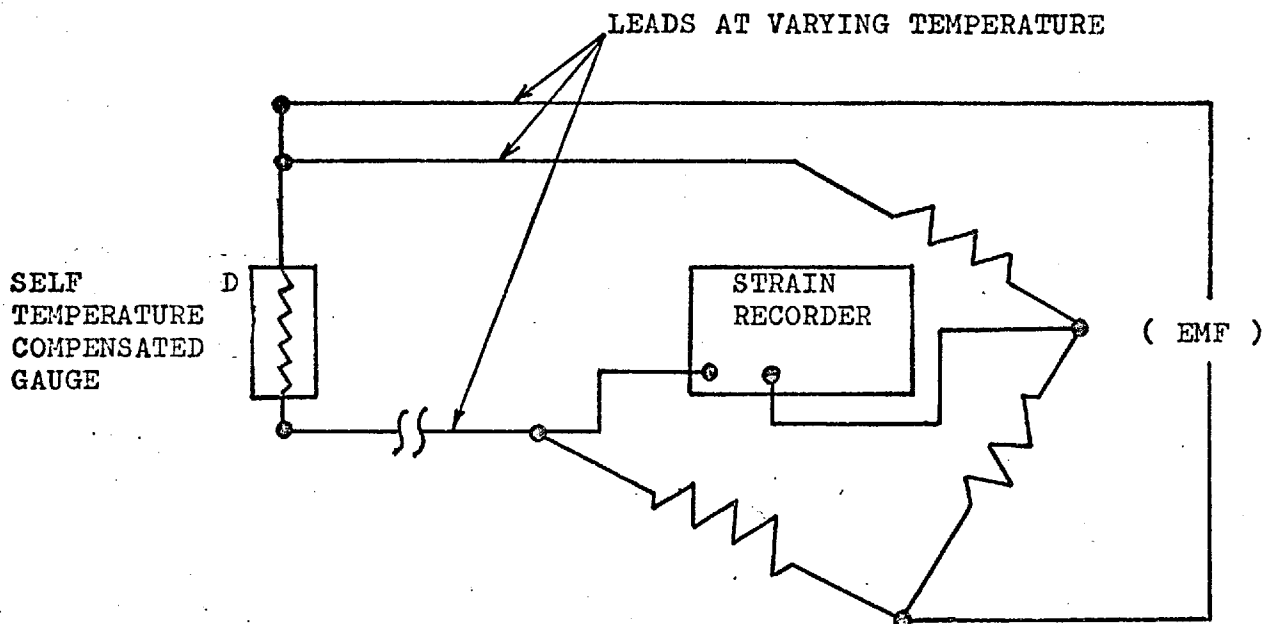
Account of errors involved in the theoretical and experimental analysis

Assumptions made for the theoretical analysis and possible errors involved in the experiments both influence the final results. An attempt is made here to discuss all the possible factors which the author can identify as important, without implying that these errors are the only ones present.

1. Finite element analysis divides the structure into small parts and applies the theory of elastic analysis to each of them in order to find the collective result of the entire structure. In practice the structure consists of a much greater number of elementary particles which are also smaller than the theoretical triangular elements with a behaviour similar to that of the theoretical model but not identical.
2. Convergence of computational results is achieved to a very small tolerance but exact values would require a very large number of iterations which is impractical.
3. Coefficient of thermal expansion ( $\alpha$ ), modulus of elasticity ( $E$ ), coefficient of thermal conduction ( $k$ ), Poisson's ratio ( $\nu$ ) are all temperature dependent parameters. In practice their values change continuously during the heating-up process at all points within the metal. Theoretically an average value of each parameter for the entire structure is used at the temperature of each specific time interval. This is considerably more accurate than using an average value for each parameter for the entire structure but for an average temperature for the heating-up process.
4. The temperature of the inside surface of the nozzle is recorded by the thermocouple which is set at  $450^{\circ}\text{F}$ . In theory the above temperature is assumed to be acquired at time  $\tau = 0$  but in experiment there is a time lapse of about one minute until the temperature on the inside reaches the value of  $450^{\circ}\text{F}$ . During this time a heat transfer rate is taking place which is not accounted for in theory.
5. Apparent strains indicated by the strain gauges are estimated as has been explained in an earlier section. Nevertheless



there are additional apparent strains due to temperature rise in the instrumentation leads. Every precaution is taken to keep the leads away from the hot metal but there is a certain amount of heat which is transferred to the leads through the gauges. If the gauges were not self temperature compensating and dummy gauges were used then the resistance changes in the leads will cancel each other. However with the self temperature compensated gauges only one pair of lead wires is required and if they are connected in one leg of the bridge variations in their resistance will be indicated affecting the results. The problem is solved by placing one lead in one bridge leg and the other lead in the adjacent leg as shown below.



Nevertheless there is still a small percentage of error involved due to small difference in length and temperatures of the leads.

6. Gauge voltage readings and their recording for all 45 gauges requires a total of approximately 12 seconds but when comparison to the theoretical results is made it is assumed

that experimental readings are instantaneous. Therefore stresses for the first gauge recording (gauge No.1) and the last gauge recording (gauge No.45) may vary to a maximum of  $\pm 2.8\%$  from the assumed instantaneous reading at any particular time interval given in the graphs. The above percentage is estimated by determining stress changes between successive readings of one minute and subsequently allowing for the 12 seconds of recording time.

7. Finally changes in the resistance of resistors used for the half bridge circuit introduce small amounts of error.

During the experimental measurements care is taken not to produce any currents of air near the specimen during the heating up process as heat losses from the outside surface of the specimen are assumed to take place only by natural convection.

## 7. BASIC CONSIDERATIONS OF THERMAL FATIGUE EXPERIENCED BY VESSEL AND NOZZLE

---

### 7.1 Thermal Fatigue and Fracture Mechanics

Thermal fatigue of vessels and nozzles is a direct result of the cyclic thermal stresses applied during heating-up and cooling-down of the pressure vessel. Safety of a plant is therefore often connected directly to the endurance of the pressure vessel and its components under continuous cyclic stress. Thermal cyclic stresses, unlike other stresses, imply the presence of a liquid or gas which apart from causing thermal stresses it often acts as a corrosive agent. Corrosion can accelerate the propagation of cracks with all the associate consequences.

The problem of thermal fatigue in brittle and ductile materials has been investigated extensively and research is being carried out to produce solutions for unsolved questions. In this section no account of such works is given since this is not the object of the present project. However reference to certain thermal fatigue investigations directly connected to pressure vessels is given below.

The problem of thermal fatigue in structures is now associated with fracture mechanics as it is by crack initiation and propagation that failure eventually occurs. Basically the study of fracture can be divided into two main categories.

- (a) Linear elastic fracture mechanics.
- (b) Elastic-plastic fracture mechanics.

Additionally fracture mechanics must deal separately with brittle and ductile materials. In the case of thermal fatigue of pressure vessels ductile materials are used and considerations of crack growth are associated with the fracture mechanics of ductile materials. However brittle fracture can also occur but only under the influence of high internal pressure or excessive external loads. Low-cycle fatigue is associated with very high temperatures, usually above  $1200^{\circ}\text{F}$  ( $650^{\circ}\text{C}$ ) where plastic flow at the tip of the crack is mainly responsible for propagation. A very comprehensive account of low-cycle fatigue is given by Manson (R.7-1). Some fatigue studies of pressure vessel and nozzles are given in references (R.7-2,7-3 and 7-4).

## 7.2 Mechanics of Fracture and Crack Propagation

A load operating on a structure produces normal and shear components of stress. Failure occurs when the sum of external and any internal stresses reaches a critical value. Elastic failure (yielding) occurs when the maximum shear stress or shear strain energy of distortion reaches a critical value. Since the shear stresses are related to the difference between the principal components of stress, a larger principal stress exists when yielding begins under triaxial tension or compression than under uniaxial tension or compression. Whenever a discontinuity exists in a structure stress concentrations will occur near it and local yielding can occur in the vicinity of this discontinuity. Regions away from the discontinuity will remain elastic. The structure is then in an elastic-plastic state of deformation.

The concentration of elastic stress near the discontinuity is expressed analytically in terms of an elastic stress

concentration factor

$$K = \frac{\sigma_{\text{local}}}{\sigma_{\text{nominal}}} \quad (7.2.1)$$

which is the ratio of the local stress near the discontinuity to the nominal stress acting across the gross cross section. The elastic stress distribution depends on the shape of discontinuity. Around a discontinuity when a load is increased to a certain amount (which is usually expressed as a fraction of the load that would cause yield in the absence of the discontinuity) a plastic zone appears which will spread further as the load increases. The rest of the structure will behave elastically until the plastic deformation becomes large and the plastic zones spread over sufficiently large distances to cause a significant distortion.

Fracture is an inhomogeneous form of deformation which can be viewed on different levels. On an atomistic level it occurs by the breaking of atomic bonds, either perpendicular to a plane (cleavage) or across a plane (shear). On a microscopic level cleavage occurs by the formation and propagation of microcracks and the separation of grains along cleavage planes. Shear fracture (rupture) usually occurs by the formation of voids by intense shear. On a macroscopic level cleavage occurs when a cleavage crack spreads essentially perpendicular to the axis of maximum tensile stress. Shear fracture occurs when a fibrous crack advances essentially perpendicular to the axis of maximum tensile stress (normal rupture) or along a plane of maximum shear stress (shear rupture). Fracture is said to be transgranular when microcrack propagation and void coalescence occur through the grains and intergranular when they occur along grain boundaries. More than one mode of crack propagation can

contribute to the fracture of a structure. In general, cleavage fracture is favoured by low temperatures.

In order to analyse the fracture process under various types of stress systems it is necessary to establish a co-ordinate system with respect to both the fracture plane, the direction of crack propagation and the applied stress system. At the present time there is no standard type of notation and symbols are explained in the text as they occur. The system is shown in Fig.7.2.1(a). The crack whose length =  $a$ , height =  $2h$ , and tip radius =  $\rho$  lies in the  $xz$  plane of a plate of thickness  $t$  and width  $w$ . The propagation of the crack is treated as a two-dimensional process since this introduces a relatively small error in computation and considerably simplifies the treatment of the problem. In practice a crack will also propagate in one plane as long as that plane is the one on which maximum principal stresses occur. The direction of the crack propagation is along the  $x$  axis and  $x = 0$  at the centre of the crack. The leading edge of the crack is parallel to the  $z$  axis. At the centre of the plate  $z = 0$  and equals  $\pm t/2$  at the outer surfaces of the plate;  $(r, \theta)$  are the co-ordinates of a point in the  $xy$  plane near the crack tip. Three distinct modes of separation at the crack tip can occur, as shown in Fig.7.2.1(b).

Mode 1. The tensile component of stress is applied in the  $y$  direction, normal to the faces of the crack, either under plane strain (thick plate,  $t$  large) or plane-stress (thin plate,  $t$  small) conditions.

Mode 2. The shear component of stress is applied normal to the leading edge of the crack either under plane-strain or plane-stress conditions.

Mode 3. The shear component of stress is applied parallel to the leading edge of the crack (antiplane strain).

### 7.2.1 Crack propagation

Over a wide range, the growth of fatigue cracks in both fully plastic and elastic-plastic situations is by a continuum controlled process. Direct observations at high applied strain levels indicates a mechanism which depends on the crack tip low field and results fractographically in striation formation. The growth of a fatigue crack from its nucleation to final unstable propagation involves amounts of crack extension per cycle which vary from the atomic to macroscopic scale.

In general fatigue failure consists of at least three distinct stages. These involve the initiation or production of a microcrack, steady crack growth at a measurable rate and catastrophic fracture in one cycle. In a simple polished specimen for instance the initiation time occupies most of the life to fracture. However in most welded structures crack-like defects will be present before the structure enters service or, failing this, high stress concentration regions will probably provide cracks, running into low stress regions, soon after service loading commences.

Griffith (R.7-5) and Irwin (R.7-6) were the first to investigate the crack propagation in materials. They consider the necessary conditions for the propagation of the elliptical, elastic crack and the stress concentration around an elastic crack. Irwin noticed that the local stresses near a flaw depend on the product of the nominal stress  $\sigma$  and the square root of the flaw depth  $2c$  and that they are proportional to a term  $K$  which is called the stress intensity factor and has dimensions  $[\text{stress } \sqrt{\text{length}}]$ . For an infinitely sharp elastic crack, in an

infinitely wide plate, the stress intensity factor  $K$  is defined as

$$K = \sigma \sqrt{\pi c}$$

and the local stresses near the crack can also be expressed in terms of the stress intensity factor.

Since the introduction of the stress intensity factor the approach to crack growth has been expressed in the form of the law

$$\frac{da}{dN} = M (\Delta K)^n \quad (7.2.1.1)$$

where  $M$  and  $n$  are material constants.

The exponent  $n$  was originally taken (R.7-7) to be equal to four but in recent work (R.7-8) it has been shown to vary widely, although this could be due to the limited range of data used. Coffin (R.7-9) has shown that plastic strain range considerations could produce something much closer to a universal criterion. Propagation laws have been examined and presented in a paper by Paris and Erdogan (R.7-7) and a comprehensive work on fracture is given by Liebowitz (R.7-10). In equation above  $a$  is the amount of crack growth and  $N$  the number of cycles. Therefore  $\frac{da}{dN}$  is the fatigue crack growth per cycle and  $\Delta K$  is the stress intensity range.

There is a threshold level  $\Delta T_c$  below which growth does not occur. For most materials the threshold range of stress intensity factor is determined experimentally for the various modes of failures described in Section 7.2. It is found that aggressive environments, especially corrosive agents, tend to decrease the stress intensity threshold range and hence encourage crack growth at lower values of the stress intensity factor  $K$ .

The range  $\Delta K$  is in fact the alternating stress intensity, given by the difference between the maximum and minimum values for each cycle. Therefore  $\Delta K = K_{\max} - K_{\min}$ . This equation has



been found to represent the behaviour of a large number of materials (R.7-7), but it is now recognised that it is only valid for the intermediate range of growth rates ( $10^{-5}$ -  $10^{-3}$  mm/cycle). The complete relationship between stress intensity and growth rate (R.7-11) is shown schematically in Fig.7.2.2, where it can be seen that Eqn.7.2.1.1 does not hold at very low values of  $\Delta K$ , where  $K$  approaches the threshold value  $K_c$  (Region A), nor for very high values which approach the material's fracture toughness  $K_{IC}$  (region C). For the mid-range of growth rates (region B), values of the exponent 'n', i.e. the slope of this "crack growth-rate" curve, have been found to lie mainly in the range 2 to 4. These values are consistent with most analytical theories of fatigue (R.7-12 to R.7-14) which are modelled on a mechanism involving one growth increment per cycle. This pertains to the generally accepted metallurgical theories which involve the production of ductile striations, by alternate blunting and re-sharpening of the crack tip, and where growth is controlled by the local crack tip alternating plastic deformation. In such situations Eqn.(7.2.1.1) can be used with confidence to predict growth rates in service components and to provide the basis for designs against failure by fatigue.

However, there is recent evidence that, in medium and high strength steels, much higher values of the exponent  $n$  (up to 10) can be obtained for a particular material or heat-treated condition (R.7-15 to R.7-17).

### 7.3 A Theoretical Investigation of Crack Growth for Case C

A theoretical analysis is made for Case C in order to determine the stress intensity factor  $K$  under the stress loads during heating-up of the structure. This is done for a region of high

stress concentration where crack propagation is most likely to occur under cyclic thermal loading. The boundary collocation method is used for the determination of  $K$ . The method is used as an alternative to the finite element analysis and it has the advantage of being able to calculate the stress intensity factor at any point including the tip of the crack.

No attempt is made to determine the constants  $M$  and  $n$  in Eqn.(7.2.1.1) since this requires experimental work directly concerned with the material used. However from the designer's point of view the determination of  $K$  is very important in order to predict if an existing crack will propagate and, according to the magnitude of  $K$ , if this crack propagation will be such as to cause extensive damage to the structure.

### 7.3.1 Regions of high stress concentration for Case C

Cracks already existing in the structure will propagate under the condition that the value of the stress intensity factor  $K$  is above the threshold value  $K_c$ . During heating-up the maximum value of the factor  $K_{max}$ , which will be attained when the maximum thermal stresses are reached, has to be determined in order to find out if it is sufficient to cause crack growth.

Initially it is necessary to determine the regions of the section where the maximum principal stresses develop. Cracks propagate under Mode I perpendicular to the lines of maximum principal stress, the rate of propagation being determined by  $K$ . Maximum principal stresses have been determined for Case C by program STREN3 and in Fig.7.3.1.1 the lines of maximum principal stresses are plotted for the section of Case C.

It can be seen that the area surrounded by the square is a region of stress concentration. The area is defined by the square whose corners are the nodes 285, 283, 200, 180 of the mesh

of Fig.5.3.1 for Case C. It is assumed that a small crack, similar to the ones present in the material due to machining and welding, exists at node 284. The crack length is taken as  $a = 0.04\text{in}$  which is a typical magnitude of a crack produced due to fabrication of the structure. During heating-up the nozzle expands and bending at the junction will cause growth of the crack assuming of course that the stress intensity factor  $K$  reaches the required value. In fact growth will occur for that period of heating-up during which the thermal stresses developed are large enough to produce a stress intensity factor  $K$  greater than  $K_c$ . On the other hand during cooling-down existing cracks could propagate from nodes 21 or 25 towards the interior of the structure.

### 7.3.2 Determination of stress intensity factor $K$ by boundary collocation theory

If the state of stress in a two-dimensional solid is considered, it is found (R.7-18) that it is specified by three stress components  $\sigma_x$ ,  $\sigma_y$ ,  $\tau_{xy}$  which satisfy the equilibrium equations

$$\frac{\partial \sigma_x}{\partial x} + \frac{\partial \tau_{xy}}{\partial y} + \rho X = 0 \quad (7.3.2.1)$$

$$\frac{\partial \tau_{xy}}{\partial x} + \frac{\partial \sigma_y}{\partial y} + \rho Y = 0 \quad (7.3.2.2)$$

where  $X$  and  $Y$  are the components of the body force per unit mass.

If  $X$  and  $Y$  are zero then the expressions

$$\sigma_x = \frac{\partial^2 \chi}{\partial y^2}, \quad \tau_{xy} = -\frac{\partial^2 \chi}{\partial x \partial y}, \quad \sigma_y = \frac{\partial^2 \chi}{\partial x^2} \quad (7.3.2.3)$$

satisfy the equilibrium equations for an arbitrary function  $\chi$ .

If the body is elastic then the components of stress satisfy the compatibility relations of the form

$$\frac{\partial^2}{\partial y^2} \{ \sigma_x - \nu(\sigma_x + \sigma_y) \} + \frac{\partial^2}{\partial x^2} \{ \sigma_y - \nu(\sigma_x + \sigma_y) \} = 2 \frac{\partial^2 \tau_{xy}}{\partial x \partial y}$$

(7.3.2.4)

Substituting Eqn. (7.3.2.3) into Eqn. (7.3.2.4) it is seen that  $\chi$  must satisfy the fourth-order linear partial differential equation

$$\frac{\partial^2 \chi}{\partial x^4} + 2 \frac{\partial^4 \chi}{\partial x^2 \partial y^2} + \frac{\partial^2 \chi}{\partial y^4} = 0 \quad (7.3.2.5)$$

which can be written as

$$\nabla^4 \chi = 0 \quad (7.3.2.6)$$

which is the two-dimensional biharmonic equation and  $\chi$  in the stress function.

In Fig. 7.3.2.1 the area where the crack is introduced is shown. The method of analysis consists in finding a stress function  $\chi$  that satisfies the biharmonic equation  $\nabla^4 \chi = 0$  and also the boundary conditions at a finite number of stations along the boundary BC and AD. The biharmonic equation and the boundary conditions along the crack are satisfied by the Williams stress function (R.7-19), therefore

$$\begin{aligned} \chi(r, \theta) = \sum_{n=1, 2, \dots}^{\infty} \left\{ (-1)^{n-1} d_{2n-1} r^{n+\frac{1}{2}} \left[ -\cos\left(n - \frac{3}{2}\right)\theta \right. \right. \\ \left. \left. + \frac{2n-3}{2n+1} \cos\left(n + \frac{1}{2}\right)\theta \right] + (-1)^n d_{2n} r^{n+1} \left[ -\cos(n-1)\theta \right. \right. \\ \left. \left. + \cos(n+1)\theta \right] \right\} \end{aligned} \quad (7.3.2.7)$$

The remaining boundary conditions to be satisfied are as follows (Derivations in Appendix 7).

Boundary BC:

$$\begin{aligned} \chi = -\frac{12M}{\nu^3} \left( \frac{a^3}{6} + \frac{a^2 y}{2} + \frac{ay^2}{2} + \frac{y^3}{6} \right) + \frac{6M}{\nu^2} \left( \frac{y^2}{2} + ay + \frac{a^2}{2} \right) \\ + \sigma_x \left( \frac{y^2}{2} + ay + \frac{a^2}{2} \right), \end{aligned}$$

where the first term is the moment effect and the second term is the stress effect.  $M$  is the moment of the sum of the components of  $\sigma_x$  along boundaries BC and AD.

Also along BC

$$\frac{\partial \chi}{\partial x} = 0$$

Boundary CD:

$$\chi = M/V, \quad \frac{\partial \chi}{\partial x} = 0 \quad (\text{Moment effect})$$

$$\chi = \frac{\sigma_x V^2}{2}, \quad \frac{\partial \chi}{\partial y} = \sigma_x V \quad (\text{x-stress effect})$$

The total effect will then be

$$\chi = \frac{M}{V} + \frac{\sigma_x V^2}{2}$$

$$\frac{\partial \chi}{\partial x} = 0$$

Boundary AB: The moment effect is

$$\chi = 0 \text{ and } \frac{\partial \chi}{\partial y} = 0, \text{ and the stress effect is}$$

$$\chi = 0, \quad \frac{\partial \chi}{\partial y} = 0$$

therefore the total effect will be:

$$\chi = 0, \quad \frac{\partial \chi}{\partial y} = 0$$

From here the procedure consists of solving  $2m$  simultaneous algebraic equations corresponding to the value of the stress function  $\chi$  and  $\frac{\partial \chi}{\partial y}$  at  $m$  selected boundary stations. In this way the values for the first  $2m$  coefficients in the Williams stress function are obtained, the remaining terms are neglected. Only the value of the first coefficient  $d_1$  is needed for the present purpose because this is directly proportional to the stress-intensity factor  $K$ . According to Irwin (R.7-20), the stress component  $\sigma_y$  in the immediate vicinity of the crack tip (as  $r$  approaches zero) is given by

$$\sigma_y = \frac{K}{\sqrt{2\pi r}} \cos \frac{\theta}{2} \left( 1 + \sin \frac{\theta}{2} \sin \frac{3\theta}{2} \right)$$

while in terms of the Williams stress function, as  $r$  approaches zero

$$\sigma_y = \frac{-d_1}{\sqrt{r}} \cos \frac{\theta}{2} \left( 1 + \sin \frac{\theta}{2} \sin \frac{3\theta}{2} \right)$$

and similarly for the other stress components, hence

$$K = -\sqrt{2\pi} d_1 \quad (7.3.2.8)$$

Once the value of  $d_1$  has been determined for values of  $r$  near the tip of the crack (where  $\theta = 0$ ) the stress intensity factor at the tip of the crack can be calculated. Now Eqn. 7.3.2.7 by neglecting coefficients of higher order than 1 we have

$$\chi(r, \theta) = (-1)^{n-1} d_{2n-1} r^{n+(\frac{1}{2})} \left[ -\cos\left(n - \frac{3}{2}\right) + \frac{2n-3}{2n+1} \cos\left(n+\frac{1}{2}\right)\theta \right]$$

where  $n = 1$

hence  $\chi(r, \theta = 0) = -d_1 r^{3/2} \left(-\frac{4}{3}\right)$

and

$$\chi(r, \theta = 0) = -\frac{4}{3} r^{3/2} d_1 \quad (7.3.2.9)$$

In order to determine the stress function  $\chi$  for the area A of Fig. 7.3.1.1 a finite element mesh is constructed shown in Fig. 7.3.2.2. This enables the calculation of stresses at a much smaller scale than they were calculated before for Case C. Program STREN4 is used to solve this finer mesh. It does not use the temperature differences to calculate the thermal stresses but it sets as boundary conditions the stresses obtained by STREN3 for Case C around the boundaries of area A. Program STREN4 is listed in Appendix 7.

When the stresses are determined for the area, program FUNSTR is used to determine the stress function  $\chi$  for a total of 2025 nodal points (a grid of 45 x 45). Program FUNSTR performs the following calculations:

Using finite difference analysis it determines the stress function  $\chi$  which satisfies the biharmonic equation at the prescribed boundary points and at all interior mesh points. The grid is shown in Fig.7.3.2.3.

The following steps are performed by the program:

1. Read constants and dimensions parameters such as:  
mesh points, crack length, cell width and height, boundary co-ordinates.
2. Read boundary stresses in y-direction. These are provided as data from the results of STREN4.
3. Calculate moment for x-stress component.
4. Using finite difference equation solve for interior mesh points. The finite difference approximation for the biharmonic equation  $\nabla^4\chi = 0$  is derived from the cell shown in Fig.7.3.2.3 and is given below as:

$$\begin{aligned} \nabla^4\chi \doteq & 20\chi_{jk} - 8(\chi_{j,k+1} + \chi_{j,k-1} + \chi_{j+1,k} \\ & + \chi_{j-1,k}) + 2(\chi_{j+1,k+1} + \chi_{j+1,k-1} \\ & + \chi_{j-1,k+1} + \chi_{j-1,k-1}) + (\chi_{j+2,k} + \chi_{j-2,k} \\ & + \chi_{j,k+2} + \chi_{j,k-2}) = 0 \end{aligned}$$

5. Perform convergence test until predetermined tolerance.
6. Print the stress function  $\chi$  for all nodal points.

The listing and designations of program FUNSTR are given in Appendix 7.

Having determined  $\chi$  the first matrix coefficient  $d_1$  is calculated by subroutine DMATRIX which is linked to program FUNSTR. The subroutine calculates  $d_1$  using Eqn.(7.3.2.9). The matrix coefficient  $d_1$  is a function of  $\chi$  and the distance  $r$  from the tip of the crack. The subroutine prints  $d_1$  for each value of  $\chi$  and  $r$  at every nodal point. Intermediate points are obtained by

specifying the co-ordinates x,y between two nodal points. The subroutine is also listed in Appendix 7.

#### Stress Intensity Factor K Results

The theoretical values of K obtained by the analysis are those developed at time  $\tau = 11$  minutes when the maximum stresses are set up for Case C. In Table 7.3.2.1 the values of the first matrix coefficient  $d_1$  and the equivalent values of K are shown for distances r away from the tip of the crack. The values are calculated by subroutine DMATRX using the values of the stress function  $\chi$  along the y axis of the crack where  $\theta = 0$ . It can be seen from the table that K increases as the tip of the crack is approached. It attains its maximum value of 2112.3 at the tip of the crack. This is the maximum value which will be attained during heating-up at that particular point under the present conditions of thermal loading.

From reference R.7-21 the critical or threshold value of K for austenitic steel estimated by experimental analysis is of the order of  $5.5 \times 10^3$ . This value is considerably higher than the maximum value of 2112.3 obtained above, and it can be safely assumed that an existing crack will not propagate under the applied thermal load. In practice corrosion of the metal by the fluid responsible for the thermal stresses may lower the critical value of K, but such an effect is not likely to alter the value more than 10%. The critical value of K mentioned above is valid under the condition that a crack already exists and is not less than 0.02in in length. If the crack length is very small (0.001-0.010in) the critical value of K will tend to be lower. However as the crack grows K must be increased for further propagation and if this does not happen then the crack growth will be arrested permanently at a particular stress level. Therefore



in order to have a catastrophic crack growth the value of  $K$  must be higher than the critical or threshold value at every stage of the growth until the length of the crack is such to cause fracture of the structure or the component. The theoretical analysis can estimate  $K$  at every stage of the growth by taking into account the various lengths of the crack and by determining the stress function  $\chi$  from the existing stress field.

If a crack does not exist at all, the stress intensity factor must be very high in order to initiate one. This is not possible unless the loads applied on the structure are quite large and generally at least 50% of the tensile strength of the material, if cyclic loading is applied.

Summarizing, the theoretical analysis for the determination of the stress intensity factor  $K$  consists of the following steps:

- (i) Determine the stresses at the area where the crack is located.
- (ii) Using the calculated stresses determine the stress function  $\chi$  by solving the biharmonic equation  $\nabla^4\chi = 0$ . Use the boundary collocation analysis to define boundary conditions.
- (iii) The calculated values of  $\chi$  are then used to determine the first matrix coefficient  $d_1$  at the tip of the crack and at various distances  $r$  from the tip of the crack.
- (iv) The stress intensity factor  $K$  is a function of the first matrix coefficient  $d_1$  (Eqn.7.3.2.8) and therefore it can be calculated at any point including the tip of the crack using the values of  $d_1$ .
- (v) The calculated value of  $K$  at the tip of the crack can then be compared to the threshold value  $K_c$  determined by experiments, and if  $K > K_c$  then crack growth will take place.

- (vi) By experimentally determining the values of M and n in the equation  $\frac{da}{dN} = M(\Delta K)^n$  for the material considered, the rate of crack growth per cycle can be assessed.

#### 7.4 Experimental Thermal Cycling of Specimen

In order to check if any cracks would develop in the specimen under investigation by subjecting it to thermal cycling, the experimental rig is slightly modified. Heating is still achieved by means of the heater but for cooling water is used which flows over the nozzle and the block as shown in the photograph of Fig.6.1.3.

Rapid cooling by water ensures that reverse stresses will develop of approximately the same order like the ones developed during the heating up process.

The inside of the nozzle is kept at 450°F for twelve minutes, enough time for the maximum thermal stresses to develop. Cooling is subsequently switched on for approximately six minutes until the inside of the nozzle is cooled down to 65°F (18.3°C). Therefore the specimen is subjected to a thermal cycle of 18 minutes and an alternating maximum principal stress which ranges from  $\pm 8247$  lb/in<sup>2</sup> at node (21) to  $\pm 4583$  lb/in<sup>2</sup> at node (43). The thermal cycling of the specimen at maximum stresses continued for four months at 12 hours daily to produce a total of 4783 cycles. Then the water valve failed and therefore it was decided to examine the specimen for possible cracks without inducing further cycles. This was decided in the light of the theoretical analysis which has predicted that the thermal stresses and therefore the stress intensity factors were not high enough to initiate cracks or cause growth of possible existing ones.

The specimen was cut in half through the longitudinal plane as shown in the photographs of Fig.7.4.1. It was then polished and examined under the microscope for possible cracks. The area shown within the square in Fig.7.4.1 was given special attention since it is in this area of high stress concentration and high stress intensity factors where existing cracks would most probably propagate. The results were negative and no cracks of detectable length were revealed.

It is therefore concluded that under the above thermal loadings the specimen will not fail within its possible service life unless the thermal stresses increase appreciably.

## 8. CONCLUSIONS

---

### 8.1 General Conclusions

To conclude the present work the following questions are answered in this section:

(1) Are the numerical and computational methods produced and developed in the theoretical part of the work satisfactory and reliable for the determination of thermal stresses and fatigue aspects in pressure vessel nozzles? Can they be used for design purposes and can they be applied to other parts of the vessel?

(2) What is the nature and magnitude of thermal stresses which develop in the various cases of vessel nozzles examined and how do they compare?

(3) Are the experimental techniques for measuring thermal strains (and consequently stresses) accurate enough, and how do theoretical predictions agree with experimental results?

The transient thermal distributions are determined for all three cases (A, B and C) by using the finite difference method to solve the heat convection and conduction equations at various time intervals during heating-up. The advantage of the method is that any heating conditions can be treated including transient convection at the boundary. The thermal programs developed can be used for other geometries by simply changing the input data. The method is reliable and converges fast. Truncation and round-off errors are present but are greatly reduced for small time

intervals and pre-determined tolerance. The heat transfer coefficient at the convective boundaries is a source of error since it is computed separately by using approximate relationships described in Section 4.1. Nevertheless this only affects the accuracy of the method indirectly and the values of heat transfer coefficients can be improved at any stage without disturbing the general structure of the program.

In Appendix 2 the finite element method is used to obtain thermal distributions with curvature taken into consideration. Its main advantage lies in the fact that the temperatures can be obtained at any time interval for every point within a square element. With the finite difference method the temperatures are obtainable at the nodes. However the method is not as fast as the finite difference method and it converges much slower.

The thermal stresses are calculated by the developed elastic stress-strain programs using the finite element method, and the thermal results obtained by the temperature distribution programs. Again stresses can be determined at any time and at any point of the structure where the temperature is known. The programs can be used extensively for other parts of the vessel and stresses can therefore be assessed for design purposes.

It is found that in all three cases the thermal stress pattern during heating-up is generally similar for both the outside and inside boundaries and for direct as well as principal and shear stresses. The outside vessel wall is in compression with the nozzle in tension. On the inside the wall is in compression. Additionally the maximum shear stress  $\tau_{\max}$  (12) develops in the xy plane for all three cases.

In CASE A, where the heating takes place from both the inside boundary of the vessel and nozzle, the magnitude of the stresses is the highest, and this is due to higher temperatures in the structure. Stresses in CASE B are generally higher than in CASE C although the rate of heating is the same. This is because in CASE B the inside vessel wall and the outside of the structure are insulated and this contributes to higher temperatures for CASE B at the corresponding time intervals during heating-up. In CASE C heat is transferred to the surroundings by natural convection. A considerable number of vessels are not insulated on the outside and this makes the analysis of CASE C useful with respect to the determination of thermal distributions when natural convection conditions prevail around the vessel.

In the experimental part of the project the temperature self compensating strain gauge is proved to be the most appropriate device to record strains under continuously changing temperature. The automatic strain recorder (Data-Log) is adequate for recording transient strains, but the printer's selection speed is limited and it takes 11.2 seconds to scan all 45 gauges. The experimental results are generally in good agreement with the theoretical model of CASE C with the experimental values higher than the theoretical by an average of 16%. The agreement indicates that both methods of finite difference and finite elements for the determination of temperatures and stresses can be used reliably for design assessments.

## 8.2 Conclusion to Chapter 7

The determination of the stress intensity factor  $K$  along the crack axis by the boundary collocation analysis for a structure other than a plate of thickness  $t$  poses a number of problems

directly associated with the loading at the boundaries. However it is thought that boundary collocation analysis can be used to determine  $K$  in a region of a structure as long as the stress loading at the boundary can be determined.

To achieve this the stress field of the entire structure determined in CASE C is used and region A (Fig.7.3.1.1) is isolated with the stress loading on the boundary uniformly distributed as shown in Fig.7.3.2.1. It is found that the value of  $K$  at various distances from the tip of the crack can be obtained from the stress function  $\chi$ . The method is mathematically accurate and as long as the maximum principal stress  $\sigma_{\max}$  is in one plane, and in this case the  $xy$  plane, the values of  $K$  are reliable and the crack will propagate, if  $K > K_c$  perpendicular to the lines of maximum principal stress. The value of  $K$  for CASE C at the tip of the crack is found to be  $2112.3 \text{ lb}\sqrt{\text{in}^{-3}}$ , which is less than the critical value  $K_c \approx 5500 \text{ lb}\sqrt{\text{in}^{-3}}$  determined by experiments for the same material. Although for this low value of  $K$  no cracks are detected in the region A of the specimen, it should be emphasised that more experimental work is required in order to establish fully that the theoretical model predictions coincide with experimental results. However it is believed that the theoretical analysis developed in Chapter 7 can be used reliably in conjunction with experiments to assist the designer of pressure vessels in his effort to improve his ability to predict fatigue crack initiation and propagation.

## 9. DISCUSSION OF NUMERICAL METHODS

---

### 9.1 Finite Difference and Finite Element Methods for the Determination of Temperatures and How They Compare

The solution of the time-dependent heat transfer equation for the heat flow within a solid body in two-dimensional unsteady-state conduction has been solved by both finite difference and the finite element method. An account of the relative merits and disadvantages of each method thrown up <sup>by</sup> this work will be given in this section.

#### (a) Finite Difference Method

As is shown in Appendix 1, to solve the partial differential equation of heat flow the derivatives are replaced by finite difference approximations. The entire region of interest for the solution is divided into a mesh or grid over which the approximate solution is obtained. The solution at each point is equal to the average value of the quantity at the four adjacent points. In steady state problems the difference equations set up are solved by the iterative procedure over the entire grid until no point changes by more than the prescribed error; that is, the solution converges to the pre-determined accuracy. This accuracy depends on the problem and the available computing facilities. Now when time is one of the independent variables a sequence of solutions corresponding to each time increment must be obtained. The solution of the time dependent equation is an explicit solution, that is the expression used uses forward difference representation to give the future temperature  $T_i$  at node  $i$  in terms of the



current temperatures of its surrounding nodes. From the computational point of view the method is stable for small time increments  $\Delta\tau$  and very fast.

Now the space increments  $\Delta x$  and  $\Delta y$  must be small enough to give the required accuracy. Of course the size of  $\Delta x$ ,  $\Delta y$  depends on the overall dimensions of the body. Once the value of  $\Delta x$ ,  $\Delta y$  (and in this case  $\Delta x = \Delta y$ ) has been established, two other quantities are automatically fixed as well. The first is the time increment  $\Delta\tau$  which is now fixed and the second is the total number of nodal points. It is clear that the larger the value of  $\Delta x$  and  $\Delta\tau$  the more rapidly the solution will proceed. On the other hand, the smaller the value of these increments the more accuracy will be obtained. At first glance one might assume that small distance increments could be used for greater accuracy in combination with large time increments to speed the solution. This is not the case since the finite-difference equation (A 1.13, Appendix 1) limits the value of  $\Delta\tau$  which may be used once  $\Delta x$  is chosen. It can also be seen that when  $\Delta x$  is increased  $\Delta\tau$  is increased and when  $\Delta x$  decreases  $\Delta\tau$  also decreases. This dependency of  $\Delta\tau$  on  $\Delta x$  poses a computational problem. If for example the temperatures of a large structure were to be determined, the distance increment  $\Delta x$  cannot be taken as very small, which will otherwise be desirable for accuracy, because it will result in a very large number of nodal points which may be outside the storage capacity of the available computer facilities. At the same time, a small  $\Delta x$  means an equally small time increment  $\Delta\tau$ . A small time increment will unavoidably lead to a large number of time iterations to cover a fairly long heating-up process and therefore a considerable amount of computing time will be necessary. On the other hand if  $\Delta x$  is chosen to be large in order to make  $\Delta\tau$  large and thus speed the solution the accuracy of the results will be limited.

It is therefore highly desirable under the above circumstances for the method of finite difference to converge rapidly. Rapid convergence saves computing time and it has been proved that finite difference method converges fast.

(b) Finite Element Method

In the Finite Element Method the temperature is approximated within the element by using shape functions which are defined piecewise element by element. Since the values of temperatures are known at time  $\tau_0$ , values at time  $\tau_1 = \tau_0 + \Delta\tau$  can be obtained by summing around the nodes at this latter step and then solving the system of simultaneous linear algebraic equations that results. At each new step an identical procedure is used until a required time is reached. The accuracy of the results still depends on the size of the element but for the same  $\Delta x, \Delta y$  coordinate spacing the finite element method is more accurate than the finite difference method. This is mainly due to the fact that the temperature is defined better by the shape functions for the isoparametric elements used. On the other hand the finite element method is not as easily programmed as the finite difference and it does not converge to the exact solution as fast as the finite difference. The finite element method has the advantage that the determination of temperature at any point  $x, y$  within an element at time  $\tau$  is obtained relatively more easily than for the finite difference method where the interpolation is time-consuming and not as accurate. The geometry of the domain under investigation often favours the use of the finite element method. For example in the case of the spherical vessel where the boundary shape is curved it is difficult to fit a finite difference grid to the boundary and therefore the finite element method is more appropriate for this particular geometric configuration. The finite element method is also unconditionally stable for any time

step  $\Delta t$  although in certain cases where  $\Delta t$  is very large some condition between the space increment  $\Delta x$  and the time increment  $\Delta t$  must be imposed to obtain meaningful results.

Finally we can conclude in general that :

(1) The finite difference method is less accurate than the finite element method for large areas (greater than about 50,000 nodal points) and for relatively long times (greater than about 10,000  $\Delta t$ ) but it is more economical and computationally faster. On the other hand the finite element method is generally unconditionally stable for any time step  $\Delta t$ .

(2) For smaller areas and shorter times than those mentioned above the finite difference method should be preferred since the accuracy obtained is comparable to that of the finite element and at the same time it is faster. It must be emphasized that the area and time dimensions given above are based on the available computing facilities and the figures mentioned are of the computer systems used for this work (namely the CDC 6400 and CDC 6600 computers). For other computer systems the storage capacity and the central peripheral time must be taken into account in order to assess the relative value of the two methods in relation to any particular problem.

## 9.2 Comparisons of Finite Difference and Finite Element Methods for the Determination of Stresses

In this work the finite element method was used to calculate the thermal stresses and the finite difference method was used to solve the biharmonic equation  $\nabla^4 \chi = 0$  in order to determine the stress function  $\chi$ .

An advantage of the finite difference method, as has already been mentioned in Section 9.1, is the ease with which it may be formulated and programmed for solution by a digital computer. This is mainly due to the use of regular grids. In almost all finite difference methods the grid lines are parallel to the coordinate axes and therefore the

method is best suited to solving problems where the rows of points can terminate with points on the boundary (see Fig.7.3.2.3, p.337 for the finite difference solution of  $\nabla^4 \chi = 0$ ).

Nevertheless, a disadvantage of finite difference method is a lack of geometric flexibility in fitting irregular boundary shapes and in concentration points in regions of the solution domain where the stresses for example change most rapidly (although it is possible to use irregular grids with varying distances between successive rows, this increases the complexity of the formulation).

The finite difference method is applied to the governing partial differential equations for the problem concerned while the finite element is formulated directly from the physical arguments used to derive such equations and therefore by using shape functions to describe the displacements the finite element method becomes more accurate.

Generally it can be concluded that:

- (a) The finite difference method can be formulated and programmed more easily than the finite element and is faster.
- (b) The finite element method is more accurate and has greater geometric flexibility, especially at irregular boundaries and at regions where the stresses change most rapidly. Computationally it is more complex and expensive than using finite differences.

# APPENDICES

---

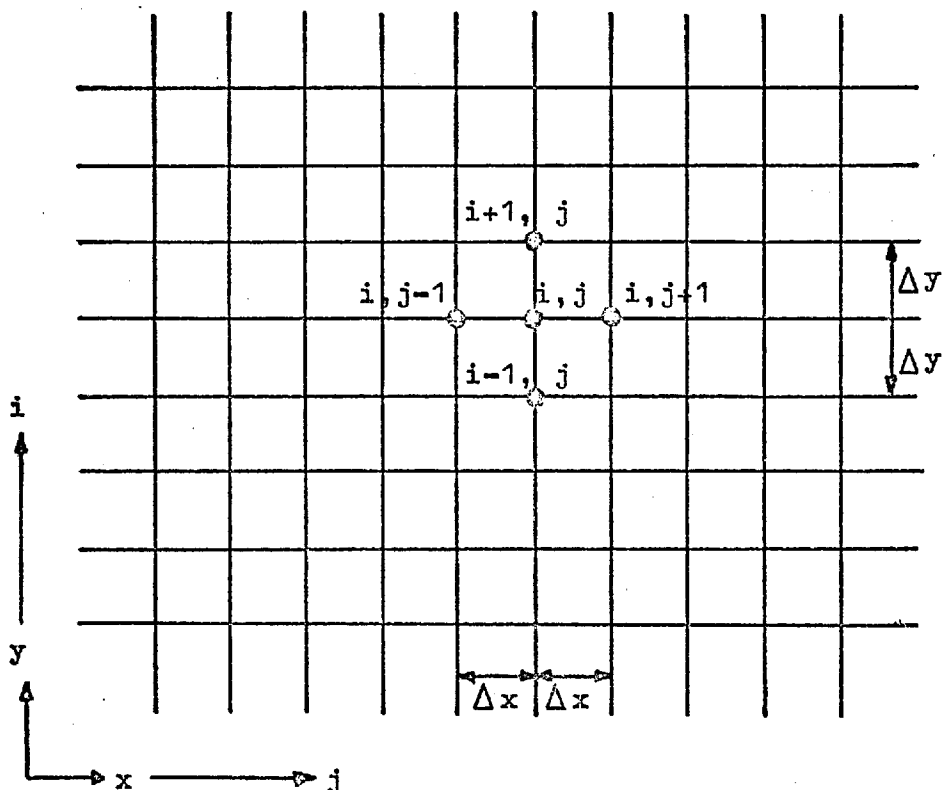
## APPENDIX 1

# Transient Heat Conduction and Convection

### 1.1 Transient Heat Conduction Finite Difference Equations inside the Walls

The difference equations derived below apply only within the walls where heat is transferred by conduction. The equations across the convection boundary between fluid and nozzle-vessel section are derived in 1.2.

Consider the nozzle-vessel section divided into a two-dimensional net of space increments  $\Delta x$  and  $\Delta y$ ,  $\Delta x$  being equal to  $\Delta y$ . The co-ordinates of the nodal points are represented by increments of  $i$  and  $j$ .



Finite differences are used to approximate differential increments in the temperature and space co-ordinates. The temperature gradients are written as follows:

$$\begin{aligned} \left. \frac{\partial T}{\partial x} \right|_{i+\frac{1}{2},j} &\approx \frac{T_{i+1,j} - T_{i,j}}{\Delta x} \\ \left. \frac{\partial T}{\partial x} \right|_{i-\frac{1}{2},j} &\approx \frac{T_{i,j} - T_{i-1,j}}{\Delta x} \\ \left. \frac{\partial T}{\partial y} \right|_{i,j+\frac{1}{2}} &\approx \frac{T_{i,j+1} - T_{i,j}}{\Delta y} \\ \left. \frac{\partial T}{\partial y} \right|_{i,j-\frac{1}{2}} &\approx \frac{T_{i,j} - T_{i,j-1}}{\Delta y} \end{aligned}$$

The second partial derivatives will be:

$$\begin{aligned} \frac{\partial^2 T}{\partial x^2} \Big|_{i,j} &\approx \frac{\left. \frac{\partial T}{\partial x} \right|_{i+\frac{1}{2},j} - \left. \frac{\partial T}{\partial x} \right|_{i-\frac{1}{2},j}}{\Delta x} \\ &= \frac{T_{i+1,j} + T_{i-1,j} - 2T_{i,j}}{\Delta x^2} \end{aligned} \quad (A1.1)$$

and,

$$\begin{aligned} \frac{\partial^2 T}{\partial y^2} &\approx \frac{\left. \frac{\partial T}{\partial y} \right|_{i,j+\frac{1}{2}} - \left. \frac{\partial T}{\partial y} \right|_{i,j-\frac{1}{2}}}{\Delta y} \\ &= \frac{T_{i,j+1} + T_{i,j-1} - 2T_{i,j}}{\Delta y^2} \end{aligned} \quad (A1.2)$$

The differential equation of transient heat conduction is:

$$k \left( \frac{\partial^2 T}{\partial x^2} + \frac{\partial^2 T}{\partial y^2} \right) = \rho c \frac{\partial T}{\partial \tau} \quad (A1.3)$$

Substituting the gradients  $\frac{\partial^2 T}{\partial x^2}$  and  $\frac{\partial^2 T}{\partial y^2}$  in equation (A1.1)

above the time derivative equations is approximated by

$$\frac{\partial T}{\partial \tau} \approx \frac{T_{i,j}^{n+1} - T_{i,j}^n}{\Delta \tau} \quad (A1.4)$$

where  $n$  is the time increment. By combining the equations (A1.1), (A1.2), (A1.3) and (A1.4) the equation of the temperature  $T$  at a

particular time is derived in terms of the temperatures at the surrounding nodes at the beginning of the time increment.

$$\begin{aligned} & \frac{T_{i+1,j}^n + T_{i-1,j}^n - 2T_{i,j}^n}{(\Delta x)^2} + \frac{T_{i,j+1}^n + T_{i,j-1}^n - 2T_{i,j}^n}{(\Delta y)^2} \\ &= \left[ \frac{T_{i,j}^{n+1} - T_{i,j}^n}{\Delta \tau} \right] \left[ \frac{1}{\alpha} \right] \end{aligned} \quad (A1.5)$$

where  $\alpha$  is the thermal diffusivity in  $\text{ft}^2/\text{hr}$  and is equal to  $\frac{k}{\rho c}$ .

Since the space increments are equal, that is  $\Delta x = \Delta y$  the equation (A1.5) above becomes

$$\begin{aligned} T_{i,j}^{n+1} &= \frac{\alpha' \Delta \tau}{(\Delta x)^2} (T_{i,j}^n + T_{i-1,j}^n + T_{i,j+1}^n + T_{i,j-1}^n) \\ &+ \left[ 1 - \frac{4\alpha' \Delta \tau}{(\Delta x)^2} \right] T_{i,j}^n \end{aligned} \quad (A1.6)$$

By choosing the distance and time increment such as

$$\frac{(\Delta x)^2}{\alpha' \Delta \tau} = 4$$

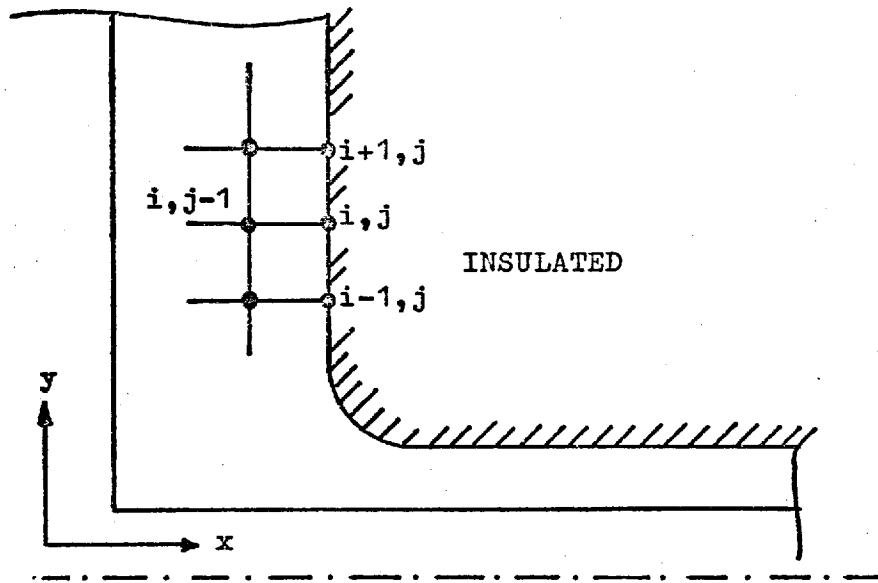
the last term of the equation disappears and the temperature of the node  $(i,j)$  after a time increment is the arithmetic average of the four surrounding nodal temperatures at the beginning of the time increment.

Therefore,

$$T_{i,j}^{n+1} = \frac{1}{4} (T_{i,j}^n + T_{i-1,j}^n + T_{i,j+1}^n + T_{i,j-1}^n) \quad (A1.7)$$

For the insulated boundaries, but not the junction, the energy balance gives the equation for the temperature  $T^{n+1}$ .





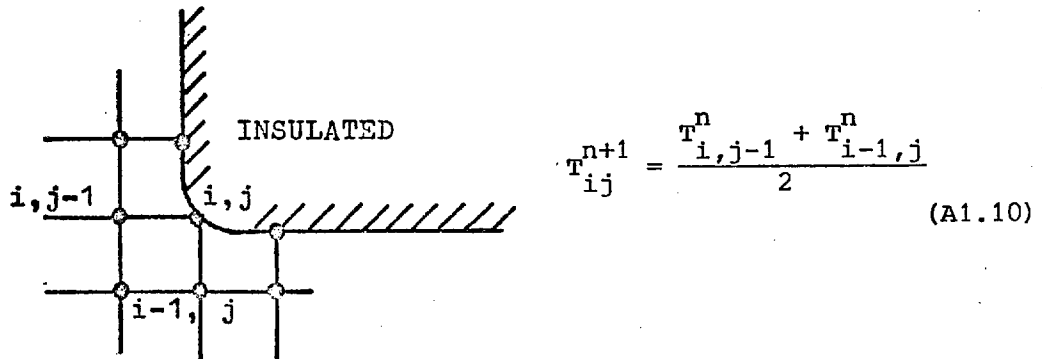
For the vertical nodal points

$$T_{i,j}^{n+1} = \frac{T_{i,j-1}^n}{2} + \frac{T_{i-1,j}^n + T_{i+1,j}^n}{4} \tag{A1.8}$$

For the horizontal nodal points

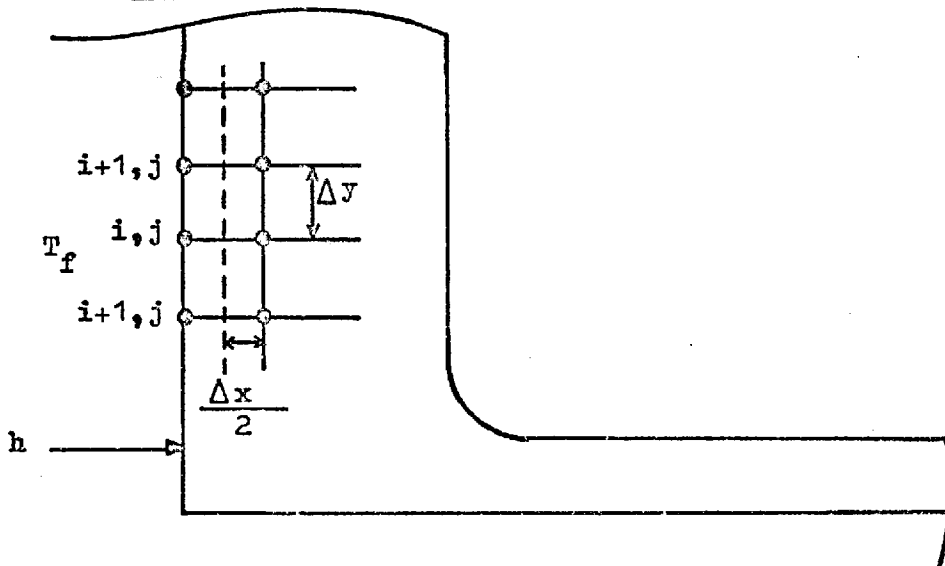
$$T_{i,j}^{n+1} = \frac{T_{i-1,j}^n}{2} + \frac{T_{i,j-1}^n + T_{i,j+1}^n}{4} \tag{A1.9}$$

The insulated boundary on the outside at the junction when the junction is curved the energy balance gives,



$$T_{ij}^{n+1} = \frac{T_{i,j-1}^n + T_{i-1,j}^n}{2} \tag{A1.10}$$

1.2 Difference Equations for Convective Boundary Condition



The boundary of the inside walls of the vessel and nozzle is exposed to a convection boundary condition. The transient energy balance on the node  $(i,j)$  is made by setting the sum of the energy conducted and converted into the node equal to the increase in the internal energy of the node. Therefore

$$\begin{aligned}
 & k\Delta y \frac{T_{i,j+1}^n - T_{i,j}^n}{\Delta x} + k \frac{\Delta x}{2} \frac{T_{i+1,j}^n - T_{i,j}^n}{\Delta y} \\
 & + k \frac{\Delta x}{2} \frac{T_{i-1,j}^n - T_{i,j}^n}{\Delta y} + h\Delta y (T_f - T_{i,j}^n) \\
 & = \rho c \frac{\Delta x}{2} \Delta y \frac{T_{i,j}^{n+1} - T_{i,j}^n}{\Delta \tau}
 \end{aligned} \tag{A1.11}$$

For  $\Delta x = \Delta y$  the above equation for  $T_{i,j}^{n+1}$  becomes

$$\begin{aligned}
 T_{i,j}^{n+1} = \frac{\alpha' \Delta \tau}{(\Delta x)^2} & \left\{ 2 \frac{h\Delta x}{k} T_f + 2 T_{i,j+1}^n + T_{i+1,j}^n \right. \\
 & \left. + T_{i-1,j}^n + \left[ \frac{(\Delta x)^2}{\alpha' \Delta \tau} - 2 \frac{h\Delta x}{k} - 4 \right] T_{i,j}^n \right\}
 \end{aligned} \tag{A1.12}$$

No attempt to choose the value of  $\frac{(\Delta a)^2}{\alpha' \Delta \tau}$  to make the coefficient of  $T_j^n$  or  $T_{i,j}^n$  zero, since the heat transfer coefficient influences the choice and also the time interval has been defined appropriately to give the value of  $\frac{(\Delta x)^2}{\alpha' \Delta \tau}$  equal to 4 for the interior difference equations.

The equation for the nozzle inside convection boundary will be the same with the  $i$  and  $j$  subscripts interchanged and a different heat transfer coefficient. Thus,

$$\begin{aligned}
 T_{i,j}^{n+1} = \frac{\alpha' \Delta \tau}{(\Delta x)^2} & \left\{ 2 \frac{h\Delta x}{k} T_f + 2 T_{i+1,j}^n + T_{i,j+1}^n \right. \\
 & \left. + T_{i,j-1}^n + \left[ \frac{(\Delta x)^2}{\alpha' \Delta \tau} - 2 \frac{h\Delta x}{k} - 4 \right] T_{ij}^n \right\}
 \end{aligned} \tag{A1.13}$$

### 1.3 Natural Convection to Air for Case C

In Case C there is no insulation on the outside of the nozzle and vessel (see Fig.3.2.3) and therefore when the heat wave reaches the outside boundaries, heat is lost to the surrounding air by natural convection. Every precaution is taken during the experimental measurements of stresses not to create any air draughts near the specimen which will upset the condition of natural convection. During the transient period the heat lost to the gas is less than the heat input and the temperatures of the nodal points inside the wall will keep rising until steady state is reached. At steady state the heat input is equal to the heat lost to the gas plus the heat used to maintain the nodal temperatures of the structure at their steady state values. In order to determine the heat loss to the air the heat transfer coefficient  $h$  is determined for the vessel, junction and nozzle parts of the outside wall at the end of each time interval.

The equation of heat transfer for the vessel and junction wall for laminar flow (R.4-4) is given by:

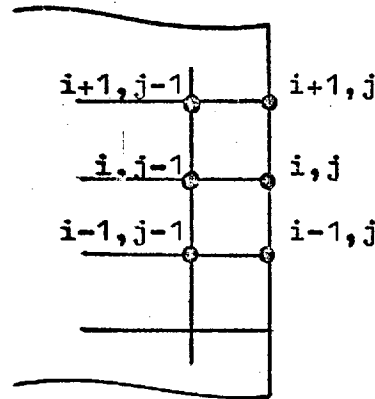
$$\frac{hL}{k_a} = 0.13 \left[ \frac{L^3 g \beta (T_w - T_\infty)}{\nu^2} (Pr) \right]^{0.33} \quad (A1.14)$$

where,  $L$  is the length of the vessel or junction wall,  $T_w$  is the wall temperature at the end of each time interval, and  $T_\infty$  is the air temperature ( $60^\circ\text{F}$ ). The temperature of the wall  $T_w$  is taken as the mean of all the nodal temperatures along the wall at the end of each time interval and the heat transfer coefficient thus obtained is the mean for the particular section of the wall under consideration.

For the vessel outside wall the equation is

$$\frac{hL}{k_a} = 0.54 \left[ \left( \frac{L^3 g \beta (T_w - T_\infty)}{\nu^2} \right) (Pr) \right]^{0.25} \quad (A1.15)$$

Again  $T_w$  is the mean temperature along the wall and  $h$  the mean coefficient for each particular time interval. Once the heat transfer coefficient  $h$  has been determined for each section of the outside wall the heat lost to the air by convection is calculated by considering the heat balance equation at the wall. This has as follows (figure below).



At the time interval  $n+1$  the heat conducted from point  $i, j-1$  to point  $i, j$  is equal to the heat used to raise the temperature of the wall at the point  $i, j$  plus the heat lost to the gas by convection. This happens for every nodal point of the structure near the inside wall.

Now the heat conducted from point  $i, j-1$  to point  $i, j = -k \frac{\Delta x}{\Delta y} (T_{i,j} - T_{i,j-1})$ . The heat which is used to raise the temperature of the wall by  $\Delta T = \rho_s C_s \Delta x \Delta y \Delta T$ . The heat lost to the air  $= h \Delta x (T_{i,j} - T_\infty)$ . Therefore the equation of heat balance will be:

$$-k \frac{\Delta x}{\Delta y} (T_{i,j} - T_{i,j-1}) = \rho_s C_s \Delta x \Delta y \Delta T + h \Delta x (T_{i,j} - T_\infty)$$

or since  $\Delta x = \Delta y$

$$-k (T_{i,j} - T_{i,j-1}) = \rho_s C_s (\Delta x)^2 \Delta T + h \Delta x (T_{i,j} - T_\infty) \quad (A1.16)$$

From this last equation  $\Delta T$  can be calculated for the time interval  $n+1$ . Nevertheless in the computation of the temperatures at the nodal points on the outside wall an approximation has to be made. The temperature of each node on the outside wall  $T_{i,j}$  at the time interval  $n$  is taken as equal to the temperature of the previous node  $T_{i,j-1}$  of the same time interval. This is an approximation which is necessary in order to establish some value for the wall temperature which will enable us to calculate  $h$ . The real value of the wall temperature at the new time interval  $n+1$  will therefore be

$$T_{i,j}^{n+1} = T_{i,j}^n - \Delta T \quad (\text{A1.17})$$

This is done for all the nodal points on the outside wall. The new heat transfer coefficient is then calculated at  $n+1$  time using the new wall temperature  $T_{i,j}^{n+1}$ . This new coefficient is used to obtain the wall temperature at time  $n+2$  and so on. A truncation error exists here since the wall temperature at any time increment is calculated using the heat transfer coefficient which is obtained by using the wall temperature at the previous time increment. This error is unavoidable because in the unsteady state, when temperature changes continuously with time, the heat transfer coefficient is a function of the wall temperature and the wall temperature cannot be calculated if the heat transfer coefficient is not known. Nevertheless the error is very small for small time increments used in this analysis.

## APPENDIX 2

---

# Transient Thermal Analysis for Spherical Vessels

---

### 2.1 Introduction

It was explained in Chapter 4 that the analysis for the determination of thermal distributions and stresses applied in the case of cylindrical vessels may be equally applied for spherical vessels. This is when the diameter of the spherical vessel is large and the curvature can be neglected. In here a method of determining the thermal distributions for spherical vessel where the curvature is taken into account is developed. The two-dimensional transient heat conduction problem is solved by the finite element method.

The finite element method was first applied by Wilson and Nickell (R.A2-1). Their method for analysing the unsteady flow of heat was based on the variational principle of Gurtin (R.A2-2). Richardson and Shunn (R.A2-3) used the same variational principle and the finite element method to solve transient heat conduction problems involving non-linear boundary conditions. Emery and Carson (R.A2-4) and Visser (R.A2-5) used the variational formulations in their finite element method applied to transient heat conduction problems. Zienkiewicz (R.A2-6), Desai and Abel (R.A2-7) have also used the finite element method for determination of two-dimensional heat conduction problems.

## 2.2 Theoretical Formulation of the Finite Element Method

The two-dimensional heat conduction equation which describes the unsteady temperature distribution in a solid which is in a domain P (Fig.A2.2.1) is given by the equation below:

$$\frac{\partial}{\partial x} \left( k_x \frac{\partial T}{\partial x} \right) + \frac{\partial}{\partial y} \left( k_y \frac{\partial T}{\partial y} \right) + Q = \rho c \frac{\partial T}{\partial \tau} \quad (\text{A2.2.1})$$

The equation subject to the conditions on the boundary surface  $S_1$

$$T = T_s \text{ on } S_1 \quad (\text{A2.2.2})$$

$$- k_x \frac{\partial T}{\partial x} \ell_x - k_y \frac{\partial T}{\partial y} \ell_y = q \text{ on } S_2 \quad (\text{A2.2.3})$$

$$- k_x \frac{\partial T}{\partial x} \ell_x - k_y \frac{\partial T}{\partial y} \ell_y = h (T - T_\alpha) \text{ on } S_3 \quad (\text{A2.2.4})$$

The initial condition is

$$T(x,y,0) = T_0(x,y) \quad (\text{A2.2.5})$$

- where  $S = S_1 + S_2 + S_3$
- $S_1$  = the part of the boundary on which T is prescribed
  - $S_2$  = the part of the boundary on which q is prescribed (the intensity of heat input)
  - $S_3$  = the part of the boundary on which  $h(T - T_\alpha)$  is prescribed
- $T(x,y,\tau)$  = temperature in the solid
- $k_x$  &  $k_y$  = thermal conductivities
- $x,y$  = principal directions of the conductivity tensor
- $c$  = specific heat
- $\rho$  = density
- $Q$  = externally applied heat flux
- $T_s$  = boundary surface temperature
- $T_0$  = initial temperature

$l_x$   
 $l_y$  } = direction cosines of the outward normal  
to the boundary surface

$h$  = heat transfer coefficient

$T_\alpha$  = temperature of the surrounding



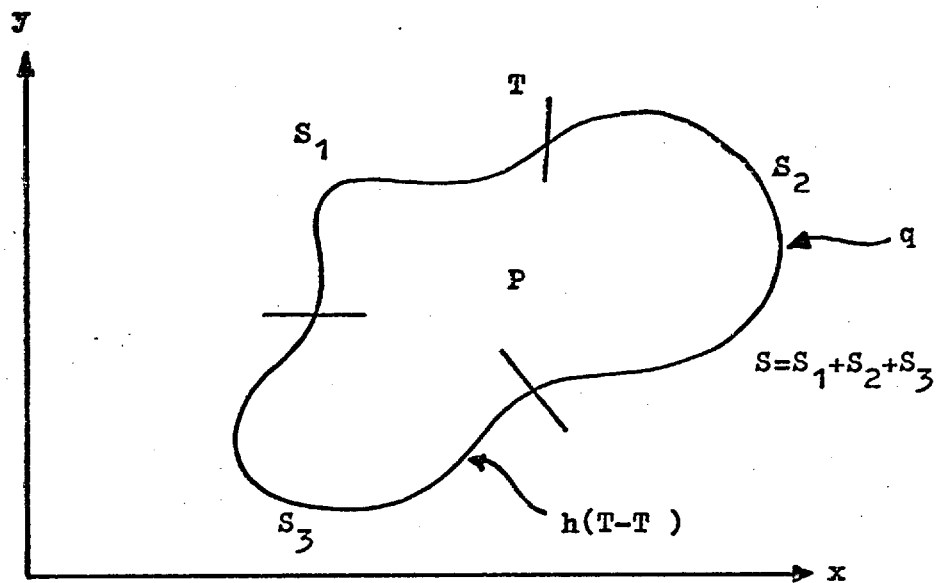


FIG.A2.2.1 P domain governed by Equation (A2.2.1)

Fig.A2.2.2 shows the P domain divided into finite elements in space and time.

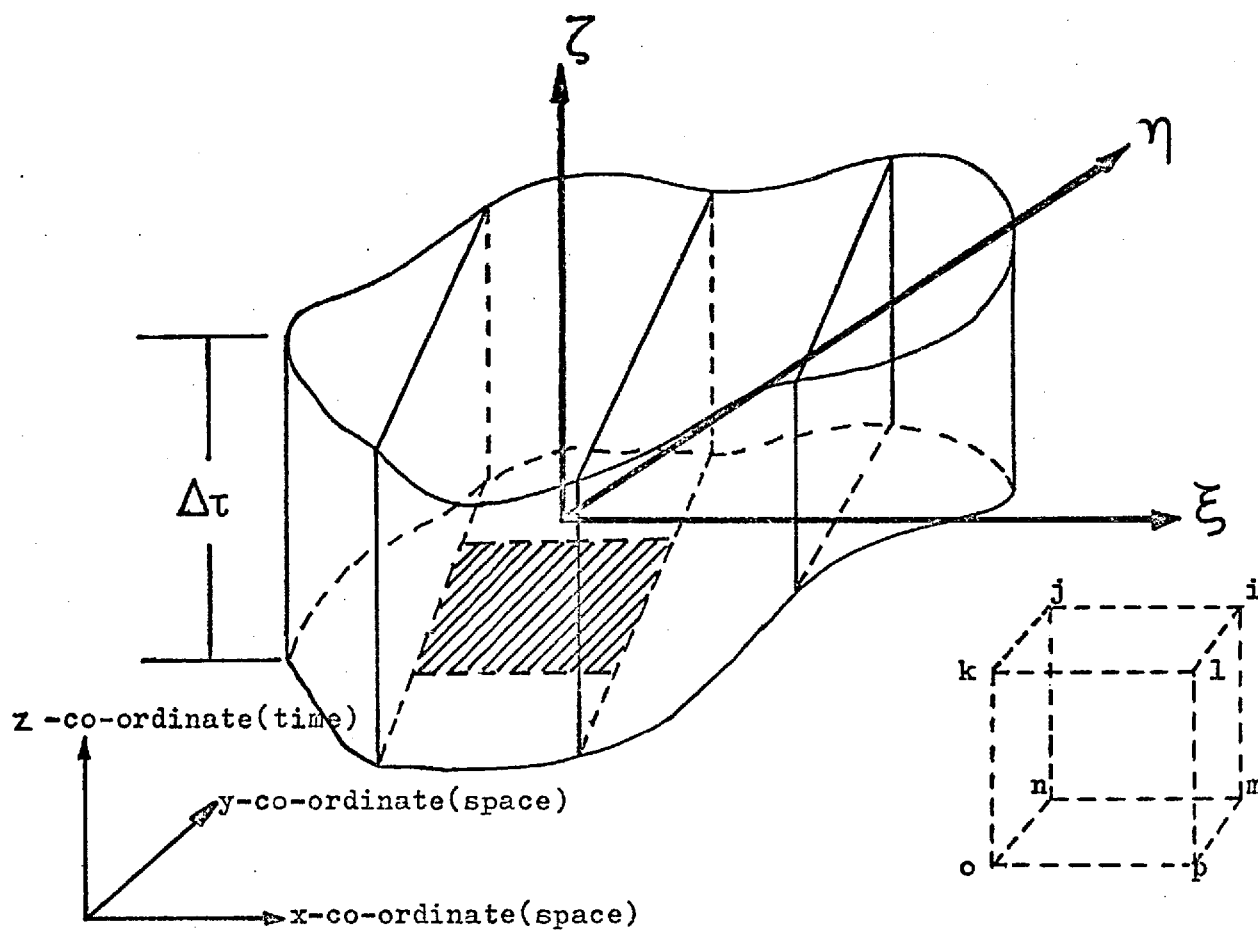


FIG.A2.2.2

The temperature within each element is approximated by

$$T(x, y, \tau) = \sum_{I=1}^{nnp} N_I(x, y, \tau) T_I$$

where,

$N_I$  = the shape functions defined element by element

$I$  = summation subscript

$T_I$  = nodal temperature representation of  $T(x, y, \tau)$

$nnp$  = number of nodes in an element

Using the weighted residual process in which the weighting function is equal to the shape function defining the approximation within the elements, the heat conduction equation

(A2.2.1) becomes,

$$\int_P N_I \left[ \frac{\partial}{\partial x} \left( k_x \frac{\partial T}{\partial x} \right) + \frac{\partial}{\partial y} \left( k_y \frac{\partial T}{\partial y} \right) + Q - \rho c \frac{\partial T}{\partial \tau} \right] dP = 0 \quad (A2.2.6)$$

where,  $P$  is the finite element domain and  $dP = dx dy d\tau$ .

Integrating by parts on the first and second terms in the equation above is simplified to

$$\begin{aligned} & - \iint \left[ k_x \frac{\partial N_I}{\partial x} \frac{\partial T}{\partial x} + k_y \frac{\partial N_I}{\partial y} \frac{\partial T}{\partial y} - N_I Q + N_I \rho c \frac{\partial T}{\partial \tau} \right] dP \\ & - \int_{S_2} N_I q dS_2 - \int_{S_3} N_I h (T - T_a) dS_3 = 0 \end{aligned} \quad (A2.2.7)$$

where  $S_2$  and  $S_3$  are defined in Fig.A2.2.1.

Using the equation for the temperature approximation within each element the  $I^{\text{th}}$  equation of the system that will allow the solution for the  $n$  values of  $T_I$  is

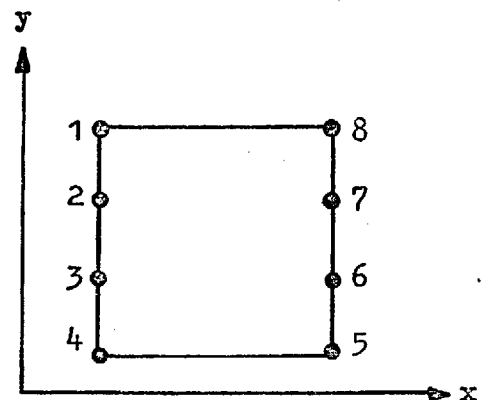
$$\begin{aligned}
 & - \int_P \left[ k_x \frac{\partial N_I}{\partial x} \frac{\partial}{\partial x} \left( \sum_1^n N_I T_I \right) + k_y \frac{\partial N_I}{\partial y} \frac{\partial}{\partial y} \left( \sum_1^n N_I T_I \right) \right. \\
 & \left. - N_I Q + N_I \rho c \frac{\partial}{\partial t} \left( \sum_1^n N_I T_I \right) \right] dx dy \\
 & - \int_{S_2} N_I q dS_2 - \int_{S_3} N_I \left( \sum_1^n N_I T_I - T_\alpha \right) S_3 = 0
 \end{aligned} \tag{A2.2.8}$$

Therefore the system consists of n linear algebraic equations in n unknowns.

2.3 Rectangular Prism (x,y,\tau). Element Shape Functions

The rectangular prism is used to represent the three dimensional element (Fig.A2.2.2). Co-ordinates x,y are space co-ordinates while \tau is the time co-ordinate. In order to establish the shape functions for a rectangular prism, the rectangular 12345678 is first considered shown below.

Let the shape function \phi be expressed in a polynomial form in x and y. In order to ensure inter-element continuity of \phi along the top and bottom sides the variation must be linear. The eight nodal points are to be determined and thus:



$$\phi = a_1 + a_2 x + a_3 y + a_4 xy + a_5 y^2 + a_6 xy^2 + a_7 y^3 + a_8 xy^3$$

Substituting co-ordinates of the various nodes a set of simultaneous equations is written in a matrix form

$$\begin{bmatrix} \phi_1 \\ \vdots \\ \phi_8 \end{bmatrix} = \begin{bmatrix} 1, x_1, y_1, x_1 y_1, y_1^2, x_1 y_1^2, y_1^3, x_1 y_1^3 \\ \dots \\ \dots \\ \dots \end{bmatrix} \begin{bmatrix} \alpha_1 \\ \vdots \\ \alpha_8 \end{bmatrix} \tag{A2.3.1}$$

or

$$\begin{bmatrix} \phi \end{bmatrix}^e = \begin{bmatrix} c \end{bmatrix} \begin{bmatrix} \alpha \end{bmatrix} \quad (\text{A2.3.2})$$

Equation (A2.3.1) can then be written

$$\phi = \begin{bmatrix} P \end{bmatrix} \begin{bmatrix} \alpha \end{bmatrix} = \begin{bmatrix} P \end{bmatrix} \begin{bmatrix} c \end{bmatrix}^{-1} \begin{bmatrix} \phi \end{bmatrix}^e \quad (\text{A2.3.3})$$

$$\text{where } \begin{bmatrix} P \end{bmatrix} = \begin{bmatrix} 1, x, y, xy, y^2, xy^2, y^3, xy^3 \end{bmatrix} \quad (\text{A2.3.4})$$

Therefore the shape functions for the elements defined by

$$\phi = \begin{bmatrix} N \end{bmatrix} \begin{bmatrix} \phi \end{bmatrix}^e = \begin{bmatrix} N_1 N_2 \dots N_8 \end{bmatrix} \begin{bmatrix} \phi \end{bmatrix}^e \quad (\text{A2.3.5})$$

$$\text{and hence } \begin{bmatrix} N \end{bmatrix} = \begin{bmatrix} P \end{bmatrix} \begin{bmatrix} c \end{bmatrix}^{-1} \quad (\text{A.2.3.6})$$

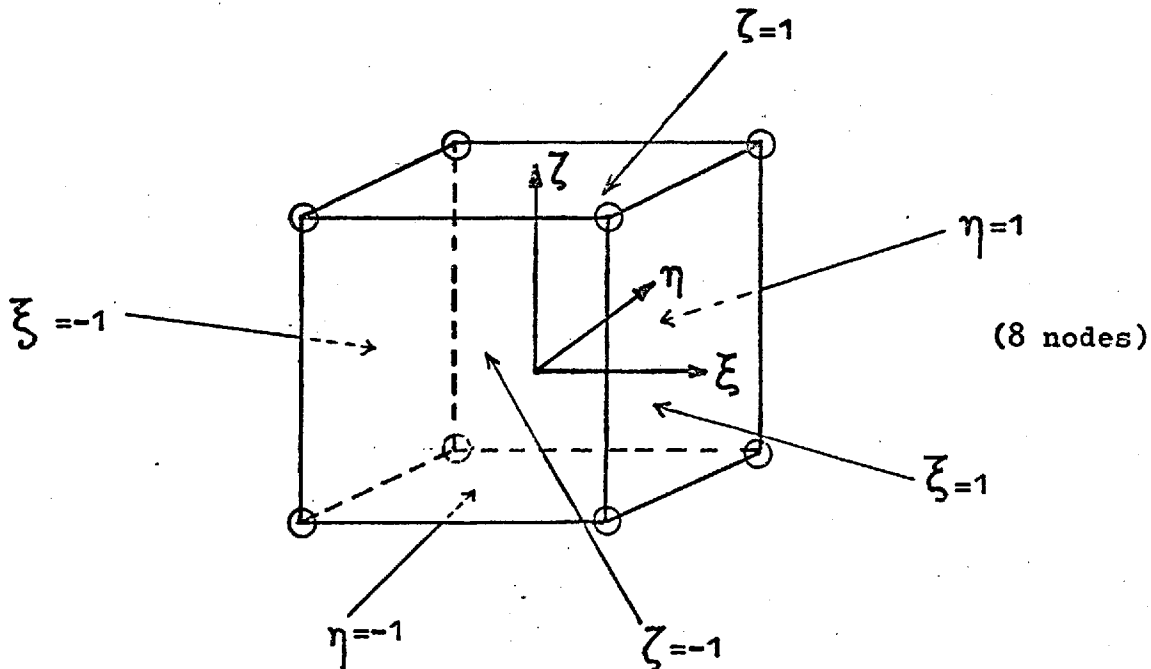
It is more convenient to use normalised co-ordinates and these are so chosen that on the faces of the rectangle their values are  $\pm 1$ .

$$\begin{aligned} \xi &= (x - x_c)/a, & d\xi &= dx/a \\ \eta &= (y - y_c)/b, & d\eta &= dy/b \end{aligned} \quad (\text{A2.3.7})$$

where  $a$  and  $b$ , the length of the sides of the rectangle. Once the shape functions are known in the normalised co-ordinates translation into actual co-ordinates can be carried out.

#### 2.4 Three Dimensional Element. Rectangular Prism

As it has already been explained the three dimensional rectangular prism is used for the element discretization of the structure. This is shown in the figure below (linear element with 8 nodes).



The shape function is thus given by

$$N_i = \frac{1}{8}(1 + \xi_o)(1 + \eta_o)(1 + \zeta_o) \quad (\text{A2.4.1})$$

where

$$\xi_o = x_c/a$$

$$\eta_o = y_c/b$$

$$\zeta_o = z_c/c$$

and  $x_c, y_c, z_c$  the co-ordinates of the centroid and  $a, b, c$  the dimensions of the element.

## 2.5 Numerical Solution of the Thermal Distribution

The section of nozzle-vessel is shown in Fig.A2.5.1(a).

The solid is symmetrical about axis  $xx'$  and  $yy'$ . In Fig.A2.5.1(b) the finite element grid is shown. This divides the structure into 426 elements. Since values of the element temperatures are known at  $\tau_o$  values at  $\tau_1 = \tau_o + \Delta\tau$  can be obtained by summing around the nodes at this latter step, an identical procedure is used until a required time is reached.

The temperature approximation for each element using rectangular prisms as the elements and linear shape functions as it was explained in Section 2.4, is as follows.

$$\begin{aligned}
T(x,y,\tau) &= \frac{1}{8} (1 + \xi) (1 + \eta) (1 + \zeta) T_i \\
&+ \frac{1}{8} (1 - \xi) (1 + \eta) (1 + \zeta) T_j \\
&+ \frac{1}{8} (1 - \xi) (1 - \eta) (1 + \zeta) T_k \\
&+ \frac{1}{8} (1 + \xi) (1 - \eta) (1 + \zeta) T_l \\
&+ \frac{1}{8} (1 + \xi) (1 + \eta) (1 - \zeta) T_m \\
&+ \frac{1}{8} (1 - \xi) (1 + \eta) (1 - \zeta) T_o \\
&+ \frac{1}{8} (1 + \xi) (1 - \eta) (1 - \zeta) T_p \\
&= N_i T_i + N_j T_j + N_k T_k + N_m T_m + N_n T_n + N_o T_o + N_p T_p
\end{aligned}$$

where  $\xi = 2(x - x_c)/(\Delta x)$

$$\eta = 2(y - y_c)/(\Delta y)$$

$$\zeta = 2(\tau - \tau_c)/(\Delta \tau)$$

$x_c, y_c, \tau_c$  = co-ordinates of the centroid of each element.

$T_i, T_j, T_k, T_l, T_m, T_n, T_o, T_p$  = values of temperatures at the appropriate nodal points.

$N_i, N_j, N_k, N_l, N_m, N_n, N_o, N_p$  = shape functions

$x$  =  $x$  co-ordinate spacing

$y$  =  $y$  co-ordinate spacing

$i, j, k, l, m, n, o, p$  = node numbers

## 2.6 Boundary Conditions

At time  $\tau = 0$  the structure is at room temperature of  $60^\circ\text{F}$ . Boundaries BCDE and AG are insulated (Fig.A2.5.2), thus making the heat gradient zero.

Fluid enters at temperature  $T_f = 450^\circ\text{F}$  and heat input  $q$  is provided along the boundary GF. Temperature of fluid is maintained steady at  $450^\circ\text{F}$  along GF. Small fluctuations will not affect the thermal distribution within the solid and the temperature of the inside surface of the nozzle is assumed to be at  $450^\circ\text{F}$ .

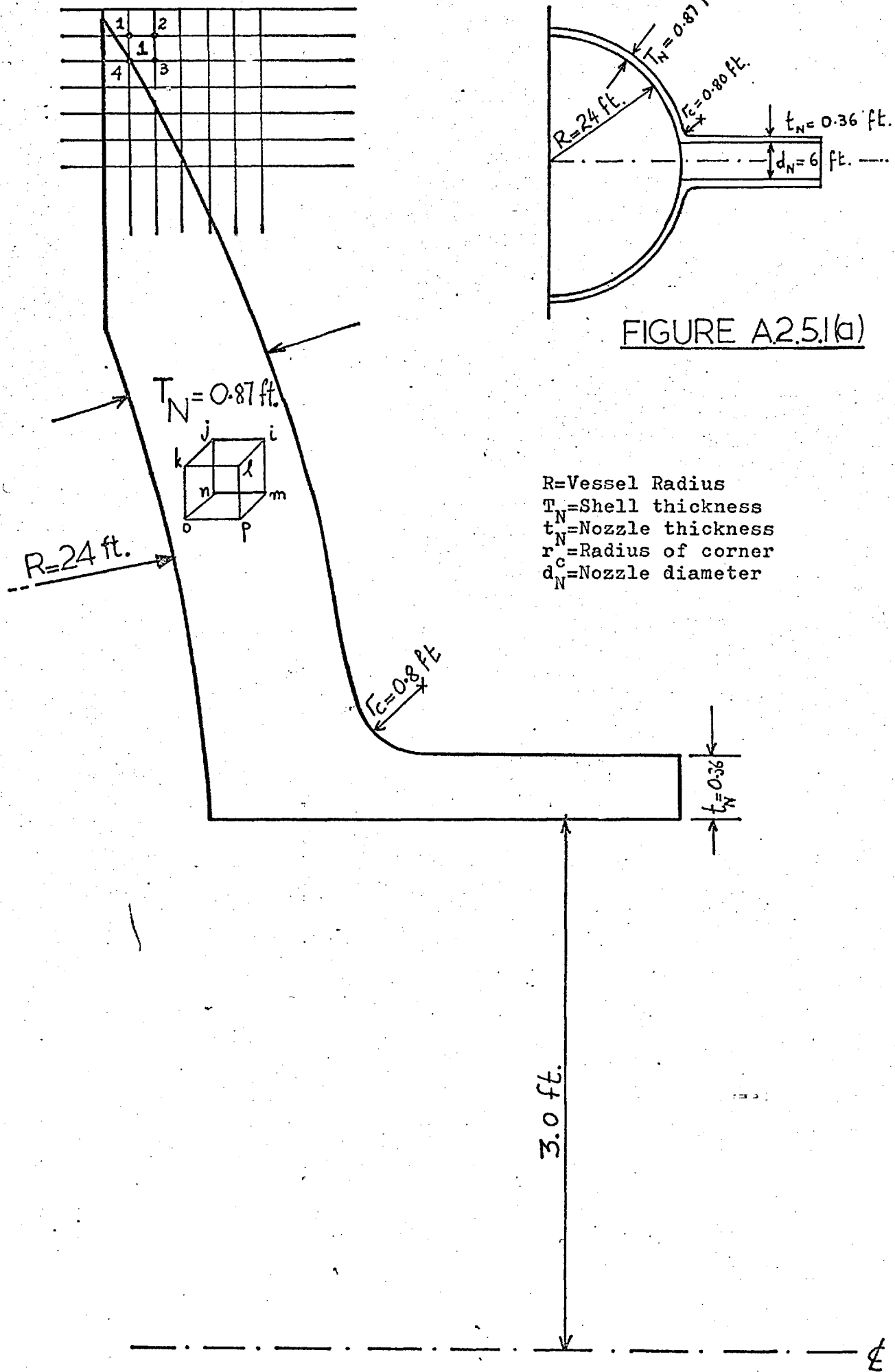


FIGURE A2.5.1(b)

$R$ =Vessel Radius  
 $T_N$ =Shell thickness  
 $t_N$ =Nozzle thickness  
 $r_N$ =Radius of corner  
 $d_N^c$ =Nozzle diameter

FIGURE A2.5.1(b) FINITE ELEMENT MESH

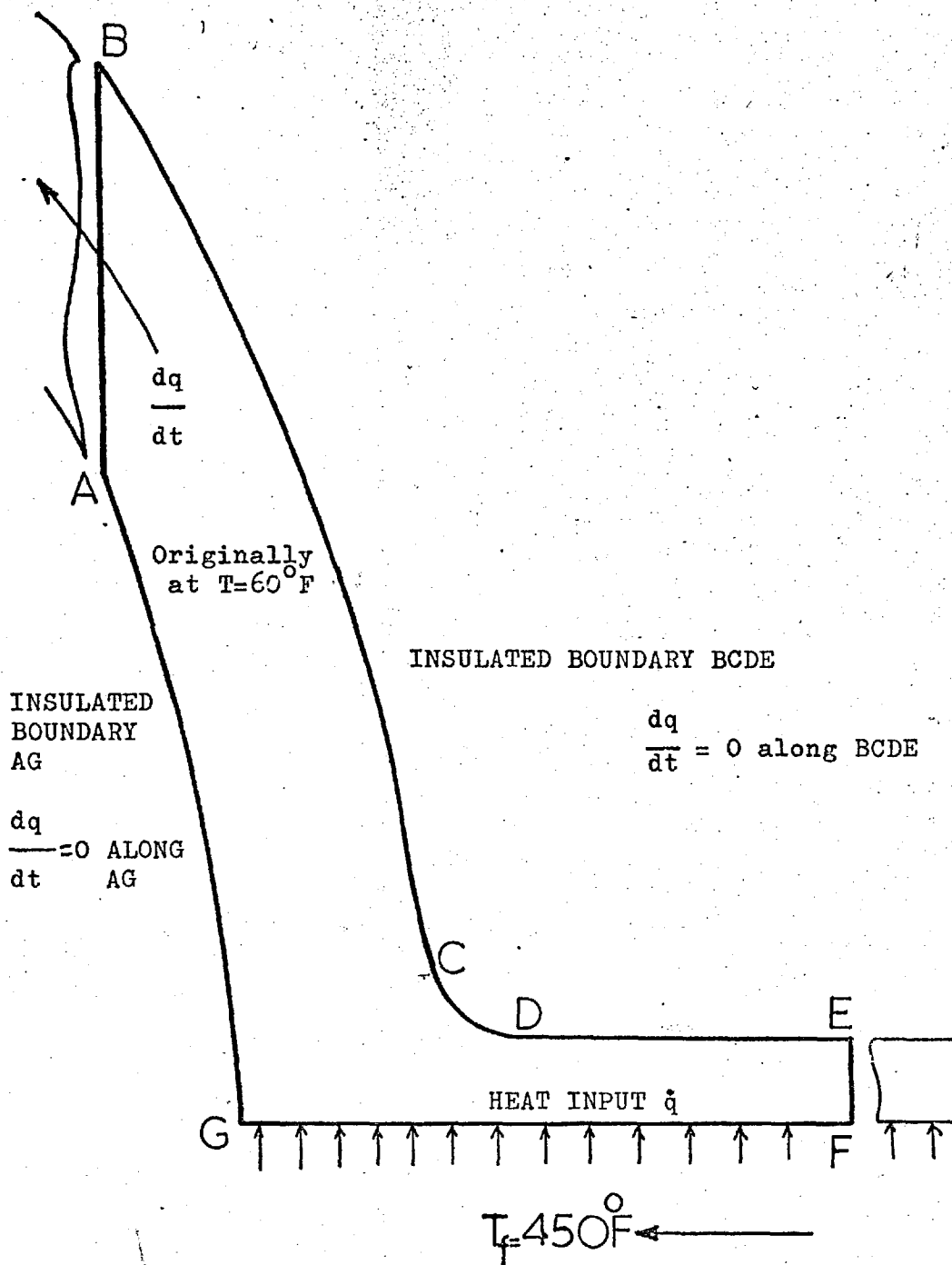


FIGURE A2.5.2



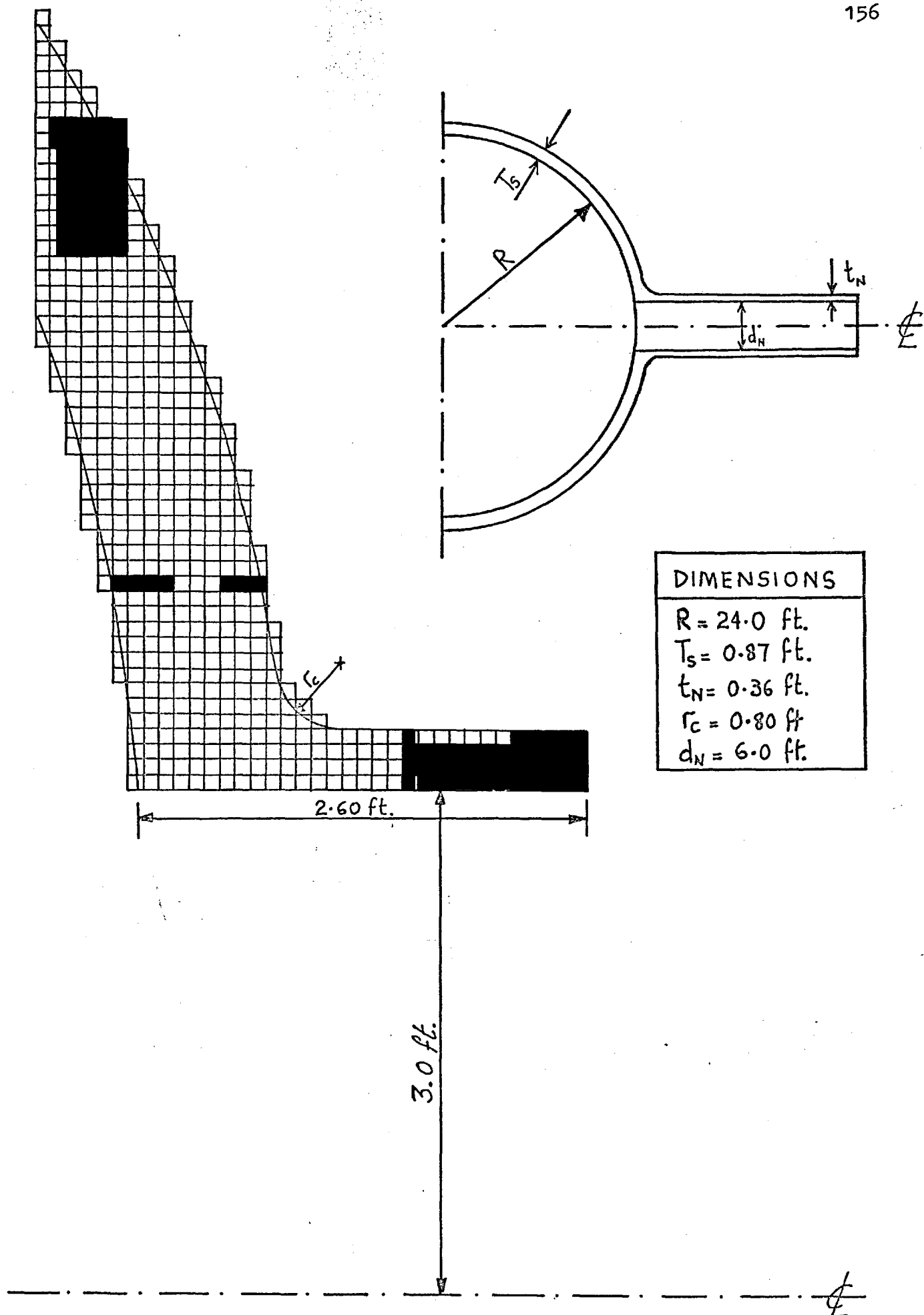


FIGURE A2.5.3 FINITE ELEMENT MESH

2.7 Computer Program TEFEL

The program is determining the temperature distribution at prescribed time intervals. Element and nodal temperatures are recorded every 3.0 minutes. The time increments may be increased or decreased to any value.

The variable data and main parameters in program TEFEL are designated as follows:

- is integer single
- ia integer array
- rs real single
- ra real array

Dimensions of the sections are in feet.

- TEL ra temperature of the element
- TEN ra temperature of nodes
- NPI ia
- NPJ ia
- NPK ia
- NPM ia
- X ra x-co-ordinate of node
- y ra y-co-ordinate of node
- TFL rs temperature of fluid
- TR rs temperature of structure at time = 0.0
- MAXIT is number of gaussian iterations
- TIME rs time interval
- TT rs time spacing
- NEL ia number of elements
- NNP ia number of nodes
- L1 } is working variables referring to elements
- L2 }
- L3 }

N1 }  
 N2 } is working variables referring to nodes  
 N3 }  
 XC rs X co-ordinate of the centroid of element  
 YC rs Y co-ordinate of the centroid of element  
 X1 rs X co-ordinate of point within element  
 Y1 rs Y co-ordinate of point within element  
 XXX }  
 YYY } rs working variables  
 XX X-spacing ( $\Delta x$ )  
 YY rs Y-spacing ( $\Delta y$ )  
 SNI }  
 SNJ } rs shape functions  
 SNK }  
 SNM }  
 ITN rs iteration index  
 SUM rs iteration summation index  
 G rs Gaussian iteration variable  
 SFT rs time shape function  
 L8 }  
 L9 } is working variables referring to input data  
 NNI }  
 NNJ } ia index of node adjacent to node  
 NNK }  
 NNM }

The listing of the program is given in the next page.

```

PROGRAM TEFEL(INPUT,OUTPUT,TAPE5=INPUT,TAPE6=OUTPUT)
COMMON TEL(451), TEN(515),
1 NPI(451), NPJ(451), NPK(451), NPM(451),
2 X(515), Y(515), X1(451), Y1(451),
3 NNI(515), NNJ(515), NNK(515), NNM(515) ,
4 SYMBOL(51), SG(41), TELL(22,41)
COMMON BLANK
C READ GRAPING SYMBOLS AND BLANKS
708 READ (5,7) (SYMBOL(J), J=1,51), BLANK
FORMAT(52A1)
DO 232 I=1,22
DO 232 J=1,41
232 TELL(I,J)=0
C DEFINE CONSTANTS AND PARAMETERS
TFL=450.
TR=60.
XX=0.5
YY=0.5
MAXIT=50
TIME=0.0
TT=0.0
NEL=451
NMP=515
C READ ELEMENTS
8 READ(5,8) (LE,NPI(LE),NPJ(LE),NPK(LE),NPM(LE),L=1,NEL)
FORMAT(5I5)
C READ NODES
C READ NODE CO-ORDINATES
10 READ(5,10) (NP,NNI(NP),NNJ(NP),NNK(NP),NNM(NP),X(NP),Y(NP),N=1,NNP)
FORMAT(5I5,2F5.4)
C PERFORM INITIAL DISTRIBUTION OF TEMPERATURE AT TIME=0.0 MIN.
C DEFINE BOUNDARY AND INTERIOR NODES AND ELEMENTS
C ELEMENTS EXTERIOR
C L1=17
C L2=24
C DO 2 L=L1,L2
C TEL(L)=TFL
C 2 CONTINUE
C ELEMENTS INTERIOR
C L3=1
C DO 3 L=L3,NEL
C TEL(L)=TR
C 3 CONTINUE
C NODES EXTERIOR
C N1=64
C N2=93
C DO 4 N=N1,N2
C TEN(N)=TFL
C 4 CONTINUE
C NODES INTERIOR
C DO 511 N=1,53
C TEN(N)=TR
511 CONTINUE
C N3=94
C DO 5 N=N3,NNP
C TEN(N)=TR
5 CONTINUE
555 GO TO 33
CONTINUE
CALL DIN(TIME)
WRITE (6, 32)
82 FORMAT (1H1 //)
1 57X, 18HINPUT ELEMENT DATA /
2 57X, 18H----- //
3 3X, 40HELMT NPI NPJ NPK NPM TEMP
4 5X, 40HELMT NPI NPJ NPK NPM TEMP
5 6X, 29HELMT NPI NPJ NPK NPM TEMP //
L9 = (NEL + 2) / 3
DO 83 L8 = 1, L9
L3 = MIN0 (L8 + 2 * L9, NEL)
83 WRITE(6,84) (L,NPI(L),NPJ(L),NPK(L),NPM(L),TEL(L),L=L8,L3,L9)
84 FORMAT(1H,5I5,F6.1,15X,5I5,F6.1,15X,5I5,F6.1)
WRITE (6, 35) (N, NNI(N), NNJ(N), NNK(N), NNM(N), TEN(N), X(N), Y(N),
1 N=1, NNP)
85 FORMAT (1H1 //)
1 53X, 15HINPUT NODE DATA /
2 58X, 15H----- //
3 13X, 56HNODE NNI NNJ NNK NNM T5M7 X Y
4 (I16,X,4I5,F7.1,2E16.5)
C START PERFORMING TIME STEPS.
C TIME SHAPE FUNCTION IS DEFINED.

```



477 WRITE(6,477)  
FORMAT(5(/))

C  
C

882 I=22  
CONTINUE  
DO 883 J=1,41  
IF (TELL(I,J).EQ.0) GO TO 839  
K1=TELL(I,J)/9 +1  
IF (K1.GT.51) GO TO 889  
PLACE APPROPRIATE SYMBOL IN APPROPRIATE POSITION

C  
C  
C

GG(J)=SYMBOL(K1)  
GO TO 883  
889 GG(J)=BLANK  
883 CONTINUE  
891 CONTINUE  
PRINT PRGFILES

C  
C  
C

893 WRITE(6,893) GG  
FORMAT(45X,41A1)  
I=I-1  
IF (I.NE.0) GO TO 882  
RETURN  
END

## 2.8 Thermal Distribution Results

The thermal profiles are plotted for the section for every 3.0 minutes. Temperatures are in degrees  $^{\circ}$ F. The method of finite element is flexible and the temperatures can be calculated at any point within the elements by defining the x and y coordinates. This is not possible with the finite difference method where values can only be obtained at the nodal points of the grid, unless an extrapolation procedure is performed which is not very accurate. On the other hand finite difference method is computationally faster and converges faster too.

Once the temperatures are determined at any point defined by x-y, the stress can be calculated by the methods described in Chapter 5.

In the next pages the temperature distributions are shown for specified time intervals of 3.0 minutes for the first 15 minutes and at various time intervals up to 100 minutes when the structure attains uniform temperature of  $450^{\circ}$ F.

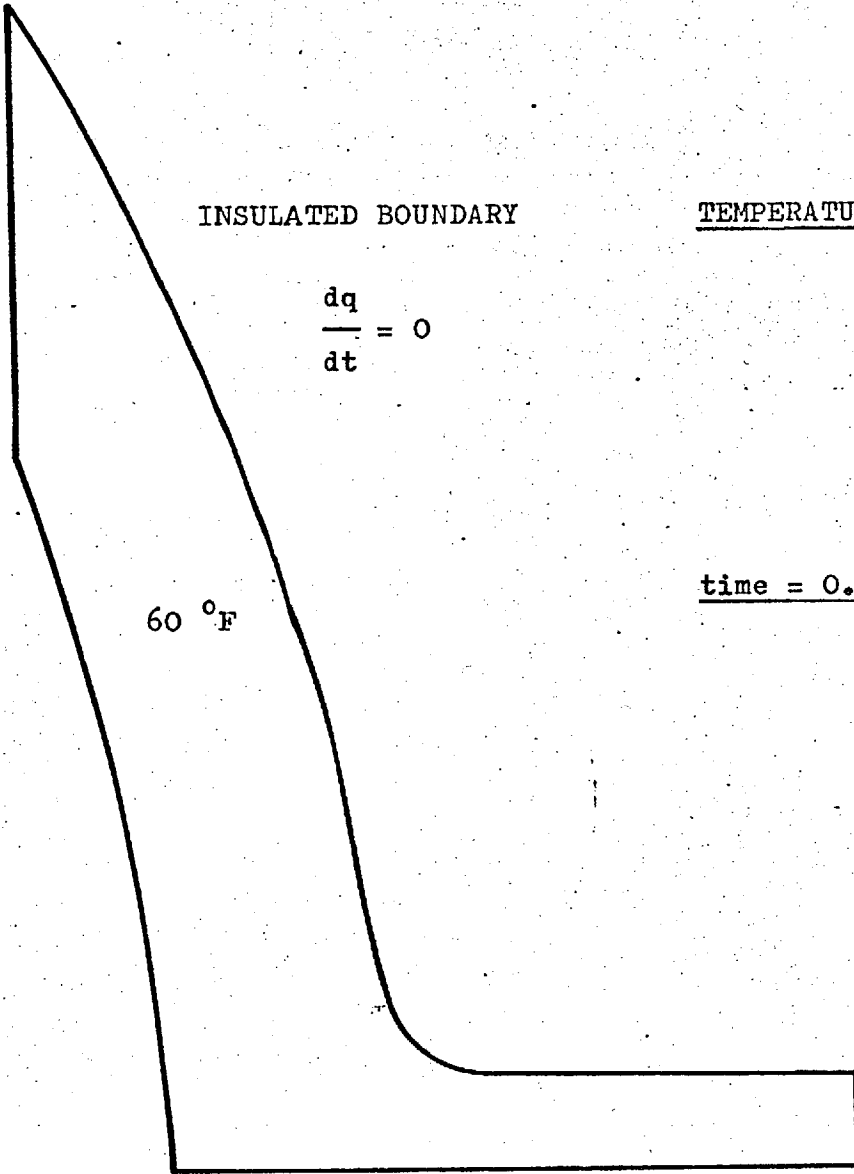
INSULATED BOUNDARY

TEMPERATURES IN DEGREES °F

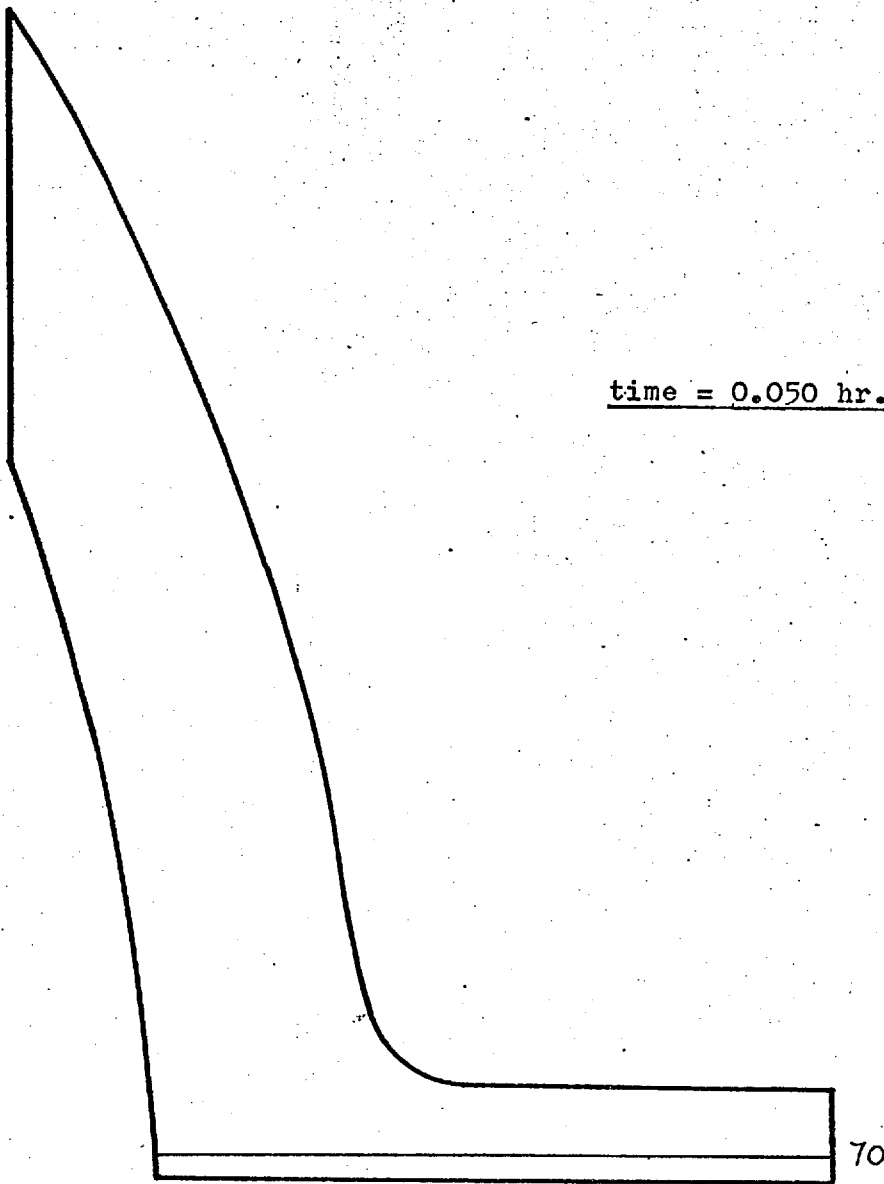
$$\frac{dq}{dt} = 0$$

time = 0.00 hr.

60 °F



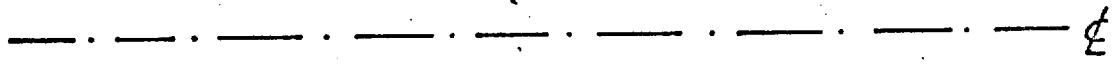
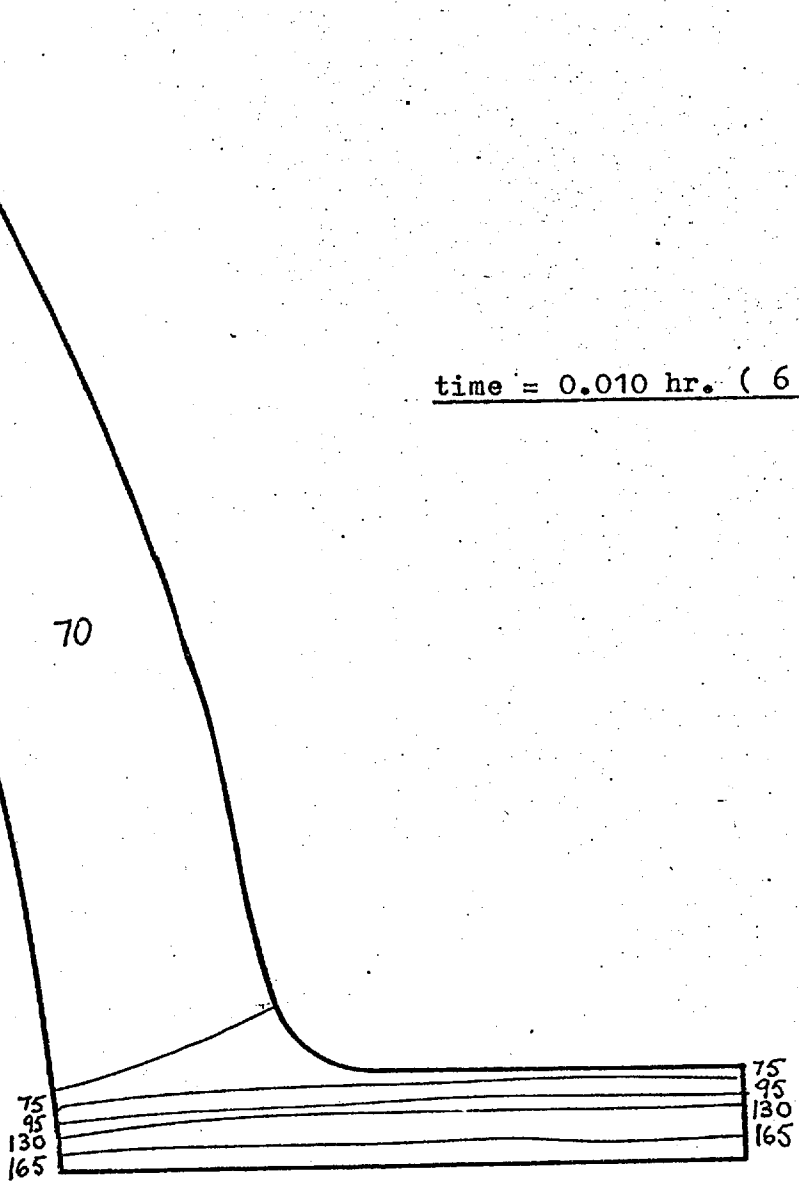




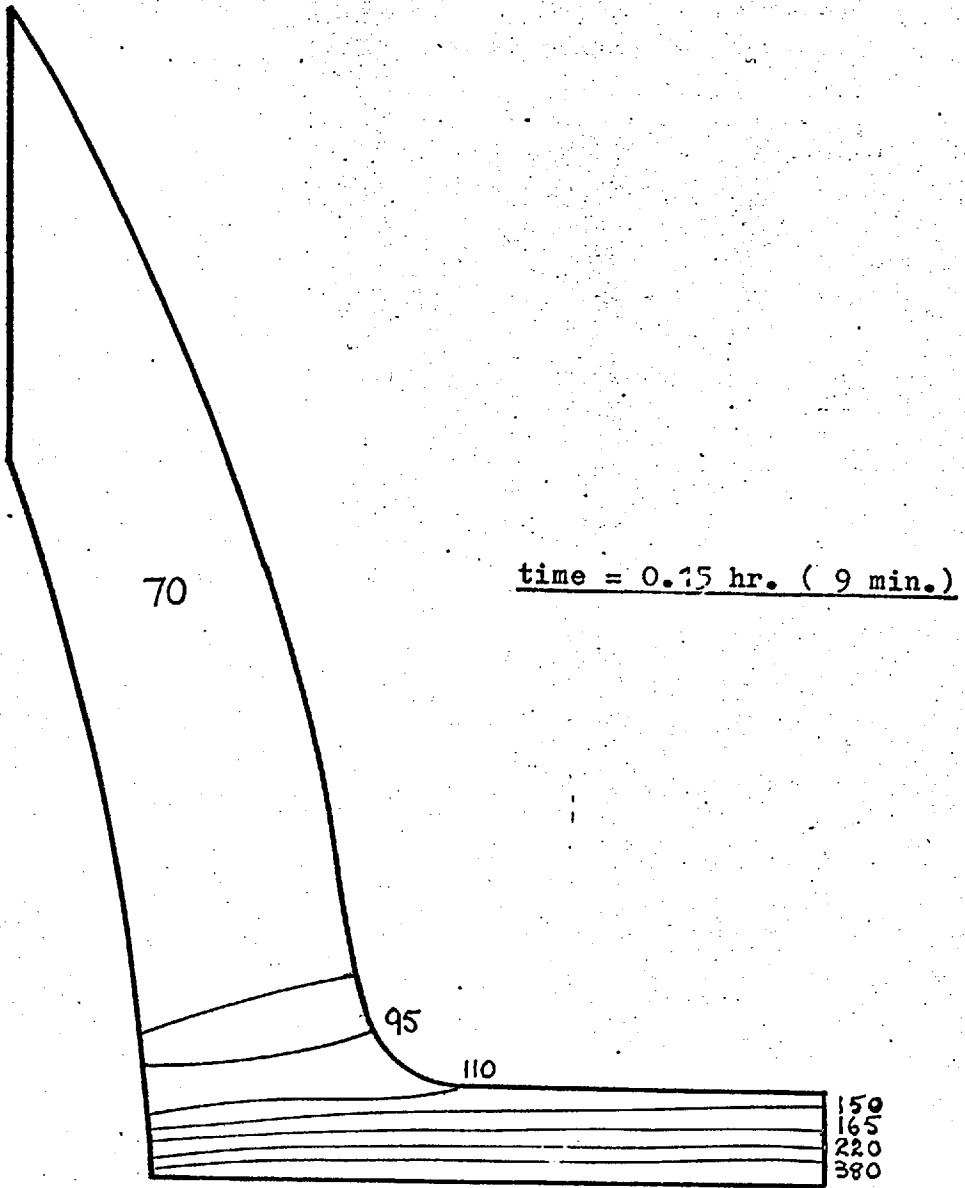
time = 0.050 hr. ( 3 min. )

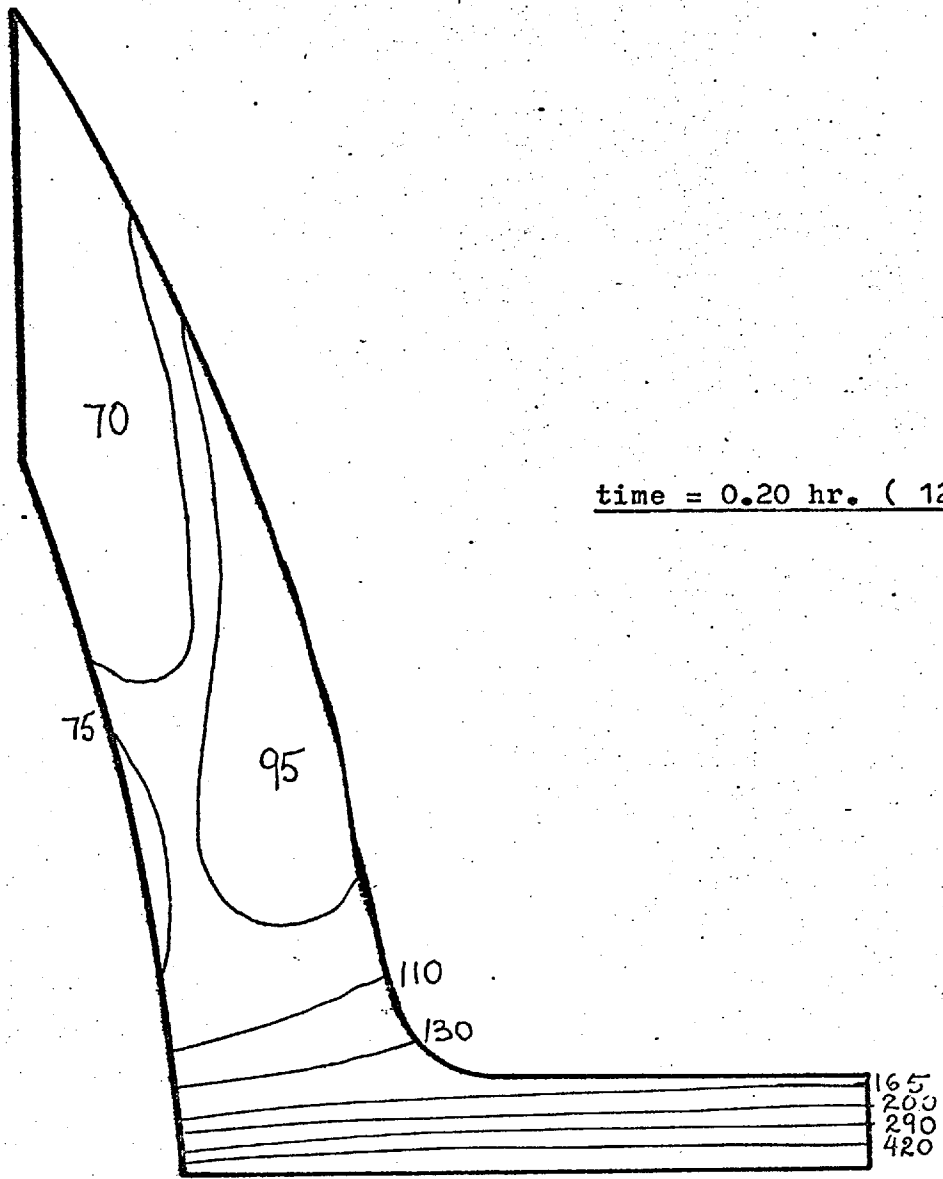
$T_f = 450 \text{ } ^\circ\text{F}$

time = 0.010 hr. ( 6 min.)

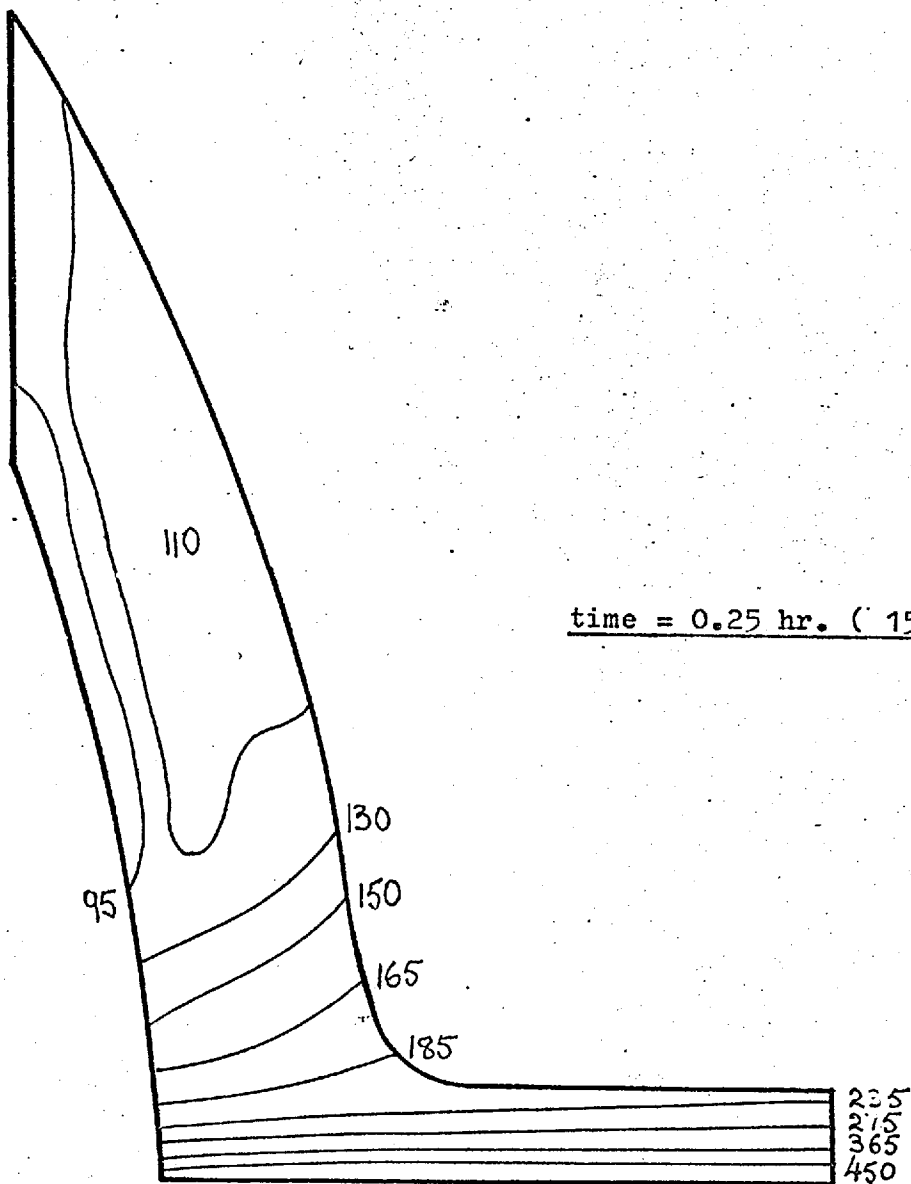


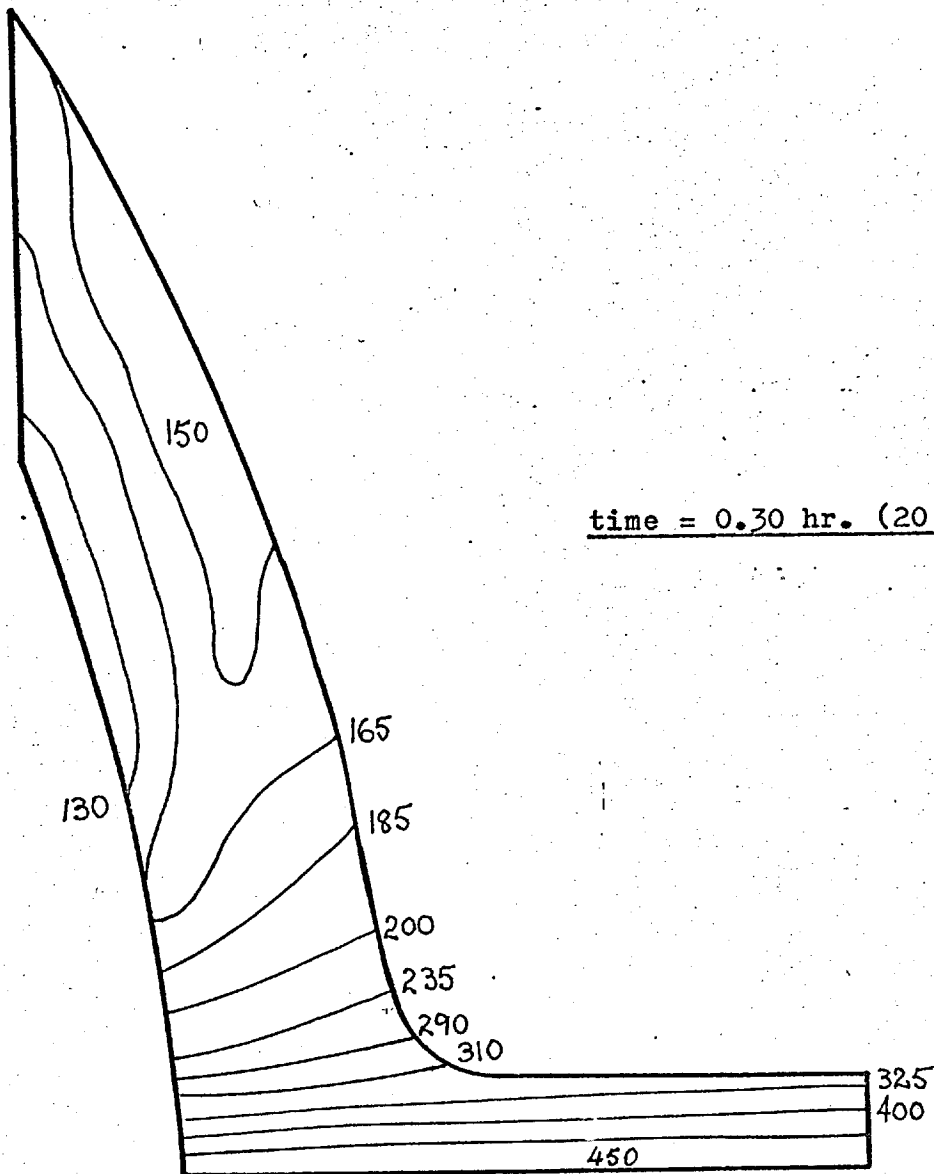
1

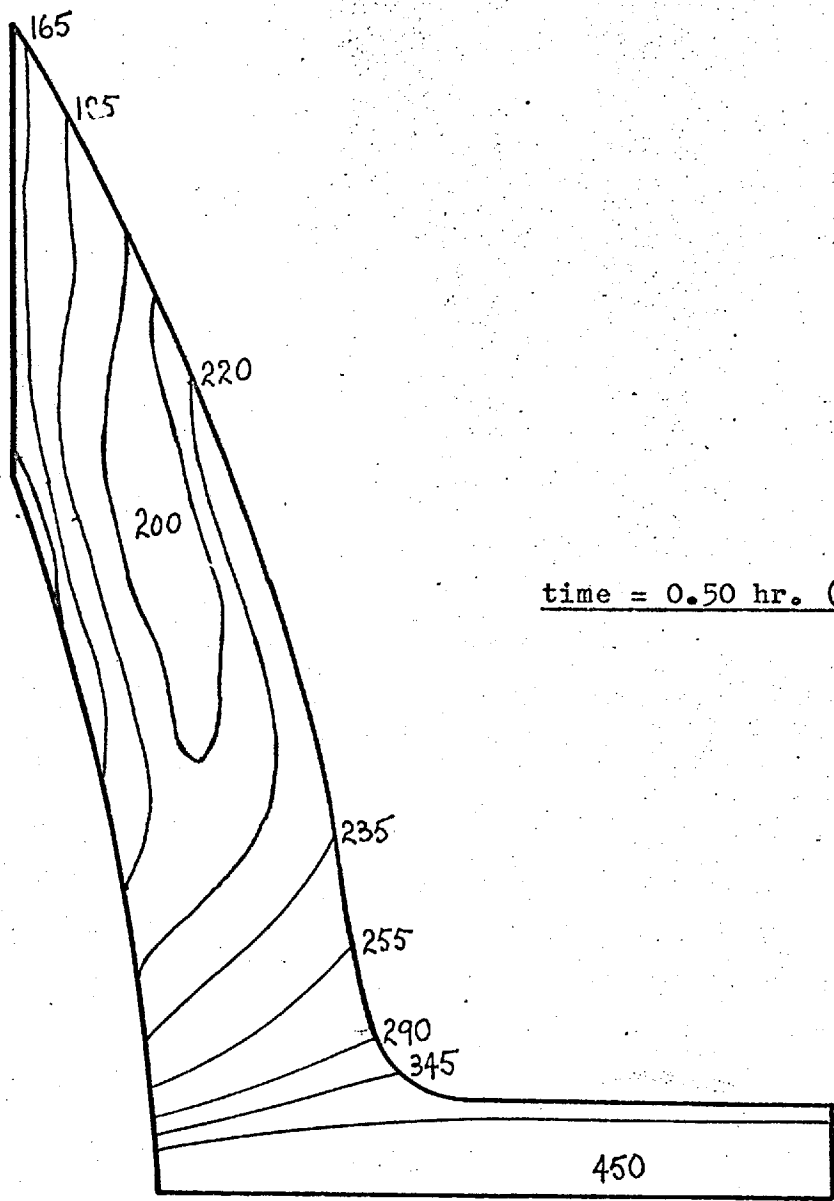




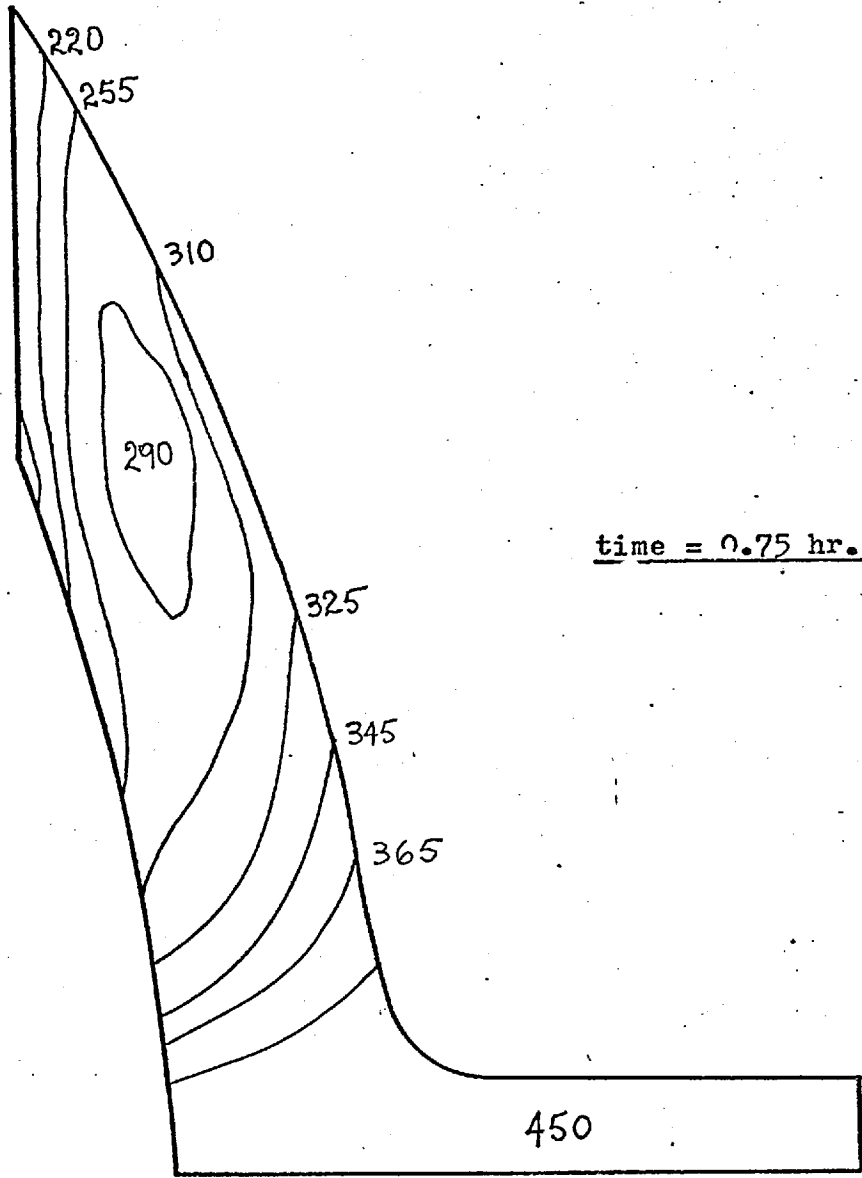
time = 0.20 hr. ( 12 min.)





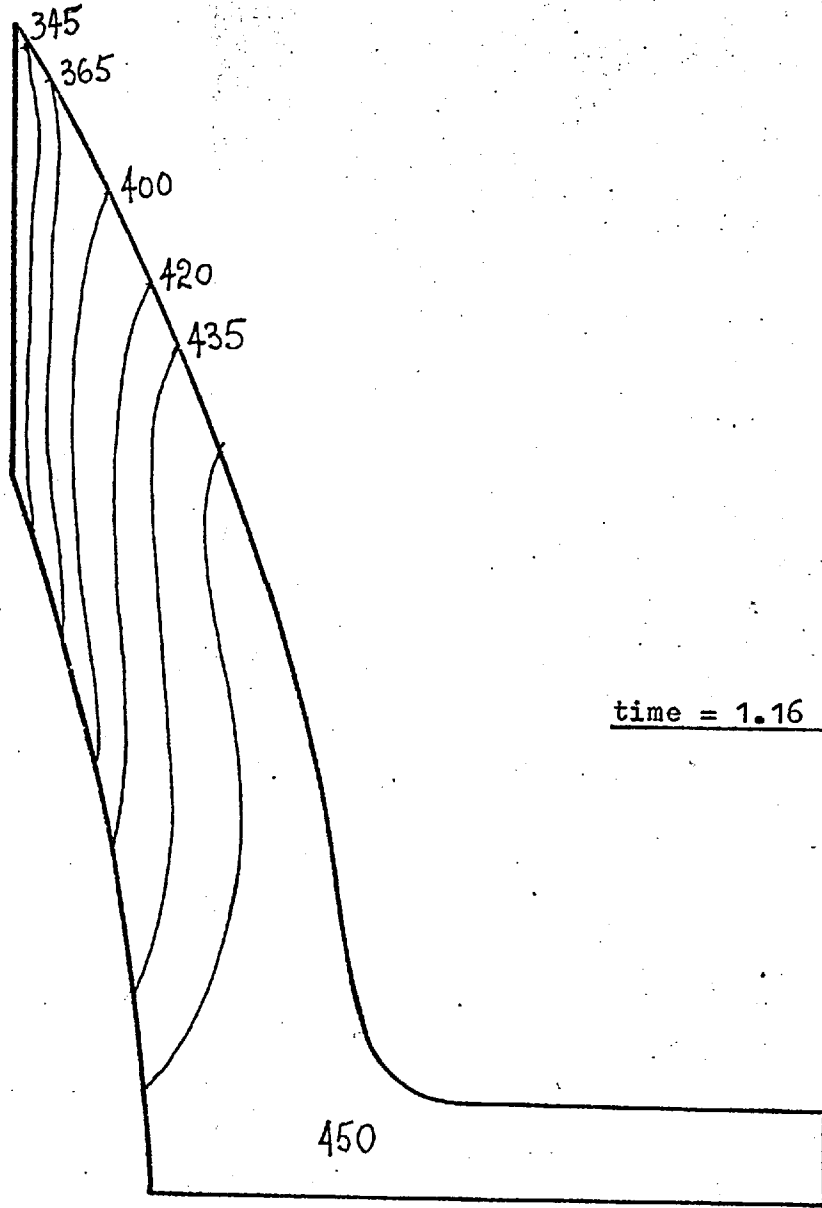


time = 0.50 hr. ( 30 min.)

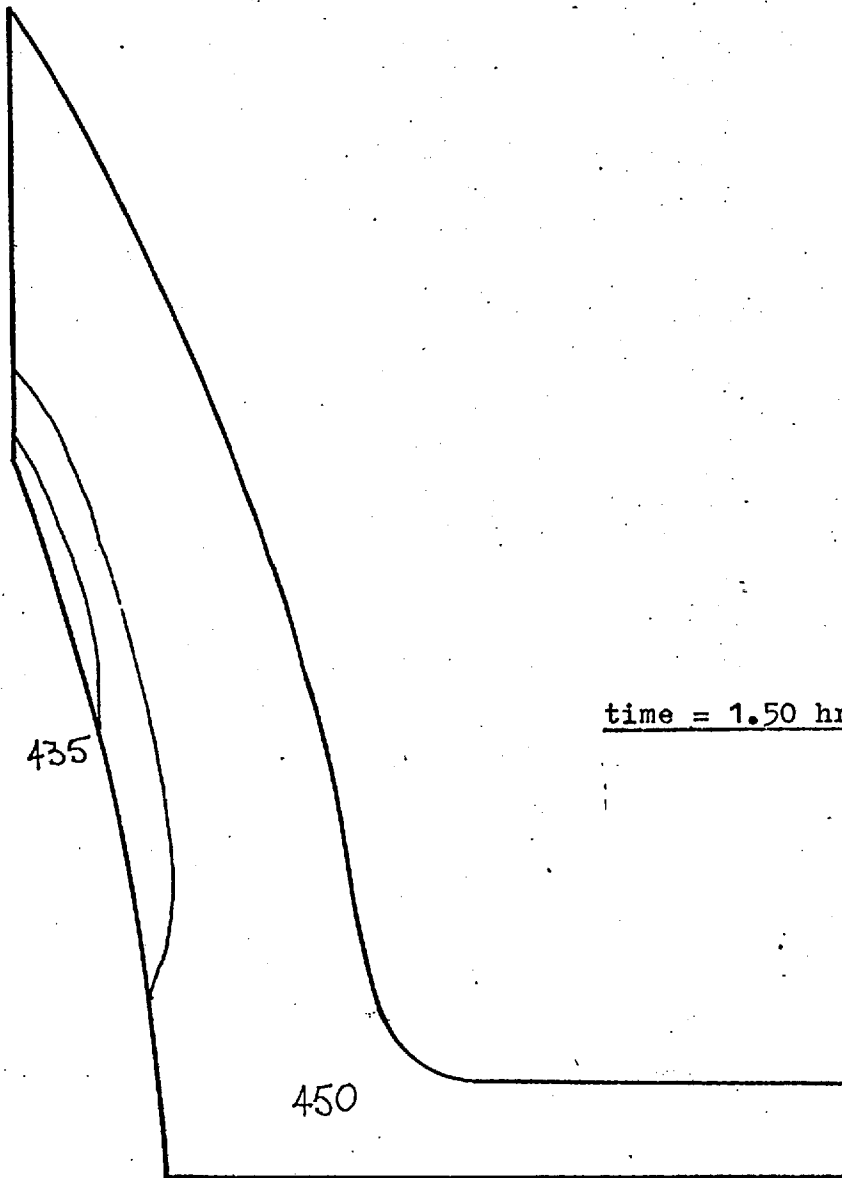


time = 0.75 hr. ( 45 min.)





time = 1.16 hr. ( 70 min.)

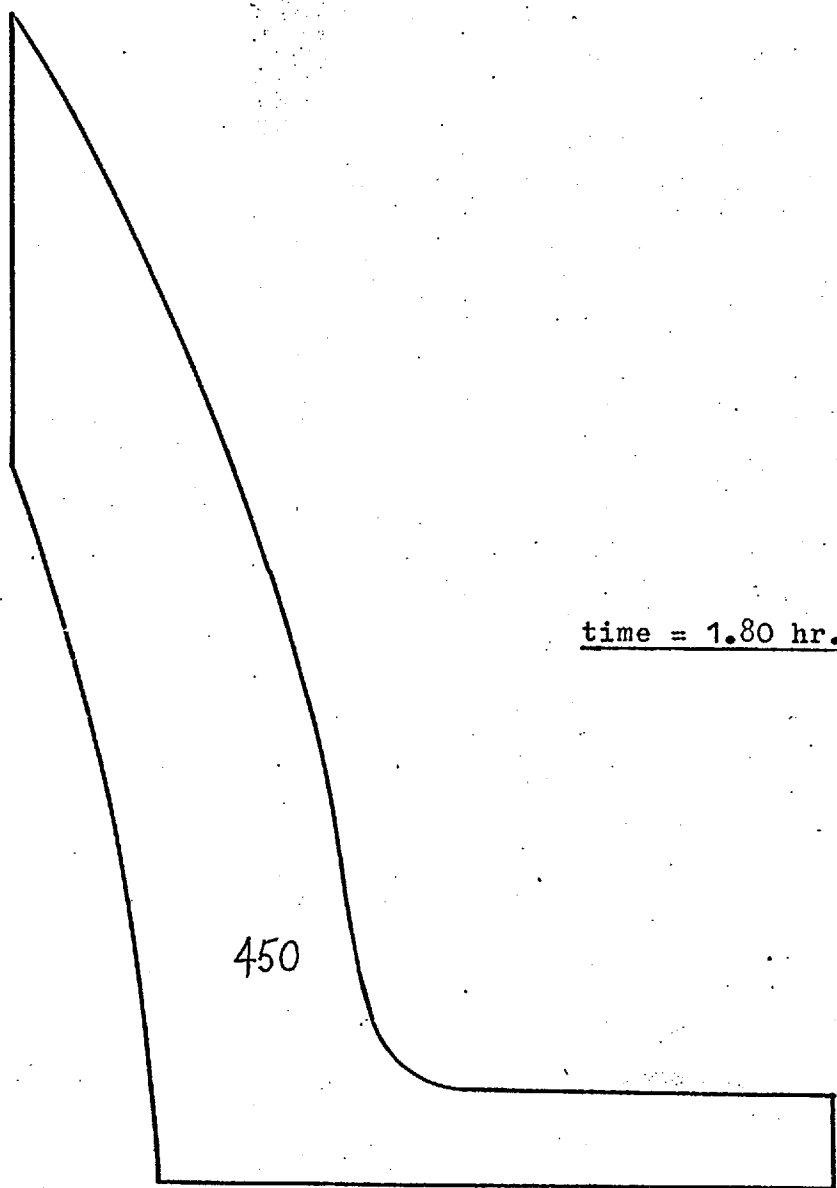


time = 1.50 hr. ( 90 min. )

435

450

-----  $\epsilon$



time = 1.80 hr. (108 min)

450

## APPENDIX 3

---

### COMPUTER PROGRAMS: TRAN 1, TRAN 2, TRAN 3. SUBROUTINE PLOT

---

#### 3.1 Data designations for Programs TRAN1, TRAN2, TRAN3 and

##### Subroutine PLOT

The data are designated as follows:

INTEGER	SINGLE	is
INTEGER	ARRAY	ia
REAL	SINGLE	rs
REAL	ARRAY	ra

The main parameters have the following names:

MAXIT	is	number of iterations (for grid)
NMAX	is	number of iterations (for time)
W	rs	dimension of nozzle-shell
Z	rs	dimension of nozzle-shell
V	rs	dimension of nozzle-shell
RA	rs	dimension of nozzle-shell
GRID	rs	size of grid increments
R	rs	generalised corner radius
COCON	rs	coefficient of thermal conductivity of metal
HTRCOV	rs	heat transfer coefficient for vessel
HTRCON	rs	heat transfer coefficient for nozzle
TIN	rs	temperature of fluid ( $^{\circ}$ F)
TIS	rs	initial temperature of structure ( $^{\circ}$ F)
RO	rs	density of metal
U	ia	nodal temperatures

G	ia	symbol for subroutine PLOT
I1	ia	generalised co-ordinate
I2	ia	generalised co-ordinate
I3	ia	generalised co-ordinate
J1	ia	generalised co-ordinate
J2	ia	generalised co-ordinate
J3	ia	generalised co-ordinate
DIFF	ra	difference of nodal temperature
SUM	ra	sum of differences of nodal temperatures for iteration process
ITN	ra	number of iterations
OMEGA	rs	convergence constant
TIME	ra	time increments
PLOT	SUBROUTINE	this subroutine plots temperature profiles
BLANK	ra	symbol designations for subroutine PLOT
L10	ia	generalised co-ordinate for boundary calculations
L15	ia	generalised co-ordinate for boundary calculations
N	ia	time increments for all nodal points
L18	ia	generalised co-ordinate for boundary calculations

MMF(I,D,R=2,F=1,P=5000)

PROGRAM TRAN1(INPUT,OUTPUT,TAPE5=INPUT,TAPE6,OUTPUT)

PROGRAM TRAN1 DETERMINES THE TRANSIENT THERMAL DISTRIBUTIONS  
FOR THE NOZZLE-VESSEL SECTION FOR CASE A BY SOLVING THE  
TWO-DIMENSIONAL UNSTEADY-STATE CONDUCTION DIFFERENTIAL  
EQUATION AND BY APPLYING THE APPROPRIATE BOUNDARY CONDITIONS.

COMMON U(70,100),

1SYMECL(51),

1G(100),

1R, I1, I2, I3, J1, J2, J3, Z, GRID

COMMON BLANK

READ GRAPHING SYMBOLS AND BLANK

READ(5,707) (SYMBOL(J), J=1,49), BLANK

707 FORMAT(52A1)

MAXIT=50

NMAX=75

MAX=10

W=4.

Z=10.

V=7.

S=1.

RA=2.

GRID=0.1

R=RA/GRID

EPS=3.

SIGMA=10.

COCCN=9.75/(12.\*3600.)

HTRCCV= 964.5/(3600.\*144.)

HTRCON= 936.1/(3600.\*144.)

TIN=450.

TIS=60.

RO=490./((12.\*\*3)

I1=V/GRID

I2=(S+RA)/GRID

I3=S/GRID

J1=Z/GRID

J2=(W+RA)/GRID

J3=W/GRID

AT INITIAL STATE THE TEMPERATURE OF THE MATERIAL IS DEFINED  
THIS MAY VARY

VESSEL PART CALCULATIONS--BOUNDARY--

J=1

DO 11 I=1, I1  
11 U(I,J)=TIN

I=1

DO 12 J=1, J1  
12 U(I,J)=TIN

DO 99 I=2, I1

DO 99 J=2, J1

99 U(I,J)=TIS

SET ITERATION COUNTER TO 1

ITN=1

START AN ITERATION BY SETTING SUM OF RESIDUES TO ZERO

9 SUM=0.0

J=1

L15=I1-1

DO 15 I=2, L15

U(I,1)=U(2,1)

U(I1,1)=U(I1-1,1)

DIFF=HTRCO/GRID\*TIN/(HTRCO/GRID+2.\*COCCN)

1+COCCN\*(2.\*U(I,J+1)+U(I+1,J)+U(I-1,J))

1/(2.\*HTRCO/GRID+4.\*COCCN)-U(I,J)

U(I,J)=U(I,J)+DIFF

15 SUM=SUM+ABS(DIFF)

IF(SUM.LE.(EPS\*I1)) GO TO 16

ITN=ITN+1

IF(ITN.GT.MAXIT) GO TO 16

NOT CONVERGED--GO BACK FOR ANOTHER ITERATION

GO TO 9

```

16 CONTINUE
   ITN=1
17 SUM=0.0
   I=1
   L18=J1-1
   DO 18 J=2,L18
   U(I,J1)=U(I,J1-1)
   DIFF=HTRCON*GRID*TIN/(HTRCON*GRID+2.*COCCCN)
1+COCCCN*(2.*U(I+1,J)+U(I,J-1)+U(I,J+1))
1/(2.*HTRCON*GRID+4.*COCCCN)-U(I,J)
   U(I,J)=U(I,J)+DIFF
18 SUM=SUM+ABS(DIFF)
   IF(SUM.LE.EPS*J1) GO TO 19
   ITN=ITN+1
   IF(ITN.GT.MAXIT) GO TO 19
   GO TO 17
19 CONTINUE

```

CCCCCCCC

### VESSEL AND NOZZLE WALL CALCULATIONS

```

THIS IS TIME ITERATION
ITN=1
300 SUM=0.0
   L1=I1-1
   L19=J3-1
   DO 100 I=2,L1
   DO 100 J=2,L18
   U(I1,J)=U(I1-1,J)
   U(I,J1)=U(I,J1-1)
   DIFF=1.8*(U(I-1,J)+U(I+1,J)+U(I,J+1)+U(I,J-1))/4.-U(I,J)
   U(I,J)=U(I,J)+DIFF
100 CONTINUE
   ITN=ITN+1
   IF(ITN.GT.MAX) GO TO 101
   GO TO 300
101 CONTINUE
   DO 120 J=J2,L18
   DO 120 I=I2,L1
120 U(I,J)=U(I2,I2)
130 CONTINUE
   N=1
   WRITE(6,65J) N
650 FORMAT(2X,'N=',I2/)
   I=I1
600 CONTINUE
   WRITE(6,2999) I
2999 FORMAT(2X,'I=',I2/)
   WRITE(6,3000) (J,J=1,10)
3000 FORMAT(2X,10(I2,10X))
   WRITE(6,3200)
3200 FORMAT(1(/))
   WRITE(6,3300) (U(I,J),J=1,J1)
3300 FORMAT(10X,10(F5.1,7X))
   WRITE(6,3400)
3400 FORMAT(1(/))
   I=I-1
   IF(I.EQ.0) GO TO 1500
   GO TO 600
   CALL PLOT(N)
1500 CONTINUE
   DO 1000 N=1,NMAX
   DO 112 I=1,I1
   J=1
112 U(I,J)=TIN
   DO 113 J=1,J1
   I=1
113 U(I,J)=TIN
   ITN=1
310 SUM=0.0
   DO 200 I=2,L1
   DO 200 J=2,L18
   U(I1,J)=U(I1-1,J)
   U(I,J1)=U(I,J1-1)
   DIFF=1.8*(U(I-1,J)+U(I+1,J)+U(I,J+1)+U(I,J-1))/4.-U(I,J)
   U(I,J)=U(I,J)+DIFF
200 CONTINUE
   ITN=ITN+1
   IF(ITN.GT.MAX) GO TO 201
   GO TO 310
201 CONTINUE
   DO 250 J=J2,L18
   DO 250 I=I2,L1

```





```
C 910 FORMAT(1H,1X,100A1)  
      MOVE TO THE NEXT ROW  
      I=I-1  
C     CHECK FOR COMPLETION  
      IF(I.NE.0) GO TO 802  
920  CONTINUE  
      RETURN  
      END
```

MAP (PART)  
 MNF (T, D, R=2, E=1, P=5000)  
 PROGRAM TRAN2 (INPUT, OUTPUT, TAPES=INPUT, TAPES=OUTPUT)

PROGRAM TRAN2 DETERMINES THE TRANSIENT THERMAL DISTRIBUTIONS FOR THE NOZZLE-VESSEL SECTION FOR CASE B BY SOLVING THE TWO-DIMENSIONAL UNSTEADY-STATE CONDUCTION DIFFERENTIAL EQUATION AND BY APPLYING THE APPROPRIATE BOUNDARY CONDITIONS.

COMMON U(70,100),  
 1SYMBOL(51),  
 IG(100),  
 1R, I1, I2, I3, J1, J2, J3, Z, GRID  
 COMMON BLANK  
 READ GRAPHING SYMBOLS AND BLANK  
 READ(5,707) (SYMBOL(J), J=1,51), BLANK  
 707 FORMAT(52A1)

MAXIT=50  
 NMAX=75  
 MAX=10  
 S=1.  
 Z=10.  
 V=7.  
 W=4.  
 GRID=0.1  
 RA=1.5  
 R=RA/GRID  
 SIGMA=10.  
 COCON=9.75/(12.\*3600.)  
 HTRCON=905.1/(3600.\*144.)  
 TIN=450.  
 TIS=60.  
 RO=490./(12.\*\*3)

I1=V/GRID  
 I2=(S+RA)/GRID  
 I3=S/GRID  
 J1=Z/GRID  
 J2=(W+RA)/GRID  
 J3=W/GRID

AT INITIAL STATE THE TEMPERATURE OF THE MATERIAL IS DEFINED THIS MAY VARY

VESSEL PART CALCULATIONS--BOUNDARY--

J=1  
 DO 11 I=2, I1  
 11 U(I,J)=TIS  
 I=1  
 DO 12 J=1, J1  
 12 U(I,J)=TIN  
 DO 99 I=2, I1  
 DO 99 J=2, J1  
 99 U(I,J)=TIS

SET ITERATION COUNTER TO 1

NOZZLE PART CALCULATIONS-BOUNDARY-

ITN=1  
 17 SUM=0.0  
 I=1  
 L18=J1-1  
 DO 18 J=2, L18  
 U(1,J1)=U(1,J1-1)  
 U(1,1)=U(1,2)  
 DIFF=HTRCON\*GRID\*TIN/(HTRCON\*GRID+2.\*COCON)  
 1+COCON\*(2.\*U(I+1,J)+U(I,J-1)+U(I,J+1))  
 1/(2.\*HTRCON\*GRID+4.\*COCON)-U(I,J)  
 U(I,J)=U(I,J)+DIFF  
 18 SUM=SUM+ABS(DIFF)  
 ITN=ITN+1  
 IF (ITN.GT.MAXIT) GO TO 19  
 GO TO 17

## VESSEL-NOZZLE WALL CALCULATIONS

CCCCC

```

THIS IS TIME ITERATION
ITN=1
300 SUM=0.0
L1=I1-1
L10=J3-1
DO 100 I=2,L1
DO 100 J=2,L10
U(I1,J)=U(I1-1,J)
U(I,J1)=U(I,J1-1)
U(I,1)=U(I,2)
DIFF=1.8*(U(I-1,J)+U(I+1,J)+U(I,J+1)+U(I,J-1))/4.-U(I,J)
U(I,J)=U(I,J)+DIFF
100 CONTINUE
ITN=ITN+1
IF(ITN.GT.MAX) GO TO 101
GO TO 300
101 CONTINUE
DO 120 J=J2,L18
DO 120 I=I2,L1
120 U(I,J)=U(J2,I2)
130 CONTINUE
N=1
CALL PLOT(N)
WRITE(6,650) N
650 FORMAT(2X,'N=',I2/)
I=I1
600 CONTINUE
WRITE(6,2999) I
2999 FORMAT(2X,'I=',I2/)
WRITE(6,3000) (J,J=1,10)
3000 FORMAT(2X,'(I2,10X)')
WRITE(6,3200)
3200 FORMAT(1(/))
WRITE(6,3300) (U(I,J),J=1,J1)
3300 FORMAT(11X,10(F5.1,7X))
WRITE(6,3400)
3400 FORMAT(1(/))
I=I-1
IF(I.EQ.0) GO TO 1500
GO TO 600
1500 CONTINUE
DO 1000 N=1,NMAX
DO 113 J=1,J1
I=1
113 U(I,J)=TIN
ITN=1
310 SUM=0.0
DO 200 I=2,L1
DO 200 J=2,L10
U(I1,J)=U(I1-1,J)
U(I,J1)=U(I,J1-1)
U(I,1)=U(I,2)
DIFF=1.8*(U(I-1,J)+U(I+1,J)+U(I,J+1)+U(I,J-1))/4.-U(I,J)
U(I,J)=U(I,J)+DIFF
200 CONTINUE
ITN=ITN+1
IF(ITN.GT.MAX) GO TO 201
GO TO 310
201 CONTINUE
DO 250 J=J2,L18
DO 250 I=I2,L1
250 U(I,J)=U(I2,J2)
IF((N+2)/3.NE.N/3) GO TO 1000
IF(N.EQ.12) GO TO 1000
WRITE(6,550) N
550 FORMAT(2X,'N=',I2/)
I=I1
JJ=J3
500 CONTINUE
WRITE(6,1999) I
1999 FORMAT(2X,'I=',I2/)
WRITE(6,2000) (J,J=1,10)
2000 FORMAT(2X,'(I2,10X)')
WRITE(6,2200)
2200 FORMAT(1(/))
WRITE(6,2300) (U(I,J),J=1,JJ)
2300 FORMAT(11X,10(F5.1,7X))
WRITE(6,2400)

```

```
2400 FORMAT(1(/))
      I=I-1
      IF(I.LT.I2.AND.I.GT.I3) GO TO 670
      IF(I.LE.I3) JJ=J1
      IF(I.EQ.0) GO TO 145
      GO TO 500
670  C=65.-FLOAT(I)
      JJ=INT(C)
      GO TO 500
145  CONTINUE
145  CALL PLOT(N)
1000 CONTINUE
      STOP
      END
      SUBROUTINE PLOT(N)
      COMMON U(72,133),
1     SYMBOL(51),
1     IG(100),
1     IR,I1,I2,I3,J1,J2,J3,Z,GRID
      COMMON BLANK
```

```
FROM HERE THE TEMPERATURES ARE PLOTTED
```

```
CCCCCCCC
```

```
MOVE TO A NEW PAGE
WRITE(6,845)
845  FORMAT(1H1)
      IF(N.GE.60) GO TO 852
      GO TO 853
852  TIME=FLOAT(N)/60.
853  WRITE(6,847) N,TIME
847  FORMAT('N=',I2,10X,'TIME=',F10.2)
      SET ROW INDEX I TO I1 FOR TOP ROW
      I=I1
      RUN THROUGH COMPLETE ROW
802  CONTINUE
      IF(I.LT.I2.AND.I.GT.I3) GO TO 808
      GO TO 805
808  CONTINUE
      C=65.-FLOAT(I)
      J1=INT(C)
806  CONTINUE
      DO 901 J=1,J1
      CHECK IF POINT IS OUTSIDE LIMIT
      IF(I.LT.I2.AND.I.GT.I3.AND.J.GT.J3.AND.J.LT.J2) GO TO 809
      IF(I.GE.I2.AND.J.GT.J3) GO TO 809
809  CONTINUE
      NOT OUTSIDE--SELECT LETTER OR BLANK TO REPRESENT TEMPERATURE
      K1=UNI(J)/9.+1.
      IF(K1.GT.51) GO TO 880
      PLACE APPROPRIATE SYMBOL IN APPROPRIATE POSITION IN LINE
      G(J)=SYMBOL(K1)
      GO TO 901
      INSERT BLANK IF OUTSIDE LIMIT
880  G(J)=BLANK
901  CONTINUE
      IF(I.LT.I3) GO TO 807
      IF(I.GE.I2) GO TO 902
      L809=Z/GRID
      L808=INT(C+1.)
      DO 807 J=L808,L809
      G(J)=BLANK
807  CONTINUE
      J1=Z/GRID
902  CONTINUE
      WRITE ENTIRE LINE
905  WRITE(6,910) G
910  FORMAT(1H,1X,100A1)
      MOVE TO THE NEXT ROW
      I=I-1
      CHECK FOR COMPLETION
      IF(I.NE.0) GO TO 802
920  CONTINUE
      RETURN
      END
```

4 JOB(UMEHM18,J13,T620,CM50000,LC5120) OIKONOMIDES.C.N.

MNF(T,D,R=2,E=1,L=BIN)  
 MAP(P)  
 BIN.

PROGRAM TRANS(INPUT,OUTPUT,TAPE5=INPUT,TAPE6=OUTPUT)  
 PROGRAM TRANS DETERMINES THE TRANSIENT THERMAL DISTRIBUTION  
 FOR THE NOZZLE-VESSEL SECTION FOR THE CASE C BY SOLVING THE  
 TWO-DIMENSIONAL UNSTEADY STATE CONDUCTION DIFFERENTIAL  
 EQUATION AND BY APPLYING THE APPROPRIATE BOUNDARY CONDITIONS.

COMMON U(35,100),  
 I1,I2,I3,J1,J2,J3,Z,GRID

DATA DESIGNATIONS--DIMENSIONS--  
 DIMENSIONS OF THE STRUCTURE IN INCHES.  
 TEMPERATURES IN DEGREES FAHRENHEIT

TIN=450.  
 TIS=60.  
 S=0.5  
 Z=10.0  
 V=3.5  
 W=3.0  
 GRID=0.1  
 RA=0.5  
 RB=0.5  
 R=RA/GRID  
 TI=5.  
 AMINUT=60.  
 TIMEB=2.5

PROPERTIES OF STEEL-BRITISH UNITS--

THERMAL CONDUCTIVITY IN BTU/FT-HR-F  
 CONDS=35.0  
 DENSITY OF STEEL IN LB/CUBIC FEET  
 DENST=491.3  
 SPECIFIC HEAT OF STEEL IN BTU/LB-F  
 SPEST=0.11  
 CHARACTERISTIC LENGTHS IN FEET  
 XCHAR1=2.5/12.  
 XCHAR2=.707/12.  
 XCHAR3=6.5/12.

PROPERTIES OF AIR AT 60 DEGREES F-BRITISH UNITS-

THERMAL CONDUCTIVITY OF AIR IN BTU/FT-HR-F  
 GASK=0.0146  
 SPECIFIC HEAT OF AIR IN BTU/LB-F  
 SPHEAT=0.240  
 DYNAMIC VISCOSITY OF AIR IN LB/FT-HR  
 DYNVIS=0.0437  
 KINEMATIC VISCOSITY OF AIR IN FEET SQUARE/HR  
 VISCK=0.579  
 VOLUME COEFFICIENT OF EXPANSION OF AIR PER/DEG.F  
 B=0.00164

DATA RELATED TO CONDITIONS-BRITISH UNITS-

ACCELERATION DUE TO GRAVITY IN FEET/HR.SQUARE  
 ACCEG=4.173\* (10.E+08)  
 TEMPERATURE OF AIR -DEGREES F--  
 TGAS=60.  
 UNIT DIMENSION OF ELEMENT-FEET-  
 RCY=1.0

I1=V/GRID  
 I2=(S+RB)/GRID  
 I3=S/GRID  
 J1=Z/GRID  
 J2=(W+RA)/GRID  
 J3=W/GRID

AT INITIAL STATE THE TEMPERATURE OF THE MATERIAL IS DEFINED  
 THIS MAY VARY

VESEL PART CALCULATIONS--BOUNDARY--

J=1  
DO 11 I=1, I1  
U(I,J)=TIN

I=1  
DO 12 J=2, J1  
U(I,J)=TIS

-----  
L1=I1-1  
L18=J1-1  
I22=I2-1  
I33=I3+1  
J33=J3+1  
-----

DO 95 I=2, I33  
DO 95 J=2, J1  
U(I,J)=TIS

DO 96 I=I33, I22  
THE EQUATION OF THE INCLINED INSIDE SURFACE OF THE VESSEL  
WALL DETERMINES THE VALUE OF J CO-ORDINATE FOR EACH VALUE OF I  
JJ=43-I  
JJJ=JJ+1  
DO 95 J=2, JJJ  
U(I,J)=TIS  
DO 97 I=I2, I1  
DO 97 J=2, J33  
U(I,J)=TIS  
-----

VESEL WALL CALCULATIONS

THIS IS TIME ITERATION

TIME=2.50

NV=1

299 CONTINUE

300 CONTINUE

DO 100 I=2, I3  
DO 100 J=2, L18

U(I,J)=U(I-1, J)

U(I,J)=(U(I-1, J)+U(I+1, J)+U(I, J+1)+U(I, J-1))/4.

U(I, J1)=U(I, J1-1)

100 CONTINUE  
-----

HEAT IS CONVECTED TO AIR BY NATURAL CONVECTION.

CALCULATE THE HEAT TRANSFER COEFFICIENT AT THE WALL TEMPERATURE  
OF THIS TIME INTERVAL

PRAND=(SPHLAT\*DYNVIS)/GASK

CALCULATE GRASHOFF NUMBER AS A FUNCTION OF THE WALL  
TEMPERATURE AT THE END OF THIS TIME INTERVAL-----

UM=(U(I3, J2)+U(I3, J1))/2.

GRASH=((XCHAR1\*\*3)\*ACCEG\*\*3\*(UM-TGAS))/(VISCK\*\*2)

ANSL=0.54\*(GRASH\*PRAND)\*\*0.25

HEATCO=(GASK\*ANSL)/XCHAR1

FROM THE HEAT BALANCE EQUATION ON THE INSIDE BOUNDARY

CALCULATE THE TEMPERATURE DROP OF THE WALL NOZAL

TEMPERATURES DUE TO CONVECTION AT THIS TIME INTERVAL

DO 480 J=J2, J1

AA1=-CONDS\*(GRID/12.)\*RCY\*(U(I3, J)-U(I3-1, J))

IF(AA1, EQ, 0.) GO TO 480

BB1=HEATCO\*(GRID/12.)\*RCY\*(U(I3, J)-TGAS)

IF(BB1, EQ, 0.) GO TO 480

CC1=DENST\*SPLEST\*(GRID/12.)\*(GRID/12.)\*RCY

DIFF=(-AA1-BB1)/CC1

FOIFF=(DIFF\*TIME)/3600.

U(I3, J)=U(I3, J)-FOIFF

480 CONTINUE  
-----

DO 120 I=I33, I22

```

C THE EQUATION OF THE INCLINED INSIDE SURFACE OF THE VESSEL
C WALL DETERMINES THE VALUE OF J CO-ORDINATE FOR EACH VALUE OF I
  JJ=40-I
  DO 120 J=0, JJ
  U(I, JJ)=U(I, JJ-1)
  U(I, J)=(U(I-1, J)+U(I+1, J)+U(I, J+1)+U(I, J-1))/4.
  U(I, JJ+1)=U(I, JJ)
120 CONTINUE

```

```

  UM=(U(I2, J1)+U(I3, J2))/2.
  GRASH=((XCHAR2**3)*ACCEG**3*(UM-TGAS))/(VISCK**2)
  ANSL=0.13*(GRASH+PRAND)**0.33
  HEATCO=(GASK+ANSL)/XCHAR2
  DO 481 I=I33, I22
  JJ=41-I
  AA2=-CONDS*(GRID/12.)*RCY*(U(I, JJ)-U(I, JJ-1))
  IF(AA2.EQ.0.) GO TO 481
  BB2=HEATCO*(GRID/12.)*RCY*(U(I, JJ)-TGAS)
  IF(BB2.EQ.0.) GO TO 481
  CC2=DENST*SP*EST*(GRID/12.)*(GRID/12.)*RCY
  DIFF2=(-AA2-BB2)/CC2
  FDIFF2=(DIFF2+TIMER)/3600.
  U(I, JJ)=U(I, JJ)-FDIFF2
481 CONTINUE

```

```

-----
  DO 130 I=I2, I1
  DO 130 J=2, J3
  U(I, J)=(U(I-1, J)+U(I+1, J)+U(I, J+1)+U(I, J-1))/4.
  U(I1, J)=U(I-1, J)
  U(I, J1)=U(I, J1-1)
130 CONTINUE
  UM=(U(I1, J2)+U(I2, J3))/2.
  GRASH=((XCHAR3**3)*ACCEG**3*(UM-TGAS))/(VISCK**2)
  ANSL=0.13*(GRASH+PRAND)**0.33
  HEATCO=(GASK+ANSL)/XCHAR3
  DO 482 I=I2, I1
  AA3=-CONDS*(GRID/12.)*RCY*(U(I, J3)-U(I, J3-1))
  IF(AA3.EQ.0.) GO TO 482
  BB3=HEATCO*(GRID/12.)*RCY*(U(I, J3)-TGAS)
  IF(BB3.EQ.0.) GO TO 482
  CC3=DENST*SP*EST*(GRID/12.)*(GRID/12.)*RCY
  DIFF3=(-AA3-BB3)/CC3
  FDIFF3=(DIFF3+TIMER)/3600.
  U(I, J3)=U(I, J3)-FDIFF3
482 CONTINUE

```

```

-----
  IF (TIME.EQ.32.5) TI=10.
  IF (TIME.EQ.42.5) TI=30.
  IF (TIME.EQ.70.5) TI=60.
  IF (TIME.EQ.180.5) TI=120.
  IF (TIME.EQ.32.5) NV=4
  IF (TIME.EQ.42.5) NV=5
  IF (TIME.EQ.70.5) NV=6
  IF (TIME.EQ.180.5) NV=16
  TINT=TI*FLOAT(NV)
  IF (TIME.EQ.TINT) GO TO 101
  TIME=TIME+2.5
  GO TO 300
101 CONTINUE
  NV=NV+1

```

```

-----
CALCULATE THE MEAN TEMPERATURES FOR THE SECTIONS OF THE VESSEL
WALL.

```

```

  SUM=J.0
  NNP=0
  DO 2000 I=I2, I1
  DO 2000 J=1, J3
  SUM=SUM+U(I, J)
  NNP=NNP+1
  THEAN1=SUM/FLOAT(NNP)
2000 CONTINUE

```

```

  SUM=J.0
  NNP=1
  DO 2010 I=I33, I22

```

```

JJ=40-I
DO 2010 J=1, JJ
SUM=SUM+U(I, J)
NNP=NNP+1
TMEAN2=SUM/FLOAT(NNP)
2010 CONTINUE

SUM=0.0
NNP=0
DO 2020 I=1, I3
DO 2020 J=J2, J1
SUM=SUM+U(I, J)
NNP=NNP+1
TMEAN3=SUM/FLOAT(NNP)
2020 CONTINUE

CALCULATE THE MEAN DIFFERENCES IN TEMPERATURE BETWEEN SECTIONS

DELT12=TMEAN1-TMEAN2
DELT23=TMEAN2-TMEAN3
IF (TIME.GT.60.AND.TIME.LT.180.) GO TO 1000
IF (TIME.GE.180.) GO TO 523
TIME=TIME+TIMEB

-----

PRINT ALL NODAL TEMPERATURES AT SPECIFIED TIME INTERVALS

523 CONTINUE
STIME=TIME/60.
WRITE(6,2430)
2400 FORMAT(1(/))
WRITE(6,550) STIME, TIME
550 FORMAT(2X, 'TIME IN MINUTES=* ,F9.3,10X, *TIME IN SECONDS=* ,F9.2)
WRITE(6,2450)
2450 FORMAT(1(/))
WRITE(6,2460) DELT12, DELT23
2460 FORMAT(2X, 'DIFFERENCE DELT12=* ,F9.2,10X, *DIFFERENCE DELT23=* ,F9.2)
I=I-1
JJ=J3
500 CONTINUE
WRITE(6,1999) I
1999 FORMAT(2X, 'I=* ,I3)
WRITE(6,2030) (J, J=1, 10)
2030 FORMAT(2X, ' (I2,10X))
WRITE(6,2300) (U(I, J), J=1, JJ)
2300 FORMAT((1X,10(F5.1,7X)))
I=I-1
IF (I.LT.I2.AND.I.GT.I3) GO TO 670
IF (I.LE.I3) JJ=J1
IF (I.EQ.0) GO TO 1010
GO TO 500
670 C=40.-FLOAT(I)
JJ=INT(C)
GO TO 500
1010 IF (TIME.LE.150.) GO TO 528
GO TO 1000
528 TIME=TIME/TIMEC
1000 IF (STIME.EQ.4MINUT) GO TO 1001
GO TO 299

-----

1001 CONTINUE
STOP
END

```



## APPENDIX 4

# Stress Analysis by Finite Elements

### 4.1 Finite Elements

The structure is considered as an assemblage of elements interconnected at a discrete number of nodal points. If the force displacement relationships for the individual elements are known it is possible to derive the properties and study the behaviour of the assembled structure. In an elastic continuum the real number of interconnection points is infinite. The concept of finite elements attempts to overcome the difficulty of an infinite number of points by assuming the real continuum to be divided into elements interconnected only at a finite number of nodal points at which some imaginary forces, representative of the distributed stresses actually acting on the element boundaries, were supposed to be introduced. With this idealisation the problem reduces to that of a conventional structural type which can be solved by numerical treatment.

### 4.2 Equations

In Cartesian co-ordinates  $(x,y,z)$  the stresses are:

Direct stresses:  $\sigma_{xx}, \sigma_{yy}, \sigma_{zz}$

Shear stresses:  $\tau_{xy}, \tau_{yz}, \tau_{zx}$

First subscript denotes the direction of the stress and the second subscript the direction of the outward normal to the surface on which it acts. Tensile stresses are positive.

Strains are:

$$\epsilon_{xx} = \frac{\partial u}{\partial x} \quad \epsilon_{yy} = \frac{\partial v}{\partial y} \quad , \quad \epsilon_{zz} = \frac{\partial w}{\partial z}$$

$$\epsilon_{xy} = \frac{\partial u}{\partial y} + \frac{\partial v}{\partial x} \quad , \quad \epsilon_{yz} = \frac{\partial v}{\partial z} + \frac{\partial w}{\partial y} \quad , \quad \epsilon_{zx} = \frac{\partial w}{\partial x} + \frac{\partial u}{\partial z}$$

where  $u, v, w$  are the corresponding displacements in  $x, y, z$  direction.

For the isotropic elastic solid with thermal strains

$$\epsilon_{xx} = \frac{1}{E} \left[ \sigma_{xx} - \nu(\sigma_{yy} + \sigma_{zz}) \right] + \alpha \Delta T$$

$$\epsilon_{yy} = \frac{1}{E} \left[ \sigma_{yy} - \nu(\sigma_{zz} + \sigma_{xx}) \right] + \alpha \Delta T$$

$$\epsilon_{zz} = \frac{1}{E} \left[ \sigma_{zz} - \nu(\sigma_{xx} + \sigma_{yy}) \right] + \alpha \Delta T$$

$$\epsilon_{xy} = \frac{\tau_{xy}}{G} = \frac{2(1+\nu)}{E} \sigma_{xy}$$

$$\epsilon_{yz} = \frac{\tau_{yz}}{G} = \frac{2(1+\nu)}{E} \sigma_{yz}$$

$$\epsilon_{zx} = \frac{\tau_{zx}}{G} = \frac{2(1+\nu)}{E} \sigma_{zx}$$

where  $E$  = Young's modulus

$G$  = Shear modulus

$\nu$  = Poisson's ratio

$\alpha$  = Coefficient of thermal expansion

$\Delta T$  = Temperature rise

For this particular project the elementary part in which the sections of vessel/nozzle are divided is the triangular element. The displacements are given by  $u$  and  $v$  in the direction of the  $x$  and  $y$  axes. Due to thermal expansion of the solid the stress in a direction perpendicular to the  $x$ - $y$  plane is not zero. This is the case of plane strain. By definition the strain in the  $z$ -direction is zero, and therefore no contribution to internal work is made by the stress in this direction, which is evaluated from the three main components. The displacements within an element are given by two linear polynomials.

$$u = \alpha_1 + \alpha_2 x + \alpha_3 y$$

$$v = \alpha_4 + \alpha_5 x + \alpha_6 y$$

The six constants  $\alpha$  can be evaluated by solving the two sets of three simultaneous equations which will arise if the nodal co-ordinates are inserted and the displacements equated to the appropriate nodal displacements.

$$u_i = \alpha_1 + \alpha_2 x_i + \alpha_3 y_i$$

$$u_j = \alpha_1 + \alpha_2 x_j + \alpha_3 y_j$$

$$u_m = \alpha_1 + \alpha_2 x_m + \alpha_3 y_m$$

Solving for  $\alpha_1, \alpha_2, \alpha_3$  in terms of the nodal displacements  $u_i, u_j, u_m$  and obtain

$$u = \frac{1}{2\Delta} \left[ (a_i + b_i x + c_i y) u_i + (a_j + b_j x + c_j y) u_j + (a_m + b_m x + c_m y) u_m \right] \quad (\text{A4.2.1})$$

where,

$$a_i = x_j y_m - x_m y_j$$

$$b_i = y_j - y_m = y_{jm}$$

$$c_i = x_m - x_j = x_{mj}$$

The other coefficients can be obtained by a cyclic process of subscripts in the order  $i, j, m$  and where

$$2\Delta = \det \begin{vmatrix} 1 & x_i & y_i \\ 1 & x_j & y_j \\ 1 & x_m & y_m \end{vmatrix} = 2(\text{area of triangular element } ijm)$$

For the vertical displacement  $v$

$$v = \frac{1}{2\Delta} \left[ \begin{aligned} &(a_i + b_i x + c_i y)v_i + (a_j + b_j x + c_j y)v_j \\ &+ (a_m + b_m x + c_m y)v_m \end{aligned} \right] \quad (\text{A4.2.2})$$

The displacement function guarantees continuity of displacements with adjacent elements because the displacements vary linearly along any side of the triangle and, with identical displacement imposed at the nodes, the same displacement will exist all along the interface. The total strain at any point within the element can be defined by its three components which contribute to internal work.

$$[\epsilon] \begin{bmatrix} \epsilon_{xx} \\ \epsilon_{yy} \\ \gamma_{xy} \end{bmatrix} = \begin{bmatrix} \frac{\partial u}{\partial x} \\ \frac{\partial v}{\partial y} \\ \frac{\partial u}{\partial y} + \frac{\partial v}{\partial x} \end{bmatrix}$$

Using equations (A4.2.1) and (A4.2.2) we have

$$\begin{aligned} \epsilon & \begin{bmatrix} \frac{\partial N'_i}{\partial x} & 0 & \frac{\partial N'_j}{\partial x} & 0 & \frac{\partial N'_m}{\partial x} & 0 \\ 0 & \frac{\partial N'_i}{\partial y} & 0 & \frac{\partial N'_j}{\partial y} & 0 & \frac{\partial N'_m}{\partial y} \\ \frac{\partial N'_i}{\partial y} & \frac{\partial N'_i}{\partial x} & \frac{\partial N'_j}{\partial y} & \frac{\partial N'_j}{\partial x} & \frac{\partial N'_m}{\partial y} & \frac{\partial N'_m}{\partial x} \end{bmatrix} \begin{bmatrix} u_i \\ v_i \\ u_j \\ v_j \\ u_m \\ v_m \end{bmatrix} \\ &= \frac{1}{2\Delta} \begin{bmatrix} b_i & 0 & b_j & 0 & b_m & 0 \\ 0 & c_i & 0 & c_j & 0 & c_m \\ c_i & b_i & c_j & b_j & c_m & b_m \end{bmatrix} [\delta]^c \end{aligned}$$

where

$$\delta = \begin{pmatrix} u_i \\ v_i \end{pmatrix}$$

$$N_i^x = (a_i + b_i x + c_i y)/2$$

$$N_j^x = (a_j + b_j x + c_j y)/2 \quad \text{e.t.c.}$$

The matrix thus derived is independent of the position within the element and hence the strains are constant throughout it.

In the case of plane strain for the case of isotropic thermal expansion  $\sigma_z$  exists and we have

$$\begin{aligned} \epsilon_{xx} &= \frac{\sigma_{xx}}{E} - \frac{\nu\sigma_{yy}}{E} - \frac{\nu\sigma_{zz}}{E} + \alpha\Delta T^e \\ \epsilon_{yy} &= -\frac{\nu\sigma_{xx}}{E} + \frac{\sigma_{yy}}{E} - \frac{\nu\sigma_{zz}}{E} + \alpha\Delta T^e \\ \gamma_{xy} &= \frac{2(1+\nu)\tau_{xy}}{E} \end{aligned}$$

but also

$$\epsilon_{zz} = 0 = -\frac{\nu\sigma_{xx}}{E} - \frac{\nu\sigma_{yy}}{E} + \frac{\sigma_{zz}}{E} + \alpha\Delta T^e$$

By eliminating  $\sigma_{zz}$  and solving for the three remaining stresses the matrix  $[D]$  is obtained as

$$[D] = \frac{E(1-\nu)}{(1+\nu)(1-2\nu)} \begin{bmatrix} 0 & \nu/(1-\nu) & 0 \\ \nu/(1-\nu) & 1 & 0 \\ 0 & 0 & \frac{(1-2\nu)}{2(1-\nu)} \end{bmatrix}$$

The direct stresses are then calculated from

$$\{\sigma\} = \begin{Bmatrix} \sigma_{xx} \\ \sigma_{yy} \\ \tau_{xy} \end{Bmatrix} = [D] \left[ \begin{Bmatrix} \epsilon_{xx} \\ \epsilon_{yy} \\ \gamma_{xy} \end{Bmatrix} - \{\epsilon_0\} \right]$$

where

$$\{\epsilon_0\} = \begin{Bmatrix} \alpha\Delta T_{xx} \\ \alpha\Delta T_{yy} \\ 0 \end{Bmatrix} \quad \text{and}$$

$\sigma_{zz}$  is determined from Equation (A4.2.3). The principal stresses are subsequently calculated from

$$\{\sigma_1\} = \frac{1}{2} \{\sigma_{xx} + \sigma_{yy}\} + \left\{ \frac{1}{2} \sqrt{(\sigma_{xx} - \sigma_{yy})^2 + 4 \tau_{xy}^2} \right\}$$

$$\{\sigma_2\} = \frac{1}{2} \{\sigma_{xx} + \sigma_{yy}\} - \left\{ \frac{1}{2} \sqrt{(\sigma_{xx} - \sigma_{yy})^2 + 4 \tau_{xy}^2} \right\}$$

As the condition of plane strain is valid for the present problem due to large thickness of the vessel in the z-direction (closed ring) and as  $\epsilon_z = 0$ , the stress  $\sigma_z$  can be assumed to represent the principal stress  $\sigma_3$  in the z-direction.

## APPENDIX 5

---

### COMPUTER PROGRAMS: STREN 1, STREN 2, STREN 3

---

#### 5.1 Data Designations for Programs STREN1, STREN2, STREN3

The data are categorised by the following designations:

is	integer single
ia	integer array
rs	real single
ra	real array
hs	Hollerith single
ha	Hollerith array

The units can be any consistent set, with angles in degrees.

ALPHA	ra	coefficients of thermal expansion
ANGLEL	rs	angle of the major principal in plane stress on an element, counter-clockwise from the x-axis
ANGLEN	rs	angle of the major principal in plane stress at a node, counter-clockwise from the x-axis
ANP	ia	indices of the forced node and of the displaced nodes adjacent to it
AREA	rs	area of an element
B	ra	the B-matrix in the compatibility or in the equilibrium equation for an element
BI	ra	$y_j - y_m$ for the elements
BJ	ra	$y_m - y_i$ for the elements
BM	ra	$y_i - y_j$ for the elements
BODYF	rs	gravitational body force per unit thickness on an element taken to be in the -y direction

CASCTL hs constant with the value NFCASE used for testing  
for the termination of the job

CI ra  $-(x_j - x_m)$  for the elements

CJ ra  $-(x_m - x_i)$  for the elements

CM ra  $-(x_i - x_j)$  for the elements

CØND ia specified conditions of restraint for boundary  
nodes with the three possible values  
0 fixed in both x and y directions  
1 fixed in the x direction only  
2 allowed to move along a line at an in plane angle  
 $\phi$  measured counter-clockwise from the x-axis

D ra the elasticity D-matrix for an element

DELTAT ra temperature rise in the elements above their  
initial constant value

DELTAU rs x-component of the cyclic increment in the  
iteration to the displacement of a node

DELTAV rs y-component of the cyclic increment in the  
iteration to the displacement of a node

E ra moduli of elasticity in the elements

EEXX rs linear total strain in the x-direction in an  
element

EEXY rs total shear strain in the plane of an element

EEYY rs linear total strain in the y-direction in an  
element

ETH rs thermal strain in an element

EXX rs linear elastic strain in the x-direction in an  
element

EXY rs elastic shear strain in the plane of an element

EYY rs linear elastic strain in the y-direction in an  
element



**FXX** ra components for each node of flexibility times thickness in the x-direction due to a force per unit thickness on itself in the x-direction

**FXY** ra components for each node of flexibility times thickness in the x-direction due to a force per unit thickness on itself in the y-direction

**FYX** ra components for each node of flexibility times thickness in the y-direction due to a force per unit thickness on itself in the x-direction

**FYY** ra components for each node of flexibility times thickness in the y-direction due to a force per unit thickness on itself in the y-direction

**I** is working index of the first node of an element

**J** is working index of the second node of an element

**K** ra matrix of stiffness per unit thickness for an element

**KXX** ra components for each node of stiffness per unit thickness in the x-direction due to displacements in the x-direction of itself and of nodes adjacent to it

**KXY** ra components for each node of stiffness per unit thickness in the x-direction due to displacements in the y-direction of itself and of nodes adjacent to it

**KYX** ra components for each node of stiffness per unit thickness in the y-direction due to displacements in the x-direction of itself and of nodes adjacent to it

**KYY** ra components for each node of stiffness per unit thickness in the y-direction due to displacements in the y-direction of itself and of nodes adjacent to it

L is running index of the elements

L<sub>1</sub> is working variable used in the output of element data

L<sub>2</sub> is working variable used in the output of element data

L<sub>3</sub> is working variable used in the output of element data

LE is index of particular element

LN ia working indices of the three nodes of an element

M is working index of the third node of an element

MAT ia indices of materials specified for the elements

MATN is index of a particular material

N is running index of the nodes

N<sub>1</sub> is working variable used in the output of node displacements

N<sub>2</sub> is working variable used in the output of node displacements

N<sub>3</sub> is working variable used in the output of node displacements

NAP ia numbers of nodes adjacent to each node plus one added for itself

NAP1 is number of nodes adjacent to a particular node plus one added for itself

NB ia indices of the restrained boundary nodes with values corresponding to those of NP

NBR is number of restrained boundary nodes

NC is cycle count in the iteration

NCC is cycle interval for writing the iteration progress

NCY is maximum number of cycles for the case

NEL is number of elements

NM is running index of materials  
 NMAT is number of materials  
 NNP is number of nodes  
 NP is index of a particular node  
 NPI ia indices of the first nodes of the elements  
 NPJ ia indices of the second nodes of the elements  
 NPM ia indices of the third nodes of the elements  
 NR is running index of restrained boundary nodes with values 1, 2, ....  
 NU ra Poisson's ratios in the elements  
 Ø is working row or column index used in matrix multiplication  
 ØMEGA rs over-relaxation factor  
 F is working row index of a matrix  
 PS hs control parameter specifying the type of deformation in the body with the two possible values  
     STRESS plane stress  
     STRAIN plane strain  
 Q is working column index of a matrix  
 QA is running index of a reference node and the nodes adjacent to it  
 RELDIF rs relative sum of absolute cyclic component increments in displacements  
 RHØ ra densities in the elements  
 RX ra x-components of forces per unit thickness acting on the nodes, external or total  
 RX1 rs x-component of an out-of-balance force per unit thickness acting on a node plus the force per unit thickness acting on the node due to its own displacement

RY	ra	y-components of forces per unit thickness acting on the nodes, external or total
RY1	rs	y-component of an out-of-balance force per unit thickness acting on a node plus the force per unit thickness acting on the node due to its own displacement
SD	rs	sum of the absolute components of displacements
SDD	rs	sum of the absolute components of cyclic displacement increments
SIGLM	rs	the second invariant of stress in an element
SIGLXX	ra	normal stress in the x-direction in the elements
SIGLXY	ra	shear in plane components of stress in the elements
SIGLYY	ra	normal stress in the y-direction in the elements
SIGLZZ	ra	normal stress in the z-direction in the elements
SIGL1	ra	maximum principal in plane stress on an element
SIGL2	rs	minimum principal in plane stress on an element
SIGL3	rs	principal anti-plane stress on an element
SIGNM	rs	the second invariant of stress at a node
SIGNXX	rs	normal stress in the x-direction at a node
SIGNXY	rs	shear in plane component of stress at a node
SIGNYY	rs	normal stress in the y-direction at a node
SIGNZZ	rs	normal stress component in the z-direction at a node
SIGN1	rs	maximum principal in plane stress at a node
SIGN2	rs	minimum principal in plane stress at a node
SIGN3	rs	principal anti-plane stress at a node
SIGTH	rs	thermal stress in an element
SIØPE	ra	$\tan \phi$ for the condition CØND - 2 at the restrained boundary nodes

SR is control parameter specifying stresses to be output,  
with the four possible values

- 0 none
- 1 elements only
- 2 nodes only
- 3 both elements and nodes

STRAIN hs constant with the value STRAIN used in testing  
which type of deformation is specified

STRESS hs constant with the value STRESS used in testing  
which type of deformation is specified

TITLE ha input text being the case title

TOLER rs cyclic convergence test constant

U ra x-components of displacements of the nodes,  
the input guessed values or the solution values

V ra y-components of displacements of the nodes,  
the input guessed values or the solution values

W ra working matrix

WI is control parameter specifying how much of the  
input data is to be output, with the two possible  
values

- 0 case title and control parameters only
- 1 all input data

W<sub>1</sub> rs working variable

W<sub>2</sub> rs working variable

W<sub>3</sub> rs working variable

W<sub>4</sub> rs working variable

W<sub>5</sub> rs working variable

W<sub>6</sub> rs working variable

W<sub>7</sub> rs working variable

X ra abscissae of the nodes

Y ra ordinates of the nodes

## 5.2 Listing of Program STREN1

```
PROGRAM STREN1(INPUT=1002,OUTPUT=1002,TAPE5=INPUT,TAPE6=OUTPUT)
```

```
0 SPECIFICATION AND DATA INITIALIZATION STATEMENTS.
```

```
1 INTEGER TITLE, PS, SR, QA, O, NP,  
2 CASCTL, STRESS, WI, ANP, P,  
3 STRAIN, COND, G
```

```
1 REAL NU, K, KXX,  
2 KXY,  
3 KXX,  
4 KYY
```

```
COMMON TITLE(13), NPI(377), X(221),  
1 E(5), NPJ(377), Y(221),  
2 NU(5), NPM(377), RX(221),  
3 RHO(5), MAT(377), RY(221),  
4 ALPHA(5), DELTAT(377), U(221),  
5 V(221),  
6 BI(377), KXX(221,9), ANP(221,9), SIGLXX(377),  
7 EJ(377), KXY(221,9), NAP(221), SIGLYY(377),  
8 BM(377), KYX(221,9), LN(3), SIGLZZ(377),  
9 CI(377), KYY(221,9), E(3,6), SIGLXY(377),  
10 CJ(377), FXX(221), D(3,3),  
11 CM(377), FXY(221), W(3,6),  
12 FXX(221), K(6,6),  
13 FYY(221)
```

```
DATA CASCTL, STRESS, STRAIN / 6HNFCASE, 6HSTRESS, 6HSTRAIN /
```

```
10 INPUT THE CASE TITLE BUT STOP IF THERE IS NO FURTHER CASE.
```

```
11 READ (5, 12) TITLE
```

```
12 FORMAT (13A6)
```

```
IF (TITLE(1) .EQ. CASCTL) STOP
```

```
20 INPUT THE CONTROL PARAMETERS AND PREPARE TO INPUT THE ARRAY DATA.
```

```
READ (5, 21) NEL, NNP, NMAT, NCV, NCC,
```

```
1 TOLER, CMEGA, PS, SR, WI
```

```
21 FORMAT (5I5, E13.5, F7.3, 2X, A6, 2I3)
```

```
DO 22 NM = 1, NMAT
```

```
22 E(NM) = -1.
```

```
DO 23 L = 1, NEL
```

```
23 NPI(L) = -1.
```

```
DO 24 N = 1, NNP
```

```
24 X(N) = -J.123456789E35
```

```
30 INPUT AND CHECK THE ARRAY DATA.
```

```
READ (5, 31) (MAIN, E(MATN), NU(MATN),
```

```
1 RHO(MATN), ALPHA(MATN), NM = 1, NMAT)
```

```
31 FORMAT (I5, 4E13.5)
```

```
DO 33 NM = 1, NMAT
```

```
IF (E(NM) .NE. -1.) GO TO 33
```

```
WRITE(6, 333) NM
```

```
333 FORMAT(1X, 7H E(NM)=, I5)
```

```
WRITE(6, 32) TITLE
```

```
32 FORMAT (1H1 // // // EH IN 1, 13A6, 1H' /
```

```
1 35H THERE IS A MISSING INPUT DATA CARD.,
```

```
2 24H THE JOB IS ABANDONED.)
```

```
STOP
```

```
33 CONTINUE
```

```
READ (5, 34) (LE, NPI(LE), NPJ(LE), NPM(LE),
```

```
1 DELTAT(LE), MAT(LE), L=1, NEL)
```

```
34 FORMAT(4I5, F10.3, I5)
```

```
DO 35 L = 1, NEL
```

```
IF (NPI(L) .NE. -1) GO TO 35
```

```
WRITE(6, 334) L
```

```
334 FORMAT(1X, 7H L=, I5)
```

```
WRITE(6, 32) TITLE
```

```
STOP
```

```
35 CONTINUE
```

```
DO 350 N=1, 45
```

```
READ(5, 36) A1, B1, NP1, A2, B2, NP2, A3, B3, NP3, A4, B4, NP4, A5, B5, NP5
```

```
36 FORMAT(5(F4.0, 1X, F4.0, I4, 3X))
```

```
WRITE(6, 371) NP1, NP2, NP3, NP4, NP5
```

```
371 FORMAT(1X, 5(I20))
```

```
X(NP1)=(A1-6848.)/254. EX(NP2)=(A2-6848.)/254.
```

```
X(NP3)=(A3-6848.)/254. EX(NP4)=(A4-6848.)/254.
```

```
X(NP5)=(A5-6848.)/254.
```

```
Y(NP1)=(B1-811.)/254. EY(NP2)=(B2-811.)/254.
```

```
Y(NP3)=(B3-811.)/254. EY(NP4)=(B4-811.)/254.
```

```
Y(NP5)=(B5-811.)/254.
```

```
350 CONTINUE
```

```
DO 361 N=1, NNP
```

```
RX(N)=0.
```

```

361 CONTINUE
DO 37 N = 1, NNP
IF (X (N) .NE. -0.123456789E35) GO TO 37
WRITE (6, 335) N
335 FORMAT (1X, 3H N=, I5)
WRITE (6, 32) TITLE
STOP
37 CONTINUE

40 OUTPUT THE TITLE AND THE CONTROL PARAMETERS.
WRITE (6, 41)
41 FORMAT (1H1 //)
1 45X, 41H THE CASE TITLE AND THE CONTROL PARAMETERS /
2 45X, 41H ----- //)
WRITE (6, 42) TITLE
42 FORMAT (1H, 13A6)
WRITE (6, 43) NEL, NNP, N3R, NMAT, NCY, MCC, TOLER, OMEGA, PS
43 FORMAT (25H THE NUMBER OF ELEMENTS IS, I5, 1H. /
1 33H THE NUMBER OF NODAL POINTS IS, I5, 1H. /
2 43H THE NUMBER OF RESTRAINED BOUNDARY NODES IS, I5, 1H. /
3 43H THE NUMBER OF DIFFERENT MATERIALS IS, I5, 1H. /
4 23H THE ITERATION LIMIT IS, I5, 8H CYCLES. /
5 36H THE INTERVAL FOR PROGRESS OUTPUT IS, I5, 8H CYCLES. /
6 29H THE CONVERGENCE TOLERANCE IS, F13.5, 1H. /
7 39H THE OVER-RELAXATION FACTOR IS, F7.3, 1H. /
8 37H THE CASE HAS THE CONDITION OF PLANE, A6, 1H. /
9 23H STRESSES ARE FOUND FOR)
IF (SR .EQ. 0) WRITE (6, 44)
44 FORMAT (1H+, 23X, 42H NEITHER THE ELEMENTS NOR THE NODAL POINTS.)
IF (SR .EQ. 1) WRITE (6, 45)
45 FORMAT (1H+, 23X, 18H THE ELEMENTS ONLY.)
IF (SR .EQ. 2) WRITE (6, 46)
46 FORMAT (1H+, 23X, 22H THE NODAL POINTS ONLY.)
IF (SR .EQ. 3) WRITE (6, 47)
47 FORMAT (1H+, 23X, 39H BOTH THE ELEMENTS AND THE NODAL POINTS.)
IF (WI .EQ. 0) WRITE (6, 48)
48 FORMAT (37H THE INPLT ARRAY DATA ARE NOT OUTPUT.)
IF (WI .EQ. 1) WRITE (6, 49)
49 FORMAT (33H THE INPLT ARRAY DATA ARE OUTPUT.)

50 OUTPUT THE ARRAY DATA.
NPI(376)=132 & NPJ(376)=181
IF (WI .EQ. 0) GO TO 61
WRITE (6, 51) (N, E (NM), NU (NM), RHC (NM),
1 ALPHA (NM), NM = 1, NMAT)
51 FORMAT (1H1 //)
1 56X, 19H INPUT MATERIAL DATA /
2 56X, 19H ----- //)
3 28X, 42H MATERIAL ELASTIC MODULUS POISSON'S RATIO,
4 34H DENSITY THIL EXPN CCEFF //
5 (I33, X, 4E17.5))
WRITE (6, 52)
52 FORMAT (1H1 //)
1 57X, 18H INPUT ELEMENT DATA /
2 57X, 18H ----- //)
3 3X, 45H ELMT NPI NPJ NPM MTRL DELTA T
4 48H ELMT NPI NPJ NPM MTRL DELTA T
5 33H ELMT NPI NPJ NPM MTRL DELTA T //)
L1 = (NEL + 2) / 3
DO 53 L2 = 1, L1
L3 = MIN0 (L2 + 2 * L1, NEL)
53 WRITE (6, 54) (L, NPI (L), NPJ (L), NPM (L),
1 MAT (L), DELTAT (L), L = L2, L3, L1)
54 FORMAT (1H, 5I5, F10.3, 13X, 5I5, F10.3, 13X, 5I5, F10.3)
DO 540 N=1, NNP
U(N)=0.
V(N)=0.
540 CONTINUE
WRITE (6, 55) (N, X (N), Y (N), RX (N), RY (N),
1 U (N), V (N), N = 1, NNF)
55 FORMAT (1H1 //)
1 53X, 15H INPUT NODE DATA /
2 53X, 15H ----- //)
3 13X, 49H NCDE X Y
4 31H RX RY
5 21H U V //
6 (I16, X, 6E17.5))

60 DO GEOMETRIC CALCULATIONS ON THE ELEMENTS.
61 DO 72 L = 1, NEL
I = NPI (L)

```

CCC

CCC

CCC

```

M = NPM (L)
BI (L) = Y (J) - Y (M)
BJ (L) = Y (M) - Y (I)
BM (L) = Y (I) - Y (J)
CI (L) = - X (J) + X (M)
CJ (L) = - X (M) + X (I)
CM (L) = - X (I) + X (J)
AREA = (BJ (L) * CM (L) - BM (L) * CJ (L)) / 2.
IF (AREA .GT. 1.E-35) GO TO 71
WRITE (6, 62) L
62 FORMAT (1H1 // 'ELEMENT, IS, 25H HAS A NON-POSITIVE AREA. /
1 23H THE CASE IS ABANDONED.')
GO TO 221

```

```

70 SUM THE TOTAL NODAL POINT FORCES.
71 MATN = MAT (L)
IF (PS .EQ. STRESS) SIGTH = 1. - NU (MATN)
IF (PS .EQ. STRAIN) SIGTH = (1. + NU (MATN))
1 * (1. - 2. * NU (MATN))
SIGTH = - (MATN) * ALPHA (MATN) * DELTAT (L) / SIGTH
BODYF = AREA * RHO (MATN) / 3.
RX (I) = RX (I) - 0.5 * BI (L) * SIGTH
RY (I) = RY (I) - 0.5 * CI (L) * SIGTH - BODYF
RX (J) = RX (J) - 0.5 * BJ (L) * SIGTH
RY (J) = RY (J) - 0.5 * CJ (L) * SIGTH - BODYF
RX (M) = RX (M) - 0.5 * BM (L) * SIGTH
72 RY (M) = RY (M) - 0.5 * CM (L) * SIGTH - BODYF

```

```

80 PREPARE TO SUM THE STIFFNESS COEFFICIENTS.
DO 82 N = 1, NNP
DO 81 GA = 1, 9
KXX (N, GA) = 0.
KXY (N, GA) = 0.
KXX (N, GA) = 0.
KYY (N, GA) = 0.
81 ANP (N, GA) = 0
ANP (N, 1) = N
82 NAF (N) = 1

```

```

90 FORM THE STIFFNESS MATRIX FOR THE ELEMENT.
DO 105 L = 1, NEL
DO 92 P = 1, 3
DO 91 Q = 1, 6
91 B (P, Q) = 0.
DO 92 Q = 1, 3
92 C (P, Q) = 0.
B (1, 1) = BI (L)
B (1, 3) = BJ (L)
B (1, 5) = BM (L)
B (2, 2) = CI (L)
B (2, 4) = CJ (L)
B (2, 6) = CM (L)
B (3, 1) = CI (L)
B (3, 2) = BI (L)
B (3, 3) = CJ (L)
B (3, 4) = BJ (L)
B (3, 5) = CM (L)
B (3, 6) = BM (L)
MATN = MAT (L)
W1 = NU (MATN)
W2 = 1. - W1
W3 = 1. + W1
W4 = 1. - 2. * W1
IF (PS .EQ. STRAIN) GO TO 93
W5 = E (MATN) / (W2 * W3)
W6 = W1
W7 = W2 / 2.
GO TO 94
93 W5 = E (MATN) * W2 / (W3 * W4)
W6 = W1 / W2
W7 = W4 / W2 * W2
94 AREA = (BJ (L) * CM (L) - BM (L) * CJ (L)) / 2.
W5 = W5 / (4. * AREA)
E (1, 1) = W5 * W6
E (1, 2) = W5 * W6
E (2, 1) = W5 * W6
E (2, 2) = W5 * W6
E (3, 3) = W5 * W7
DO 95 P = 1, 3
DO 95 Q = 1, 6
DO 95 O = 1, 3
95 W (P, Q) = W (P, Q) + D (P, Q) + B (O, Q)

```



```

CO 96 P = 1, 6
CO 96 C = 1, 6
K (P, Q) = 0.
DO 96 O = 1, 3
96 K (P, Q) = K (P, Q) + B (O, P) * W (C, Q)

CCCC
100 SUM AND STORE FOR EACH (FORCED) NODE THE NON-ZERO STIFFNESS
COEFFICIENTS FOR THE ADJACENT (DISPLACED) NODES.
LN (1) = NPT (L)
LN (2) = NPJ (L)
LN (3) = NPM (L)
DO 105 P = 1, 3
NP = LN (P)
DO 105 Q = 1, 3
QA = 0
101 QA = QA + 1
IF (QA .LE. 9) GO TO 103
WRITE (6, 102) NP
102 FORMAT (1H1 // // // // 5H NODE, IS,
1 36H HAS MORE THAN EIGHT ADJACENT NODES. /
2 23H THE CASE IS ABANDONED.)
GO TO 221
103 IF (ANP (NP, QA) .EQ. LN (Q)) GO TO 104
IF (ANP (NP, QA) .NE. 0) GO TO 101
ANP (NP, QA) = LN (Q)
NAP (NP) = QA
104 KXX (NP, QA) = KXX (NP, QA) + K (2 * P - 1, 2 * Q - 1)
KXY (NP, QA) = KXY (NP, QA) + K (2 * P - 1, 2 * Q)
KYX (NP, QA) = KYX (NP, QA) + K (2 * P, 2 * Q - 1)
105 KYY (NP, QA) = KYY (NP, QA) + K (2 * P, 2 * Q)

CCCC
110 BY INVERSION OF THE MAIN DIAGONAL STIFFNESS SUBMATRIX, FIND THE
FLEXIBILITY SUBMATRIX AT EACH NODE DISPLACED BY FORCES AT ITSELF.
DO 112 N = 1, NNP
W1 = KXX (N, 1) * KYY (N, 1) - KXY (N, 1) * KYX (N, 1)
FXX (N) = KYY (N, 1) / W1
FXY (N) = - KXY (N, 1) / W1
FYX (N) = - KYX (N, 1) / W1
112 FYY (N) = KXX (N, 1) / W1

CCCC
125 CONTINUE

CCCC
130 PERFORM A GAUSS - SEIDEL ITERATION ON THE STIFFNESS MATRIX FOR
THE ENTIRE STRUCTURE.
IF (NCC .GT. NCY) GO TO 132
WRITE (6, 131)
131 FORMAT (1H1 // // // //
1 34X, 35H THE PROGRESS OF THE GAUSS - SEIDEL ,
2 23H ITERATION TOWARD CONVERGENCE /
3 34X, 35H -----,
4 23H ----- // // //
5 33X, 39H CYCLE CONVERGENCE CRITERION,
6 26H CURRENT DIFFERENCE)
132 NC = 0
133 SD = 0.
SDD = 0.
DO 136 N = 1, NNP
IF (FXX (N) + FYY (N) .EQ. 0.) GO TO 136
RX1 = RX (N)
RY1 = RY (N)
NAP1 = NAP (N)
DO 134 CA = 1, NAP1
NP = ANP (N, QA)
134 RX1 = RX1 - KXX (N, QA) * U (NP) - KXY (N, QA) * V (NP)
RY1 = RY1 - KYX (N, QA) * U (NP) - KYY (N, QA) * V (NP)
IF (FXX (N) .EQ. 0.) GO TO 135
DELTAU = FXX (N) * RX1 + FXY (N) * RY1
U (N) = U (N) + CMEGA * DELTAU
SD = SD + ABS (U (N))
SDD = SDD + ABS (DELTAU)
IF (FYY (N) .EQ. 0.) GO TO 136
135 DELTAV = FYX (N) * RX1 + FYY (N) * RY1
V (N) = V (N) + CMEGA * DELTAV
SD = SD + ABS (V (N))
SDD = SDD + ABS (DELTAV)
136 CONTINUE
SD = AMAX1 (SD, 1.E-35)
RELDIF = SDD / SD

```

```

NC = NC + 1
IF (NCC .GT. NCV .OR. MCC (NC, NCC) .LE. 0) GO TO 142
WRITE (6, 141) NC, TOLER, RELODIF
141 FORMAT (1H3, I36, 3X, 2E27.5)
142 IF (RELODIF .GT. TOLER) GO TO 144
WRITE (6, 143) NC
143 FORMAT (1H1 //) 28H THE ITERATION HAS CONVERGED,
1 6H AFTER, I5, 6H CYCLES.)
GO TO 151
144 IF (NC .LT. NCV) GO TO 133
WRITE (6, 145) NC, RELODIF, TOLER
145 FORMAT (1H1 //) 28H THE ITERATION HAS COMPLETED, I5, 5H THE ,
1 52H MAXIMUM NUMBER OF CYCLES WITHOUT CONVERGING, BUT HAS /
2 34H ACHIEVED A RELATIVE DIFFERENCE OF, E13.5,
3 33H AGAINST A SPECIFIED TOLERANCE OF, E13.5, 1H. /
4 43H THE UNCONVERGED RESULTS ARE WRITTEN BELOW.)

```

```

150 OUTPUT THE NODE DISPLACEMENTS.
151 WRITE (6, 152)
152 FORMAT (1H1 //)
1 49X, 33H THE CALCULATED NODE DISPLACEMENTS /
2 49X, 33H -----
3 3X, 47H NCDE U V
4 U V
5 30H NCDE U V //
N1 = (NNP + 2) / 3
DO 153 N2 = 1, N1
N3 = MIN0 (N2 + 2 * N1, NNP)
153 WRITE (6, 154) (N, U (N), V (N), N = N2, N3, N1)
154 FORMAT (1H , I5, 2E16.5, I15, 2E16.5, I15, 2E16.5)

```

```

160 CALCULATE THE ELEMENT STRESS COMPONENTS.
IF (SR .EQ. 0) GO TO 221
DO 184 L = 1, NEL
I = NPI (L)
J = NPJ (L)
M = NPM (L)
AREA = (BJ (L) * CM (L) - BM (L) * CJ (L)) / 2.
EEXX = (BI (L) * U (I) + BJ (L) * U (J)
1 + EM (L) * U (M)) / (2. * AREA)
EYY = (CI (L) * V (I) + CJ (L) * V (J)
1 + CM (L) * V (M)) / (2. * AREA)
EEXY = (CI (L) * U (I) + BI (L) * V (I)
1 + CJ (L) * U (J) + BJ (L) * V (J)
2 + CM (L) * U (M) + BM (L) * V (M)) / (2. * AREA)
MATN = MAT (L)
W1 = NU (MATN)
W2 = 1. - W1
W3 = 1. + W1
W4 = 1. - 2. * W1
IF (PS .EQ. STRAIN) GO TO 161
W5 = E (MATN) / (W2 * W3)
W6 = W1
W7 = W2 / 2.
GO TO 162
161 W5 = E (MATN) * W2 / (W3 * W4)
W6 = W1 / W2
W7 = W4 / (2. * W2)
162 ETH = ALPHA (MATN) * DELTAT (L)
EEXX = EEXX - ETH
EYY = EYY - ETH
EEXY = EEXY
SIGLXX (L) = W5 * (EEXX + W6 * EYY)
SIGLYY (L) = W5 * (W6 * EEXX + EYY)
IF (PS .EQ. STRAIN) GO TO 163
SIGLZZ (L) = 0.
GO TO 164
163 SIGLZZ (L) = W1 * (SIGLXX (L) + SIGLYY (L))
164 SIGLXY (L) = W5 * W7 * EXY

```

```

170 CALCULATE THE ELEMENT PRINCIPAL AND MEAN STRESSES.
IF (SR .EQ. 2) GO TO 184
W1 = (SIGLXX (L) + SIGLYY (L)) / 2.
W2 = (SIGLXX (L) - SIGLYY (L)) / 2.
W3 = SIGLXY (L)
W4 = SORT (W2 ** 2 + W3 ** 2)
SIGL1 = W1 + W4
SIGL2 = W1 - W4
IF (ABS (W2) .GT. 1.E-35 .OR. ABS (W3) .GT. 1.E-35) GO TO 171
ANGLEL = 0.
GO TO 172
171 ANGLEL = 23.647889756 * ATAN2 (W3, W2)

```

```

172 SIGL3 = SIGLZZ (L)
    SIGLM = SQRT ((SIGL1 + SIGL2 + SIGL3) ** 2
1      - 3. * (SIGL2 * SIGL3 + SIGL3 * SIGL1 + SIGL1 * SIGL2))
C
C
180 OUTPUT THE ELEMENT STRESSES.
    IF (L .NE. 1) GC TO 182
    WRITE (6, 181)
181 FORMAT (1H1 //)
1      27X, 40H THE CALCULATED ELEMENT STRESS COMPONENTS,
2      40H AND THE PRINCIPAL AND THE MEAN STRESSES /
3      27X, 40H-----,
4      40H-----,
5      1X, 45HELEMENT          SIGMXX          SIGMYX          SIGMY
6      45HSIGMZZ          SIGMXY          ANGLE1
7      37HSIGM1          SIGM2          SIGMM /
182 WRITE (6, 183) L, SIGLXX (L), SIGLYY (L), SIGLZZ (L),
1      SIGLXY (L), ANGLE1, SIGL1, SIGL2, SIGLM
183 FORMAT (1H , I5, 4E16.5, F12.2, X, 3E16.5)
184 CONTINUE
    IF (SR .EQ. 1) GC TO 221
C
C
190 FIND THE NODE STRESS COMPONENTS.
    DO 212 N = 1, NNP
    SIGNXX = 0.
    SIGNYY = 0.
    SIGNZZ = 0.
    SIGNXY = 0.
    QA = 1
    DO 191 L = 1, NEL
    IF (NPI (L) .NE. N .AND. NPJ (L) .NE. N .AND. NPM (L) .NE. N)
1      GO TO 191
    SIGNXX = SIGNXX + SIGLXX (L)
    SIGNYY = SIGNYY + SIGLYY (L)
    SIGNZZ = SIGNZZ + SIGLZZ (L)
    SIGNXY = SIGNXY + SIGLXY (L)
    QA = QA + 1
    IF (QA .EQ. NAP (N)) GO TO 192
191 CONTINUE
192 W1 = FLOAT (QA - 1)
    SIGNXX = SIGNXX / W1
    SIGNYY = SIGNYY / W1
    SIGNZZ = SIGNZZ / W1
    SIGNXY = SIGNXY / W1
C
C
200 CALCULATE THE NODE PRINCIPAL AND MEAN STRESSES.
201 W1 = (SIGNXX + SIGNYY) / 2.
    W2 = (SIGNXX - SIGNYY) / 2.
    W3 = SIGNXY
    W4 = SQRT (W2 ** 2 + W3 ** 2)
    SIGN1 = W1 + W4
    SIGN2 = W1 - W4
    IF (ABS (W2) .GT. 1.E-35 .OR. ABS (W3) .GT. 1.E-35) GO TO 202
    ANGLE1 = 0.
    GO TO 203
202 ANGLE1 = 28.647889756 * ATAN2 (W3, W2)
203 SIGN3 = SIGNZZ
    SIGNM = SQRT ((SIGN1 + SIGN2 + SIGN3) ** 2
1      - 3. * (SIGN2 * SIGN3 + SIGN3 * SIGN1 + SIGN1 * SIGN2))
C
C
210 OUTPUT THE NODE STRESSES.
    IF (N .NE. 1) GC TO 212
    WRITE (6, 211)
211 FORMAT (1H1 //)
1      29X, 37H THE CALCULATED NODE STRESS COMPONENTS,
2      40H AND THE PRINCIPAL AND THE MEAN STRESSES /
3      29X, 37H-----,
4      40H-----,
5      3X, 43H NODE          SIGMXX          SIGMYX          SIGMY
6      45HSIGMZZ          SIGMXY          ANGLE1
7      37HSIGM1          SIGM2          SIGMM /
212 WRITE (6, 213) N, SIGNXX, SIGNYY, SIGNZZ, SIGNXY,
1      ANGLE1, SIGN1, SIGN2, SIGNM
213 FORMAT (1H , I5, 4E16.5, F12.2, X, 3E16.5)
C
C
220 RETURN TO THE BEGINNING OF THE PROGRAM FOR THE NEXT CASE.
221 GO TO 11
    END

```

## 5.3 Listing of Program STREN2

```

PROGRAM STREN2(INPUT=1002,OUTPUT=1002,TAPE5=INPUT,TAPE6=OUTPUT)
C 0 SPECIFICATION AND DATA INITIALIZATION STATEMENTS.
  INTEGER TITLE, PS, SR, QA, O, NP,
  1 CASCTL, STRESS, WI, ANP, P,
  2 STRAIN, CONO, Q.
  REAL NU, K, KXX,
  1 KXY,
  2 KYY,
  3 COMMON TITLE(13), NPI(277), X(166),
  1 E(1), NPJ(277), Y(166),
  2 NU(1), NPM(277), RX(166),
  3 RHO(1), MAT(277), RY(166),
  4 ALPHA(1), DELTAT(277), U(166),
  5 V(166),
  1 BI(277), KXX(166,9), ANP(166,9), SIGLXX(277),
  2 BJ(277), KXY(166,9), NAP(166), SIGLYY(277),
  3 BM(277), KYX(166,9), LN(3), SIGLZZ(277),
  4 CI(277), KYY(166,9), E(3,6), SIGLXY(277),
  5 CJ(277), FXX(166), D(3,3),
  6 CM(277), FXY(166), W(3,6),
  7 FYY(166), K(6,6),
  8
  DATA CASCTL, STRESS, STRAIN / 6HNFCASE, 6HSTRESS, 6HSTRAIN /
C C C
10 INPUT THE CASE TITLE BUT STOP IF THERE IS NO FURTHER CASE.
11 READ (5, 12) TITLE
12 FORMAT (13A6)
  IF (TITLE(1) .EQ. CASCTL) STOP
C C C
20 INPUT THE CONTROL PARAMETERS AND PREPARE TO INPUT THE ARRAY DATA.
  READ (5, 21) NEL, NNP, NMAT, NCV, NCC,
  1 TOLER, OMEGA, PS, SR, WI
21 FORMAT (5I5, E13.5, F7.3, 2X, A6, 2I3)
  DO 22 NM = 1, NMAT
22 E (NM) = -1.
  DO 23 L = 1, NEL
23 NPI (L) = -1
  DO 24 N = 1, NNP
24 X (N) = -0.123456789E35
C C C
30 INPUT AND CHECK THE ARRAY DATA.
  READ (5, 31) (MATN, E (MATN), NU (MATN),
  1 RHO (MATN), ALPHA (MATN)), NM = 1, NMAT)
31 FORMAT (I5, 4E13.5)
  DO 33 NM = 1, NMAT
  IF (E (NM) .NE. -1.) GO TO 33
  WRITE(6,333) NM
333 FORMAT(1X,7H E(NM)=, I5)
  WRITE (6, 32) TITLE
32 FORMAT (1H1 // // // 5H IN ' : 13A6, 1H' /
  1 35H THERE IS A MISSING INPUT DATA CARD.,
  2 24H THE JOB IS ABANDONED.)
  STOP
33 CONTINUE
  READ (5, 34) (LE, NPI (LE), NPJ (LE), NPM (LE),
  1 DELTAT(LE), MAT(LE), L=1, NEL )
34 FORMAT(4I5, F10.3, I5)
  DO 35 L = 1, NEL
  IF (NPI (L) .NE. -1) GO TO 35
  WRITE(6,334) L
334 FORMAT(1X, 3H L=, I5)
  WRITE (6, 32) TITLE
  STOP
35 CONTINUE
  DO 350 N=1,34
  READ(5,36) A1,E1,NP1,A2,32,NP2,A3,33,NP3,A4,34,NP4,A5,E5,NP5
36 FORMAT(5(F4.0,1X,F4.0,I4,3X))
  WRITE(6,37) NP1,NP2,NP3,NP4,NP5
371 FORMAT(1X,5(I20))
  X(NP1)=(A1-3607.)/505. EX(NP2)=(A2-3607.)/505.
  X(NP3)=(A3-3607.)/505. EX(NP4)=(A4-3607.)/505.
  X(NP5)=(A5-3607.)/505.
  Y(NP1)=(E1-1101.)/505. E Y(NP2)=(E2-1101.)/505.
  Y(NP3)=(E3-1101.)/505. E Y(NP4)=(E4-1101.)/505.
  Y(NP5)=(E5-1101.)/505.
350 CONTINUE
  DO 361 N=1,NNP
  RX(N)=0.
  RY(N)=0.
361 CONTINUE
  DO 37 N = 1, NNP

```

```

IF (X (N) .NE. -G.123456789E35) GO TO 37
WRITE (6, 335) N
335 FORMAT (1X, 3H N=: I5)
WRITE (6, 32) TITLE
STOP
37 CONTINUE

40 OUTPUT THE TITLE AND THE CONTROL PARAMETERS.
WRITE (6, 41)
41 FORMAT (1H1 //)
1 45X, 41H THE CASE TITLE AND THE CONTROL PARAMETERS /
2 45X, 41H ----- //)
WRITE (6, 42) TITLE
42 FORMAT (1H, 13A6)
WRITE (6, 43) NEL, NNP, NBR, NPMAT, NCV, NCC, TOLER, OMEGA, PS
43 FORMAT (26H THE NUMBER OF ELEMENTS IS, I5, 1H. /
1 30H THE NUMBER OF NODAL POINTS IS, I5, 1H. /
2 43H THE NUMBER OF RESTRAINED BOUNDARY NODES IS, I5, 1H. /
3 25H THE NUMBER OF DIFFERENT MATERIALS IS, I5, 1H. /
4 25H THE ITERATION LIMIT IS, I5, 8H CYCLES. /
5 36H THE INTERVAL FOR PROGRESS OUTPUT IS, I5, 8H CYCLES. /
6 29H THE CONVERGENCE TOLERANCE IS, E13.5, 1H. /
7 37H THE OVER-RELAXATION FACTOR IS, F7.3, 1H. /
8 37H THE CASE HAS THE CONDITION OF PLANE, A6, 1H. /
9 23H STRESSES ARE FOUND FOR)
IF (SR .EQ. 0) WRITE (6, 44)
44 FORMAT (1H+, 23X, 42H NEITHER THE ELEMENTS NOR THE NODAL POINTS.)
IF (SR .EQ. 1) WRITE (6, 45)
45 FORMAT (1H+, 23X, 18H THE ELEMENTS ONLY.)
IF (SR .EQ. 2) WRITE (6, 46)
46 FORMAT (1H+, 23X, 22H THE NODAL POINTS ONLY.)
IF (SR .EQ. 3) WRITE (6, 47)
47 FORMAT (1H+, 23X, 39H BOTH THE ELEMENTS AND THE NODAL POINTS.)
IF (WI .EQ. 0) WRITE (6, 48)
48 FORMAT (37H THE INPUT ARRAY DATA ARE NOT OUTPUT.)
IF (WI .EQ. 1) WRITE (6, 49)
49 FORMAT (33H THE INPUT ARRAY DATA ARE OUTPUT.)

50 OUTPUT THE ARRAY DATA.
IF (WI .EQ. 0) GO TO 61
WRITE (6, 51) (NM, E (NM), NU (NM), RHC (NM),
1 ALPHA (NM), NH = 1, NPMAT)
51 FORMAT (1H1 //)
1 55X, 19H INPUT MATERIAL DATA /
2 55X, 19H ----- //)
3 28X, 42H MATERIAL ELASTIC MODULUS POISSON'S RATIO,
4 34H DENSITY THIL EXPN COEFF //
5 (I33, X, 4E17.5))
WRITE (6, 52)
52 FORMAT (1H1 //)
1 57X, 18H INPUT ELEMENT DATA /
2 57X, 18H ----- //)
3 3X, 48HELMT NPI NPM MTRL DELTA T
4 48HELMT NPI NPM MTRL DELTA T
5 33HELMT NPI NPM MTRL DELTA T //)
L1 = (NEL + 2) / 3
DO 53 L2 = 1, L1
L3 = MIN0 (L2 + 2 * L1, NEL)
53 WRITE (6, 54) (L, NPI (L), NPM (L), NPM (L),
1 MAT (L), DELTAT (L), L = L2, L3, L1)
54 FORMAT (1H, 5I5, F10.3, 13X, 5I5, F10.3, 13X, 5I5, F10.3)
DO 540 N=1, NNP
U(N)=0.
V(N)=0.
540 CONTINUE
WRITE (6, 55) (N, X (N), Y (N), RX (N), RY (N),
1 U (N), V (N), N = 1, NNP)
55 FORMAT (1H1 //)
1 58X, 15H INPUT NODE DATA /
2 58X, 15H ----- //)
3 13X, 49H NODE X Y
4 31HRX RY
5 21H U V //
6 (I15, X, 6E17.5))

60 DO GEOMETRIC CALCULATIONS ON THE ELEMENTS.
61 DO 72 L = 1, NEL
I = NPI (L)
J = NPJ (L)
M = NPM (L)
EI (L) = Y (J) - Y (M)
EJ (L) = Y (M) - Y (I)

```

```

BH (L) = Y (I) - Y (J)
CI (L) = - X (J) + X (M)
CJ (L) = - Y (M) + X (I)
CM (L) = - X (I) + X (J)
AREA = (BJ (L) * CM (L) - BM (L) * CJ (L)) / 2.
IF (AREA .GT. 1.E-35) GO TO 71
WRITE (6, 62) L
62 FORMAT (1H1, '///// 8H ELEMENT, 15, 25H HAS A NON-POSITIVE AREA. /
1 23H THE CASE IS ABANDONED.')
GO TO 221

```

```

70 SUM THE TOTAL NCDAL PCINT FORCES.

```

```

71 MATN = MAT (L)
IF (PS .EQ. STRESS) SIGTH = 1. - NU (MATN)
IF (PS .EQ. STRAIN) SIGTH = (1. + NU (MATN))
1 (1. - 2. * NU (MATN))
SIGTH = - E (MATN) * ALPHA (MATN) * DELTAT (L) / SIGTH
BODYF = AREA * RHO (MATN) / 3.
RX (I) = RX (I) - 0.5 * BI (L) * SIGTH
RY (I) = RY (I) - 0.5 * CI (L) * SIGTH - BODYF
RX (J) = RX (J) - 0.5 * BJ (L) * SIGTH
RY (J) = RY (J) - 0.5 * CJ (L) * SIGTH - BODYF
RX (M) = RX (M) - 0.5 * BI (L) * SIGTH
72 RY (M) = RY (M) - 0.5 * CM (L) * SIGTH - BODYF

```

```

80 PREPARE TO SUM THE STIFFNESS COEFFICIENTS.

```

```

DO 82 N = 1, NNP
DO 81 QA = 1, 9
KXX (N, QA) = 0.
KXY (N, QA) = 0.
KYY (N, QA) = 0.
81 ANP (N, QA) = 0
ANP (N, 1) = N
82 NAP (N) = 1

```

```

90 FORM THE STIFFNESS MATRIX FOR THE ELEMENT.

```

```

DO 105 L = 1, 277
DO 92 P = 1, 3
DO 91 Q = 1, 6
91 E (P, Q) = 0.
DO 92 (P, Q) = 0.
92 DD (P, Q) = 0.
BB (1, 1) = BI (L)
BB (1, 3) = BJ (L)
BB (1, 5) = BM (L)
BB (2, 2) = CI (L)
BB (2, 4) = CJ (L)
BB (2, 6) = CM (L)
BB (3, 1) = BI (L)
BB (3, 2) = BJ (L)
BB (3, 3) = BJ (L)
BB (3, 4) = CJ (L)
BB (3, 5) = CM (L)
BB (3, 6) = CM (L)
MATN = MAT (L)
W1 = NU (MATN)
W2 = 1. - W1
W3 = 1. + W1
W4 = 1. - 2. * W1
IF (PS .EQ. STRAIN) GO TO 93
W5 = E (MATN) / (W2 * W3)
W6 = W1
W7 = W2 / 2.
GO TO 94
93 W5 = E (MATN) * W2 / (W3 * W4)
W6 = W1 / W2
W7 = W4 / (2. * W2)
94 AREA = (BJ (L) * CM (L) - BM (L) * CJ (L)) / 2.
W5 = W5 / (4. * AREA)
D (1, 1) = W5 * W6
D (1, 2) = W5 * W6
D (2, 1) = W5 * W6
D (2, 2) = W5 * W6
D (3, 3) = W5 * W7
DO 95 P = 1, 3
DO 95 Q = 1, 6
W (P, Q) = 0.
DO 95 O = 1, 3
IF (P.GT.3) P=3
IF (Q.GT.6) Q=6

```

```

95 W (P, Q) = W (P, Q) + D (P, Q) * B (Q, Q)
DO 96 P = 1, 6
DO 96 Q = 1, 6
K (P, Q) = 9.
DO 96 Q = 1, 3
96 K (P, Q) = K (P, Q) + B (Q, P) * W (Q, Q)

CCCC
100 SUM AND STORE FOR EACH (FORCED) NODE THE NON-ZERO STIFFNESS
COEFFICIENTS FOR THE ADJACENT (DISPLACED) NODES.
LN (1) = NPI (L)
LN (2) = NPJ (L)
LN (3) = NPM (L)
DO 105 P = 1, 3
NP = LN (P)
DO 105 Q = 1, 3
QA = 0
101 QA = QA + 1
IF (QA .LE. 9) GO TO 103
WRITE (6, 102) NP
102 FORMAT (1H1 ////////////// 5H NODE, I5,
1 35H HAS MORE THAN EIGHT ADJACENT NODES. /
2 23H THE CASE IS ABANDONED.)
GO TO 221
103 IF (ANP (NP, QA) .EQ. LN (Q)) GO TO 104
IF (ANP (NP, QA) .NE. 0) GO TO 101
ANP (NP, QA) = LN (Q)
NAP (NP) = QA
104 KXX (NP, QA) = KXX (NP, QA) + K (2 * P - 1, 2 * Q - 1)
KXY (NP, QA) = KXY (NP, QA) + K (2 * P - 1, 2 * Q)
KYG (NP, QA) = KYG (NP, QA) + K (2 * P, 2 * Q - 1)
105 KYY (NP, QA) = KYY (NP, QA) + K (2 * P, 2 * Q)

CCCC
110 BY INVERSION OF THE MAIN DIAGONAL STIFFNESS SUBMATRIX, FIND THE
FLEXIBILITY SUBMATRIX AT EACH NODE DISPLACED BY FORCES AT ITSELF.
DO 112 N = 1, NNP
W1 = KXX (N, 1) * KYY (N, 1) - KXY (N, 1) * KYX (N, 1)
FXX (N) = - KYY (N, 1) / W1
FXY (N) = - KXY (N, 1) / W1
FYX (N) = - KYX (N, 1) / W1

CCCC
130 PERFORM A GAUSS - SEIDEL ITERATION ON THE STIFFNESS MATRIX FOR
THE ENTIRE STRUCTURE.
IF (NCC .GT. NCY) GO TO 132
WRITE (6, 131)
131 FORMAT (1H1 //////////////
1 34X, 35H THE PROGRESS OF THE GAUSS - SEIDEL ;
2 29H ITERATION TOWARD CONVERGENCE /
3 34X, 35H -----
4 28H ----- //
5 33X, 39H CYCLE CONVERGENCE CRITERION,
6 26H CURRENT DIFFERENCE)
132 NC = 0
133 SD = 0.
SDD = 0.
DO 136 N = 1, NNP
IF (FXX (N) + FYY (N) .EQ. 0.) GO TO 136
RX1 = RX (N)
RY1 = RY (N)
NAP1 = NAP (N)
DO 134 QA = 1, NAP1
NP = ANP (N, QA)
134 RX1 = RX1 - KXX (N, QA) * U (NP) - KXY (N, QA) * V (NP)
RY1 = RY1 - KYX (N, QA) * U (NP) - KYY (N, QA) * V (NP)
IF (FXX (N) .EQ. 0.) GO TO 135
DELTAU = FXX (N) * RX1 + FXY (N) * RY1
U (N) = U (N) + CMEGA * DELTAU
SD = SD + ABS (U (N))
SDD = SDD + ABS (DELTAU)
IF (FYY (N) .EQ. 0.) GO TO 136
135 DELTAV = FYX (N) * RX1 + FYY (N) * RY1
V (N) = V (N) + CMEGA * DELTAV
SD = SD + ABS (V (N))
SDD = SDD + ABS (DELTAV)
136 CONTINUE
SD = AMAX1 (SD, 1.E-35)
RELDIF = SDD / SD

CCCC
140 TEST FOR CONVERGENCE.
NC = NC + 1
IF (NCC .GT. NCY .OR. MOD (NC, NCC) .NE. 0) GO TO 142

```

```

141 WRITE (6, 141) NC, TOLER, RELOIF
142 IF (RELOIF .GT. TOLER) GO TO 144
143 WRITE (6, 143) NC
144 FORMAT (1H1 // // // // // 28H THE ITERATION HAS CONVERGED,
1 GO TO 151
144 IF (NC .LT. NCY) GO TO 133
145 WRITE (6, 145) NC, RELOIF, TOLER
145 FORMAT (1H1 // // // // // 23H THE ITERATION HAS COMPLETED, I5, 5H THE
1 52H MAXIMUM NUMBER OF CYCLES WITHOUT CONVERGING, BUT HAS /
2 34H ACHIEVED A RELATIVE DIFFERENCE OF, E13.5,
3 33H AGAINST A SPECIFIED TOLERANCE OF, E13.5, 1H. /
4 43H THE UNCONVERGED RESULTS ARE WRITTEN BELOW.)

```

C  
C  
C

```

150 OUTPUT THE NODE DISPLACEMENTS.
151 WRITE (6, 151)
152 FORMAT (1H1 // // // // //
1 49X, 33H THE CALCULATED NODE DISPLACEMENTS /
2 43X, 33H -----
3 3X, 47H NODE U V
4 47H NODE U V
5 30H NODE U V /)
N1 = (NNP + 2) / 3
DO 153 N2 = 1, N1
N3 = MIN0 (N2 + 2 * N1, NNP)
153 WRITE (6, 154) (N, U (N), V (N), N = N2, N3, N1)
154 FORMAT (1H1, I5, 2E16.5, I15, 2E16.5, I15, 2E16.5)

```

C  
C  
C

```

160 CALCULATE THE ELEMENT STRESS COMPONENTS.
IF (SR .EQ. 0) GO TO 221
DO 164 L = 1, NEL
I = NPI (L)
J = NPJ (L)
M = NPM (L)
AREA = (BJ (L) * CM (L) - BM (L) * CJ (L)) / 2.
EEXX = (BI (L) * U (I) + BJ (L) * U (J)
1 + BM (L) * U (M)) / (2. * AREA)
1 EEEY = (CI (L) * V (I) + CJ (L) * V (J)
1 + CM (L) * V (M)) / (2. * AREA)
1 EEXY = (CI (L) * U (I) + BI (L) * V (I)
1 + CJ (L) * U (J) + BJ (L) * V (J)
2 + CM (L) * U (M) + BM (L) * V (M)) / (2. * AREA)
MATN = MAT (L)
W1 = NU (MATN)
W2 = 1. - W1
W3 = 1. + W1
W4 = 1. - 2. * W1
IF (PS .EQ. STRAIN) GO TO 161
W5 = E (MATN) / (W2 * W3)
W6 = W1
W7 = W2 / 2.
GO TO 162
161 W5 = E (MATN) * W2 / (W3 * W4)
W6 = W1 / W2
W7 = W4 / (2. * W2)
162 ETH = ALPHA (MATN) + DELTAT (L)
EEX = EEXX - ETH
EYY = EEEY - ETH
EXY = EEXY
SIGLXX (L) = W5 * (EEX + W6 * EYY)
SIGLYY (L) = W5 * (W6 * EEX + EYY)
IF (PS .EQ. STRAIN) GO TO 163.
SIGLZZ (L) = 0.
GO TO 164
163 SIGLZZ (L) = W1 * (SIGLXX (L) + SIGLYY (L))
164 SIGLXY (L) = W5 * W7 * EXY

```

C  
C  
C

```

170 CALCULATE THE ELEMENT PRINCIPAL AND MEAN STRESSES.
IF (SR .EQ. 2) GO TO 184
W1 = (SIGLXX (L) + SIGLYY (L)) / 2.
W2 = (SIGLXX (L) - SIGLYY (L)) / 2.
W3 = SIGLXY (L)
W4 = SQRT (W2 ** 2 + W3 ** 2)
SIGL1 = W1 + W4
SIGL2 = W1 - W4
IF (ABS (W2) .GT. 1.E-35 .OR. ABS (W3) .GT. 1.E-35) GO TO 171
ANGLEL = 0.
GO TO 172
171 ANGLEL = 28.647889756 * ATAN2 (W3, W2)
172 SIGL3 = SIGLZZ (L)
SIGLM = SQRT ((SIGL1 + SIGL2 + SIGL3) ** 2)

```



```

1          - 3. * (SIGL2 * SIGL3 + SIGL3 * SIGL1 + SIGL1 * SIGL2))
C C C
180 OUTPUT THE ELEMENT STRESSES.
IF (L .NE. 1) GO TO 182
WRITE (6, 181)
181 FORMAT (1H1 //)
1 27X, 40H THE CALCULATED ELEMENT STRESS COMPONENTS,
2 40H AND THE PRINCIPAL AND THE MEAN STRESSES /
3 27X, 40H-----
4 40H----- //
5 1X, 45H ELEMENT          SIGMXX          SIGMY
6 45H SIGMZZ          SIGMXY          ANGLE1
7 37H SIGM1          SIGM2          SIGMM //
182 WRITE (6, 183) L, SIGLXX (L), SIGLYY (L), SIGLZZ (L),
1  SIGLXY (L), ANGLE1, SIGL1, SIGL2, SIGLM
183 FORMAT (1H , I5, 4E16.5, F12.2, X, 3E16.5)
184 CONTINUE
IF (SR .EQ. 1) GO TO 221

C C C
190 FIND THE NODE STRESS COMPONENTS.
DO 212 N = 1, NNP
SIGNXX = 0.
SIGNYY = 0.
SIGNZZ = 0.
SIGNXY = 0.
QA = 1
DO 191 L = 1, NEL
IF (NPI (L) .NE. N .AND. NPJ (L) .NE. N .AND. NPM (L) .NE. N)
1 GO TO 191
SIGNXX = SIGNXX + SIGLXX (L)
SIGNYY = SIGNYY + SIGLYY (L)
SIGNZZ = SIGNZZ + SIGLZZ (L)
SIGNXY = SIGNXY + SIGLXY (L)
QA = QA + 1
IF (QA .EQ. NAP (N)) GO TO 192
191 CONTINUE
192 W1 = FLCAT (QA - 1)
SIGNXX = SIGNXX / W1
SIGNYY = SIGNYY / W1
SIGNZZ = SIGNZZ / W1
SIGNXY = SIGNXY / W1

C C C
200 CALCULATE THE NODE PRINCIPAL AND MEAN STRESSES.
201 W1 = (SIGNXX + SIGNYY) / 2.
W2 = (SIGNXX - SIGNYY) / 2.
W3 = SIGNXY
W4 = SQRT (W2 ** 2 + W3 ** 2)
SIGN1 = W1 + W4
SIGN2 = W1 - W4
IF (ABS (W2) .GT. 1.E-35 .OR. ABS (W3) .GT. 1.E-35) GO TO 202
ANGLN = 0.
GO TO 203
202 ANGLN = 28.647889756 * ATAN2 (W3, W2)
203 SIGN3 = SIGNZZ
SIGNM = SQRT ((SIGN1 + SIGN2 + SIGN3) ** 2
1 - 3. * (SIGN2 * SIGN3 + SIGN3 * SIGN1 + SIGN1 * SIGN2))

C C C
210 OUTPUT THE NODE STRESSES.
IF (N .NE. 1) GO TO 212
WRITE (6, 211)
211 FORMAT (1H1 //)
1 29X, 37H THE CALCULATED NODE STRESS COMPONENTS,
2 40H AND THE PRINCIPAL AND THE MEAN STRESSES /
3 29X, 37H-----
4 40H----- //
5 3X, 43H NODE          SIGMXX          SIGMY
6 45H SIGMZZ          SIGMXY          ANGLE1
7 37H SIGM1          SIGM2          SIGMM //
212 WRITE (6, 213) N, SIGNXX, SIGNYY, SIGNZZ, SIGNXY,
1 ANGLN, SIGN1, SIGN2, SIGNM
213 FORMAT (1H , I5, 4E16.5, F12.2, X, 3E16.5)
X, 3E16.5)

C C C
220 RETURN TO THE BEGINNING OF THE PROGRAM FOR THE NEXT CASE.
221 GO TO 11
END

```

```

C      PROGRAM STREN3(INPUT,CUTPUT,TAPES=INPUT,TAPE6=OUTPUT)
0 SPECIFICATION AND DATA INITIALIZATION STATEMENTS.
  INTEGER  TITLE, PS, SR, OA, O, NP,
1          CASCTL, STRESS, WI, AMP, P,
2          REAL  NU, K, KXX,
3          KXY,
4          KYY
COMMON  TITLE(13), NPI(549), X(340),
1        E(1), NPJ(549), Y(340),
2        NU(1), NPY(549), RX(340),
3        RHO(1), MAT(549), RY(340),
4        ALPHA(1), DELTAT(549), U(340),
5        V(340),
6        BI(549), KXX(340,9), AMP(340,9), SIGLXX(549),
7        BJ(549), KXY(340,9), NAP(340), SIGLYY(549),
8        BM(549), KYX(340,9), LN(3), SIGLZZ(549),
9        CI(549), KYY(340,9), B(3,6), SIGLXY(549),
10       CJ(549), FXX(340), C(3,3),
11       CM(549), FXY(340), W(3,6),
12       FYY(340), K(6,6),
13
DATA  CASCTL, STRESS, STRAIN / 6HNFCASE, 6HSTRESS, 6HSTRAIN /

C
10 INPUT THE CASE TITLE BUT STOP IF THERE IS NO FURTHER CASE.
11 READ (5, 12) TITLE
12 FORMAT (13A6)
   IF (TITLE (1) .EG. CASCTL) STOP

C
20 INPUT THE CONTROL PARAMETERS AND PREPARE TO INPUT THE ARRAY DATA.
  READ (5, 21) NEL, NNP, NMAT, NCY, NCC,
1          TOLER, OMEGA, PS, SR, WI
21 FORMAT (5I5, E13.5, F7.3, 2X, A6, 2I3)
  DO 22 NM = 1, NMAT
22 E (NM) = -1.
  DO 23 L = 1, NEL
23 NPI (L) = -1
  DO 24 N = 1, NNP
24 X (N) = -.123456789E35

C
30 INPUT AND CHECK THE ARRAY DATA.
  READ (5, 31) (MATN, E (MATN), NU (MATN),
1          RHC (MATN), ALPHA (MATN), NM = 1, NMAT)
31 FORMAT (I5, 4E13.5)
  DO 33 NM = 1, NMAT
  IF (E (NM) .NE. -1.) GO TO 33
  WRITE (6, 333) NM
333 FORMAT (1X, 7H E(NM)=, I5)
  WRITE (6, 32) TITLE
32 FORMAT (1H1 // // // // 5H IN ', 13A6, 1H' /
1          36H THERE IS A MISSING INPUT DATA CARD.,
2          24H THE JOB IS ABANDONED.)
  STOP
33 CONTINUE
  READ (5, 34) (LE, NPI (LE), NPJ (LE), NPY (LE),
1          DELTAT(LE), MAT(LE), L=1, NEL)
34 FORMAT(4I5, F10.3, I5)
  DO 35 L = 1, NEL
  IF (NPI (L) .NE. -1) GO TO 35
  WRITE (6, 334) L
334 FORMAT(1X, 3H L=, I5)
  WRITE (6, 32) TITLE
  STOP
35 CONTINUE
  DO 350 N=1,68
  READ(5,36) A1,91,NP1,A2,32,NP2,A3,83,NP3,A4,B4,NP4,A5,E5,NP5
36 FORMAT(5(F4.0,1X,F4.0,I4,3X))
  WRITE(6,37) NP1,NP2,NP3,NP4,NP5
371 FORMAT(1X,5(I20))
  X(NP1)=(A1-1693.)/797. EX(NP2)=(A2-1693.)/797.
  X(NP3)=(A3-1698.)/797. EX(NP4)=(A4-1693.)/797.
  X(NP5)=(A5-1698.)/797.
  Y(NP1)=(B1-1477.)/797. E Y(NP2)=(B2-1477.)/797.
  Y(NP3)=(B3-1477.)/797. E Y(NP4)=(B4-1477.)/797.
  Y(NP5)=(B5-1477.)/797.
350 CONTINUE
  DO 361 N=1,NNP
  RX(N)=0.
  RY(N)=0.
361 CONTINUE
  DO 37 N = 1, NNP

```



```

    PH (L) = Y (I) - Y (J)
    CI (L) = - X (J) + X (M)
    CJ (L) = - Y (M) + X (I)
    CM (L) = - X (I) + X (J)
    AREA = (BJ (L) * CM (L) - BM (L) * CJ (L)) / 2.
    IF (AREA .GT. 1.E-35) GO TO 71
    WRITE (6, 62) L
62  FORMAT (1H1 // // // 8H ELEMENT, IS, 25H HAS A NON-POSITIVE AREA. /
1    23H THE CASE IS ABANDONED.)
    GO TO 221

```

```

70  SUM THE TOTAL NODAL POINT FORCES.
71  MATN = MAT (L)
    IF (PS .EQ. STRESS) SIGTH = 1. - NU (MATN)
    IF (PS .EQ. STRAIN) SIGTH = 1. + NU (MATN)
1    SIGTH = - E (MATN) * ALPHA (MATN) * DELTAT (L) / SIGTH
    BODYF = AREA * RHO (MATN) / 3.
    RX (I) = RX (I) - 0.5 * BI (L) * SIGTH
    RY (I) = RY (I) - 0.5 * CI (L) * SIGTH - BODYF
    RX (J) = RX (J) - 0.5 * BJ (L) * SIGTH
    RY (J) = RY (J) - 0.5 * CJ (L) * SIGTH - BODYF
    RX (M) = RX (M) - 0.5 * BM (L) * SIGTH
    RY (M) = RY (M) - 0.5 * CM (L) * SIGTH - BODYF
72

```

```

80  PREPARE TO SUM THE STIFFNESS COEFFICIENTS.
    DO 82 N = 1, NNP
    DO 81 QA = 1, 9
    KXX (N, QA) = 0.
    KXY (N, QA) = 0.
    KYY (N, QA) = 0.
    KXX (N, QA) = 0.
    KYY (N, QA) = 0.
81  ANP (N, QA) = 0
    ANP (N, 1) = N
82  NAP (N) = 1

```

```

90  FORM THE STIFFNESS MATRIX FOR THE ELEMENT.
    DO 105 L = 1, NEL
    DO 92 P = 1, 3
    DO 91 Q = 1, 6
91  B (P, Q) = 0.
    DO 92 O = 1, 3
92  D (P, O) = 0.
    B (1, 1) = BI (L)
    B (1, 3) = BJ (L)
    B (1, 5) = BM (L)
    B (2, 2) = CI (L)
    B (2, 4) = CJ (L)
    B (2, 6) = CM (L)
    B (3, 1) = CI (L)
    B (3, 2) = BI (L)
    B (3, 3) = BJ (L)
    B (3, 4) = BM (L)
    B (3, 5) = CM (L)
    B (3, 6) = CM (L)
    MATN = MAT (L)
    W1 = NU (MATN)
    W2 = 1. - W1
    W3 = 1. + W1
    W4 = 1. - 2. * W1
    IF (PS .EQ. STRAIN) GO TO 93
    W5 = E (MATN) / (W2 * W3)
    W6 = W1
    W7 = W2 / 2.
    GO TO 94
93  W5 = E (MATN) * W2 / (W3 * W4)
    W6 = W1 / W2
    W7 = W4 / (2. * W2)
94  AREA = (BJ (L) * CM (L) - BM (L) * CJ (L)) / 2.
    W5 = W5 / (4. * AREA)
    D (1, 1) = W5 * W6
    D (1, 2) = W5 * W6
    D (2, 1) = W5 * W6
    D (2, 2) = W5 * W6
    D (3, 3) = W5 * W7
    DO 95 P = 1, 3
    DO 95 Q = 1, 6
    H (P, Q) = 0.
    DO 95 O = 1, 3
    IF (P.GT.3) P=3
    IF (O.GT.6) O=6
    IF (C.GT.3) O=3

```

```

95 W (P, Q) = W (P, Q) + D (P, Q) * B (O, Q)
DO 96 P = 1, 6
DO 96 Q = 1, 6
K (P, Q) = K (P, Q) + B (O, P) * W (O, Q)
DO 96 O = 1, 3
96 K (P, Q) = K (P, Q) + B (O, P) * W (O, Q)

```

CCCCC

```

100 SUM AND STORE FOR EACH (FORCED) NODE THE NON-ZERO STIFFNESS
    COEFFICIENTS FOR THE ADJACENT (DISPLACED) NODES.
    LN (1) = NPI (L)
    LN (2) = NPJ (L)
    LN (3) = NPM (L)
    DO 105 P = 1, 3
    NP = LN (P)
    DO 105 Q = 1, 3
    QA = 0
101 QA = QA + 1
    IF (QA .LE. 9) GO TO 103
    WRITE (6, 102) NP
102 FORMAT (1H // 5H NODE, I5,
1 36H HAS MORE THAN EIGHT ADJACENT NODES. /
2 23H THE CASE IS ABANDONED.)
    GO TO 221
103 IF (ANP (NP, QA) .EQ. LN (Q)) GO TO 104
    IF (ANP (NP, QA) .NE. 0) GO TO 101
    ANP (NP, QA) = LN (Q)
    NAP (NP) = QA
104 KXX (NP, QA) = KXX (NP, QA) + K (2 * P - 1, 2 * Q - 1)
    KXY (NP, QA) = KXY (NP, QA) + K (2 * P - 1, 2 * Q)
    KYX (NP, QA) = KYX (NP, QA) + K (2 * P, 2 * Q - 1)
105 KYY (NP, QA) = KYY (NP, QA) + K (2 * P, 2 * Q)

```

CCCCC

```

110 BY INVERSION OF THE MAIN DIAGONAL STIFFNESS SUBMATRIX, FIND THE
    FLEXIBILITY SUBMATRIX AT EACH NODE DISPLACED BY FORCES AT ITSELF.
    DO 112 N = 1, NNP
    W1 = KXX (N, 1) * KYY (N, 1) - KXY (N, 1) * KYX (N, 1)
    FXX (N) = KYY (N, 1) / W1
    FXY (N) = - KXY (N, 1) / W1
    FYX (N) = - KYX (N, 1) / W1
112 FYY (N) = KXX (N, 1) / W1

```

CCCCC

```

130 PERFORM A GAUSS - SEIDEL ITERATION ON THE STIFFNESS MATRIX FOR
    THE ENTIRE STRUCTURE.
    IF (NCC .GT. NCY) GO TO 132
    WRITE (6, 131)
131 FORMAT (1H // 5H
1 34X, 35H THE PROGRESS OF THE GAUSS - SEIDEL ,
2 28H ITERATION TOWARD CONVERGENCE ?
3 34X, 35H -----
4 28H ----- // 5H
5 33X, 39H CYCLE CONVERGENCE CRITERION,
6 26H CURRENT DIFFERENCE)

```

```

132 NC = 0
133 SD = 0.
    SDD = 0.
    DO 136 N = 1, NNP
    IF (FXX (N) + FYY (N) .EQ. 0.) GO TO 136
    RX1 = RX (N)
    RY1 = RY (N)
    NAP1 = NAP (N)
    DO 134 QA = 1, NAP1
    NP = ANP (N, QA)
134 RX1 = RX1 - KXX (N, QA) * U (NP) - KXY (N, QA) * V (NP)
    RY1 = RY1 - KYX (N, QA) * U (NP) - KYY (N, QA) * V (NP)
    IF (FXX (N) .EQ. 0.) GO TO 135
    DELTAU = FXX (N) + RX1 + FXY (N) * RY1
    U (N) = U (N) + OMEGA * DELTAU
    SD = SD + ABS (U (N))
    SDD = SDD + ABS (DELTAU)
    IF (FYY (N) .EQ. 0.) GO TO 136
135 DELTAV = FYX (N) * RX1 + FYY (N) * RY1
    V (N) = V (N) + OMEGA * DELTAV
    SD = SD + ABS (V (N))
    SDD = SDD + ABS (DELTAV)
136 CONTINUE
    SJ = AMAX1 (SD, 1.E-35)
    RELDIF = SDD / SD

```

C

```

NC = NC + 1
IF (NCC .GT. 141, NCV .OR. MOD (NC, NCC) .NE. 0) GO TO 142
WRITE (6, 141) NC, TOLER, RELODIF
141 FORMAT (1H0, I36, 3X, 2E27.5)
142 IF (RELODIF .GT. TOLER) GO TO 144
WRITE (6, 143) NC
143 FORMAT (1H1, 143) '//////// 28H THE ITERATION HAS CONVERGED,
1 6H AFTER, 15, 8H CYCLES.)
GO TO 151
144 IF (NC .LT. NCV) GO TO 133
144 WRITE (6, 145) NC, RELODIF, TOLER
145 FORMAT (1H1, 145) '//////// 28H THE ITERATION HAS COMPLETED, 15, 5H THE,
1 52H MAXIMUM NUMBER OF CYCLES WITHOUT CONVERGING, BUT HAS /
34H ACHIEVED A RELATIVE DIFFERENCE OF, E13.5,
33H AGAINST A SPECIFIED TOLERANCE OF, E13.5, 1H. /
43H THE UNCONVERGED RESULTS ARE WRITTEN BELCW.)

```

```

150 OUTPUT THE NODE DISPLACEMENTS.
151 WRITE (6, 152)
152 FORMAT (1H1, 152) '////////
1 49X, 33H THE CALCULATED NODE DISPLACEMENTS /
43X, 33H -----
3X, 47H NCDE U V
47H NCDE U V
30H NCDE U V /)
N1 = (NNP + 2) / 3
DO 153 N2 = 1, N1
N3 = MIN0 (N2 + 2 * N1, NNP)
153 WRITE (6, 154) (N, U (N), V (N), N = N2, N3, N1)
154 FORMAT (1H , 154) (N, U (N), V (N), N = N2, N3, N1)

```

```

160 CALCULATE THE ELEMENT STRESS COMPONENTS.
IF (SR .EQ. 0) GO TO 221
DO 161 L = 1, NEL
I = NPI (L)
J = NPJ (L)
M = NPM (L)
AREA = (BJ (L) * CM (L) - BM (L) * CJ (L)) / 2.
EEXX = (BI (L) * U (I) + BJ (L) * U (J)
+ BM (L) * U (M)) / (2. * AREA)
EYY = (CI (L) * V (I) + CJ (L) * V (J)
+ CM (L) * V (M)) / (2. * AREA)
EEXY = (CI (L) * U (I) + BI (L) * V (I)
+ CJ (L) * U (J) + BJ (L) * V (J)
+ CM (L) * U (M) + BM (L) * V (M)) / (2. * AREA)
MATN = MAT (L)
W1 = NU (MATN)
W2 = 1. - W1
W3 = 1. + W1
W4 = 1. - 2. * W1
IF (PS .EQ. STRAIN) GO TO 161
W5 = E (MATN) / (W2 * W3)
W6 = W1
W7 = W2 / 2.
GO TO 162
161 W5 = E (MATN) * W2 / (W3 * W4)
W6 = W1 / W2
W7 = W4 / (2. * W2)
162 ETH = ALPHA (MATN) * DELTAT (L)
EEXX = EEXX - ETH
EYY = EYY - ETH
EEXY = EEXY - ETH
SIGLXX (L) = W5 * (EEXX + W6 * EYY)
SIGLYY (L) = W5 * (W6 * EEXX + EYY)
IF (PS .EQ. STRAIN) GO TO 163
SIGLZZ (L) = 0.
GO TO 164
163 SIGLZZ (L) = W1 * (SIGLXX (L) + SIGLYY (L))
164 SIGLXY (L) = W5 * W7 * EXY

```

```

170 CALCULATE THE ELEMENT PRINCIPAL AND MEAN STRESSES.
IF (SR .EQ. 2) GO TO 184
W1 = (SIGLXX (L) + SIGLYY (L)) / 2.
W2 = (SIGLXX (L) - SIGLYY (L)) / 2.
W3 = SIGLXY (L)
W4 = SQRT (W2 ** 2 + W3 ** 2)
SIGL1 = W1 + W4
SIGL2 = W1 - W4
IF (ABS (W2) .GT. 1.E-35 .OR. ABS (W3) .GT. 1.E-35) GO TO 171
ANGLEL = 0.

```

```

172 SIGL3 = SIGLZZ (L)
    SIGLM = SQRT ((SIGL1 + SIGL2 + SIGL3) ** 2
1      - 3. * (SIGL2 * SIGL3 + SIGL3 * SIGL1 + SIGL1 * SIGL2))
C
C
180 OUTPUT THE ELEMENT STRESSES.
    IF (L .NE. 1) GO TO 182
    WRITE (6, 181)
181 FORMAT (1H1 //)
1      27X, 40H THE CALCULATED ELEMENT STRESS COMPONENTS,
2      40H AND THE PRINCIPAL AND THE MEAN STRESSES /
3      27X, 40H-----
4      40H----- //
5      1X, 45HELEMENT          SIGMXX          SIGMYX          /
6      45HSIGMZZ          SIGMXY          ANGLE1          /
7      37HSIGM1          SIGM2          SIGMM /
182 WRITE (6, 183) L, SIGLXX (L), SIGLYY (L), SIGLZZ (L),
1      SIGLXY (L), ANGLE1, SIGL1, SIGL2, SIGLM
183 FORMAT (1H, I5, 4E16.5, F12.2, X, 3E16.5)
184 CONTINUE
    IF (SR .EQ. 1) GO TO 221
C
C
190 FIND THE NODE STRESS COMPONENTS.
    DO 212 N = 1, NNP
    SIGNXX = 0.
    SIGNYY = 0.
    SIGNZZ = 0.
    SIGNXY = 0.
    QA = 1
    DO 191 L = 1, NEL
    IF (NPI (L) .NE. N .AND. NPJ (L) .NE. N .AND. NPM (L) .NE. N)
1      GO TO 191
    SIGNXX = SIGNXX + SIGLXX (L)
    SIGNYY = SIGNYY + SIGLYY (L)
    SIGNZZ = SIGNZZ + SIGLZZ (L)
    SIGNXY = SIGNXY + SIGLXY (L)
    QA = QA + 1
    IF (QA .EQ. NAP (N)) GO TO 192
191 CONTINUE
192 W1 = FLCAT (QA - 1)
    SIGNXX = SIGNXX / W1
    SIGNYY = SIGNYY / W1
    SIGNZZ = SIGNZZ / W1
    SIGNXY = SIGNXY / W1
C
C
200 CALCULATE THE NODE PRINCIPAL AND MEAN STRESSES.
201 W1 = (SIGNXX + SIGNYY) / 2.
    W2 = (SIGNXX - SIGNYY) / 2.
    W3 = SIGNXY
    W4 = SQRT (W2 ** 2 + W3 ** 2)
    SIGN1 = W1 + W4
    SIGN2 = W1 - W4
    IF (ABS (W2) .GT. 1.E-35 .OR. ABS (W3) .GT. 1.E-35) GO TO 202
    ANGLEN = 0.
    GO TO 203
202 ANGLEN = 28.647889756 * ATAN2 (W3, W2)
203 SIGN3 = SIGNZZ
    SIGMM = SQRT ((SIGN1 + SIGN2 + SIGN3) ** 2
1      - 3. * (SIGN2 * SIGN3 + SIGN3 * SIGN1 + SIGN1 * SIGN2))
C
C
210 OUTPUT THE NODE STRESSES.
    IF (N .NE. 1) GO TO 212
    WRITE (6, 211)
211 FORMAT (1H1 //)
1      29X, 37H THE CALCULATED NODE STRESS COMPONENTS,
2      40H AND THE PRINCIPAL AND THE MEAN STRESSES /
3      29X, 37H-----
4      40H----- //
5      3X, 43H NODE          SIGMXX          SIGMYX          /
6      45HSIGMZZ          SIGMXY          ANGLE1          /
7      37HSIGM1          SIGM2          SIGMM /
212 WRITE (6, 213) N, SIGNXX, SIGNYY, SIGNZZ, SIGNXY,
1      ANGLEN, SIGN1, SIGN2, SIGMM
213 FORMAT (1H, I5, 4E16.5, F12.2, X, 3E16.5)
      X, 3E16.5)
C
C
220 RETURN TO THE BEGINNING OF THE PROGRAM FOR THE NEXT CASE.
221 GO TO 11
    END

```

## APPENDIX 6

# Experimental Determination of Stresses

### 6.1 Determination of Apparent Strain for Temperatures above 180°C

Strains conform to the following designations:

$\epsilon_I$  = strain indicated by strain gauge.

$\epsilon_R$  = real strain due to thermal expansion of the material.

$\epsilon_A$  = apparent strain due to heating of the gauge (above 180°C).

The indicated strain will then be:

$$\epsilon_I = \epsilon_R + \epsilon_A \quad (\text{A6.1.1})$$

The relation is valid for the stresses

$$\sigma_I = \sigma_R + \sigma_A \quad (\text{A6.1.2})$$

Therefore the real strain and stress

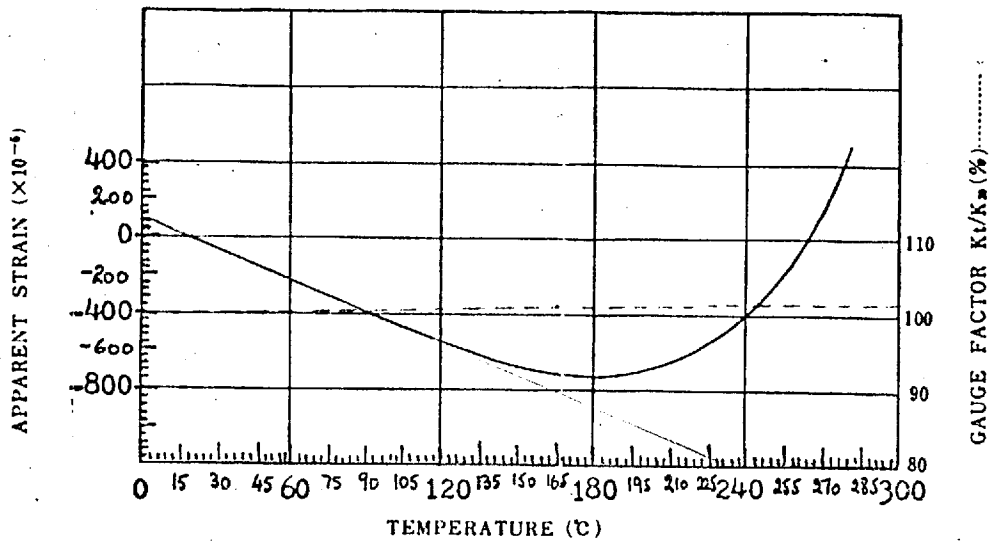
$$\epsilon_R = \epsilon_I - \epsilon_A \quad (\text{A6.1.3})$$

and

$$\sigma_R = \sigma_I - \sigma_A \quad (\text{A6.1.4})$$

The figure below gives the relation between apparent strain and temperature. It can be seen that the gauge is self compensating up to 180°C since the apparent strain is negative and decreases with temperature. For temperatures over 180°C the apparent strain increases, that is the gauge expands, and therefore the indicated strain is not the real strain but the combination of the real and apparent strains as it is described in Equation (A6.1.1).





**Tokyo Sokki Kenkyujo Co., Ltd.**

TSK Co. Ltd advise: that no correction needed up to  $180^{\circ}\text{C}$  for gauge apparent strain, due to self compensating feature, presumably non-linear at upper end.

FIG.A6.1.1

#### Calculations

At time interval 12 minutes during heating-up the following rosettes along the nozzle have temperatures above  $180^{\circ}\text{C}$ .

Rosette	Gauge	Temperature $^{\circ}\text{C}$	Degrees above $180^{\circ}\text{C}$ $^{\circ}\text{C}$
1	1,2,3	198.0	18.0
2	4,5,6	197.9	17.9
3	7,8,9	197.9	17.9
4	10,11,12	197.8	17.8
5	13,14,15	189.4	9.4
6	16,17,18	188.4	8.4
7	19,20,21	186.3	6.3

The determination of the apparent strain can be calculated as follows:

For rosette (1) the temperature is  $198.0^{\circ}\text{C}$ . The apparent strain for  $180^{\circ}\text{C}$ , read from Fig.A6.1.1, is  $-720 \times 10^{-6}$  and for  $198.0^{\circ}\text{C}$  is  $-680 \times 10^{-6}$ . Therefore the apparent strain is:

$\epsilon_A = -680 \times 10^{-6} - (-720 \times 10^{-6}) = 40 \times 10^{-6}$ . For the rest of the rosettes the calculation is similar.

Rosette	Gauge	Apparent Strain
1	1,2,3	$40 \times 10^{-6}$
2	4,5,6	$33 \times 10^{-6}$
3	7,8,9	$33 \times 10^{-6}$
4	10,11,12	$28 \times 10^{-6}$
5	13,14,15	$10 \times 10^{-6}$
6	16,17,18	$7 \times 10^{-6}$
7	19,20,21	$5 \times 10^{-6}$

## 6.2 Determination of Direct Stresses and Strains. Principal Strains and Stresses, Direction Angles and Maximum Shear Stresses

The determination of all the strain and stress components of the experimental results is performed by the computer program EXPER2 which was constructed for this purpose. The various processes and their mathematical analysis is as follows.

1. The program converts the millivolt readings recorded by the Data-Log into strain (in/in).

This is done by using the relationship

$$\epsilon_{\text{indicated}} = \frac{1}{250(F)} \times \frac{\Delta V}{V} \quad (\text{A6.2.1})$$

where:

$F$  = the gauge factor

$\Delta V$  = voltage indicated in mV ( $10^{-3}$  volts)

$V$  = voltage across the bridge in volts

(This is set to 6 volts.)

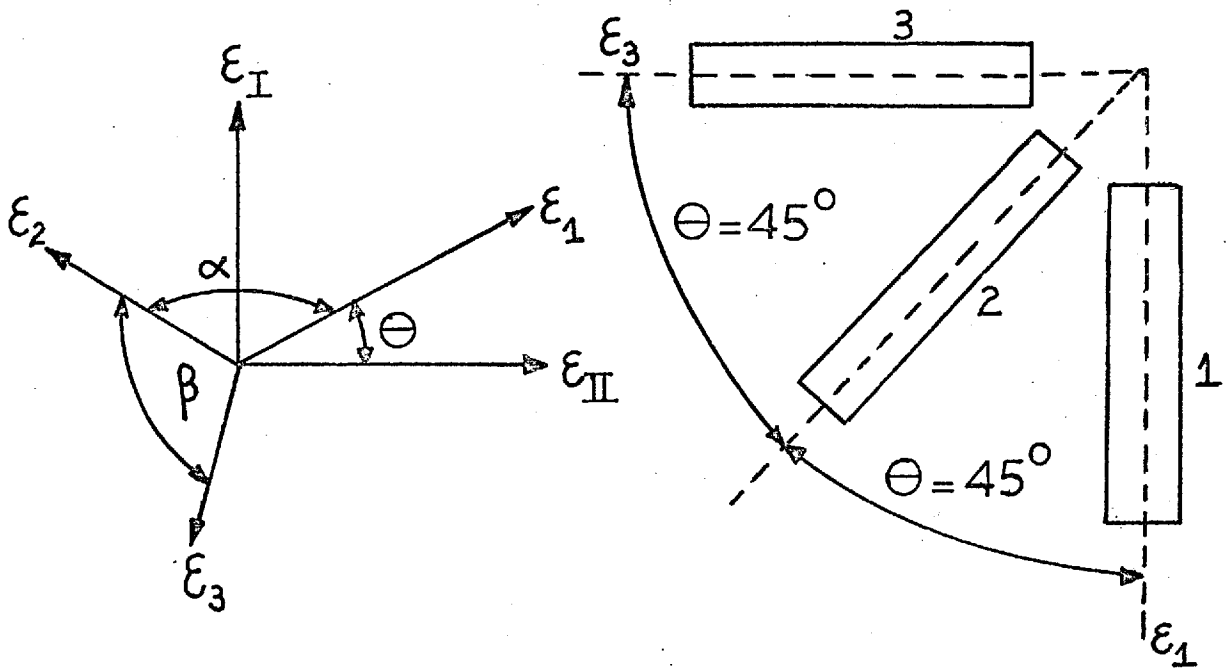
The conversion is performed for all 45 gauges for every one minute interval during heating-up and cooling-down.

2. Calculate the direct stresses for each gauge by using the relationship:

$$\sigma = E\epsilon$$

(A6.2.2)

3. Calculate principal strains for all fifteen rosettes.



If the principal strains in a two-dimensional system are  $\epsilon_I$  and  $\epsilon_{II}$  then the direct strains  $\epsilon_1$ ,  $\epsilon_2$ ,  $\epsilon_3$  in directions inclined at  $\theta$ ,  $(\theta + \alpha)$ ,  $(\theta + \alpha + \beta)$  to  $\epsilon_I$  are

$$\epsilon_1 = \frac{1}{2} (\epsilon_I + \epsilon_{II}) + \frac{1}{2} (\epsilon_I - \epsilon_{II}) \cos 2\theta$$

$$\epsilon_2 = \frac{1}{2} (\epsilon_I + \epsilon_{II}) + \frac{1}{2} (\epsilon_I - \epsilon_{II}) \cos 2(\theta + \alpha) \quad (\text{A6.2.3})$$

$$\epsilon_3 = \frac{1}{2} (\epsilon_I + \epsilon_{II}) + \frac{1}{2} (\epsilon_I - \epsilon_{II}) \cos 2(\theta + \alpha + \beta)$$

In practice the directions of the principal strains are not known usually but if the three direct strains  $\epsilon_1, \epsilon_2, \epsilon_3$  are measured in known directions, then the three unknowns in Equation (A6.2.3) are

$$\epsilon_I, \epsilon_{II} \text{ and } \theta$$

Now if three strain gauges are arranged so that  $\alpha = \beta = 45^\circ$  they form a  $45^\circ$  rosette like the one in the figure which is used for this work. Equations (A6.2.3) become

$$\epsilon_1 = \frac{1}{2}(\epsilon_I + \epsilon_{II}) + \frac{1}{2}(\epsilon_I - \epsilon_{II})\cos 2\theta$$

$$\epsilon_2 = \frac{1}{2}(\epsilon_I + \epsilon_{II}) - \frac{1}{2}(\epsilon_I - \epsilon_{II})\sin 2\theta$$

$$\epsilon_3 = \frac{1}{2}(\epsilon_I + \epsilon_{II}) - \frac{1}{2}(\epsilon_I - \epsilon_{II})\cos 2\theta$$

On eliminating  $\theta$  from these equations we find that  $\epsilon_I, \epsilon_{II}$  are the roots of the quadratic equation

$$\epsilon^2 - (\epsilon_1 + \epsilon_3)\epsilon - \frac{1}{4}(\epsilon_1 + \epsilon_3 - 2\epsilon_2)^2 = 0 \quad (\text{A6.2.4})$$

and the two principal strains are given by

$$\epsilon_I = \{(\epsilon_1 + \epsilon_3) + \sqrt{(\epsilon_1 + \epsilon_3)^2 + (\epsilon_1 + \epsilon_3 - 2\epsilon_2)^2}\}/2$$

$$\epsilon_{II} = (\epsilon_1 + \epsilon_3) - \sqrt{(\epsilon_1 + \epsilon_3)^2 + (\epsilon_1 + \epsilon_3 - 2\epsilon_2)^2}/2$$

4. Calculate the principal stresses for all fifteen rosettes.

When the principal strains  $\epsilon_I$  and  $\epsilon_{II}$  have been estimated, the corresponding principal stresses are deduced from the relations

$$\sigma_I = \frac{E}{1 - \nu^2}(\epsilon_I + \nu \epsilon_{II}) \quad (\text{A6.2.5})$$

$$\sigma_{II} = \frac{E}{1 - \nu^2}(\epsilon_{II} + \nu \epsilon_I) \quad (\text{A6.2.6})$$

5. Determine the angle  $\theta$  between the directions of  $\epsilon_I$  and  $\epsilon_1$  measured clockwise from the direction of  $\epsilon_I$ .

The equation for the angle  $\theta$  is

$$\tan 2\theta = \frac{2\epsilon_2 - \epsilon_1 - \epsilon_3}{\epsilon_3 - \epsilon_1} \quad (\text{A6.2.7})$$

The angle is determined in degrees.

6. Print all the results for the first time interval and then repeat the above procedure for the second time interval.

The millivolt readings for each gauge at each time interval are given to the program as data. The data designation and the listing of the program are given in the next pages.

PROGRAM EXPER2

DATA DESIGNATION

---

is integer single

ia integer array

rs real single

ra real array

---

MVOLTS	ra	millivolts readings of strain gauges
NU	rs	Poisson's ratio
SGFACT	ra	strain gauge factor
THETA	ra	angle of direction of principal stress
PSTRE1	ra	principal stress I
PSTRE2	ra	principal stress II
DSTRAN	ra	direct strain
DSTRES	ra	direct stress
PSTAN1	ra	principal strain I
PSTAN2	ra	principal strain II
NG	ra	number of gauge
ITINI	is	iteration parameter
ITMAX	is	maximum iteration parameter
NSG1	} is	number of strain gauge
NSG2		
NRO1	} is	number of rosette
NRO2		
VOLT	rs	voltage across the bridge

E	rs	modulus of elasticity
L1	is	working parameter
L2	is	working parameter
L3	is	working parameter
B	}	rs working constants
C		
D		
F		

JOB (UHEIM18, J1)

OIKCNGHIDES.C,N

PROGRAM EXPER2 (INPUT, OUTPUT, TAPE5=INPUT, TAPE6=OUTPUT)

PROGRAM EXPER2 INITIALLY CALCULATES THE DIRECT STRAINS IN THE LONGITUDINAL AND TRANSVERSE PLANES FOR ALL 45 STRAIN GAUGES OF 15 ROSETTES BY CONVERTING VOLTAGE READINGS FROM A MULTI CHANNEL WHEASTON BRIDGE INTO DIRECT STRAIN FOR VARIOUS TIME INTERVALS DURING HEATING AND COOLING CYCLES. IT DETERMINES FOR THE SAME TIME INTERVALS THE DIRECT STRESSES, THE PRINCIPAL STRESSES AS WELL AS THEIR DIRECTION

```

REAL    MVOLTS,  NU
COMMON  MVOLTS(45),      DSTRAN(45),
1        SGFACT(45),      DSTRES(45),
2        THETA(15),      PSTAN1(15),
3        PSTRE1(15),     PSTAN2(15),
4        PSTRE2(15),     NG(45)

```

```

ITINI=1
ITMAX=16
NSG1=1
NSG2=45
NRO1=1
NRO2=15

```

```

READ DATA FOR SPECIFIED TIME INTERVALS
READ NUMBER OF STRAIN GAUGES AND ROSETTES
READ MILLIVOLTS OUTPUT AND STRAIN GAUGE FACTORS.
NUMBER OF STRAIN GAUGES =45

```

```

DO 100  IT=ITINI,ITMAX
READ(5,10) (NG(N),MVOLTS(N),SGFACT(N),N=NSG1,NSG2)
100 FORMAT(5(I4,F6.2,F6.2))
T=FLCAT(IT)

```

```

DEFINE VOLTAGE (IN VOLTS) ACROSS THE BRIDGE
CONVERT VOLTAGE READINGS INTO DIRECT STRAIN FOR ALL GAUGES
VOLT=6.00

```

```

DO 15  N=NSG1,NSG2
DSTRAN(N)=(0.004*MVOLTS(N))/(VOLT*SGFACT(N))
15 CONTINUE

```

```

MODULUS OF ELASTICITY
E=30.0*(10.**8)
CALCULATE DIRECT STRESSES FOR ALL GAUGES

```

```

DO 20  N=NSG1,NSG2
DSTRES(N)=E*DSTRAN(N)
20 CONTINUE

```

```

CALCULATE PRINCIPAL STRAINS FOR ALL FIFTEEN ROSETTES

```

```

N=0
DO 25  M=NSG1,NSG2,3
N=N+1
L1=M
L2=M+1
L3=M+2
B=DSTRAN(L1)+DSTRAN(L3)
C=DSTRAN(L1)+DSTRAN(L3)-2.*DSTRAN(L2)
PSTAN1(N)=(B+SQRT((E**2)+(C**2)))/2.
PSTAN2(N)=(B-SQRT((E**2)+(C**2)))/2.

```

```

CALCULATE PRINCIPAL STRESSES FOR ALL FIFTEEN ROSETTES

```

```

POISSON'S RATIO  NU=0.3
PSTRE1(N)=(E*(PSTAN1(N)+0.3*PSTAN2(N)))/0.91
PSTRE2(N)=(E*(PSTAN2(N)+0.3*PSTAN1(N)))/0.91
CALCULATE THE DIRECTION OF PRINCIPAL STRESSES
THE ANGLE IS MEASURED IN DEGREES
D=2.*DSTRAN(L2)-DSTRAN(L1)-DSTRAN(L3)
F=DSTRAN(L3)-DSTRAN(L1)
THETA(N)=57.29577794*(ATAN(D/F))/2.

```

```

25 CONTINUE

```

```

PRINT ALL RESULTS

```

```

WRITE(6,55)
55 FORMAT(5(/))
WRITE(6,56)  T
56 FORMAT(1X,'CYCLE*',8X,'*TIME=*',F5.2)
WRITE(6,57)
57 FORMAT(1X,24('*-'))
WRITE(6,53)
58 FORMAT(2(/))
WRITE(6,59)
59 FORMAT(1X,30HGAUGE NO

```

MVOLTS READINGS

DIR

```

1CT STRAINS          DIRECT STRESSES /
21X, 83H-----
3----- //)
65 WRITE (6, 65) 4NG(N), MVOLTS(N), DSTRES(N), DSTRES(N), N=NSG1, NSG2)
   FORMAT(1X, 15, 19X, F6.3, 13X, L16.4, 18X, F3.1)
70 WRITE (6, 70)
   FORMAT(5(//))
75 WRITE (6, 75)
   FORMAT(1X, 97HROSETTE NO          PRINCIPAL STRAINS          PR
1INCIPAL STRESSES          DIRECTION ANGLE /
21X, 97H-----
3----- //)
80 WRITE (6, 80) (N, PSTAN1(N), PSTAN2(N), PSTRE1(N),
1PSTRE2(N), THETA(N), N=NR01, NR02)
   FORMAT(1X, 16, 5X, E16.4, E16.4, 7X, F8.1, 2X, F8.1, 16X, F6.2)
90 WRITE (6, 90)
   FORMAT(1X, 132(+--*))
100 CONTINUE
    STOP
    END

```



## APPENDIX 7

# Boundary Collocation Analysis

### 7.1 Boundary Collocation Analysis.

#### Derivation of Boundary Conditions.

The Williams stress function is given by

$$\chi(r, \theta) = \sum_{n=1, 2, \dots}^{\infty} \left\{ (-1)^{n-1} d_{2n-1} r^{n+\frac{1}{2}} \left[ -\cos\left(n-\frac{3}{2}\right)\theta \right. \right. \\ \left. \left. + \frac{2n-3}{2n+1} \cos\left(n+\frac{1}{2}\right)\theta \right] + (-1)^n d_{2n} r^{n+1} \left[ -\cos(n-1)\theta \right. \right. \\ \left. \left. + \cos(n+1)\theta \right] \right\}$$

The stress components are given by

$$\sigma_x = \frac{\partial^2 \chi}{\partial x^2} = \frac{\partial^2 \chi}{\partial r^2} \cos^2 \theta - 2 \frac{\partial^2 \chi}{\partial \theta \partial r} \frac{\sin \theta \cos \theta}{r} + \frac{\partial \chi}{\partial r} \frac{\sin^2 \theta}{r} \\ + 2 \frac{\partial \chi}{\partial \theta} \frac{\sin \theta \cos \theta}{r^2} + \frac{\partial^2 \chi}{\partial \theta^2} \frac{\sin^2 \theta}{r^2} \quad (\text{A7.1.1})$$

$$\sigma_y = \frac{\partial^2 \chi}{\partial y^2} = \frac{\partial^2 \chi}{\partial r^2} \sin^2 \theta + 2 \frac{\partial^2 \chi}{\partial \theta \partial r} \frac{\sin \theta \cos \theta}{r} + \frac{\partial \chi}{\partial r} \frac{\cos^2 \theta}{r} \\ - 2 \frac{\partial \chi}{\partial \theta} \frac{\sin \theta \cos \theta}{r^2} + \frac{\partial^2 \chi}{\partial \theta^2} \frac{\cos^2 \theta}{r^2} \quad (\text{A7.1.2})$$

$$-\tau_{xy} = \frac{\partial^2 \chi}{\partial x \partial y} = \sin \theta \cos \theta \frac{\partial^2 \chi}{\partial r^2} + \frac{\cos 2\theta}{r} \frac{\partial^2 \chi}{\partial r \partial \theta} \\ - \frac{\sin \theta \cos \theta}{r} \frac{\partial^2 \chi}{\partial r \partial \theta} - \frac{\sin \theta \cos \theta}{r} \frac{\partial \chi}{\partial r} \\ - \frac{\cos 2\theta}{r^2} \frac{\partial \chi}{\partial \theta} \quad (\text{A7.1.3})$$

Therefore  $\sigma_x$ ,  $\sigma_y$ ,  $-\tau_{xy}$  are all functions of  $\chi, r, \theta$ . The conditions at different points will be as follows:

Along the crack surface:

$$\sigma_x = f(\cos\theta, \sin\theta) \quad \cos\theta = \cos(\pm\pi), \quad \sin\theta = \sin(\pm\pi) = 0$$

$$\text{hence } \sigma_x = 0, \quad \text{and } -\tau_{xy} = f(\cos\theta\sin\theta)$$

therefore  $-\tau_{xy} = 0$ . Hence the normal and shearing stresses are zero along the surface of the crack.

BOUNDARY  $\overrightarrow{AB}$ :

At boundary AB  $\theta = +\pi/2$

$$\chi = f(\cos\theta, r) = f(\cos(\frac{\pi}{2}), r) = 0$$

$$\text{and therefore } \chi = 0, \quad \frac{\partial\chi}{\partial y} = 0$$

BOUNDARY  $\overrightarrow{BC}$ :

Equation (A7.1.1) for  $\sigma_x$  for  $\theta = 0$  becomes

$$\sigma_x = \frac{\partial^2\chi}{\partial r^2}$$

Integrating

$$\frac{\partial\chi}{\partial r} = \sigma_x r + A \quad (\text{A7.1.4})$$

$$\chi = \frac{\sigma_x r^2}{2} + Ar + B \quad (\text{A7.1.5})$$

Using conditions on boundary AB to determine the constants,

$$\text{for } r = -a \text{ (on boundary AB) } \chi = 0, \quad \frac{\partial\chi}{\partial y} = 0$$

Therefore Equation (A7.1.4) becomes

$$0 = -\sigma_x a + A$$

hence,  $A = \sigma_x a$

$$\text{Equation (A7.1.5) becomes } \chi = \frac{\sigma_x r^2}{2} + \sigma_x ar + B$$

at  $r = a$ ,  $\chi = 0$  (at tip of the crack)

$$\text{hence } \chi = 0 = \frac{\sigma_x a^2}{2} - \sigma_x a^2 + B$$

$$\text{and hence, } B = \sigma_x a^2 - \sigma_x \frac{a^2}{2} = \frac{\sigma_x a^2}{2}$$

Therefore the force component of the stress function is given by

$$\chi = \sigma_x \left( \frac{y^2}{2} + ay + \frac{a^2}{2} \right) \text{ along } \vec{BC} \quad (\text{A7.1.6})$$

BOUNDARY  $\vec{CD}$ :

In Equation (A7.1.6) above at  $\vec{CD}$   $y = V, a = 0$

$$\therefore \chi = \frac{\sigma_x V^2}{2}$$

and  $\frac{\partial \chi}{\partial x} = 0$  ,  $\frac{\partial \chi}{\partial y} = \sigma_x V$

## 7.2 PROGRAM STREN4

Data designations for program STREN4 are the same as the ones given in Appendix 5. The listing of the program is given in the next page.

PROGRAM STREN4 (INPUT=1002, OUTPUT=1002, TAPE5=INPUT, TAPE6=OUTPUT)

CCC  
C  
C

0 SPECIFICATION AND DATA INITIALIZATION STATEMENTS.

```

1 INTEGER TITLE, PS, SR, QA, O,
2 CASCTL, STRESS, WI, ANP, P,
3 REAL NU, K, KXX, KXY, KYX, KYY
COMMON TITLE (13), NPI (430), X (256), NE(15),
1 F (5), NPJ (430), Y (256), COND(15),
2 NU (15), NPH (430), RX (256), SLOPE(15),
3 RHO (15), MAT (430), RY (256),
4 ALPHA (15), DELTAT (430), U (256),
5 V (256),
1 RI (430), KXX (256, 9), ANP (256, 9), SIGLXX (430),
2 RJ (430), KXY (256, 9), NAP (256), SIGLYY (430),
3 RM (430), KYX (256, 9), LN (3), SIGLZZ (430),
4 CI (430), KYY (256, 9), B (3, 6), SIGLXY (430),
5 CJ (430), FXX (256), D (3, 3),
6 CM (430), FXY (256), W (3, 6),
7 FYY (256), K (6, 6),
8
DATA CASCTL, STRESS, STRAIN / 6HNF CASE, 6HSTRESS, 6HSTRAIN /

```

CCC  
C  
C

```

10 INPUT THE CASE TITLE BUT STOP IF THERE IS NO FURTHER CASE.
11 READ (5, 10) TITLE
12 FORMAT (13, 6)
IF (TITLE (1) .EQ. CASCTL) STOP

```

CCC  
C  
C

```

20 INPUT THE CONTROL PARAMETERS AND PREPARE TO INPUT THE ARRAY DATA.
READ (5, 21) NEL, NNP, NBR, NMAT, NOY, NCC,
1 TOLER, OMEGA, PS, SR, WI
21 FORMAT (6I5, E13.5, F7.3, 2X, A6, 2I3)
DO 22 NM = 1, NMAT
22 E (NM) = -1.
DO 23 L = 1, NEL
23 NPI (L) = -1.
DO 24 N = 1, NNP
24 X (N) = -0.123456789E35

```

CCC  
C  
C

```

30 INPUT AND CHECK THE ARRAY DATA.
READ (5, 31) (MATN, E (MATN), NU (MATN),
1 RHO (MATN), ALPHA (MATN), NM = 1, NMAT)
31 FORMAT (15, 4E13.5)
DO 33 NM = 1, NMAT
IF (E (NM) .NE. -1.) GO TO 33
WRITE (6, 32) TITLE
32 FORMAT (11H1 // // // // 5H IN ' , 13A6, 1H' /
1 36H THERE IS A MISSING INPUT DATA CARD.,
2 24H THE JOB IS ABANDONED.)
STOP

```

```

33 CONTINUE
READ (5, 34) (LE, NPI (LE), NPJ (LE), NPH (LE),
1 MAT (LE), DELTAT (LE), L = 1, NEL)
34 FORMAT (5I5, F10.3)
DO 35 L = 1, NEL
IF (NPI (L) .NE. -1) GO TO 35
WRITE (6, 32) TITLE
STOP

```

```

35 CONTINUE
READ (5, 36) (NP, X (NP), Y (NP), RX (NP), RY (NP),
1 U (NP), V (NP), N = 1, NNP)
36 FORMAT (15, 4F12.4, 2F12.5)
DO 37 N = 1, NNP
IF (X (N) .NE. -0.123456789E35) GO TO 37
WRITE (6, 32) TITLE
STOP

```

```

37 CONTINUE
READ (5, 38) (NR, COND (NR), SLOPE (NR), NR = 1, NR)
38 FORMAT (2I5, F10.5)

```

CCC  
C  
C

```

40 OUTPUT THE TITLE AND THE CONTROL PARAMETERS.
WRITE (6, 41)
41 FORMAT (11H1 // // // //
1 45X, 41H THE CASE TITLE AND THE CONTROL PARAMETERS /
2 45X, 41H- - - - - // // // //)
WRITE (6, 42) TITLE
42 FORMAT (11H, 13A6)

```

```

WRITE (6, 43) NEL, NNP, NBR, NMAT, NCV, NCC, TOLER, OMEGA, PS
43 FORMAT (26H THE NUMBER OF ELEMENTS IS, I5, 1H, /
1 30H THE NUMBER OF NODAL POINTS IS, I5, 1H, /
2 43H THE NUMBER OF RESTRAINED BOUNDARY NODES IS, I5, 1H, /
3 37H THE NUMBER OF DIFFERENT MATERIALS IS, I5, 1H, /
4 23H THE ITERATION LIMIT IS, I5, 8H CYCLES, /
5 36H THE INTERVAL FOR PROGRESS OUTPUT IS, I5, 8H CYCLES, /
6 29H THE CONVERGENCE TOLERANCE IS, E13.5, 1H, /
7 35H THE OVER-RELAXATION FACTOR IS, F7.3, 1H, /
8 37H THE CASE HAS THE CONDITION OF PLANE, A6, 1H, /
9 23H STRESSES ARE FOUND FOR)
IF (SR .EQ. 0) WRITE (6, 44)
44 FORMAT (1H+, 23X, 42H NEITHER THE ELEMENTS NOR THE NODAL POINTS.)
IF (SR .EQ. 1) WRITE (6, 45)
45 FORMAT (1H+, 23X, 18H THE ELEMENTS ONLY.)
IF (SR .EQ. 2) WRITE (6, 46)
46 FORMAT (1H+, 23X, 22H THE NODAL POINTS ONLY.)
IF (SR .EQ. 3) WRITE (6, 47)
47 FORMAT (1H+, 23X, 39H BOTH THE ELEMENTS AND THE NODAL POINTS.)
IF (WI .EQ. 0) WRITE (6, 48)
48 FORMAT (37H THE INPUT ARRAY DATA ARE NOT OUTPUT.)
IF (WI .EQ. 1) WRITE (6, 49)
49 FORMAT (33H THE INPUT ARRAY DATA ARE OUTPUT.)

50 OUTPUT THE ARRAY DATA.
IF (WI .EQ. 0) GO TO 61
WRITE (6, 51) (NM, 2 (NH), NU (NM), RHO (NM),
1 ALPHA (NM), NM = 1, NMAT)
51 FORMAT (1H1 // // // //
1 56X, 19H INPUT MATERIAL DATA /
2 56X, 19H ----- // // //
3 23X, 42H MATERIAL ELASTIC MODULUS POISSON'S RATIO,
4 34H DENSITY THML EXPN COEFF //
5 (I33, X, 4E17.5))
WRITE (6, 52)
52 FORMAT (1H1 // // // //
1 57X, 18H INPUT ELEMENT DATA /
2 57X, 18H ----- // // //
3 3X, 48H ELMT NPI NPJ NPN MTRL DELTA T
4 48H ELMT NFI NPJ NFM MTRL DELTA T
5 33H ELMT NPI NPJ NPM MTRL DELTA T //)
L1 = (NEL + 2) / 3
DO 53 L2 = 1, L1
L3 = MIN0 (L2 + 2 * L1, NEL)
53 WRITE (6, 54) (L, NPI (L), NPJ (L), NPM (L),
1 MAT (L), DELTAT (L), L = L2, L3, L1)
54 FORMAT (1H, 5I5, F10.3, 13X, 5I5, F10.3, 13X, 5I5, F10.3)
WRITE (6, 55) (N, X (N), Y (N), RX (N), RY (N),
1 U (N), V (N), N = 1, NNP)
55 FORMAT (1H1 // // // //
1 58X, 15H INPUT NODE DATA /
2 58X, 15H ----- // // //
3 13X, 49H NODE X Y
4 31H RX RY
5 21H U V //
6 (I16, X, 6E17.5))
WRITE (6, 56) (NB (NR), COND (NR), SLOPE (NR), NR = 1, NBR)
56 FORMAT (1H1 // // // //
1 48X, 35H INPUT RESTRAINED BOUNDARY NODE DATA /
2 48X, 35H ----- // // //
3 33X, 28H RESTND BNDY NODE
4 37H RESTND CONDITION SLOPE //
5 (I42, I27, F30.5))

60 DO GEOMETRIC CALCULATIONS ON THE ELEMENTS.
61 DO 72 L = 1, NEL
I = NPI (L)
J = NPJ (L)
M = NPM (L)
BI (L) = Y (J) - Y (M)
EJ (L) = Y (M) - Y (I)
EM (L) = Y (I) - Y (J)
CI (L) = - Y (J) + X (M)
CJ (L) = - X (M) + X (I)
CM (L) = - X (I) + X (J)
AREA = (BJ (L) * CM (L) - BM (L) * CJ (L)) / 2.
IF (AREA .GT. 1.E-35) GO TO 71
WRITE (6, 62) L
62 FORMAT (1H1 // // // // 3H ELEMENT, I5, 25H HAS A NON-POSITIVE AREA. /
1 23H THE CASE IS ABANDONED.)
GO TO 221

```

```

C 70 SUM THE TOTAL NODAL POINT FORCES.
71 MATN = MAT (L)
IF (PS .EQ. STRESS) SIGTH = 1. - NU (MATN)
IF (PS .EQ. STRAIN) SIGTH = (1. + NU (MATN))
      * (1. - 2. * NU (MATN))
      1 SIGTH = - E (MATN) * ALPHA (MATN) * DELTAT (L) / SIGTH
BODYF = AREA * RHO (MATN) / 3.
RX (I) = RX (I) - 0.5 * CI (L) * SIGTH
RY (I) = RY (I) - 0.5 * CI (L) * SIGTH - BODYF
RX (J) = RX (J) - 0.5 * CJ (L) * SIGTH
RY (J) = RY (J) - 0.5 * CJ (L) * SIGTH - BODYF
RX (M) = RX (M) - 0.5 * CM (L) * SIGTH
RY (M) = RY (M) - 0.5 * CM (L) * SIGTH - BODYF
72

C C C
80 PREPARE TO SUM THE STIFFNESS COEFFICIENTS.
DO 82 N = 1, NNP
DO 81 QA = 1, 9
KXX (N, QA) = 0.
KXY (N, QA) = 0.
KYX (N, QA) = 0.
KYY (N, QA) = 0.
81 ANP (N, QA) = 0.
ANP (N, 1) = N
82 NAP (N) = 1

C C C
90 FORM THE STIFFNESS MATRIX FOR THE ELEMENT.
DO 105 L = 1, NEL
DO 92 P = 1, 3
DO 91 Q = 1, 6
E (P, Q) = 0.
DO 92 Q = 1, 3
92 D (P, Q) = 0.
B (1, 1) = BI (L)
B (1, 3) = BJ (L)
B (1, 5) = BM (L)
B (2, 2) = CI (L)
B (2, 4) = CJ (L)
B (2, 6) = CM (L)
B (3, 1) = BI (L)
B (3, 2) = BJ (L)
B (3, 3) = CJ (L)
B (3, 4) = CM (L)
B (3, 5) = BM (L)
B (3, 6) = BM (L)
MATN = MAT (L)
W1 = NU (MATN)
W2 = 1. - W1
W3 = 1. + W1
W4 = 1. - 2. * W1
IF (PS .EQ. STRAIN) GO TO 93
W5 = E (MATN) / (W2 * W3)
W6 = W1
W7 = W2 / 2.
GO TO 94
93 W5 = E (MATN) * W2 / (W3 * W4)
W6 = W1 / W2
W7 = W4 / (2. * W2)
94 AREA = (CJ (L) * CM (L) - BM (L) * CJ (L)) / 2.
W5 = W5 / (4. * AREA)
D (1, 1) = W5
D (1, 2) = W5 * W6
D (2, 1) = W5 * W6
D (2, 2) = W5 * W6
D (3, 3) = W5 * W7
DO 95 P = 1, 3
DO 95 Q = 1, 6
W (P, Q) = 0.
DO 95 Q = 1, 3
IF (Q.GT.3) O=2
95 W (P, Q) = W (P, Q) + D (P, Q) * B (Q, Q)
DO 96 P = 1, 6
DO 96 Q = 1, 6
K (P, Q) = 0.
DO 96 Q = 1, 3
96 K (P, Q) = K (P, Q) + B (Q, P) * W (Q, Q)

C C C
100 SUM AND STORE FOR EACH (FORCED) NODE THE NON-ZERO STIFFNESS
COEFFICIENTS FOR THE ADJACENT (DISPLACED) NODES.
LN (1) = NPI (L)
LN (2) = NPJ (L)
LN (3) = NPM (L)
DO 105 P = 1, 3

```

```

NP = LN (P)
DO 105 Q = 1, 3
QA = 0
101 QA = QA + 1
IF (QA .LE. 9) GO TO 103
WRITE (6, 102) NP
102 FORMAT (1H, '////// 5H NODE, I5,
1 36H HAS MORE THAN EIGHT ADJACENT NODES. /
2 23H THE CASE IS ABANDONED.)
GO TO 221
103 IF (ANP (NP, QA) .EQ. LN (Q)) GO TO 104
IF (ANP (NP, QA) .NE. 0) GO TO 101
ANP (NP, QA) = LN (Q)
NAP (NP) = QA
104 KXX (NP, QA) = KXX (NP, QA) + K (2 * P - 1, 2 * Q - 1)
KXY (NP, QA) = KXY (NP, QA) + K (2 * P - 1, 2 * Q)
KYX (NP, QA) = KYX (NP, QA) + K (2 * P, 2 * Q - 1)
KYY (NP, QA) = KYY (NP, QA) + K (2 * P, 2 * Q)
105 CONTINUE

C
C
C
110 BY INVERSION OF THE MAIN DIAGONAL STIFFNESS SUBMATRIX, FIND THE
FLEXIBILITY SUBMATRIX AT EACH NODE DISPLACED BY FORCES AT ITSELF.
DO 112 N = 1, NNP
W1 = KXX (N, 1) * KYY (N, 1) - KXY (N, 1) * KYX (N, 1)
FXX (N) = KXX (N, 1) / W1
FXY (N) = - KXY (N, 1) / W1
FYX (N) = - KYX (N, 1) / W1
112 FYY (N) = KYY (N, 1) / W1

C
C
C
120 CALCULATE THE EFFECTIVE SELF FLEXIBILITY SUBMATRICES FOR THE
RESTRAINED BOUNDARY NODES.
DO 125 NR = 1, NBR
NP = NB (NR)
IF (COND (NP) - 1) 123, 122, 121
121 FXX (NP) = (FXX (NP) * FYY (NP) - FXY (NP) * FYX (NP))
/ (FXX (NP) * SLOPE (NR) ** 2
2 - (FX (NP) + FY (NP)) * SLOPE (NR) + FYY (NP))
1 FXY (NP) = FXX (NP) * SLOPE (NR)
2 FXY (NP) = FXY (NP)
3 FYY (NP) = FXY (NP) * SLOPE (NR)
GO TO 125
122 FYY (NP) = FYY (NP) - FYX (NP) * FXY (NP) / FXX (NP)
GO TO 124
123 FXY (NP) = 0.
124 FXX (NP) = 0.
124 FXY (NP) = 0.
124 FYX (NP) = 0.
125 CONTINUE

C
C
C
130 PERFORM A GAUSS - SEIDEL ITERATION ON THE STIFFNESS MATRIX FOR
THE ENTIRE STRUCTURE.
IF (NCC .GT. NCY) GO TO 132
WRITE (6, 131)
131 FORMAT (1H, '//////
1 34X, 35H THE PROGRESS OF THE GAUSS - SEIDEL ,
2 23H ITERATION TOWARD CONVERGENCE /
3 34X, 35H -----,
4 28H ----- // //
5 33X, 33H CYCLE CONVERGENCE CRITERION,
6 26H CURRENT DIFFERENCE)
132 NC = 0
133 SD = 0.
SDD = 0.
DO 136 N = 1, NNP
IF (FXX (N) + FYY (N) .EQ. 0.) GO TO 136
RX1 = RX (N)
RY1 = RY (N)
NAP1 = NAP (N)
DO 134 QA = 1, NAP1
NP = ANP (N, QA)
134 RX1 = RX1 - KXX (N, QA) * U (NP) - KXY (N, QA) * V (NP)
RY1 = RY1 - KYX (N, QA) * U (NP) - KYY (N, QA) * V (NP)
IF (FXX (N) .EQ. 0.) GO TO 135
DELTAU = FXY (N) * RX1 + FXY (N) * RY1
U (N) = U (N) + OMEGA * DELTAU
SD = SD + ABS (U (N))
SDD = SDD + ABS (DELTAU)
IF (FYY (N) .EQ. 0.) GO TO 136
135 DELTAV = FYY (N) * RX1 + FYY (N) * RY1
V (N) = V (N) + OMEGA * DELTAV
SD = SD + ABS (V (N))
SDD = SDD + ABS (DELTAV)

```

```

136 CONTINUE
SD = AMAX1 (SD, 1.E-35)
RELDIF = SDD / SD

C
C
C 140 TEST FOR CONVERGENCE.
NC = NC + 1
IF (NCC .GT. NCV .OR. MOD (NC, NCC) .NE. 0) GO TO 142
WRITE (6, 141) NC, TOLR, RELDIF
141 FORMAT (1H0, 141) NC, TOLR, RELDIF
142 IF (RELDIF .GT. TOLR) GO TO 144
WRITE (6, 143) NC
143 FORMAT (1H1 // // // // 28H THE ITERATION HAS CONVERGED,
1 6H AFTER, I5, 8H CYCLES.)
GO TO 151
144 IF (NC .LT. NCV) GO TO 133
WRITE (6, 145) NC, RELDIF, TOLR
145 FORMAT (1H2 // // // // 28H THE ITERATION HAS COMPLETED, I5, 5H THE ,
1 52H MAXIMUM NUMBER OF CYCLES WITHOUT CONVERGING, BUT HAS /
2 34H ACHIEVED A RELATIVE DIFFERENCE OF, E13.5,
3 33H AGAINST A SPECIFIED TOLERANCE OF, E13.5, 1H. /
4 43H THE UNCONVERGED RESULTS ARE WRITTEN BELOW.)

C
C
C 150 OUTPUT THE NODE DISPLACEMENTS.
151 WRITE (6, 152)
152 FORMAT (1H2 // // // //
1 49X, 33H THE CALCULATED NODE DISPLACEMENTS /
2 49X, 33H ----- // // // //
3 3X, 47H NODE U V
4 47H NODE U V
5 30H NODE U V //)
N1 = (NPN + 2) / 3
DO 153 N2 = 1, N1
N3 = MIN0 (N2 + 2 * N1, NPN)
153 WRITE (6, 154) (N, U (N), V (N), N = N2, N3, N1)
154 FORMAT (1H , I5, 2E16.5, I15, 2E16.5, I15, 2E16.5)

C
C
C 160 CALCULATE THE ELEMENT STRESS COMPONENTS.
IF (SR .EQ. 0) GO TO 221
DO 164 L = 1, NEL
I = NPI (L)
J = NPJ (L)
M = NPM (L)
AREA = (BJ (L) * CN (L) - BM (L) * CJ (L)) / 2.
EEXX = (BI (L) * U (I) + BJ (L) * U (J)) / (2. * AREA)
1 EEYY = (CI (L) * V (I) + CJ (L) * V (J)) / (2. * AREA)
1 EEXY = (CI (L) * U (I) + BI (L) * V (I)
+ CJ (L) * U (J) + BJ (L) * V (J)) / (2. * AREA)
2 + CH (L) * U (M) + BM (L) * V (M)) / (2. * AREA)
MATN = MAT (L)
W1 = NU (MATN)
W2 = 1. - W1
W3 = 1. + W1
W4 = 1. - 2. * W1
IF (PS .EQ. STRAIN) GO TO 161
W5 = E (MATN) / (W2 * W3)
W6 = W1
W7 = W2 / 2.
GO TO 162
161 W5 = E (MATN) * W2 / (W3 * W4)
W6 = W1 / W2
W7 = W4 / (2. * W2)
162 ETH = ALPHA (MATN) * DELTAT (L)
EXX = EEXX - ETH
EYY = EEYY - ETH
EXY = EEXY
SIGLXX (L) = W5 * (EXX + W6 * EYY)
SIGLYY (L) = W5 * (W6 * EXX + EYY)
IF (PS .EQ. STRAIN) GO TO 163
SIGLZZ (L) = 0.
GO TO 164
163 SIGLZZ (L) = W1 * (SIGLXX (L) + SIGLYY (L))
164 SIGLXY (L) = W5 * W7 * EXY

C
C
C 170 CALCULATE THE ELEMENT PRINCIPAL AND MEAN STRESSES.
IF (SR .EQ. 2) GO TO 184
W1 = (SIGLXX (L) + SIGLYY (L)) / 2.
W2 = (SIGLXX (L) - SIGLYY (L)) / 2.
W3 = SIGLXY (L)
W4 = SQRT (W2 ** 2 + W3 ** 2)

```



```

SIGL1 = W1 + W4
SIGL2 = W1 - W4
IF (ABS (W2) .GT. 1.E-35 .OR. ABS (W3) .GT. 1.E-35) GO TO 171
ANGLEL = 0.
GO TO 172
171 ANGLEL = 28.647889756 * ATAN2 (W3, W2)
172 SIGL3 = SIGLZZ (L)
SIGLM = SQRT ((SIGL1 + SIGL2 + SIGL3) ** 2
1 - 3. * (SIGL2 * SIGL3 + SIGL3 * SIGL1 + SIGL1 * SIGL2))

C
C
C 180 OUTPUT THE ELEMENT STRESSES.
IF (L .NE. 1) GO TO 182
WRITE (6, 181)
181 FORMAT (1H1 //)
1 27X, 40H THE CALCULATED ELEMENT STRESS COMPONENTS,
2 40H AND THE PRINCIPAL AND THE MEAN STRESSES /
3 27X, 40H-----
4 40H----- //
5 1X, 45HELEMENT SIGMXX SIGMY SIGMY
6 45HSIGMZZ SIGMXY ANGLE1 /
7 37HSIGM1 SIGM2 SIGMM //
182 WRITE (6, 183) L, SIGLXX (L), SIGLYY (L), SIGLZZ (L),
1 SIGLXY (L), ANGLEL, SIGL1, SIGL2, SIGLM
183 FORMAT (1H ; I5, 4E16.5, F12.2, X, 3E16.5)
184 CONTINUE
IF (SR .EQ. 1) GO TO 221

C
C
C 190 FIND THE NODE STRESS COMPONENTS.
DO 212 N = 1, NNP
SIGNXX = 0.
SIGNYY = 0.
SIGNZZ = 0.
SIGNXY = 0.
QA = 1
DO 191 L = 1, NEL
IF (NPI (L) .NE. N .AND. NPJ (L) .NE. N .AND. NPK (L) .NE. N)
1 GO TO 191
SIGNXX = SIGNXX + SIGLXX (L)
SIGNYY = SIGNYY + SIGLYY (L)
SIGNZZ = SIGNZZ + SIGLZZ (L)
SIGNXY = SIGNXY + SIGLXY (L)
QA = QA + 1
IF (QA .EQ. NAP (N)) GO TO 192
191 CONTINUE
192 W1 = FLOAT (QA - 1)
SIGNXX = SIGNXX / W1
SIGNYY = SIGNYY / W1
SIGNZZ = SIGNZZ / W1
SIGNXY = SIGNXY / W1

C
C
C 200 CALCULATE THE NODE PRINCIPAL AND MEAN STRESSES.
201 W1 = (SIGNXX + SIGNYY) / 2.
W2 = (SIGNXX - SIGNYY) / 2.
W3 = SIGNXY
W4 = SQRT (W2 ** 2 + W3 ** 2)
SIGN1 = W1 + W4
SIGN2 = W1 - W4
IF (ABS (W2) .GT. 1.E-35 .OR. ABS (W3) .GT. 1.E-35) GO TO 202
ANGLEL = 0.
GO TO 203
202 ANGLEL = 28.647889756 * ATAN2 (W3, W2)
203 SIGN3 = SIGNZZ
SIGMM = SQRT ((SIGN1 + SIGN2 + SIGN3) ** 2
1 - 3. * (SIGN2 * SIGN3 + SIGN3 * SIGN1 + SIGN1 * SIGN2))

C
C
C 210 OUTPUT THE NODE STRESSES.
IF (N .NE. 1) GO TO 212
WRITE (6, 211)
211 FORMAT (1H1 //)
1 29X, 37H THE CALCULATED NODE STRESS COMPONENTS,
2 40H AND THE PRINCIPAL AND THE MEAN STRESSES /
3 29X, 37H-----
4 40H----- //
5 3X, 43H NODE SIGMXX SIGMY SIGMY
6 45HSIGMZZ SIGMXY ANGLE1 /
7 37HSIGM1 SIGM2 SIGMM //
212 WRITE (6, 213) N, SIGNXX, SIGNYY, SIGNZZ, SIGNXY,
1 ANGLEL, SIGN1, SIGN2, SIGMM
213 FORMAT (1H ; I5, 4E16.5, F12.2, X, 3E16.5)

C
C
C 220 RETURN TO THE BEGINNING OF THE PROGRAM FOR THE NEXT CASE.

```

### 7.3 Program FUNSTR and Subroutine DMATRX

The data designations are as follows:

is integer single  
 ia integer array  
 rs real single  
 ra real array

#### PROGRAM FUNSTR

CRACKL rs Crack length  
 HMesh rs Height of cell  
 WIDTH rs Width of cell  
 EDIST rs Dimension  
 JJ }  
 KK } is Grid co-ordinates  
 KKE }  
 JJE }

SIGMYY ra Stresses in y-direction  
 SIGMXX ra Stresses in x-direction  
 SIGMTO ra Specified stress at boundary points

XX }  
 A1 } rs Working parameters  
 A2 }  
 A3 }  
 A4 }

AMOM rs Moment

B1 }  
B2 } rs Working parameters  
B3 }  
  
CONVER rs Convergence constant  
PREVIO rs Convergence criterion

SUBROUTINE DMATRIX

The same as above and additionally:

MCR is Crack positions  
DI ra First matrix coefficient  
CONS rs Working constant  
R ra Working constant

The listing of FUNSTR and DMATRIX is given in the next page.





C  
C  
C  
C  
C

AXIS OF THE CRACK  
MCR=23

CLEAR D1

```

DO 998 L=1, JJ
D1(L)=0.
998 CONTINUE
DO 1000 I=1, JJ
R(I)=(HMESH*FLOAT(I-3))-CRACKL
IF(R(I).LE.0.0) GO TO 1000
CONS=(-4./3.)*(R(I)**(3./2.))
D1(I)=X(I, MCR)/CONS
1000 CONTINUE
WRITE(6, 1100)
1100 FORMAT(1H1 / / / /
120X, 51HJ          X          R          D1 / / / /)
J=JJ
1140 CONTINUE
WRITE(6, 1150) J, X(J, MCR), R(J), D1(J)
1150 FORMAT(17X, I3, 5X, F12.2, 8X, F10.5, 6X, F12.2)
J=J-1
IF(J.EQ.0) GO TO 1200
GO TO 1140
1200 CONTINUE
WRITE(6, 1250)
1250 FORMAT(1H1)
RETURN
END

```

## APPENDIX 8

---

### References

---

- 1-1 CARLSON, W.B. Pressure Vessel Design Requirements in the Future. The Welding Journal, 40, (6), Research Suppl., 265-s to 271-s (1961)
- 2-1 WATERS, E.O. Stresses near a Cylindrical Outlet in a Spherical Vessel. Weld.Res.Counc.Bull., No.96, May 1964
- 2-2 LECKIE and PENNY. Stress Concentration Factors for the Stresses at Nozzle Intersections in Pressure Vessels. Weld.Res.Counc.Bull., No.90, September 1963
- 2-3 RODABAUGH, E.C. et al. Stresses at Nozzles in Spherical Shells Loaded with Pressure Moment or Thrust. Phase Rep. No.2, July 15, 1966
- 2-4 KALNINS, A. Analysis of Shells of Revolution subjected to Symmetrical and Nonsymmetrical Loads. J.Appl.Mech., September 1964
- 2-5 WILSON, E.L. Structural Analysis of Axisymmetric Solids, AIAAJ., Vol.3, pp.2269-2274, 1965
- 2-6 BESKIN, L. Strengthening of Circular Holes in Plates under Edge Loads. Trans.ASME, J.Appl.Mech., Vol.66, p.A-140, 1944
- 2-7 WATERS, E.O. Theoretical Stresses near a Cylindrical Opening in a Flat Plate with a Cylindrical Outlet. Weld.Res.Counc.Bull., No.51, June 1959

- 2-8 ERINGEN, NAGHDI and THIEL. State of Stress in a Circular Cylindrical Shell with a Circular Hole. Weld.Res.Counc. Bull., No.102, January 1962
- 2-9 VAN DYKE, P. Stresses about a Circular Hole in a Cylindrical Shell. AIAAJ., Vol.3, No.9, September 1965
- 2-10 ERINGEN, A.C. and SUHUBI, E.S. Stress Distribution at Two Normally Intersecting Cylindrical Shells. Nucl. Struct.Eng., 2, (1965), 253-270, June 1965
- 2-11 BIJLAARD, DOHRMAN and WANG. Stresses in Junction of Nozzles to Cylindrical Pressure Vessel for Equal Diameter of Vessel and Nozzle. Nucl.Eng.Des., Vol.5, pp.349-365, 1967
- 2-12 PAN and BECKETT. Stress and Displacement Analysis of a Shell Intersection. Trans.ASME., J.Eng. for Ind., Vol.92, May 1970
- 2-13 BIJLAARD, P.P. Stresses from Local Loadings in Cylindrical Pressure Vessels. Trans.ASME, Vol.77m August 1955
- 2-14 BIJLAARD, P.P. Stresses from Radial Loads and External Moments in Cylindrical Pressure Vessels. Weld.Res.Suppl., December 1955
- 2-15 BIJLAARD, P.P. Additional Data on Stresses in Cylindrical Shells under Local Loadings. Weld.Res.Counc.Bull., No.50, May 1959
- 2-16 GILL, S.S. The Limit Pressure for a Flush Cylindrical Nozzle in a Spherical Pressure Vessel. Int.J.Mech.Scie., Vol.6, pp.105-115, July 1963
- 2-17 DINNO, K.S. and GILL, S.S. The Limit Analysis of a Pressure Vessel consisting of the Junction of a Cylindrical and Spherical Shell. Int.J.Mech.Sci., Vol.7, pp.21-42, July 1964



- 2-18 CLOUD, R.L. The Limit Pressure of Radial Nozzles in Spherical Shells. *Nuc.Struct.Eng.*, 1, pp.403-413, 1965
- 2-19 COON, M.D., GILL, S.S., KITCHING, R. A Lower Bound to the Limit Pressure Vessel with an Unreinforced Hole. *Int.J.Mech.Sci.*, Vol.9, pp.69-75, 1967
- 2-20 CLOUD, R.L., RODABAUGH, E.C. Approximate Analysis of the Plastic Limit Pressures of Nozzles in Cylindrical Shells. *Trans.ASME, J.Eng. for Power*, Vol.90, Series A, pp.171-176
- 2-21 CALLADINE, C.R., GOODALL, I.W. Plastic Behaviour of Thin Cylindrical Pressure Vessels with Circular Cutouts and Radial Branches. *J.Mech.Eng.Sci.*, Vol.11, pp.351-363, 1969
- 2-22 LECKIE, F.A. Shakedown Pressures for Flush Cylinder-Sphere Shell Intersections. *J.Mech.Eng.Sci.*, Vol.7,
- 2-23 LECKIE, F.A., PENNY, R.K. Shakedown Loads for Radial Nozzles in Spherical Pressure Vessels. *Int.J.Solids Struct.*, Vol.3, pp.743-755, 1967
- 2-24 MARCAL, P.V., TURNER, C.E. Elastic-Plastic Behaviour of Flush Nozzles in Spherical Pressure Vessels. *J.Mech.Eng. Sci.*, Vol.9, No.3, pp.182-189, 1967
- 2-25 BIJLAARD, P.P., DOHRMAN, R.J., WANG, I.C. Stresses in Junction of Nozzles to Cylindrical Pressure Vessel for Equal Diameter of Vessel and Nozzle. *Nucl.Eng.Des.*, Vol.5, pp.349-365, 1967
- 2-26 HASBERRY, J.W., JONES, N. A Theoretical Study of the Elastic Behaviour of Two Normally Intersecting Cylindrical Shells. *Trans.ASME, J.Eng. for Industry*, Vol.91, pp.563-572, August 1969

- 2-27 PAN, K.C., BECKETT, R.E. Stress and Displacement Analysis of a Shell Intersection. Trans.ASME, J.Eng. for Ind., Vol.92, pp.303-308, May 1970
- 2-28 WATERS, E.O. Stresses near a Cylindrical Outlet in a Spherical Pressure Vessel. Weld.Res.Counc.Bull., No.96, May 1965
- 2-29 LIND, N.C. The Stress Concentration at Radial Outlets in Spherical Pressure Vessels. Univ. of Illinois, T&AM Report No.161, March 1960
- 2-30 LECKIE, F.A., PENNY, R.K. Stress Concentration Factors for the Stresses at Nozzle Intersections in Pressure Vessels. Weld.Res.Counc.Bull., No.90, September 1963
- 2-31 ROSE, R.T., THOMPSON, J.M.T. Calculated Stress Concentration Factors for Nozzles in Spherical Pressure Vessels. Symp. on Pressure Vessel Research towards better Design, Inst.Mech.Engrs., January 1961
- 2-32 KLINE, DIXON, JORDON and ERINGEN. Stresses in Pressurized Cylindrical Shell with Circular Cutout. Gen.Tech.Corp. Tech.Rep. No.3-1, August 1961
- 2-33 NAGHDI, A.K., ERINGEN, A.C. Stress Analysis of a Circular Cylindrical Shell with Circular Cutout. Gen.Tech.Corp. Tech.Rep.No.3-2, January 1963
- 2-34 KOH, S.L., THIEL, C.C., ERINGEN, A.C. Computations for Stress and Stress Concentration in a Circular Cylindrical Shell with Circular Cutout. Gen.Tech.Corp.Tech.Rep.No.3-3, April 1963
- 2-35 THIEL, C.C., ERINGEN, A.C. Stress Concentrations in a Capped Circular Cylindrical Shell with Circular Cutout. Gen.Tech.Corp.Tech.Rep.No.3-4, June 1963

- 2-36 KENNY, B. Effect of Poisson's Ratio on Stress Distribution. Engineer 218, 5675, 706-712, 30 October 1964
- 2-37 DUNDURS, J. Dependence of Stress on Poisson's Ratio in Plane Elasticity. Int.J.Solids Struct., 3, 1013-1021, 1967
- 2-38 EVERETT and McCUTCHAM. Investigation of Stress Conditions in a Full-Size Branch Connection, Trans,ASME, Vol.60, FSP-60-12, 1933
- 2-39 WILLIAM, C., MORGAN, P.T., BIZON. Experimental Evaluation of Theoretical Elastic Stress Distributions for Cylinder-to-Hemisphere and Cone-to-Sphere Junctions in Pressurised Shell Structures. NASA TND-1565, February 1963
- 2-40 HARDENBERGH, D.E., ZAMRIK, S.Y. Experimental Investigation of Stresses in Nozzles in Cylindrical Pressure Vessels. Weld.Res.Council, July 1963
- 2-41 KITCHING, R., JONES, N. Effect of Bending Moments on Nozzles with Forged Transition Pieces. Inst.Mech.Eng., Vol.178, 211, 1963
- 2-42 RILEY, W.F. Experimental Determination of Stress Distributions in Thin Walled Cylindrical and Spherical Pressure Vessels with Circular Nozzles. NASA CR 53580 (2), 1963
- 2-43 KITCHING, R., DUFFIELD, N.A. Stresses due to Axial Loads and Internal Pressure on Forged Nozzles in a Spherical Pressure Vessel. Inst.Mech.Eng., Vol.6, pp.77-103, 1964
- 2-44 DINNO, K.S., GILL, S.S. An Experimental Investigation into the Plastic Behaviour of Flush Nozzles in Spherical Pressure Vessels. Int.J.Mech.Sci., Vol.7, 817-839, 1965
- 2-45 COTTAM, W.J., GILL, S.S. Experimental Investigations of the Behaviour beyond the Elastic Limit of Flush Nozzles in Cylindrical Pressure Vessels. J.Mech.Eng.Sci., Vol.8, 330-350, 1966

- 4-1 WARREN, M., ROHSENOW and HARTNETT, J.P. Handbook of Heat Transfer, 6-1, 7-1
- 4-2 NUSSELT, W. Der Wärmeaustausch zwischen Wand und Wasser in Rohr. Forsch.Gebiete Ingenieurw., Vol.2, p.309, 1931
- 4-3 DITTUS, F.W., BOELTER, L.M.K. Univ. Calif.Pub.Eng., Vol.2, p.443, 1930
- 4-4 McADAMS, W.H. "Heat Transmission", 3rd Ed. McGraw-Hill, New York, 1954
- 5-1 WOOLMAN, J., MOTTRAM, R.A. Vol.3, EN40-EN363, The Mechanical and Physical Properties of the British Standard EN Steels, The British Iron and Steel Res.Assoc.
- 7-1 MANSON, S.S. Thermal Stress and Low-Cycle Fatigue. McGraw-Hill Book Co., 1966
- 7-2 BATHOLOME, G. et al. Fracture and Safety Analysis of Nuclear Pressure Vessels. Eng.Fract.Mechs., Vol.4, p.431-446, 1973
- 7-3 SESSLEG, J.G., VOLKER WEISS. Low Cycle Fatigue Damage in Pressure Vessel Materials. J.Basic Eng., ASME, p.539, December 1963
- 7-4 CLOUD, R.L., RODABAUGH, E.C. Approximate Analysis of the Plastic Limit Pressures of Nozzles in Cylindrical Shells. J.Eng. for Power, ASME, p.171, April 1968
- 7-5 GRIFFITH, A.A. Proc.Int.Congr.Appl.Mech., 55, 1924
- 7-6 IRWIN, G.R. Encyclopedia of Physics, Vol.VI, Springer, Heidelberg, 1958
- 7-7 PARIS, P., ERDOGAN, F. A Critical Analysis of Crack Propagation Laws. Trans.ASME, J.Cas.Engng., 85, 528-534 1963

- 7-8 CLARK, W.G., WESSEL, E.T. Application of Fracture Mechanics Technology to Medium Strength Steels. Review of Development on Plane Strain Fracture Toughness Testing, ASTM STP 463, 160-190, 1970
- 7-9 COFFIN, L.F. Low Cycle Fatigue. A Review, Appl.Mat.Res., 129-141, 1962
- 7-10 LIEBOWITZ, "Fracture". An Advanced Treatise, Academic Press, Vols.1-7, 1969
- 7-11 RITCHIE, R.O., KNOTT, J.F. Effects of Fracture Mechanisms of Fatigue Crack Propagation. Symp. on Fracture Mechanics, Cambridge, 1972
- 7-12 WEERTMAN, J. Int.J.Fract.Mech., 2, 460, 1966
- 7-13 BILBY, B.A., HEALD, P.T. Proc.Roy.Soc.A305, 429, 1968
- 7-14 LIU, H.W., IINO, N. Fracture 1969, Proc.2nd Int.Conf. on Fracture, Brighton, 812, 1969
- 7-15 MILLER, G.A. Trans.ASM, 61, 442, 1968
- 7-16 CLARK, W.G., WESSEL, E.T. ASTM Special Tech.Pub., No.463, 106, 1970
- 7-17 WILSON, W.K. Eng.Fract.Mech., 2, 169, 1970
- 7-18 LOVE, A.E. A Treatise of the Mathematical Theory of Elasticity, 4th Ed., Cambridge, London, 1934, p.138
- 7-19 WILLIAMS, M.L. On the Stress Distribution at the Base of a Stationary Crack. ASME, Appl.Mech.Div., March 21, 1956 Paper No.56-A-16
- 7-20 IRWIN, G.W. Analysis of Stresses and Strains near the End of a Crack Traversing a Plate. J.Appl.Mech., Vol.24, No.3, pp.361-364, September 1957
- 7-21 FROST, N.E. et al. A Fracture Mechanics Analysis of Fatigue Crack Growth. Data for various materials. Eng.Fract.Mech., Vol.3, pp.109-126, 1971

- A2-1 WILSON, E.L., NICKELL, R.E. Application of the Finite Element Method to Heat Conduction Analysis. Nuclear Engineering and Design, North Holland, Amsterdam, pp.276-286, 1966
- A2-2 GURTIN, M.E. Variational Principles for Linear Initial Value Problems. Quart.J.Appl.Math., 22, 252-256, 1964
- A2-3 RICHARDSON, P.D., SHUM, Y.M. Use of Finite Element Methods in Solution of Transient Heat Conduction Problems. ASME Winter Annual Meeting, Los Angeles, California, 1969
- A2-4 EMERY, A.F., CARSON, W.W. An Evaluation of the use of the Finite Element Method in the Computation of Temperature. Trans.ASME, J.Heat Transfer, 136-145, 1971
- A2-5 VISSER, W. A Finite Element Method for the Determination of Non-Stationary Temperature Distribution and Thermal Deformations. Proc.Conf.Matrix Meth.Struct.Mech. Wright Patterson AFB, Ohio 925-943, 1965
- A2-6 ZIENKIEWICZ, P.C. The Finite Element Method in Engineering Science, McGraw-Hill, London, 1971
- A2-7 DESAI, C.S., ABEL, J.F. Introduction to the Finite Element Method, Van Nostrand Reinhold, New York, 1972
- A2-8 Strain Gauge Techniques, Fundamental and Applications, Massachusetts Institute of Technology, Cambridge, July 1958

## APPENDIX 9

# Comparison of Temperature Distributions

### A 9.1 Finite Difference Equation in a Cylindrical System

Consider the system in a three-dimensional cylindrical co-ordinates as shown in Fig. A 9.1.1. The energy balance equation gives the following equation for the temperature  $T_o$  at node  $o$ .

$$k \frac{(r_i + \Delta r/2) \Delta \theta \Delta z}{\Delta r} (T_2 - T_o) + k \frac{(r_i - \Delta r/2) \Delta \theta \Delta z}{\Delta r} (T_4 - T_o) + k \frac{\Delta r \Delta z}{\Delta \theta r_i} (T_1 + T_3 - 2T_o) + k \frac{r_i \Delta \theta \Delta r}{\Delta z} (T_5 + T_6 - 2T_o) = 0 \quad (\text{A 9.1.1})$$

Now consider a part of a hollow cylinder subdivided into equal space increments  $\Delta r$  as shown in Fig. (A 9.1.2). The explicit difference equation for the node  $m$  is from Equation A 9.1.1 and for the one-dimensional (radial) time dependent conduction

$$\frac{k}{\Delta r} \left[ (T_{m-1}^n - T_m^n) (r_m - \frac{\Delta r}{2}) + (T_{m+1}^n - T_m^n) (r_m + \frac{\Delta r}{2}) \right] = \frac{\Delta r \rho c \Gamma_m}{\Delta \tau} \left[ T_m^{n+1} - T_m^n \right] \quad (\text{A 9.1.2})$$

$\Delta r$  = space increment in radial direction

$\Delta \tau$  = time increment, and  $n$  indicates temperature at time  $(\tau + \Delta \tau)$ .

In explicit solutions of time dependent equations the expressions used give the future temperature  $T_m$  at node  $m$  (say) in terms of the current temperatures at the surrounding nodes. The explicit formulation uses

forward-difference approximation for the non-steady conduction equation.

Now if the time and space increment is chosen so that  $\frac{(\Delta r)^2}{\alpha \Delta \tau} = 2$  then equation A 9.1.2 above becomes:

$$T_m^{n+1} = \frac{1}{2} \left[ T_{m-1}^n \left( 1 - \frac{\Delta r}{2r_m} \right) + T_{m+1}^n \left( 1 + \frac{\Delta r}{2r_m} \right) \right] \quad (\text{A 9.1.3})$$

## A 9.2 Determination of Temperature Distribution

The temperature distribution is determined by program CYL1DT (Listing at the end of the Appendix) which solves the equation

$$k \left( \frac{\partial^2 T}{\partial r^2} + \frac{1}{r} \frac{\partial T}{\partial r} \right) = \rho c \frac{\partial T}{\partial \tau} \quad (\text{N.2 p.83})$$

numerically using the forward-difference expression A 9.1.3. Temperatures are determined along the radial direction ( $r$ ) at specified time increments. The space increment  $\Delta r$  is chosen equal to 0.05 inches and this produces 11 nodal points along the radius of the cylinder as shown in Fig. A 9.2.1. The parameter  $\frac{(\Delta r)^2}{\alpha \Delta \tau} = 2$  for  $\Delta r = 0.05$  inches and  $\alpha = 0.347 \text{ ft}^2/\text{hr}$  (for steel EN58J (R.5-1) gives  $\Delta \tau = 0.09$  secs. This time increment will produce  $\frac{60 \text{ secs}}{0.09 \text{ secs}} = 667$  time iterations for every minute.

The boundary conditions are identical to that of the nozzle in Chapter 4, that is, the inside circumference is maintained at the constant temperature of  $T_f = 450^\circ \text{F}$  and there is heat loss by natural convection to the air on the outside boundary. The heat transfer coefficient is that given in Reference (R.4-4) for horizontal cylinders and pipes.

$$\frac{h D_o}{k_f} = 0.53 \left[ \frac{D_o^3 \rho_f g \beta_f \Delta t}{\mu_f^2} \left( \frac{c \mu}{k_f} \right) \right]^{0.25} \quad (\text{A 9.2.1})$$



where  $h_c$  = heat transfer coefficient

$D_o$  = outside diameter of cylinder

$k_f$  = thermal conductivity of air

$\rho_f$  = density of air

$g$  = acceleration due to gravity

$\beta_f$  = coefficient of volumetric expansion of air

$\Delta t = T_w - T_\infty$

$T_w$  = temperature on the outside surface of cylinder

$T_\infty$  = is the air temperature (60°F)

$\mu_f$  = viscosity of air

$C_p$  = specific heat of air (at atm. pressure)

The heat transfer coefficient is calculated at each time increment using the equivalent surface node temperature.

### A 9.3 Comparison of Temperature Results

The temperature distribution for the nozzle of Case C away from the vessel (grid points 91 to 100 see Fig.4.6.1, page 289) which was obtained using the two-dimensional (x,y), time dependent ( $\tau$ ) equation for a plane wall

$$k \left( \frac{\partial^2 T}{\partial x^2} + \frac{\partial^2 T}{\partial y^2} \right) = \rho c \frac{\partial T}{\partial \tau} \quad (4.3.1.1, p 71)$$

is compared to the results obtained by using the one-dimensional (radial) time dependent ( $\tau$ ) equation for the cylinder

$$k \left( \frac{\partial^2 T}{\partial r^2} + \frac{1}{r} \frac{\partial T}{\partial r} \right) = \rho c \frac{\partial T}{\partial \tau} \quad (N.2, p-83)$$

for the times 1 minute (Fig.A 9.3.1, Table A 9.3.1), 2 minutes (Fig. A 9.3.2, Table A 9.3.2), and 4 minutes (Fig. A 9.3.3, Table A 9.3.3). The cylinder results are given in Table A 9.3.4. The dimensions of both cylinder and nozzle are identical, with  $D_i = 1$  in and  $D_o = 2$  in, and the boundary conditions already referred to.

It can be seen from Fig. A 9.3.1 that at time 1 minute the temperature at  $r = 0.6$  inches for the nozzle is higher by 5.3% of the value of the cylinder and by 19.0% on the outside boundary. The average deviation is 12.2%. For time 2 minutes the average deviation is 11.8% (Fig. A 9.3.2) and for time 4 minutes 11.6%. In general the temperatures obtained in the nozzle using the two-dimensional time dependent plane wall conduction equation are higher than the temperatures obtained for the cylinder by an average of 11-12%. Near the junction where the end effects (vessel) affect the conduction in the  $z$  (axial) direction the equation for the cylinder will in fact be two-dimensional ( $r$  and  $z$ )

$$k \left( \frac{\partial^2 T}{\partial r^2} + \frac{1}{r} \frac{\partial T}{\partial r} + \frac{\partial^2 T}{\partial z^2} \right) = \rho c \frac{\partial T}{\partial \tau} \quad (N.3, p. 83-N2)$$

It can be concluded that the approximation of the plane wall heat conduction in two-dimensions ( $x, y$ ) and time ( $\tau$ ) gives reasonable results for the nozzle and can be used to overcome the difficulty in the analysis of the heat conduction at the intersection of two cylinders.

Of course the alternative of treating the problem in three-dimensional time dependent formulation will soon be possible with the expansion of the computing facilities in order to give acceptable accuracy. But even so, the economics and time consumption of three-dimensional unsteady analysis will still be subjected to considerable competition from the two-dimensional analysis especially whenever axisymmetric geometries are considered.

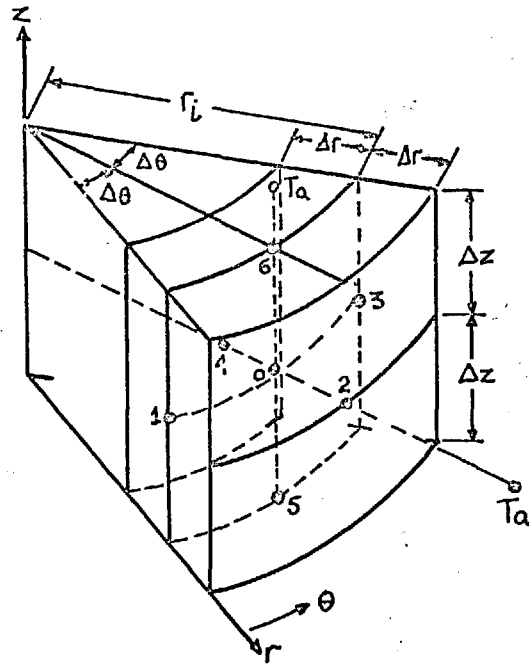


FIGURE A9.1.1

Three-dimensional cylindrical system

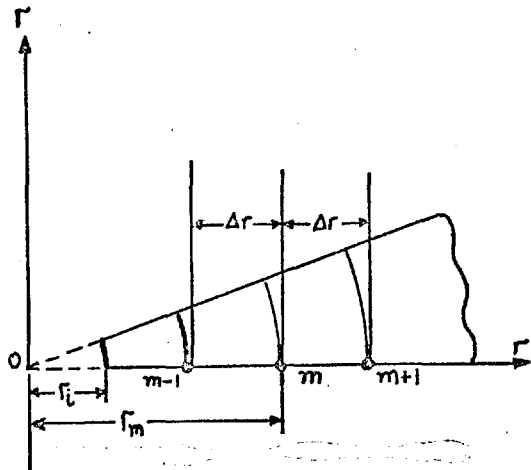
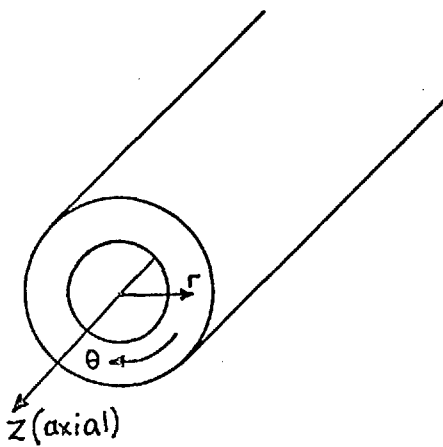
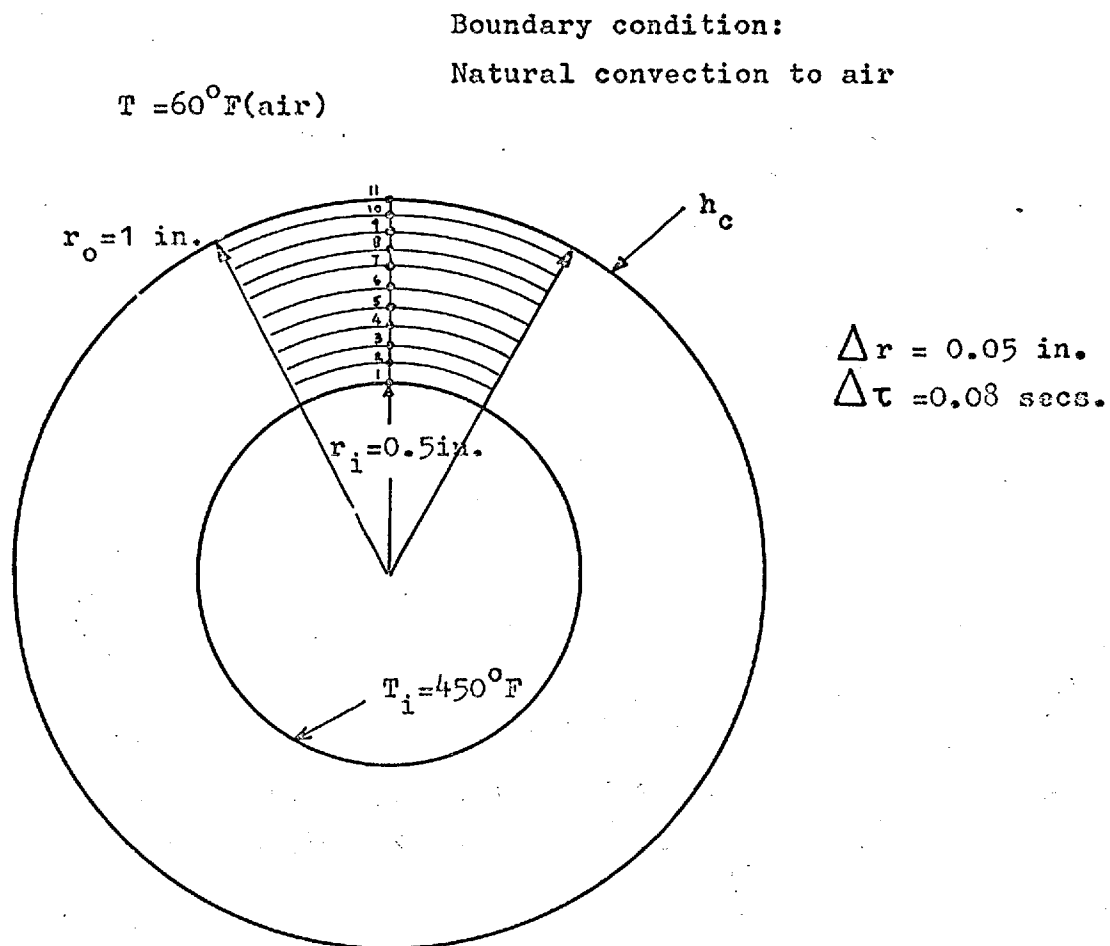


FIGURE A9.1.2

Subdivision of cylindrical wall

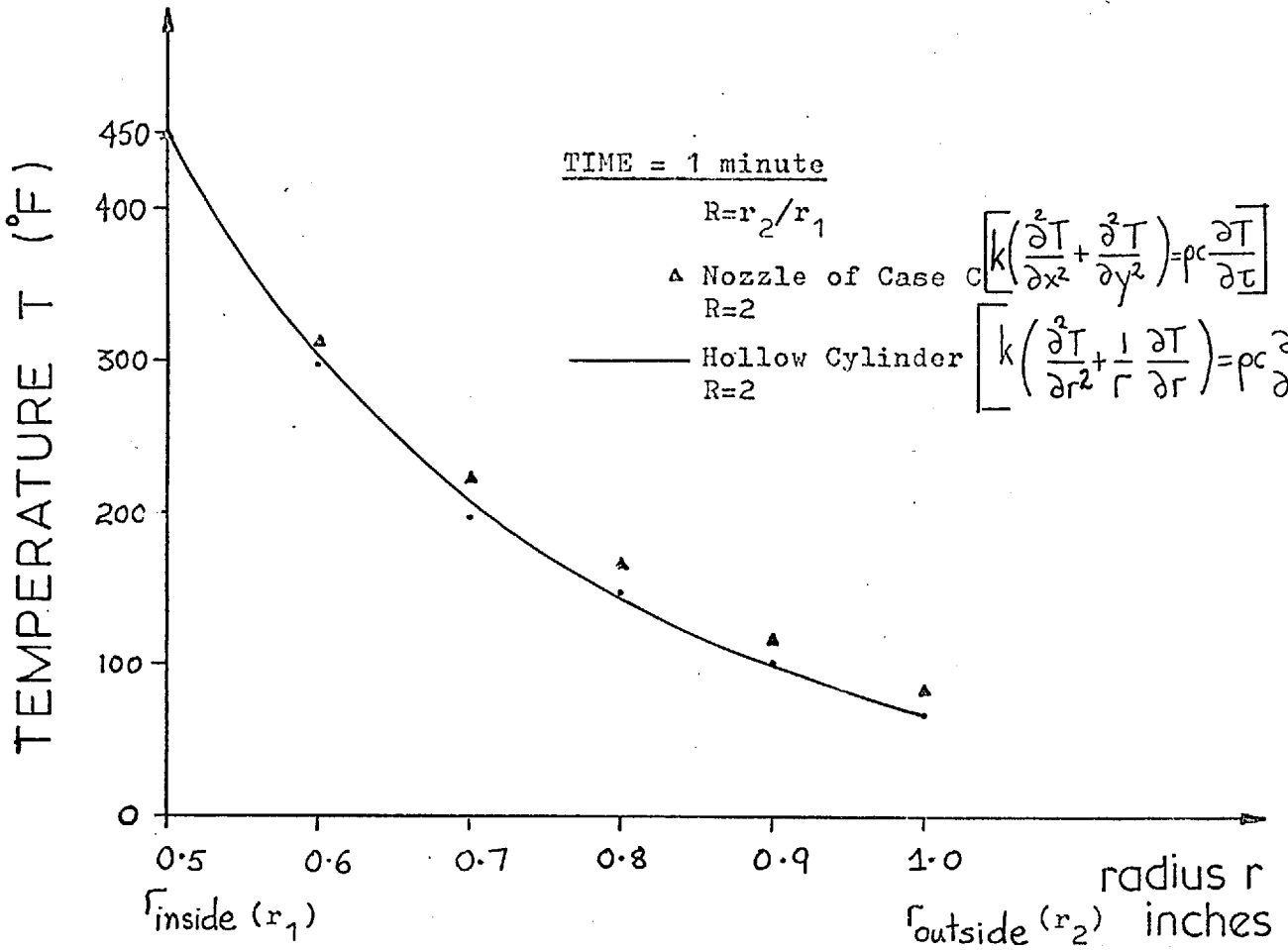
One-dimensional cylindrical system

Heat conduction(unsteady) in radial direction



Finite-Difference Grid

FIGURE A9.2.1

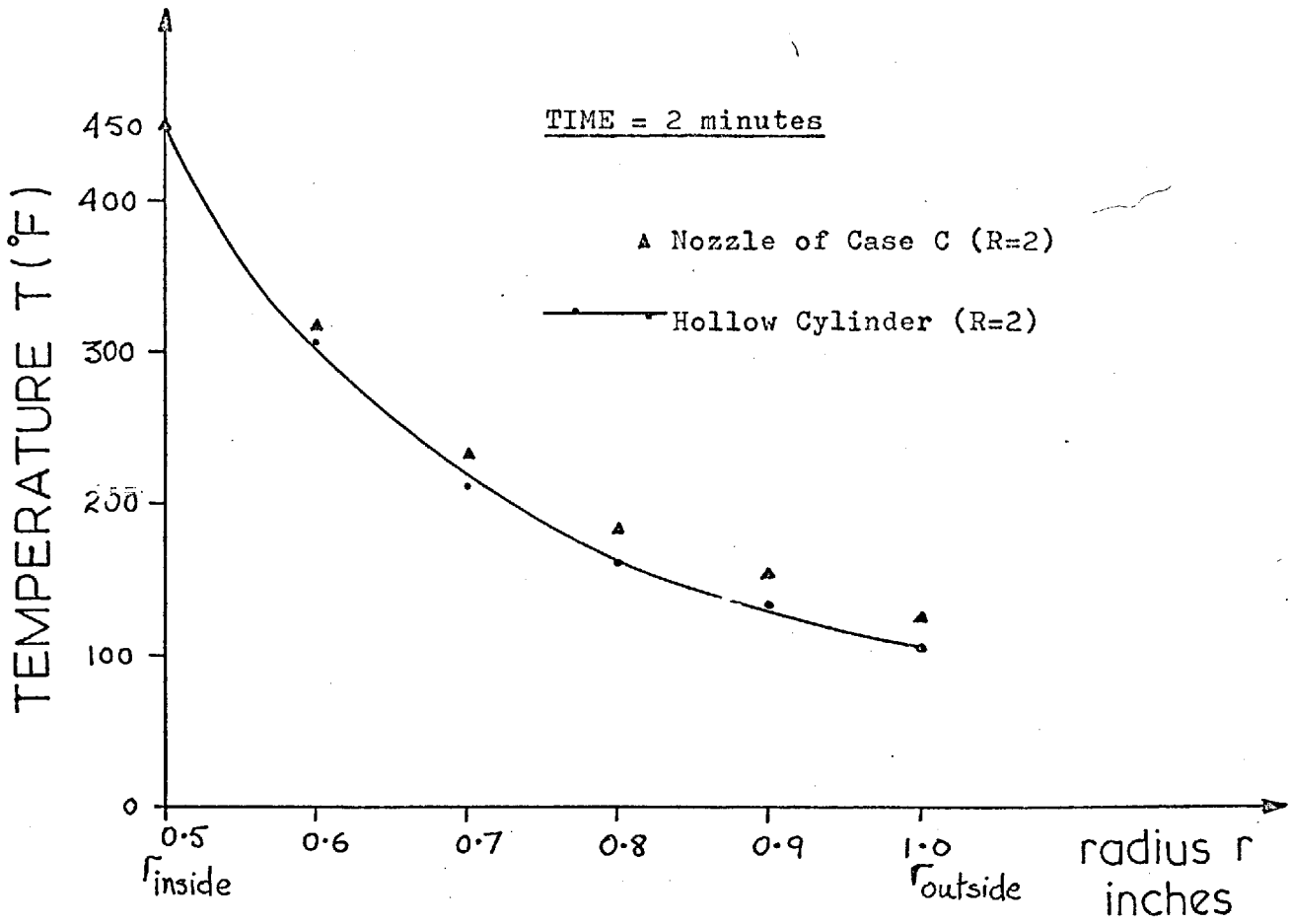


TIME = 1 minute			
RADIUS r inches	TEMPERATURE (°F) NOZZLE OF CASE C	TEMPERATURE (°F) HOLLOW CYLINDER	DEVIATION %
0.5 (r <sub>1</sub> )	450.0	450.0	
0.6	311.2	294.4	+5.7 %
0.7	220.4	195.6	+12.7 %
0.8	164.7	149.5	+10.2 %
0.9	116.8	101.7	+14.8 %
1.0 (r <sub>2</sub> )	82.6	70.2	+17.6 %

AVERAGE  
DEVIATION = 12.2 %

FIGURE A9.3.1

Comparisons of temperatures for time = 1 minute.

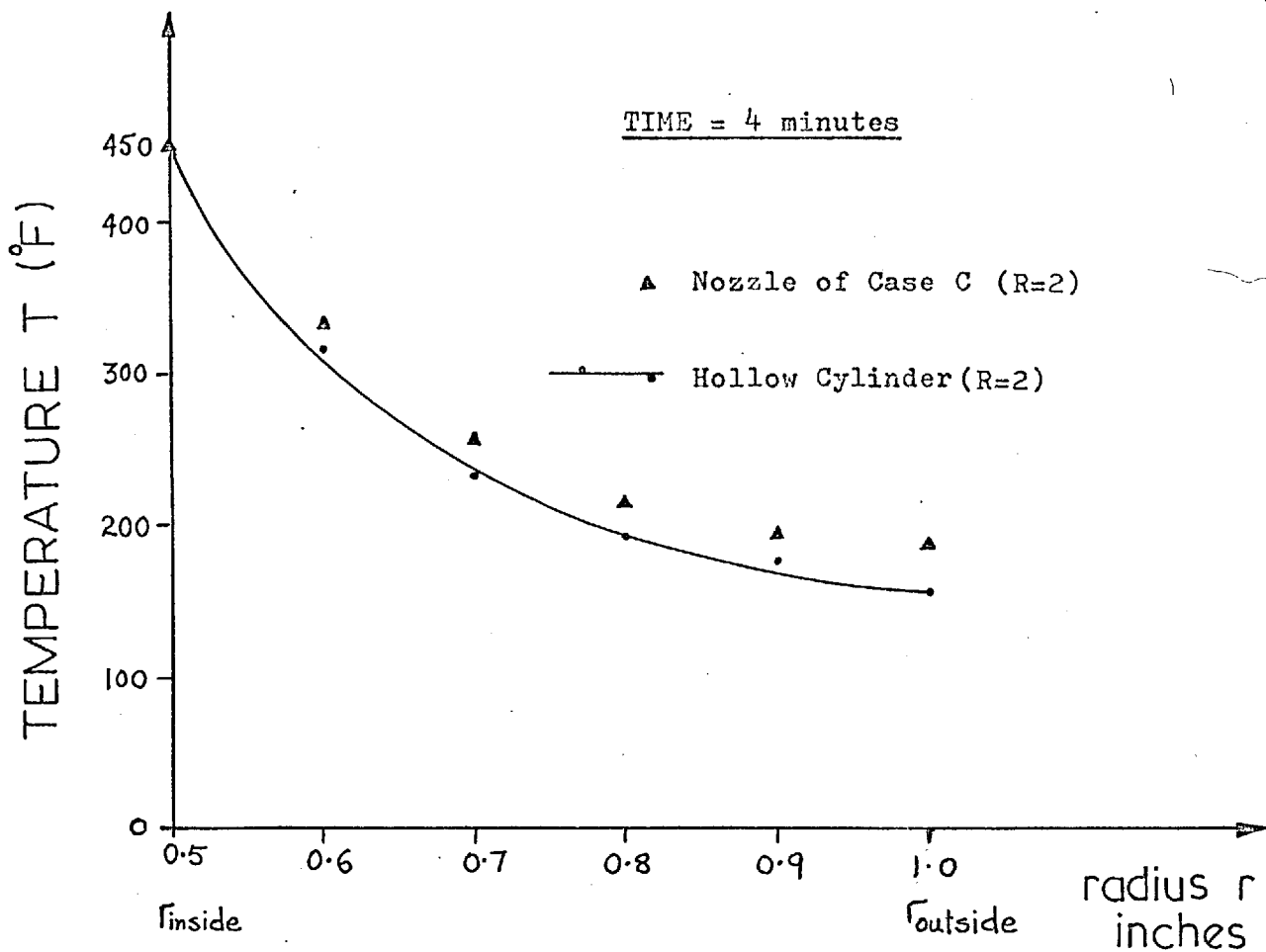


TIME = 2 minutes			
RADIUS r inches	TEMPERATURE (°F) NOZZLE CASE C	TEMPERATURE (°F) HOLLOW CYLINDER	DEVIATION %
0.5 ( $r_1$ )	450.0	450.0	
0.6	316.7	306.3	+3.4 %
0.7	231.2	211.7	+9.2 %
0.8	183.1	160.2	+14.3 %
0.9	151.8	134.5	+12.9 %
1.0	125.2	105.2	+19.0 %

AVERAGE  
DEVIATION= 11.8 %

FIGURE A9.3.2

Comparisons of temperatures for time = 2 minutes.



TIME = 4 minutes			
RADIUS r inches	TEMPERATURE (°F) NOZZLE OF CASE C	TEMPERATURE (°F) HOLLOW CYLINDER	DEVIATION %
0.5 ( $r_1$ )	450.0	450.0	
0.6	333.4	316.6	+5.3 %
0.7	255.2	232.2	+9.9 %
0.8	215.7	191.4	+12.7 %
0.9	195.4	176.0	+11.0 %
1.0	186.3	156.4	+19.0 %

AVERAGE

DEVIATION = 11.6 %

FIGURE A9.3.3

Comparisons of temperatures for time = 4 minutes

Nozzle Case C temperatures for time=1 minute.

TABLE A9.3.1

I= 1										
91	92	93	94	95	96	97	98	99	100	
450.0	450.0	450.0	450.0	450.0	450.0	450.0	450.0	450.0	450.0	450.0
I= 2										
91	92	93	94	95	96	97	98	99	100	
311.2	311.2	311.2	311.2	311.2	311.2	311.2	311.2	311.2	311.2	311.2
I= 3										
91	92	93	94	95	96	97	98	99	100	
220.4	220.4	220.4	220.4	220.4	220.4	220.4	220.4	220.4	220.4	220.4
I= 4										
91	92	93	94	95	96	97	98	99	100	
164.7	164.7	164.7	164.7	164.7	164.7	164.7	164.7	164.7	164.7	164.7
I= 5										
91	92	93	94	95	96	97	98	99	100	
116.8	116.8	116.8	116.8	116.8	116.8	116.8	116.8	116.8	116.8	116.8
I= 6										
91	92	93	94	95	96	97	98	99	100	
82.6	82.6	82.6	82.6	82.6	82.6	82.6	82.6	82.6	82.6	82.6



Nozzle Case C temperatures for time=2 minutes.

TABLE A9.3.2

I= 1										
91	92	93	94	95	96	97	98	99	100	
450.0	450.0	450.0	450.0	450.0	450.0	450.0	450.0	450.0	450.0	450.0
I= 2										
91	92	93	94	95	96	97	98	99	100	
316.7	316.7	316.7	316.7	316.7	316.7	316.7	316.7	316.7	316.7	316.7
I= 3										
91	92	93	94	95	96	97	98	99	100	
231.2	231.2	231.2	231.2	231.2	231.2	231.2	231.2	231.2	231.2	231.2
I= 4										
91	92	93	94	95	96	97	98	99	100	
183.1	183.1	183.1	183.1	183.1	183.1	183.1	183.1	183.1	183.1	183.1
I= 5										
91	92	93	94	95	96	97	98	99	100	
151.8	151.8	151.8	151.8	151.8	151.8	151.8	151.8	151.8	151.8	151.8
I= 6										
91	92	93	94	95	96	97	98	99	100	
125.2	125.2	125.2	125.2	125.2	125.2	125.2	125.2	125.2	125.2	125.2

Nozzle Case C temperatures for time=4 minutes.

TABLE A9.3.3

I= 1									
91	92	93	94	95	96	97	98	99	100
450.0	450.0	450.0	450.0	450.0	450.0	450.0	450.0	450.0	450.0
I= 2									
91	92	93	94	95	96	97	98	99	100
333.4	333.4	333.4	333.4	333.4	333.4	333.4	333.4	333.4	333.4
I= 3									
91	92	93	94	95	96	97	98	99	100
255.2	255.2	255.2	255.2	255.2	255.2	255.2	255.2	255.2	255.2
I= 4									
91	92	93	94	95	96	97	98	99	100
215.7	215.7	215.7	215.7	215.7	215.7	215.7	215.7	215.7	215.7
I= 5									
91	92	93	94	95	96	97	98	99	100
195.4	195.4	195.4	195.4	195.4	195.4	195.4	195.4	195.4	195.4
I= 6									
91	92	93	94	95	96	97	98	99	100
186.3	186.3	186.3	186.3	186.3	186.3	186.3	186.3	186.3	186.3

FL REQUIRED TO LOAD 24400  
 FL REQUIRED TO RUN 17000  
 INITIAL TRANSFER TO CYLI1DT - 4302

BLOCK ASSIGNMENTS.

BLOCK	ADDRESS	LENGTH	FILE
CYLI1DT	101	4262	SIN
ABORTE	4363	47	FORLIBB
CPUCPR	4432	201	FORLIBB
CPUCIO	4533	13	FORLIBB
CPUCPM	4646	5	FORLIBB
CPULFM	4653	10	FORLIBB
CPURDS	4663	42	FORLIBB
CPURDW	4725	133	FORLIBB
CPUSYS	5160	32	FORLIBB
CPUNTC	5113	13	FORLIBB
CPUNTS	5125	43	FORLIBB
CPUNTW	5170	104	FORLIBB
GETBA	5274	17	FORLIBB
/CJOB.F./	5313	426	
INOUTE	5741	143	FORLIBB
INPUTE	6104	1245	FORLIBB
/FREE=OR/	7351	3	
OUTPUTE	7354	1156	FORLIBB
RUNIOP	10532	324	FORLIBB
RUNSYS	11056	1106	FORLIBB
SYSTEM	12164	442	FORLIBB
TRACSAK	12020	277	FORLIBB
TRACKE	13125	750	FORLIBB
//	14075	2623	

Cylinder temperatures for times=1,2, and 4 minutes.

TABLE A9.3.4

TIME IN SECONDS= 60.0										
<u>450.0</u>	<u>366.5</u>	<u>294.4</u>	<u>245.1</u>	<u>195.6</u>	<u>170.1</u>	<u>149.5</u>	<u>114.1</u>	<u>101.7</u>	<u>75.3</u>	<u>70.2</u>
TIME IN SECONDS=120.0										
<u>450.0</u>	<u>350.1</u>	<u>306.3</u>	<u>345.6</u>	<u>211.7</u>	<u>184.5</u>	<u>160.2</u>	<u>135.1</u>	<u>134.5</u>	<u>115.8</u>	<u>105.2</u>
TIME IN SECONDS=240.0										
<u>450.0</u>	<u>355.2</u>	<u>316.6</u>	<u>260.4</u>	<u>232.2</u>	<u>205.3</u>	<u>191.4</u>	<u>176.9</u>	<u>176.0</u>	<u>163.2</u>	<u>156.4</u>

PROGRAM CYL1DT

The program solves the one-dimensional time dependent, heat conduction equation

$$k \left( \frac{\partial^2 T}{\partial r^2} + \frac{1}{r} \frac{\partial T}{\partial r} \right) = \rho c \frac{\partial T}{\partial \tau}$$

for a hollow cylinder explicitly using forward difference formulation in time ( $\tau$ ) and space (radial) increments. It assumes a constant temperature around the inside circumference and along the axis ( $z$ ) of the cylinder and heat conduction by natural convection on the outside boundary.

( The program was initially developed in November 1976 for an investigation of heat conduction in jacketed pressure vessels used by Ethylene Plastique Co. Ltd., France, for the storage of ethylene gas at low temperatures; Internal Report 2-EP-5000L/C.N.Oikonomides, Applied Mechanics, and in here the boundary conditions are changed for natural convection to air.)

JOB(UHEM13, J10, T30), C440000, LC3070) 013040 H02S.C.H  
 MNF(T,0,R=2,F=1,C=BIN)  
 MAP(P)  
 BIN.

-----  
 -----  
 PROGRAM CYL1DT(INPUT,OUTPUT,TAPE5=INPUT,TAPE6=OUTPUT)

PROGRAM CYL1DT SOLVES THE ONE DIMENSIONAL TIME DEPENDENT DIFFERENTIAL EQUATION OF HEAT CONDUCTION IN A HOLLOW CYLINDER IN THE RADIAL DIRECTION USING THE CYLINDRICAL FORWARD DIFFERENCE EXPLICIT FORMULATION IN TIME AND SPACE INCREMENTS. IT ASSUMES A CONSTANT TEMPERATURE AROUND THE INSIDE CIRCUMFERENCE AND ALONG THE AXIS OF CYLINDER AND HEAT CONDUCTION BY NATURAL CONVECTION ON THE OUTSIDE BOUNDARY.

COMMON U(510),  
 1 IRINS, IROUT,  
 2 GRID, A(300), F(300), X(300),  
 3 INFNT(12), OUTNT(12)

DATA DESIGNATIONS DIMENSIONS

100 READ(5,100) TIN  
 110 READ(5,110) TCYL  
 120 READ(5,120) SPACIN  
 130 READ(5,125) ROUT  
 140 READ(5,128) RINS  
 150 READ(5,130) RADTH  
 160 READ(5,140) GRID  
 170 READ(5,135) T1  
 180 READ(5,145) ANHVT  
 190 READ(5,150) TIMEB  
 100 FORMAT(1X,F12.6)  
 110 FORMAT(1X,F12.6)  
 120 FORMAT(1X,F12.6)  
 130 FORMAT(1X,F12.6)  
 140 FORMAT(1X,F12.6)  
 125 FORMAT(1X,F12.6)  
 128 FORMAT(1X,F12.6)  
 135 FORMAT(1X,F12.6)  
 145 FORMAT(1X,F12.6)  
 150 FORMAT(1X,F12.6)  
 IROUT=ROUT/GRID  
 IRINS=RINS/GRID

PROPERTIES OF MATERIAL

1 READ(5,160) CONDS,  
 2 DENST,  
 3 SPEST,  
 4 XCHART  
 160 FORMAT(1X,4(F12.6))

PROPERTIES OF GAS ON THE OUTSIDE  
 WHERE NATURAL CONVECTION TAKES PLACE

1 READ(5,170) GASK,  
 2 SPHEAT,  
 3 DYNVIS,  
 4 VISCK,  
 5 E,  
 6 DENSG  
 170 FORMAT(1X,6(F12.6))

DATA RELATED TO CONDITIONS

1 READ(5,175) ACCLG,  
 2 TGAS  
 175 FORMAT(1X,2(F12.6))

RCY=2\*(3.141592654)\*ROUT  
 I1=(IROUT-IRINS)/GRID+1

INITIAL STATE TIME=0. TEMPERATURE OF THE MATERIAL IS DEFINED

186 DO 186 M=1,I1  
 U(M)=TIN

```

C      L1= I1-1
C      RADIAL TEMPERATURE CALCULATION
C      THIS IS TIME ITERATION
187    READ(5,187) TIME
      FORMAT(1X,F12.6)
      NV=1
299    CONTINUE
      CONTINUE
      DO 196 M=2, I1
      U(I1)= U(I1-1)
      RM=RINS +FLOAT(M)*GRID
      G=U(M-1)*(1.-(GRID/(2.*RM)))
      C=U(M+1)*(1.+(GRID/(2.*RM)))
      U(M) = 1./2.*(G+C)
196    CONTINUE

      HEAT IS CONDUCTED TO THE SURROUNDING GAS BY NATURAL CONVECTION
      CALCULATE THE HEAT TRANSFER COEFFICIENT AT THE WALL
      TEMPERATURE OF THIS TIME INTERVAL

      PRAND=(SPHEAT *BYNVIS)/GASK

      CALCULATE THE GRASHOFF NUMBER AS A FUNCTION OF THE WALL
      TEMPERATURE AT THE END OF THIS TIME INTERVAL
      UM=(U(I1))
      GRASH=((2.*RMOUT)**3)*(DEL TSG**2)*ACC. G.*(UM-TGAS)/(VISC**2)
      ANSL=0.53*(GRASH*PRAND)**0.25
      HEATCO=(GASK*ANSL)/(2.*RMOUT)

      FROM THE HEAT BALANCE EQUATION ON THE OUTSIDE BOUNDARY
      CALCULATE THE TEMPERATURE DROP OF THE WALL NODEAL TEMPERATURE
      DUE TO CONVECTION AT THIS TIME INTERVAL

      AA1=-COND3*(GRID)*RCY*(U(I1)-U(I1-1))
      IF(AA1.EQ.0.)GO TO 489
      B31=HEATCO*(GRID)*RCY*(U(I1)-TGAS)
      IF(B31.EQ.0.) GO TO 489
      CC1=DENST*SPHEAT*(GRID**2)*RCY
      DIFF=(-AA1-B31)/CC1
      FDIFF=(DIFF*TIME**3)/3600.
      U(I1)=U(I1)*FFDIFF
489    CONTINUE

      IF (TIME.EQ. 22.5) T1=10.
      IF (TIME.EQ. 122.5) T1=30.
      IF (TIME.EQ. 302.5) T1=60.
      IF (TIME.EQ. 1812.5) T1=120.
      IF (TIME.EQ. 32.5) NV=4
      IF (TIME.EQ. 122.5) NV=5
      IF (TIME.EQ. 332.5) NV=6
      IF (TIME.EQ. 1812.5) NV=16
      TINT=T1*FLOAT(NV)
      IF (TIME.LT. TINT) GO TO 101
      TIME=TIME+TINT
101    CONTINUE
      NV=NV+1

      PRINT ALL NODEAL TEMPERATURES AT SPECIFIED TIME INTERVALS

523    CONTINUE
      STIME=TIME/26.
      WRITE(6,2400)
2400   FORMAT(1(/))
      WRITE(6,550) STIME, TIME
550    FORMAT(2X,*TIME IN MINUTLS=*, F9.3,1 X, *TIME IN SECONDS=*,F9.2)
2450   FORMAT(1(/))
      I=I1
500    CONTINUE
      WRITE(6,1099) I
1999   FORMAT(2X,*I=*, I3)
      WRITE(6,2300) (U(I),I=1,I1)
2300   FORMAT((1X,10(F9.1,7X)))
      I=I-1
      GO TO 500
1010   IF (TIME.LT.150.) GO TO 528
528    TIME=TIME/TIMER
1000   IF (STIME.LT. 1. MINUT) GO TO 1001

```

CALL DATA(N)  
 1001 CONTINUE  
 STOP  
 END

SUBROUTINE DATA(N)  
 COMMON U(500),IRINC,IROUT,GRID,  
 1 A(700),B(300),X(300),  
 2 INEFT(12),OUTEFT(12)  
 DO 505 L=1,N  
 505 X(L)=0.0  
 READ(5,875) INEFT  
 READ(5,875) OUTEFT  
 875 FORMAT(8X,2A6)  
 READ(5,105) N,EPS,MAX  
 105 FORMAT(I3,F4.0,I3)  
 REWIND 1  
 DO 605 I=1,N  
 READ(5,INEFT) (A(L),L=1,N)  
 605 WRITE(1) (A(M),M=1,N)  
 READ(5,INEFT) (B(L),L=1,N)  
 ITER=1  
 995 BIG=0.0  
 DO 1005 I=1,N  
 102 SUM=0.0  
 READ(1) (A(L),L=1,N)  
 IF(I.EQ.1) GO TO 1055  
 LAST=I-1  
 DO 1065 J=1,LAST  
 1065 SUM=SUM+A(J)\*X(J)  
 IF(I.EQ.N) GO TO 1035  
 1055 INITL=I+1  
 DO 1075 J=INITL,N  
 1075 SUM=SUM+A(J)\*X(J)  
 1035 TEMP=(B(I)-SUM)/A(I)  
 IF(ABS(TEMP-X(I)).GT.BIG) BIG=ABS(TEMP-X(I))  
 1005 X(I)=TEMP  
 IF(BIG.LT.EPS) GO TO 752  
 IF(ITER.GE.MAX) GO TO 752  
 ITER=ITER+1  
 GO TO 995  
 752 WRITE(6,147) ITER,EPS,BIG  
 147 FORMAT(1H3,TF,2=14.7)  
 WRITE(6,OUTEFT) (X(L),L=1,N)  
 RETURN  
 END

C CYL10T-CYL10T-CYL10T-CYL10T-CYL10T-CYL10T-CYL10T-CYL10T-CYL10T







TABLE 4.4.1

I=76										
1	2	3	4	5	6	7	8	9	10	
458.0	432.1	414.5	397.5	380.7	364.4	348.5	333.1	318.2	303.8	303.8
296.0	275.1	256.4	238.7	222.0	206.0	190.5	175.4	160.7	146.4	146.4
181.0	173.1	165.2	157.3	150.4	144.3	138.7	133.1	127.5	122.0	122.0
113.0	114.1	115.2	116.3	117.4	118.5	119.6	120.7	121.8	122.9	122.9
85.5	87.7	89.9	92.1	94.3	96.5	98.7	100.9	103.1	105.3	105.3
105.0	101.1	97.2	93.3	89.4	85.5	81.6	77.7	73.8	69.9	69.9
107.0	107.1	107.2	107.3	107.4	107.5	107.6	107.7	107.8	107.9	107.9
109.0	109.1	109.2	109.3	109.4	109.5	109.6	109.7	109.8	109.9	109.9
110.6	110.7	110.8	110.9	111.0	111.1	111.2	111.3	111.4	111.5	111.5

I=63										
1	2	3	4	5	6	7	8	9	10	
450.0	432.4	415.1	398.2	381.7	365.5	349.3	334.7	319.9	305.7	305.7
292.0	275.1	258.6	242.2	226.3	210.6	195.0	179.6	164.3	149.0	149.0
181.0	173.1	165.2	157.3	150.4	144.3	138.7	133.1	127.5	122.0	122.0
122.0	115.1	111.2	107.3	103.4	99.5	95.6	91.7	87.8	83.9	83.9
89.0	91.7	94.4	97.1	99.8	102.5	105.2	107.9	110.6	113.3	113.3
105.0	101.1	97.2	93.3	89.4	85.5	81.6	77.7	73.8	69.9	69.9
107.0	107.1	107.2	107.3	107.4	107.5	107.6	107.7	107.8	107.9	107.9
109.0	109.1	109.2	109.3	109.4	109.5	109.6	109.7	109.8	109.9	109.9
135.0	135.1	135.2	135.3	135.4	135.5	135.6	135.7	135.8	135.9	135.9

I=63										
1	2	3	4	5	6	7	8	9	10	
450.0	432.4	415.1	398.2	381.7	365.5	349.3	334.7	319.9	305.7	305.7
292.0	275.1	258.6	242.2	226.3	210.6	195.0	179.6	164.3	149.0	149.0
181.0	173.1	165.2	157.3	150.4	144.3	138.7	133.1	127.5	122.0	122.0
122.0	115.1	111.2	107.3	103.4	99.5	95.6	91.7	87.8	83.9	83.9
89.0	91.7	94.4	97.1	99.8	102.5	105.2	107.9	110.6	113.3	113.3
105.0	101.1	97.2	93.3	89.4	85.5	81.6	77.7	73.8	69.9	69.9
107.0	107.1	107.2	107.3	107.4	107.5	107.6	107.7	107.8	107.9	107.9
109.0	109.1	109.2	109.3	109.4	109.5	109.6	109.7	109.8	109.9	109.9
135.0	135.1	135.2	135.3	135.4	135.5	135.6	135.7	135.8	135.9	135.9

I = 2									
1	2	3	4	5	6	7	8	9	10
429.6	429.6	429.0	429.3	429.6	429.8	430.1	430.3	430.5	430.6
430.8	431.0	431.1	431.2	431.3	431.4	431.5	431.5	431.7	431.7
431.8	431.9	431.9	432.0	432.0	432.0	432.1	432.1	432.1	432.2
432.2	432.2	432.2	432.2	432.3	432.3	432.3	432.3	432.3	432.3
432.3	432.3	432.3	432.3	432.3	432.4	432.4	432.4	432.4	432.3
432.3	432.3	432.3	432.3	432.3	432.3	432.3	432.3	432.3	432.3
432.3	432.3	432.3	432.3	432.3	432.3	432.3	432.3	432.3	432.3
432.3	432.3	432.2	432.2	432.2	432.2	432.2	432.2	432.2	432.2
432.2	432.2	432.2	432.2	432.2	432.2	432.2	432.2	432.2	432.2
432.2	432.2	432.2	432.2	432.2	432.2	432.2	432.2	432.2	432.2

I = 1									
1	2	3	4	5	6	7	8	9	10
450.0	450.0	450.0	450.0	450.0	450.0	450.0	450.0	450.0	450.0
450.0	450.0	450.0	450.0	450.0	450.0	450.0	450.0	450.0	450.0
450.0	450.0	450.0	450.0	450.0	450.0	450.0	450.0	450.0	450.0
450.0	450.0	450.0	450.0	450.0	450.0	450.0	450.0	450.0	450.0
450.0	450.0	450.0	450.0	450.0	450.0	450.0	450.0	450.0	450.0
450.0	450.0	450.0	450.0	450.0	450.0	450.0	450.0	450.0	450.0
450.0	450.0	450.0	450.0	450.0	450.0	450.0	450.0	450.0	450.0
450.0	450.0	450.0	450.0	450.0	450.0	450.0	450.0	450.0	450.0
450.0	450.0	450.0	450.0	450.0	450.0	450.0	450.0	450.0	450.0
450.0	450.0	450.0	450.0	450.0	450.0	450.0	450.0	450.0	450.0

TABLE 4.5.1 CASE B. Thermal results sample  
for time = 10 minutes. (continued)

TABLE 4.5.1 (continued)

I= 4									
1	2	3	4	5	6	7	8	9	10
387.3	387.3	388.3	389.2	390.0	390.7	391.4	392.0	392.5	393.
393.5	393.9	394.3	394.7	395.0	395.3	395.5	395.8	396.0	396.2
395.4	396.6	396.7	396.8	397.0	397.1	397.2	397.3	397.4	397.4
397.5	397.6	397.4	397.7	397.7	397.8	397.8	397.8	397.9	397.9
397.9	397.9	398.0	398.0	398.0	398.0	398.0	398.0	398.0	398.0
397.9	397.9	397.9	397.9	397.8	397.8	397.8	397.8	397.8	397.8
397.8	397.8	397.8	397.8	397.8	397.7	397.7	397.7	397.7	397.7
397.7	397.7	397.7	397.7	397.7	397.7	397.7	397.7	397.7	397.7
397.7	397.7	397.7	397.7	397.7	397.7	397.7	397.7	397.7	397.7
397.7	397.7	397.7	397.7	397.7	397.7	397.7	397.7	397.7	398.0
I= 3									
1	2	3	4	5	6	7	8	9	10
407.7	407.7	408.4	409.0	409.5	410.0	410.5	410.9	411.3	411.6
412.0	412.2	412.5	412.7	413.0	413.2	413.3	413.5	413.7	413.8
413.9	414.0	414.1	414.2	414.3	414.4	414.5	414.5	414.6	414.6
414.7	414.7	414.7	414.8	414.8	414.8	414.9	414.9	414.9	414.9
414.9	415.0	415.0	415.0	415.0	415.0	415.0	415.0	415.0	415.0
414.9	414.9	414.9	414.9	414.9	414.9	414.9	414.9	414.9	414.9
414.9	414.9	414.8	414.8	414.8	414.8	414.8	414.8	414.8	414.8
414.8	414.8	414.8	414.8	414.8	414.8	414.8	414.8	414.8	414.8
414.8	414.8	414.8	414.8	414.8	414.8	414.8	414.8	414.8	414.8
414.8	414.8	414.8	414.8	414.8	414.8	414.8	414.8	414.8	414.8

TABLE 4.5.1

I=70									
1	2	3	4	5	6	7	8	9	10
60.0	60.4	60.4	60.5	60.5	60.6	60.7	60.7	60.8	60.8
60.9	60.9	61.0	61.1	61.1	61.2	61.2	61.3	61.3	61.4
61.5	61.5	61.6	61.6	61.7	61.7	61.7	61.8	61.8	61.9
61.9	61.9	62.0	62.0	62.0	62.9	63.6	64.4	65.3	65.3
I=69									
1	2	3	4	5	6	7	8	9	10
60.4	60.4	60.5	60.6	60.6	60.7	60.7	60.8	60.9	60.9
61.0	61.0	61.1	61.2	61.2	61.3	61.4	61.4	61.5	61.5
61.6	61.6	61.7	61.7	61.8	61.8	61.9	61.9	62.0	62.0
62.0	62.1	62.1	62.1	62.9	63.5	64.2	65.0	65.9	65.9
I=68									
1	2	3	4	5	6	7	8	9	10
60.5	60.5	60.5	60.6	60.6	60.7	60.8	60.8	60.9	60.9
61.0	61.1	61.1	61.2	61.3	61.3	61.4	61.4	61.5	61.5
61.6	61.7	61.7	61.8	61.8	61.9	61.9	62.0	62.0	62.1
62.1	62.1	62.2	62.2	62.9	63.5	64.2	65.0	65.9	65.9
I=67									
1	2	3	4	5	6	7	8	9	10
60.5	60.5	60.5	60.6	60.7	60.7	60.8	60.9	60.9	61.0
61.1	61.1	61.2	61.3	61.3	61.4	61.4	61.5	61.5	61.6
61.7	61.7	61.8	61.9	61.9	62.0	62.0	62.1	62.1	62.1
62.2	62.2	62.2	62.3	63.0	63.6	64.3	65.1	66.0	67.0





TABLE 4.6.1

I=35									
1	2	3	4	5	6	7	8	9	10
99.8	105.7	111.7	117.6	123.5	129.2	134.9	140.5	146.1	151.5
110.0	116.0	122.0	128.0	134.0	140.0	146.0	152.0	158.0	164.0
122.4	128.3	134.2	140.1	146.0	151.9	157.8	163.7	169.6	175.5
I=34									
1	2	3	4	5	6	7	8	9	10
97.6	103.4	109.2	115.0	120.8	126.6	132.4	138.2	144.0	149.8
107.8	113.6	119.4	125.2	131.0	136.8	142.6	148.4	154.2	160.0
120.0	125.8	131.6	137.4	143.2	149.0	154.8	160.6	166.4	172.2
I=33									
1	2	3	4	5	6	7	8	9	10
95.4	101.1	106.8	112.5	118.2	123.9	129.6	135.3	141.0	146.7
105.6	111.3	117.0	122.7	128.4	134.1	139.8	145.5	151.2	156.9
117.8	123.5	129.2	134.9	140.6	146.3	152.0	157.7	163.4	169.1
I=32									
1	2	3	4	5	6	7	8	9	10
93.2	98.9	104.6	110.3	116.0	121.7	127.4	133.1	138.8	144.5
103.4	109.1	114.8	120.5	126.2	131.9	137.6	143.3	149.0	154.7
115.6	121.3	127.0	132.7	138.4	144.1	149.8	155.5	161.2	166.9
I=31									
1	2	3	4	5	6	7	8	9	10
91.0	96.7	102.4	108.1	113.8	119.5	125.2	130.9	136.6	142.3
101.2	106.9	112.6	118.3	124.0	129.7	135.4	141.1	146.8	152.5
113.4	119.1	124.8	130.5	136.2	141.9	147.6	153.3	159.0	164.7



CASE A. OUTSIDE BOUNDARY

NODE	1 graph			1 graph	
	$\sigma_L$	$\sigma_R^*$	$\sigma_Z$	$\sigma_{maxp}$	$T_{max(12)}$
1		-963	-853		
2	-1195	-1185	-945	-4823	3468
3	-7598	-1568	-1661	-7687	4917
4	-11063	-2308	-3369	-11065	5449
5	-16438	-2981	-5828	-17921	8207
6	-18785	-3742	-6243	-17608	8528
7	-21371	-4211	-6850	-21602	10184
8	-18505	-3451	-7851	-23665	10579
9	-18274	-2708	-7753	-22560	10147
10	-15995	-1912	-6786	-20778	9902
11	-9137	-1583	-5612	-18765	8933
12	-8945	-1350	-4425	-14728	7957
13	-7142	-1002	-3779	-11605	6593
14	-6342	-953	-2691	-10471	5985
15	-4921	-810	-1920	-7813	5305
16	-3930	-792	-1668	-6198	3418
17	-2638	-543	-1119	-4725	2859
18	237	268	100	2646	2478
19	4782	1193	2029	7007	3624
20	6842	1542	3012	8067	4931
21	8239	1601	3496	10855	5029
22	10354	1921	3640	10905	5093
23	11089	1995	3766	11091	5104
24	9912	2005	2886	9515	4814
25	6756	1853	2743	6775	3335
26	6443	1648	2493	6461	2645
27	4369	1410	2158	4969	2421
28	2056	1180	1650	4420	2307
29		956	1594		

\* See note at the bottom of page 94

TABLE 5.2.1

CASE A. OUTSIDE BOUNDARY

NODES	$\tau_{\max(12)}$	$\tau_{\max(23)}$	$\tau_{\max(31)}$
1		2024	587
2	3468	2688	780
3	4917	3811	1108
4	5449	4223	1226
5	8207	6361	1846
6	8528	6610	1918
7	10184	7893	2291
8	10579	8200	2379
9	10147	7865	2282
10	9902	7675	2227
11	8933	6924	2009
12	7957	6167	1780
13	6593	5110	1483
14	5985	4639	1346
15	5305	4112	1193
16	3418	2649	769
17	2859	2216	643
18	2478	1921	557
19	3624	2809	815
20	4931	3822	1109
21	5029	3898	1131
22	5093	3948	1145
23	5104	3956	1148
24	4814	3731	1083
25	3335	2585	750
26	2645	2050	595
27	2421	1876	525
28	2307	1788	519
29		1694	491

TABLE 5.2.1.1

CASE A. INSIDE BOUNDARY

NODE	1 graph			1 graph	
	$\sigma_x$	$\sigma_y^*$	$\sigma_z$	$\sigma_{maxp}$	$\tau_{max(12)}$
206		-155	-120		
200	-772	-278	-315	-1118	592
192	-2632	-293	-865	-3026	1443
186	-4875	-302	-1528	-5157	2610
172	-8099	-361	-2538	-8489	4258
165	-10572	-580	-3085	-10572	5142
157	-10921	-1573	-3748	-10986	5150
156	-10960	-1592	-3480	-10288	5173
129	-10219	-1383	-3103	-9094	4487
128	-9012	-1100	-2803	-5509	4423
127	-5458	-1080	-1583	-3425	2639
126	-3341	-920	-1028	-1579	1712
125	-1490	-810	-1001	-1078	1525
124	-1303	-703	-958	-1022	1403
123	-1120	-702	-940	-982	1321
122	-1002	-650	-857	-916	1201
78	-952	-610	-803	-893	1194
77	-677	-601	-763	-802	1072
76	-603	-582	-745	-710	956
75		-504	-701		

\* See note at the bottom of page 94.

TABLE 5.2.2

CASE B. OUTSIDE BOUNDARY

NODE	1 graph			1 graph	
	$\sigma_L$	$\sigma_R^*$	$\sigma_z$	$\sigma_{max p}$	$\tau_{max(2)}$
133		-376	-297		
132	-1358	-480	-263	-1728	1289
131	-2758	-653	-765	-2763	5605
1	-6574	-833	-890	-4815	6113
2	-8145	-940	-980	-6345	6270
3	-10803	-1007	-1102	-8109	7607
4	-11911	-2185	-3928	-12660	10397
5	-14287	-4230	-4373	-14897	15245
6	-5074	-2355	-2153	-7786	4197
7	-2255	-1100	-956	-4474	2879
8	-1164	-840	-493	-2758	1934
9	229	105	97	-1693	1855
10	866	642	368	1904	1290
11	3846	2613	1506	3865	1354
12	2923	2541	1494	3499	1317
13	2861	2119	1048	3062	1315
14	2480	1823	1003	2974	1307
15	2473	1174	1000	2615	1095
16	2404	1020	904	2613	1009
158	2034	810	848	2509	1008
160	1005	703	777	2498	990
162		641	634		

\* See note at the bottom of page 94.

TABLE 5.2.3

CASE B. INSIDE BOUNDARY

1 graph

NODE	$\sigma_{maxp}$	$\tau_{max(12)}$
149		
147	-1481	1332
124	-2297	1595
123	-3066	1871
122	-3350	2638
121	-7498	3165
102	-10442	4924
101	-9190	4743
96	-5946	3077
95	-4489	1558
94	-3718	1369
87	-3648	1358
88	-3154	1274
89	-2016	1203
90	-1739	1091
91	-1714	1047
92	-1688	970
93	-1631	957
159	-1232	792
161	-1061	772
163		

TABLE 5.2.4

CASE C. OUTSIDE BOUNDARY

NODE	time=4 minutes			time=8 minutes			time=11 minutes		
	$\sigma_L$	$\sigma_R^*$	$\sigma_Z$	$\sigma_L$	$\sigma_R^*$	$\sigma_Z$	$\sigma_L$	$\sigma_R^*$	$\sigma_Z$
1		-32	-137		-74	-319		-102	-438
4	-520	-38	-157	-1209	-87	-365	-1663	-120	-502
7	-1274	-118	-266	-2959	-274	-619	-4069	-377	-851
10	-1573	-150	-299	-3654	-349	-1060	-5024	-480	-1458
13	-2166	-217	-519	-5031	-505	-1426	-6918	-694	-1961
16	-2226	-256	-675	-5171	-594	-1569	-7110	-817	-2157
19	-2370	-277	-776	-5506	-644	-1803	-7571	-886	-2479
21	-2581	-347	-810	-5996	-806	-1881	-8245	-1108	-2587
22	-194	-72	-87	-452	-168	-201	-622	-231	-277
25	423	136	134	983	316	311	1351	435	427
28	705	157	259	1638	365	601	2252	502	826
31	831	175	302	1930	406	700	2654	558	963
34	1009	176	356	2345	409	826	3225	562	1136
37	1145	197	405	2660	457	940	3658	628	1292
40	1246	198	433	2895	459	1006	3980	631	1383
43	1434	204	489	3330	473	1136	4579	651	1562
46	1152	87	359	2676	203	833	3680	279	1146
49	1098	84	343	2551	194	798	3508	267	1097
52	1006	59	283	2336	138	657	3212	190	904
55	906	58	256	2104	136	594	2893	187	817
58	858	57	253	1993	132	588	2740	182	808
61	784	44	179	1820	101	415	2503	139	571
64	611	41	166	1419	95	385	1951	131	529
67	591	39	151	1372	91	351	1886	125	482
70	512	35	128	1190	81	298	1636	111	410
73	421	31	100	977	73	232	1344	100	319
76	255	23	63	591	54	147	813	74	202
77		20	61		47	141		65	194

\* See note at the bottom of page 94.

TABLE 5.3.1

## CASE C. OUTSIDE BOUNDARY

NODE	time=4 minutes		time=8 minutes		time=11 minutes	
	$\sigma_{\max P}$	$\tau_{\max(12)}$	$\sigma_{\max P}$	$\tau_{\max(12)}$	$\sigma_{\max P}$	$\tau_{\max(12)}$
1						
4	-573	590	-1330	1370	-1829	1884
7	-1280	1423	-2972	3305	-4087	4545
10	-1576	1563	-3660	3631	-5033	4992
13	-2167	2011	-5033	4670	-6921	6421
16	-2246	2083	-5217	4838	-7174	6652
19	-2375	2162	-5516	5020	-7584	6903
21	-2582	2465	-5998	5725	-8247	7872
22	-550	809	-1276	1880	-1755	2585
25	433	420	1006	976	1383	1342
28	715	568	1661	1319	2284	1813
31	834	663	1938	1540	2665	2118
34	1012	838	2350	1945	3231	2675
37	1147	944	2663	2193	3662	3016
40	1253	1062	2910	2466	4001	3391
43	1435	1240	3333	2879	4583	3959
46	1159	1123	2692	2607	3702	3585
49	1099	1102	2553	2560	3511	3520
52	1009	1054	2343	2448	3221	3366
55	858	1053	1993	2447	2741	3365
58	849	962	1972	2234	2712	3072
61	795	746	1846	1732	2538	2382
64	615	677	1428	1573	1964	2163
67	601	580	1396	1347	1919	1852
70	513	557	1192	1294	1639	1779
73	445	196	1034	455	1422	625
76	160	79	372	183	512	251
77						

TABLE 5.3.2

GAUGE NO

MVOLTS READINGS

DIRECT STRAINS

DIRECT STRESSES

GAUGE NO	MVOLTS READINGS	DIRECT STRAINS	DIRECT STRESSES
1	.01	.5	177.6
2	.00	.2	85.7
3	.00	.2	84.1
4	.00	.7	224.6
5	.00	.4	142.9
6	.00	.3	112.1
7	.00	.1	308.4
8	.00	.7	219.0
9	.00	.3	102.8
10	.00	.1	317.0
11	.00	.6	200.0
12	.00	.5	156.9
13	.00	.1	336.4
14	.00	.5	171.4
15	.00	.5	177.6
16	.00	.1	304.5
17	.00	.8	259.1
18	.00	.4	140.2
19	.00	.9	285.7
20	.00	.5	171.4
21	.00	.4	130.8
22	.00	.3	102.8
23	.00	.2	85.7
24	.00	.1	56.1
25	.00	.1	56.1
26	.00	.2	67.2
27	.00	.9	235.7
28	.00	.9	261.7
29	.00	.1	50.4
30	.00	.1	276.2
31	.00	.7	215.0
32	.00	.1	181.4
33	.00	.4	121.5
34	.00	.1	165.4
35	.00	.2	176.2
36	.00	.3	112.1
37	.00	.9	209.2
38	.00	.2	69.1
39	.00	.7	227.6
40	.00	.1	52.4
41	.00	.1	140.2
42	.00	.1	260.0
43	.00	.1	32.7
44	.00	.1	27.1
45	.00	.1	32.7

TABLE 6.4.1(a)



ROSETTE NO	PRINCIPAL STRAINS		PRINCIPAL STRESSES		DIRECTION ANGLE
1	.6975E-05	-.2521E-06	293.4	80.5	22.60
2	.1128E-04	-.634E-07	371.2	109.5	12.17
3	.1372E-04	-.1463E-07	452.2	135.2	-3.72
4	.1599E-04	-.162E-06	526.1	154.8	12.88
5	.176E-04	-.4625E-06	575.5	156.3	23.57
6	.1882E-04	-.152E-06	554.6	166.3	-1.23
7	.1414E-04	-.118E-06	464.5	165.9	15.03
8	.5304E-05	-.8248E-06	174.6	52.2	-7.52
9	.5518E-05	-.1421E-04	-124.0	-463.5	-4.86
10	.3196E-05	-.2431E-04	-229.9	-798.5	15.00
11	.8908E-07	-.1442E-04	-139.7	-474.5	10.00
12	.594E-05	-.2966E-07	-155.8	-57.9	-14.16
13	.5505E-05	-.1457E-04	-125.9	-474.9	5.01
14	.452E-05	-.2569E-04	-239.1	-842.3	-17.62
15	.8034E-07	-.156E-04	-152.2	-515.4	-9.90

TABLE 6.4.1(b)

EXPERIMENTAL RESULTS. STRESSES (lb/in<sup>2</sup>)

Time=12 minutes. Heating-up.			
DIRECT STRESSES			
ROSETTE	GAUGE	CORRECTED	OBSERVED
1	1	1116	2316
	2	584	1211
	3	388	805
2	4	2254	3243
	5	1150	1655
	6	634	912
3	7	3212	4200
	8	2248	2940
	9	811	1061
4	10	3985	4824
	11	2502	3030
	12	1063	1287
5	13	3920	4218
	14	1943	2091
	15	904	973
6	16	4065	4275
	17	2444	2571
	18	993	1045
7	19	4308	4458
	20	2211	2288
	21	1098	1136
8	22	3192	-
	23	2543	-
	24	1451	-
9	25	-9122	-
	26	-4841	-
	27	-3002	-
10	28	-7345	-
	29	-4204	-
	30	-2248	-
11	31	-3231	-
	32	-2985	-
	33	-948	-

TABLE 6.4.2

EXPERIMENTAL RESULTS.

Time = 12 minutes. Heating-up.		
ROSETTE	MAXIMUM PRINCIPAL STRESS $\sigma_{\max}$ (lb/in <sup>2</sup> )	MAXIMUM SHEAR STRESS $\tau_{\max}$ (lb/in <sup>2</sup> )
1	1567	1401
2	2311	2118
3	2419	2641
4	2478	2845
5	2463	3109
6	2853	3281
7	3841	3613
8	4202	5718
9	-8194	7402
10	-7218	6348
11	-3178	3312

TABLE 6.4.3

VESSEL (NODE 12). STRESSES lb/in<sup>2</sup>.

Time(minutes)	Gauge 28	Gauge 30	Rosette 10
	$\sigma_y$	$\sigma_z$	$\sigma_{maxP}$
0	0	0	0
2	-1186	-421	-1093
4	-2243	-763	-2151
6	-3418	-1140	-3502
8	-5006	-1496	-5124
10	-6414	-1794	-6591
12	-7345	-2248	-7218
14	-7096	-2018	-6940
16	-6307	-1991	-6690
18	-4844	-1488	-5923
20	-3652	-1476	-4688
22	1364	497	1257
24	2579	874	2484
26	3931	1379	4062
28	5757	1765	5995
30	8446	2585	8301
32	8160	2341	7981
34	7253	2353	7694
36	5571	1771	6811
38	4200	1727	5391
40	3110	1452	4711
42	1448	808	3642
44	608	819	3233

TABLE 6.4.4

NOZZLE (NODE 43). STRESSES lb/in<sup>2</sup>.



Time(minutes)	Gauge 13	Gauge 15	Rosette 5	OBSERVED						
				$\sigma_x$	$\sigma_z$	$\sigma_{maxp}$				
Heating 	0	0	0							
	2	893	264				868			
	4	1754	508				1921			
	6	2614	911				3002	The same		
	8	3721	1483				3855			
	10	4891	1709				5002			
	12	5541	1890				5545			
	14	5426	1814				5294			
	16	4875	1551				4321			
	18	3762	1366				3717			
20	2918	1077	3109							
Cooling 	22	-1027	-304				-998			
	24	-2035	-584				-2209			
	26	-3045	-1048				-3452			
	28	-5674	-1705				-4433	The same		
	30	-6372	-2174				-6377			
	32	-6240	-2086				-6088			
	34	-5606	-1784				-4969			
	36	-4326	-1571				-4275			
	38	-3356	-1239				-3575			
	40	-2169	-763	-2653						
42	-1478	-491	-1627							
44	-724	-304	-1141							

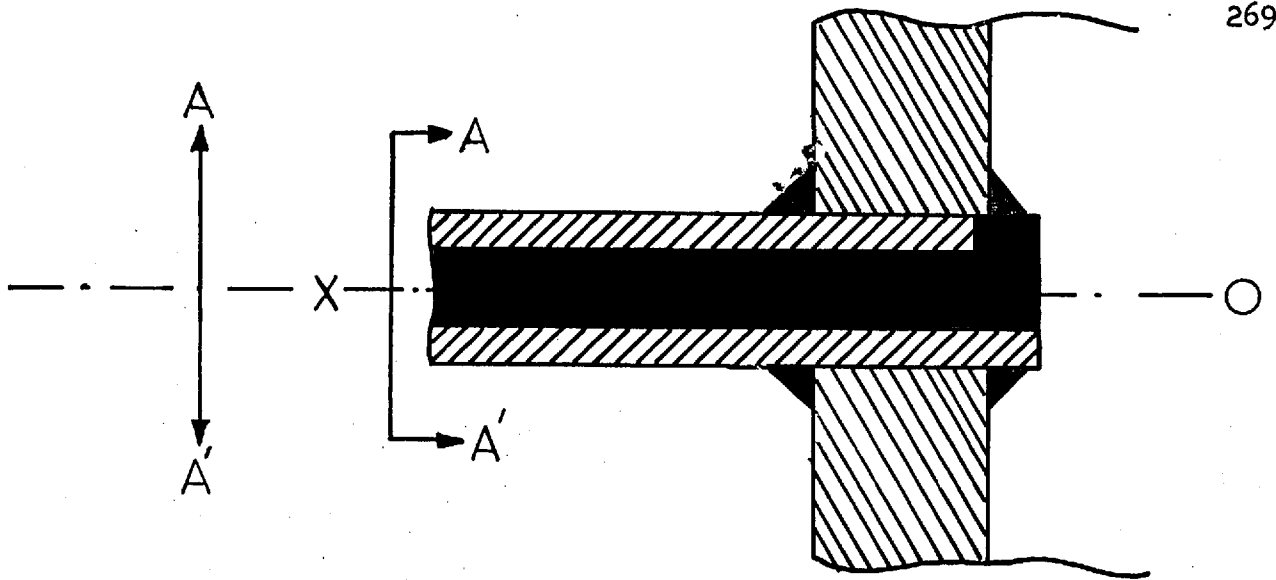
TABLE 6.4.5

r (inches) Distance from the tip of the crack along y	$d_1$ First matrix coefficient	$K = -\sqrt{2\pi}(d_1)$
0.960	-279.8	702.6
0.910	-320.4	803.1
0.885	-332.1	832.5
0.735	-421.6	1056.8
0.660	-462.7	1159.8
0.585	-507.4	1271.9
0.460	-578.9	1451.1
0.360	-637.2	1597.2
0.210	-726.7	1821.6
0.110	-782.4	1961.2
0.085	-801.6	2009.3
0.060	-813.5	2039.1
0.035	-834.2	2091.0
0.010	-839.4	2104.1
(Tip of the crack)	-842.6	2112.3

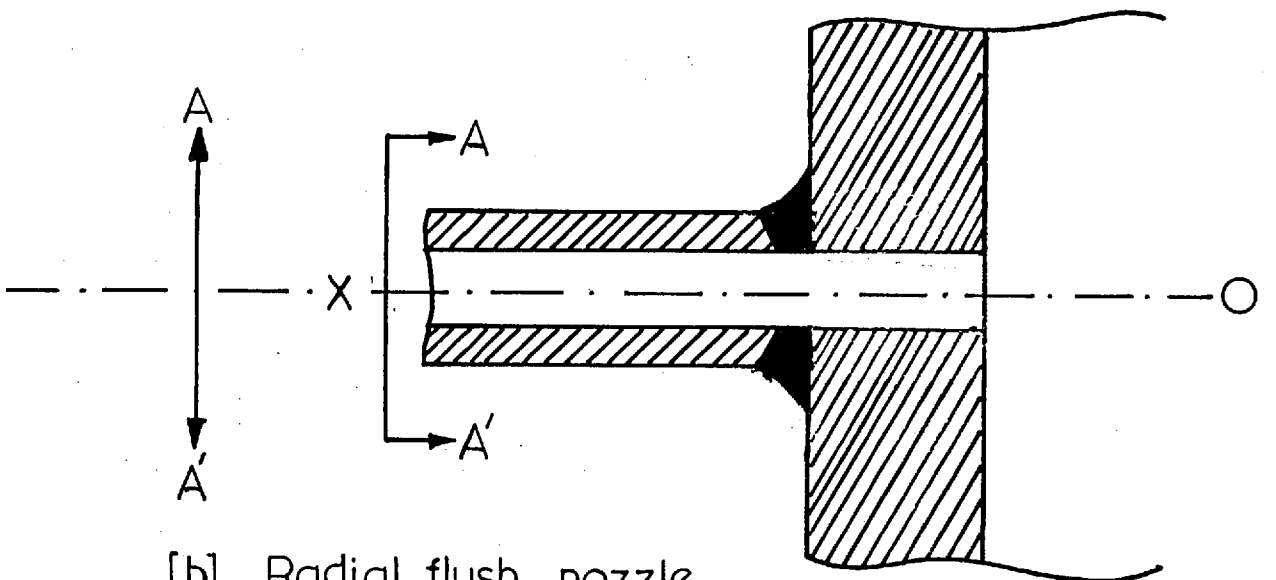
TABLE 7.3.2.1

## FIGURES

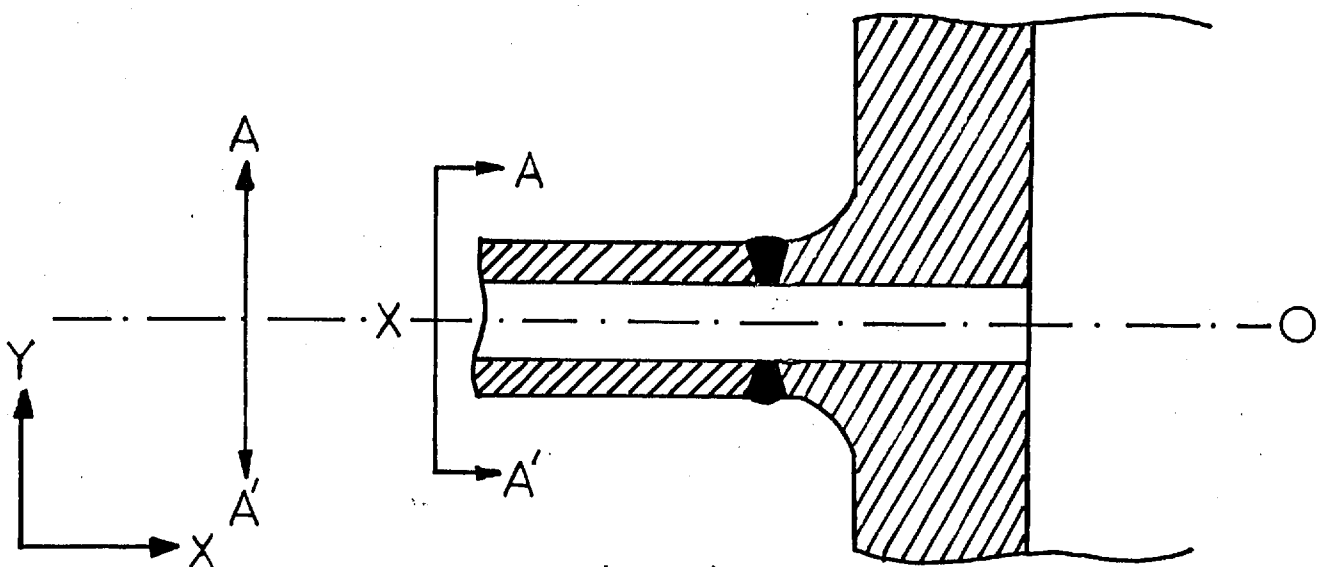
---



[a] Radial protruding nozzle



[b] Radial flush nozzle



[c] Radial nozzle directly welded on the vessel

FIGURE 3.1.1



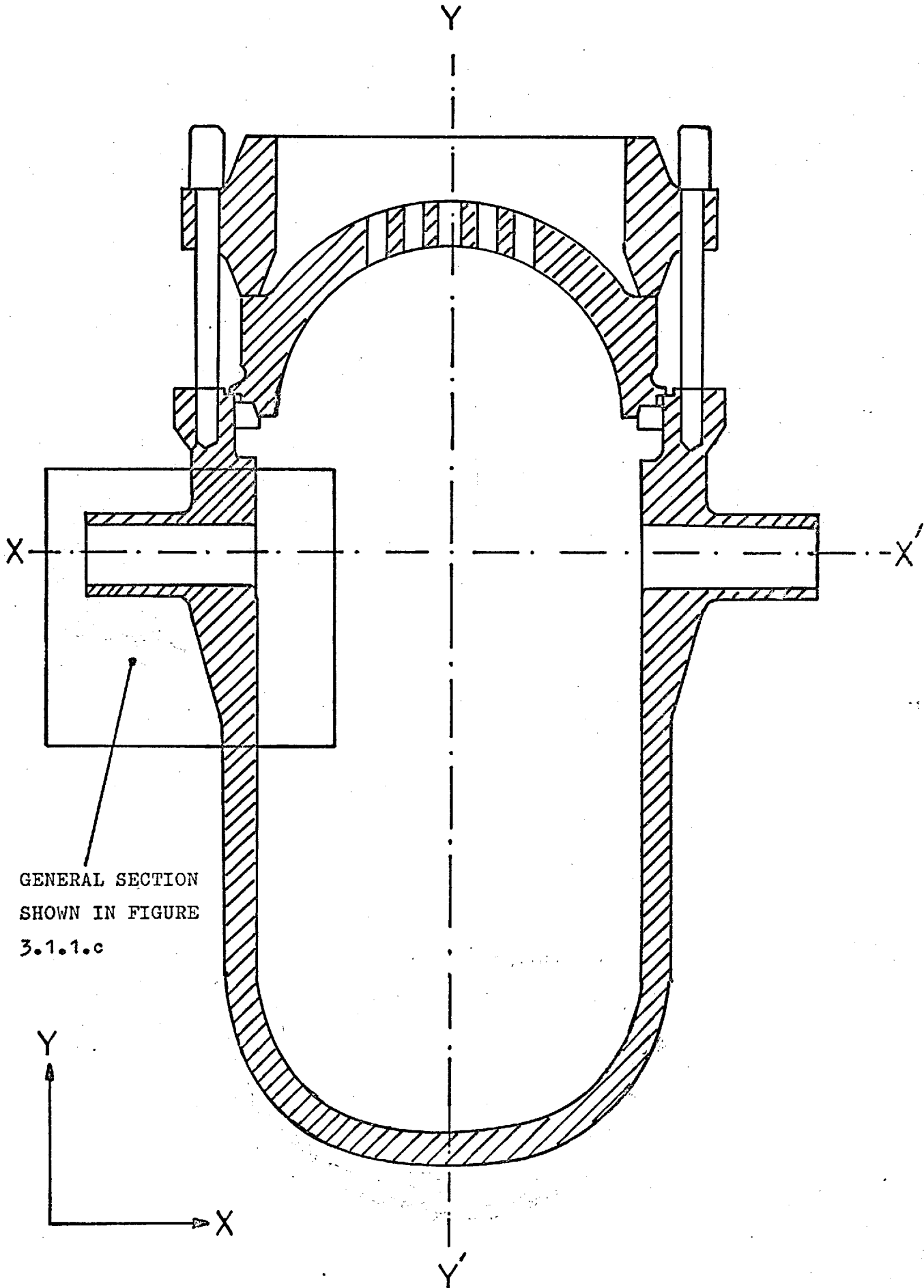
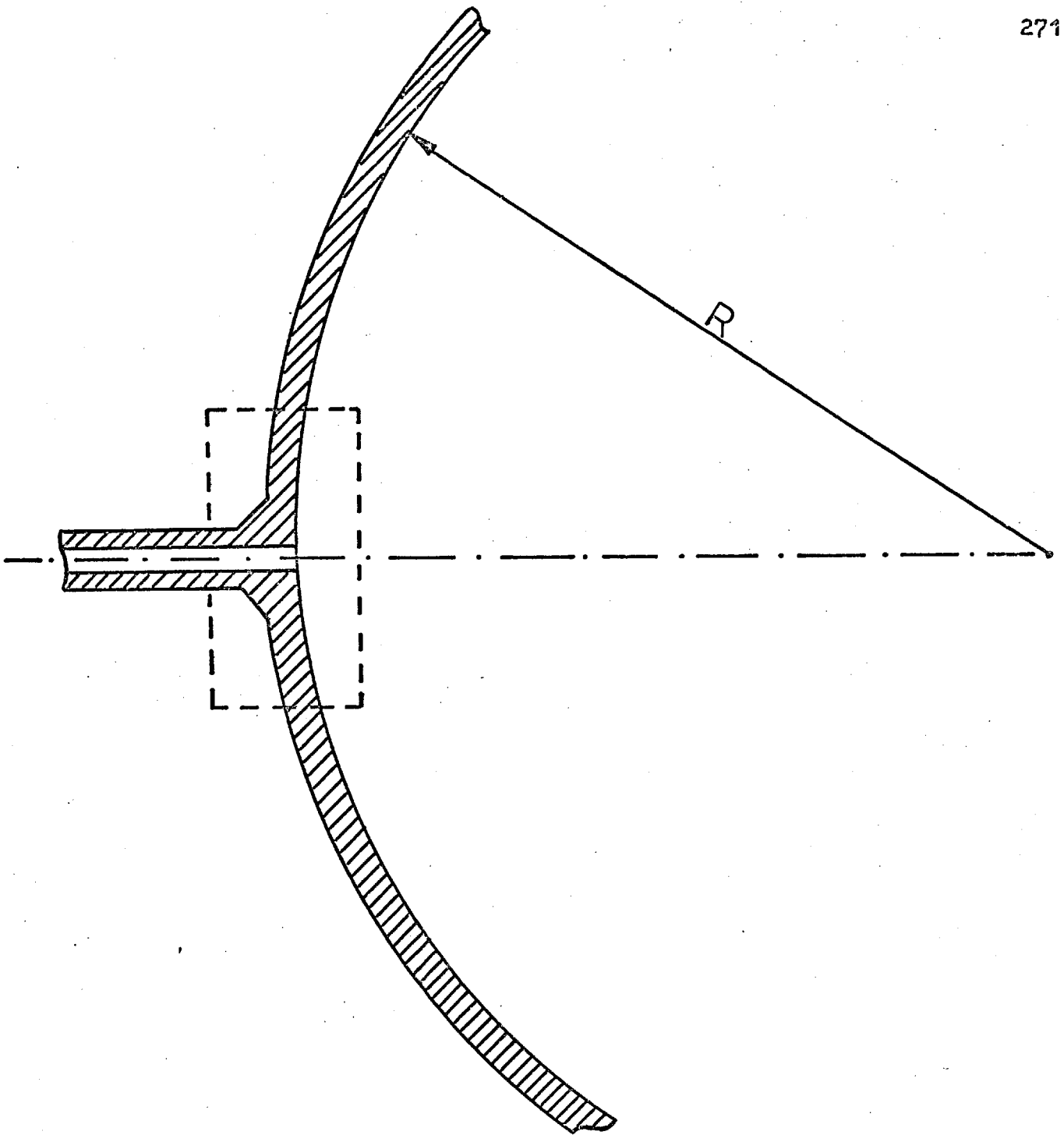


FIGURE 3.1.2 A PRESSURE VESSEL



CURVATURE OF SHELL NEAR THE JUNCTION IS  
SMALL COMPARED TO THAT OF NOZZLE.

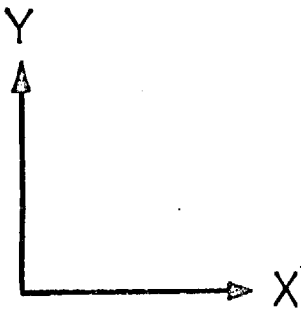


FIGURE 3.1.3

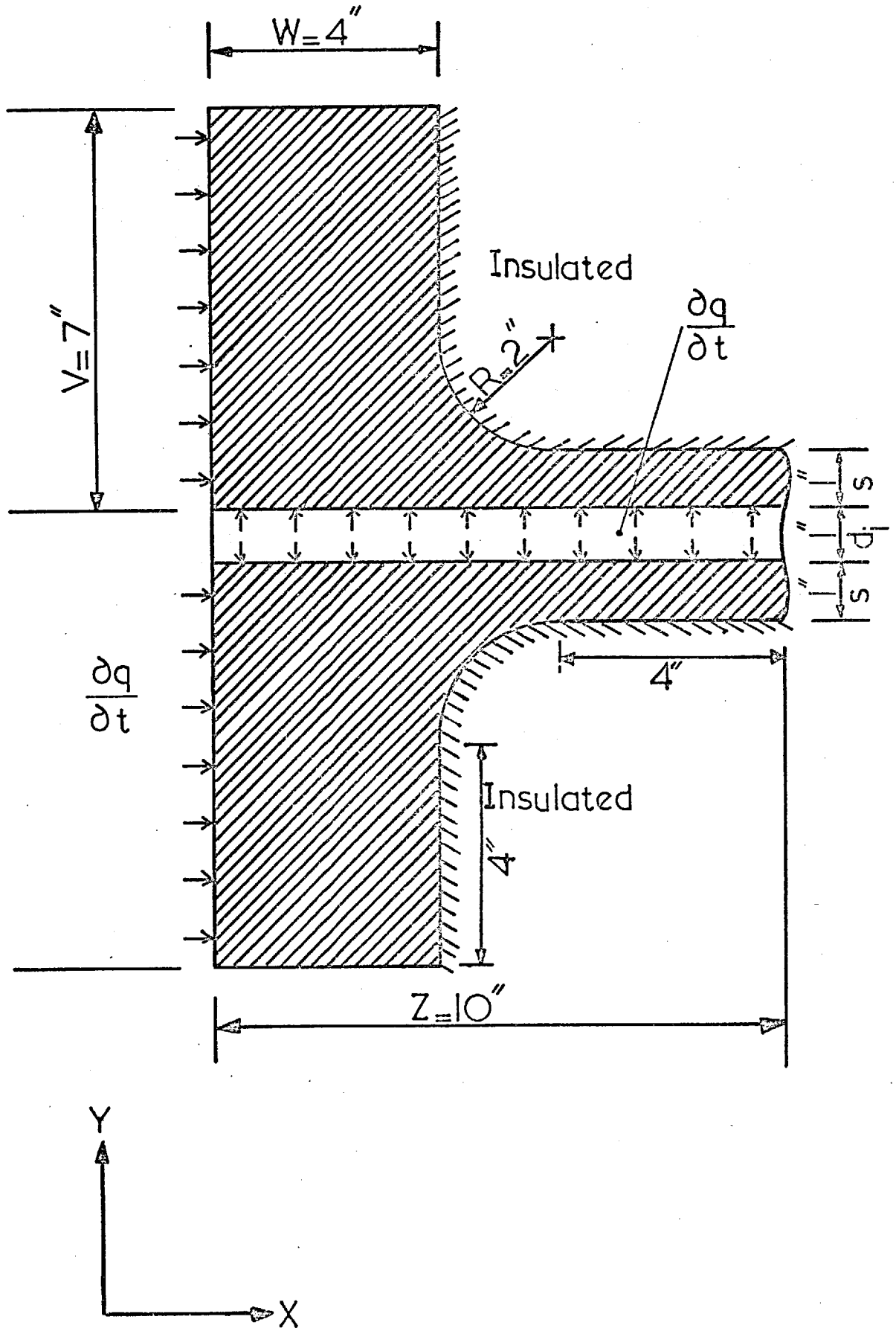


FIGURE 3.2.1 CASE A.

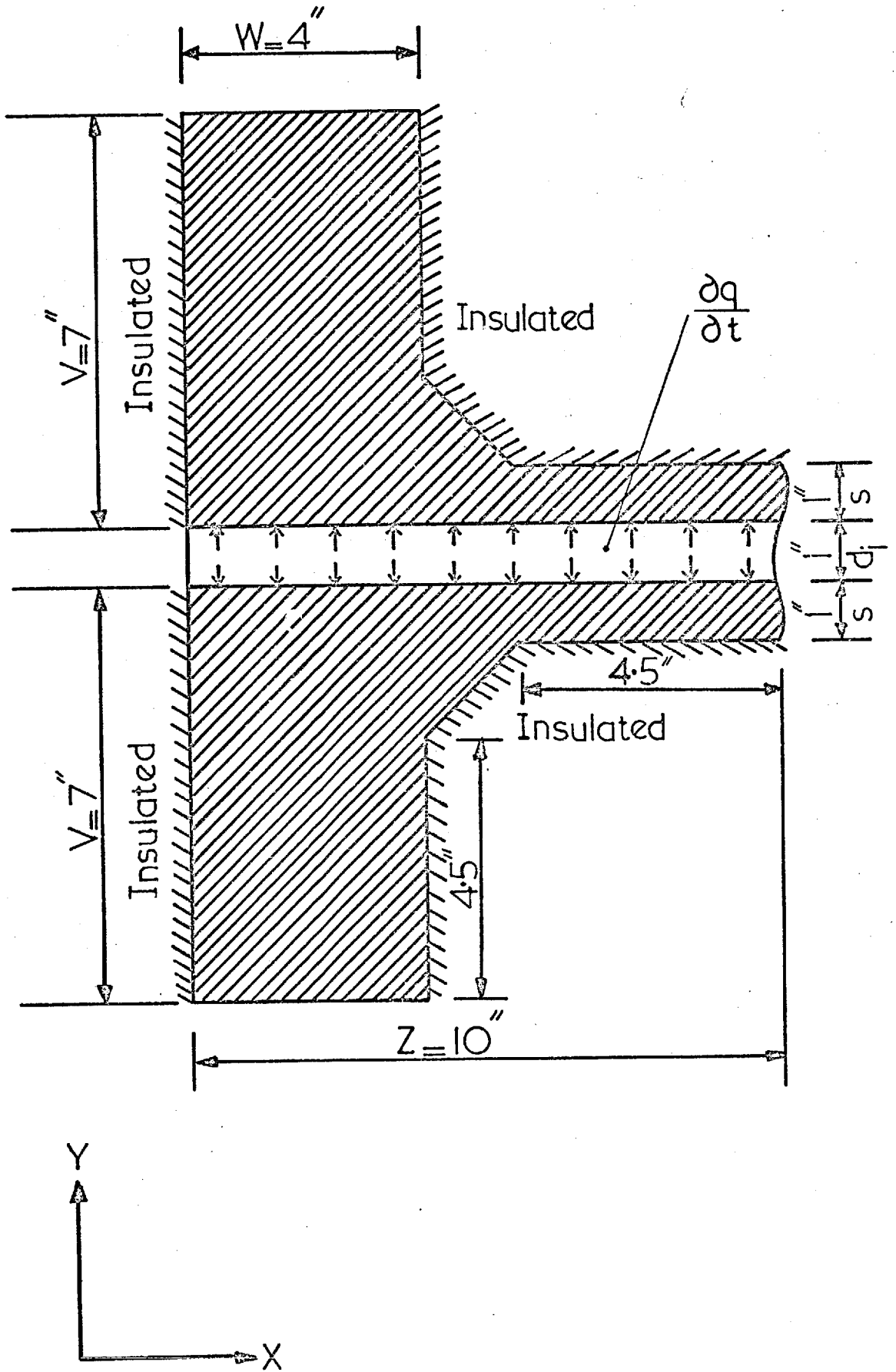


FIGURE 3.2.2. CASE B.

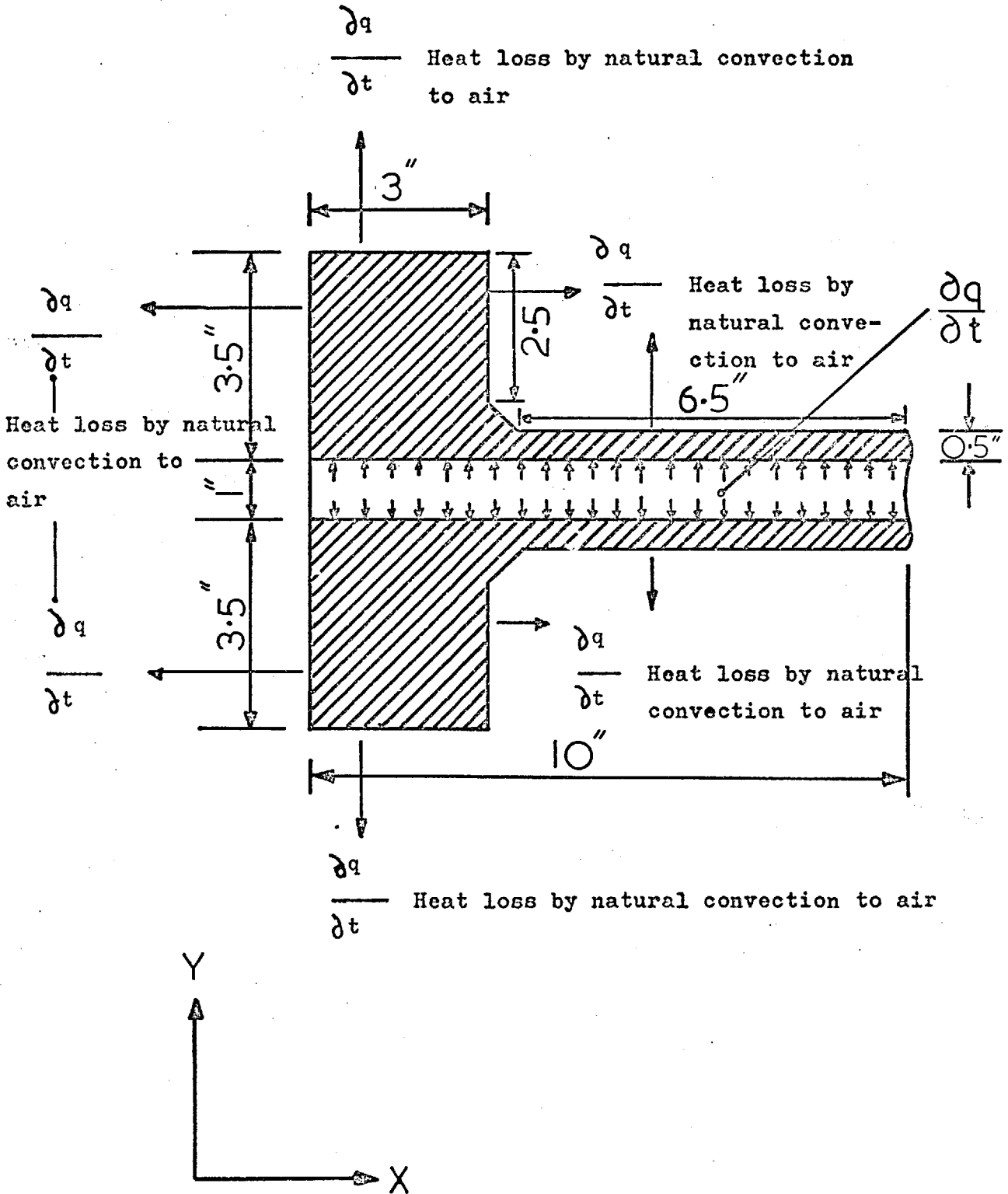
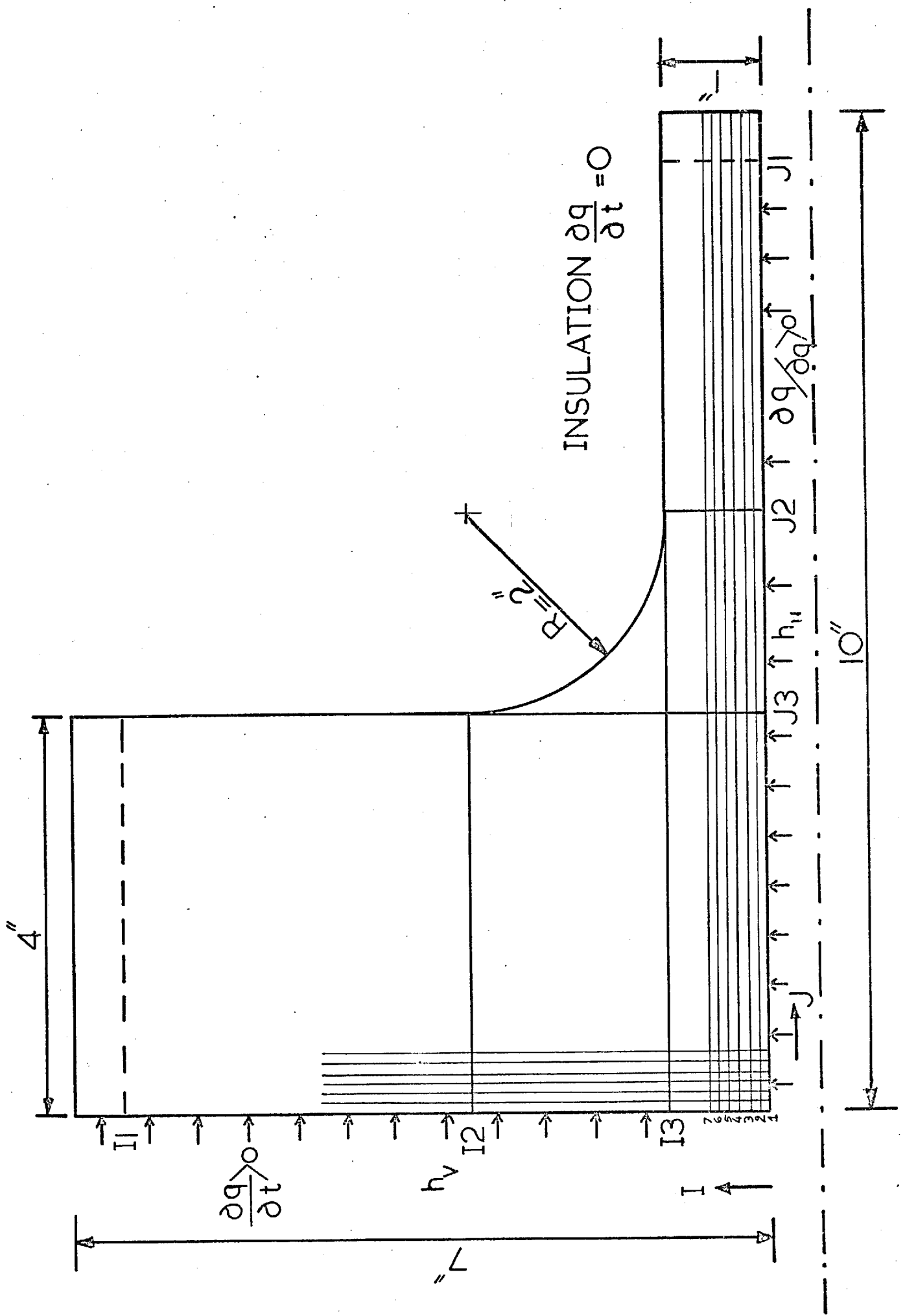


FIGURE 3.2.3

CASE C. (EXPERIMENTAL SPECIMEN)

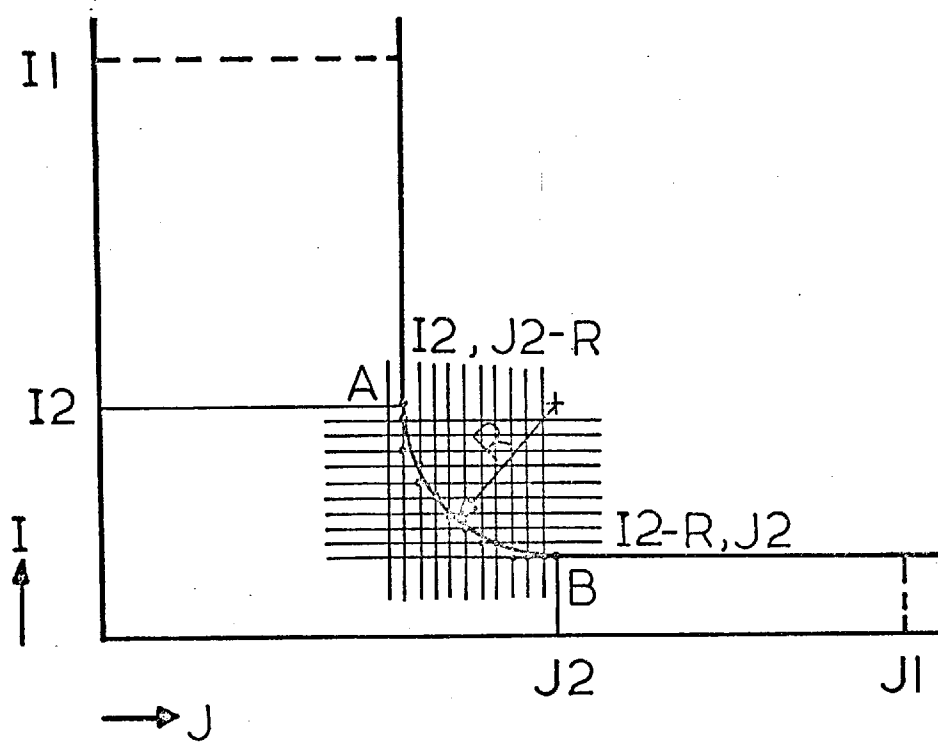


TEMPERATURE GRID FOR CASE A.



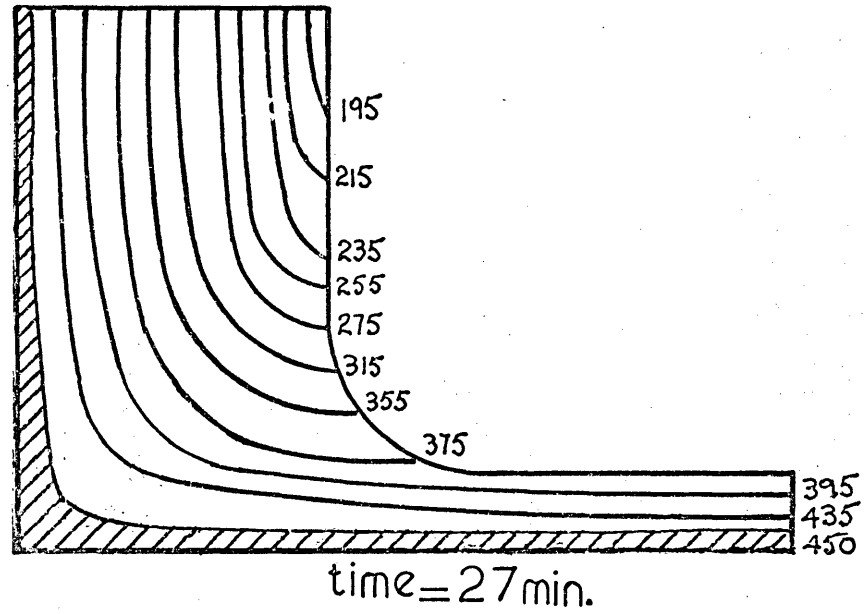
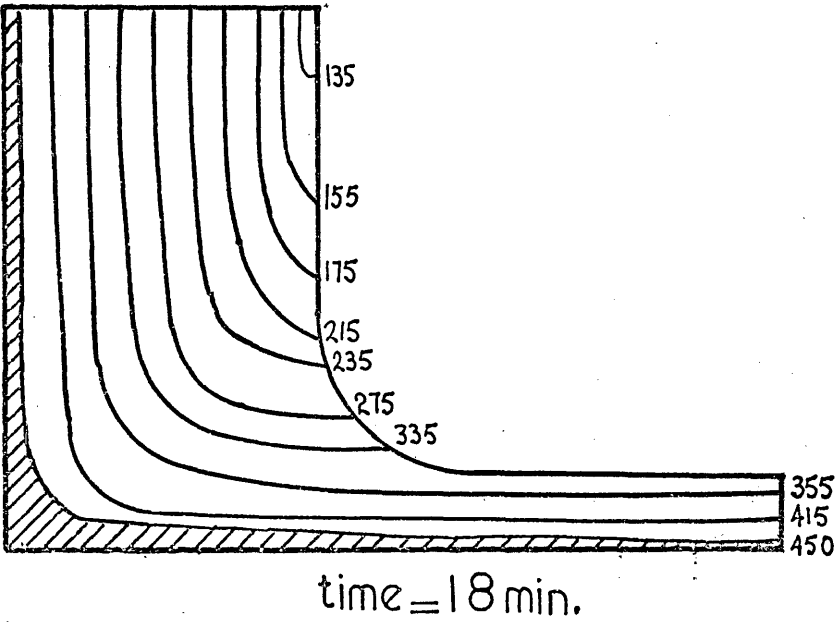
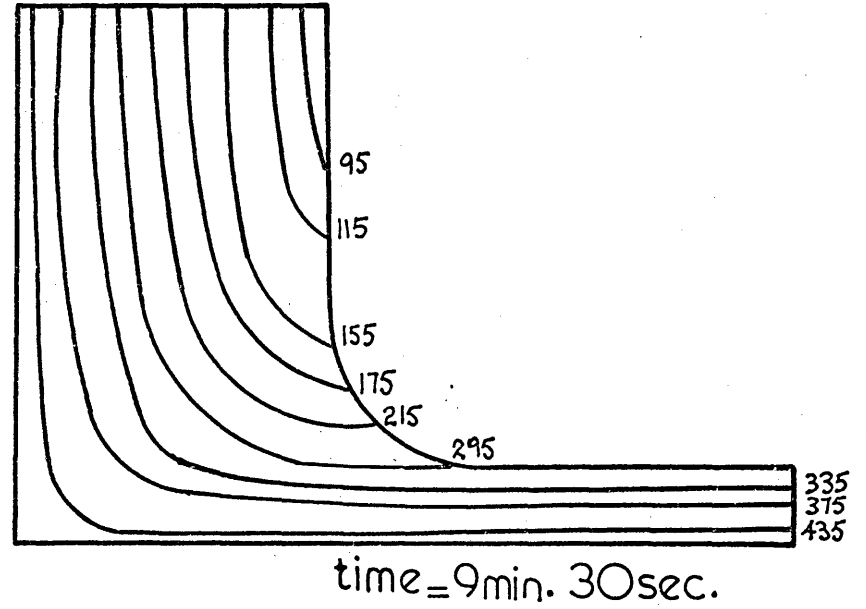
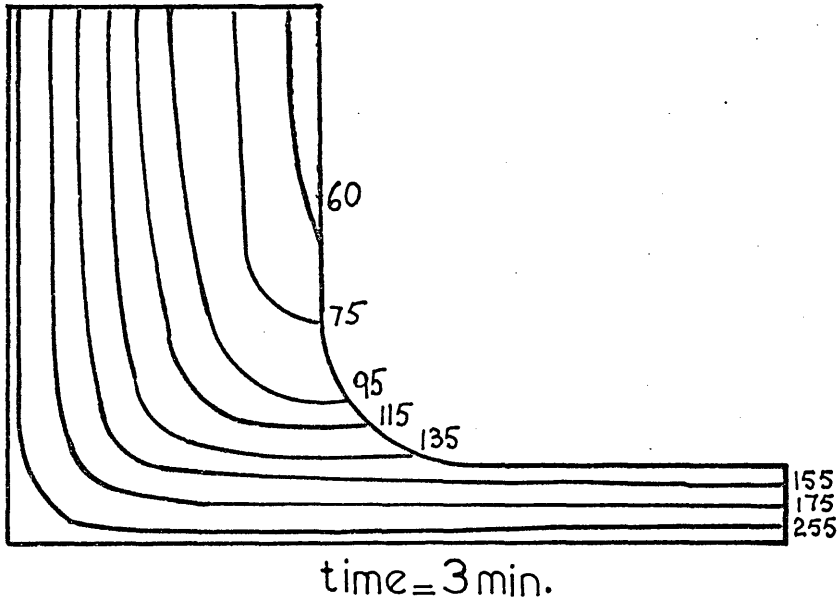






JUNCTION BOUNDARY DETERMINATION

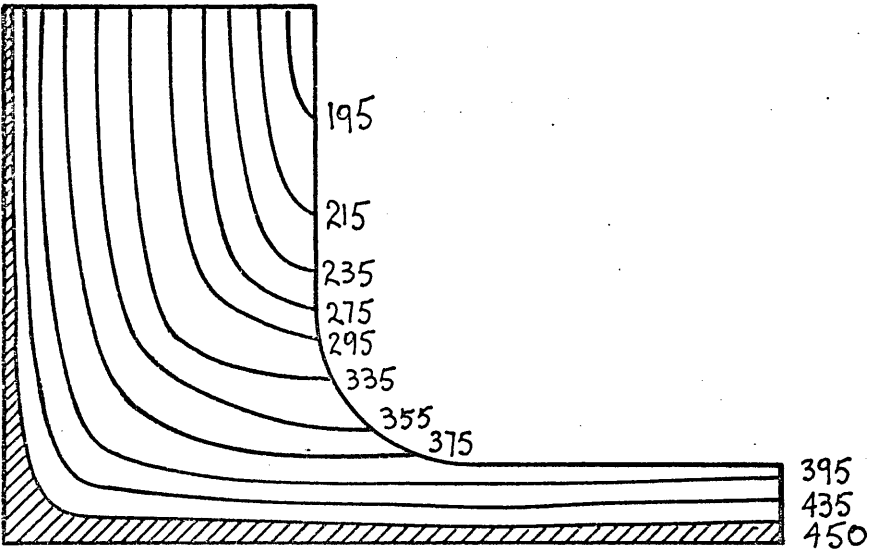
FIGURE 4.4.3



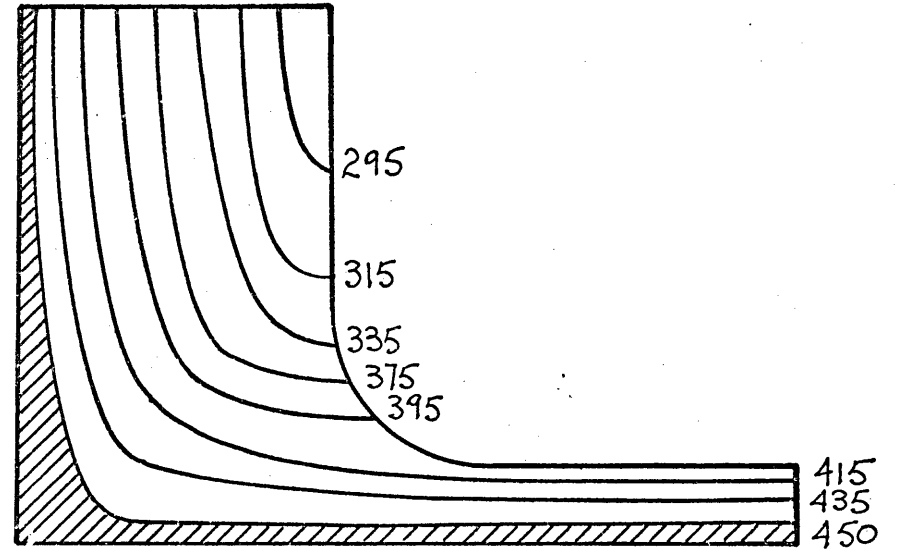
TEMPERATURE PROFILES FOR CASE A. TEMPERATURES IN DEGREES °F

FIGURE 4.4.4 (d)

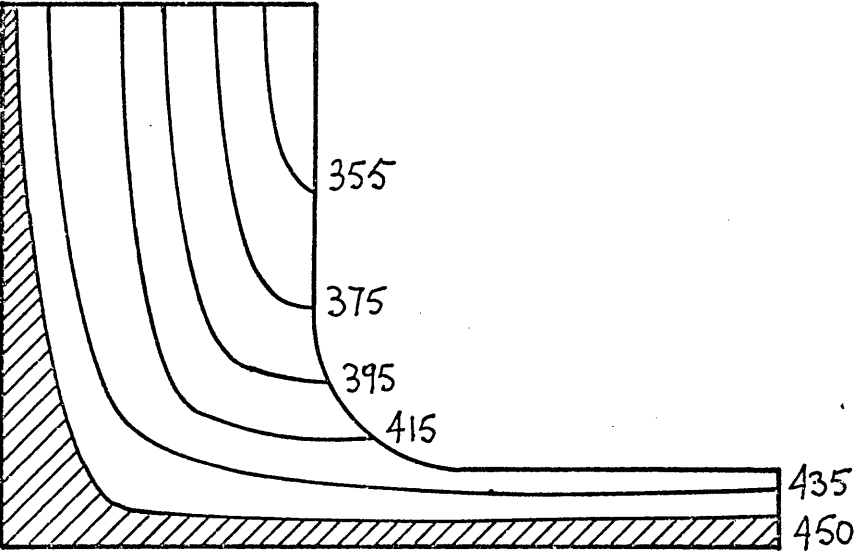
FIGURE 4.4.4(b)



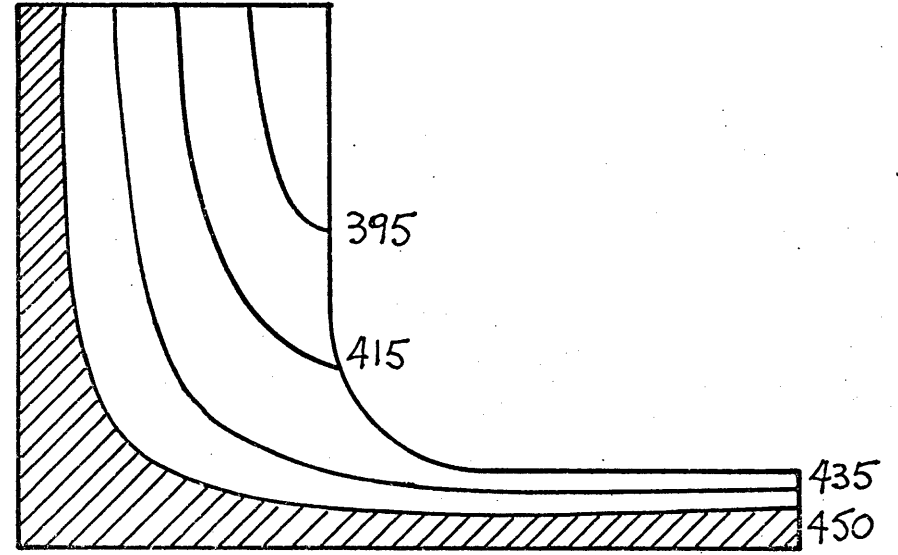
time = 36 min.



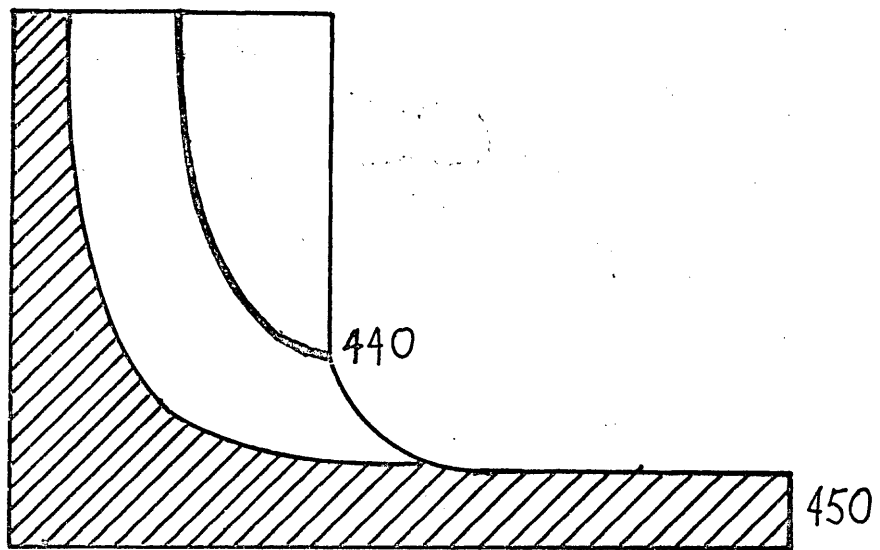
time = 45 min.



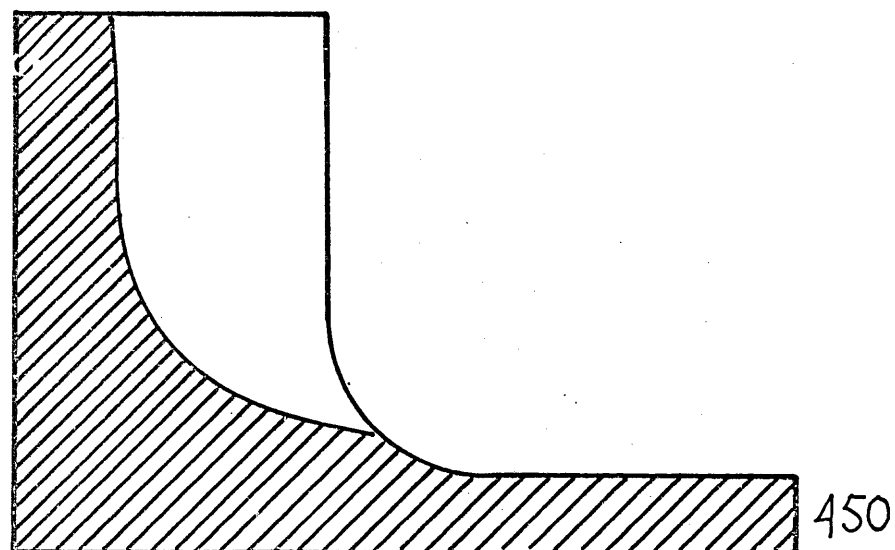
time = 63 min.



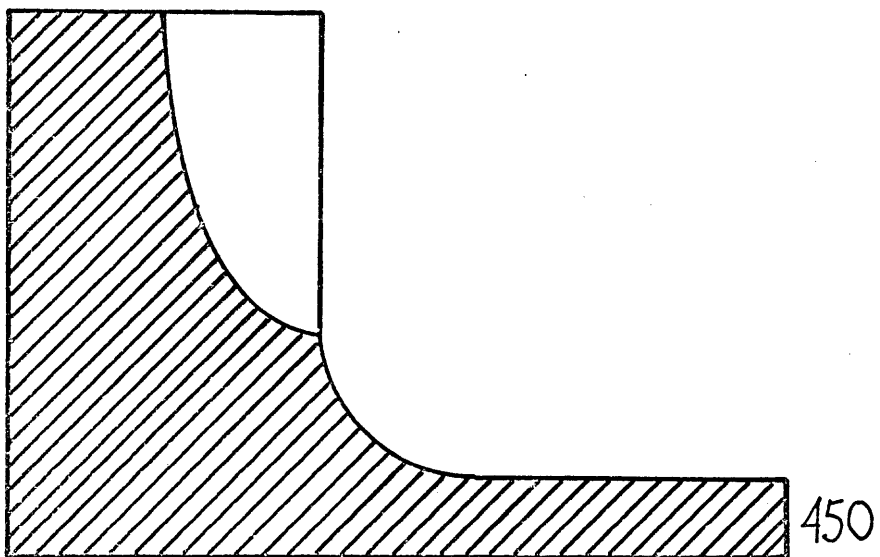
time = 81 min.



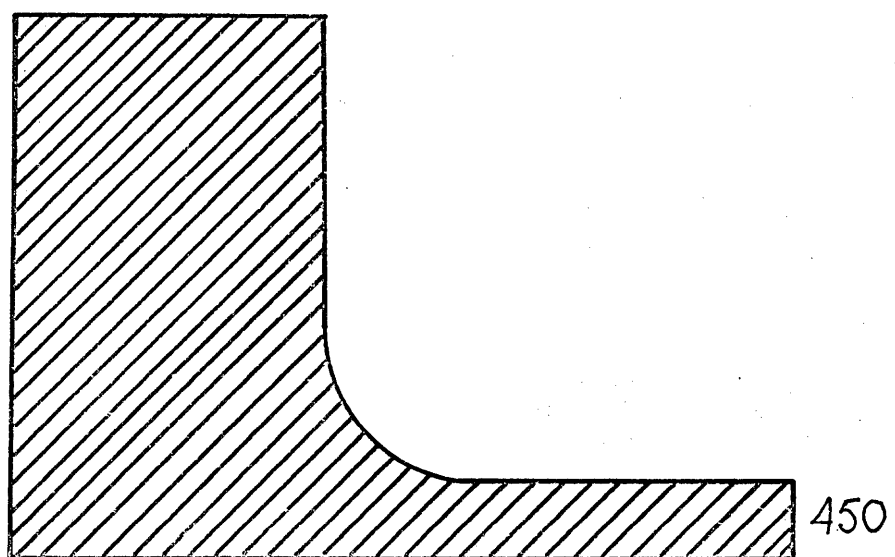
time = 126 min.



time = 144 min.



time = 162 min.



time = 200 min.

FIGURE 4 4 4 c

$$\Delta T_m = T_{\text{mean NOZZLE}} - T_{\text{mean VESSEL}}$$

$T_{\text{mean NOZZLE}}$  is the average of all the nodal temperatures in nozzle.

$T_{\text{mean VESSEL}}$  is the average of all the nodal temperatures in vessel.

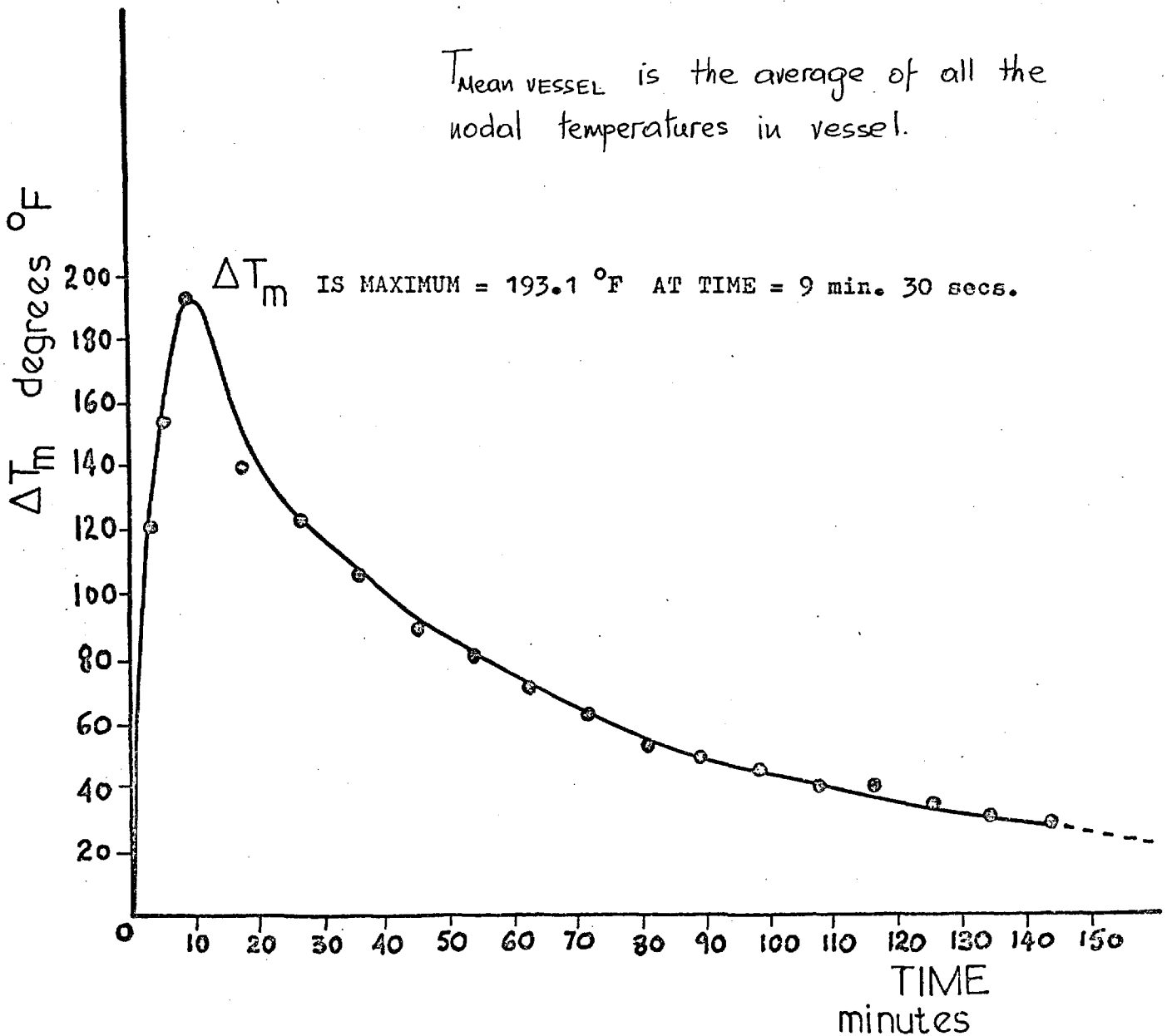
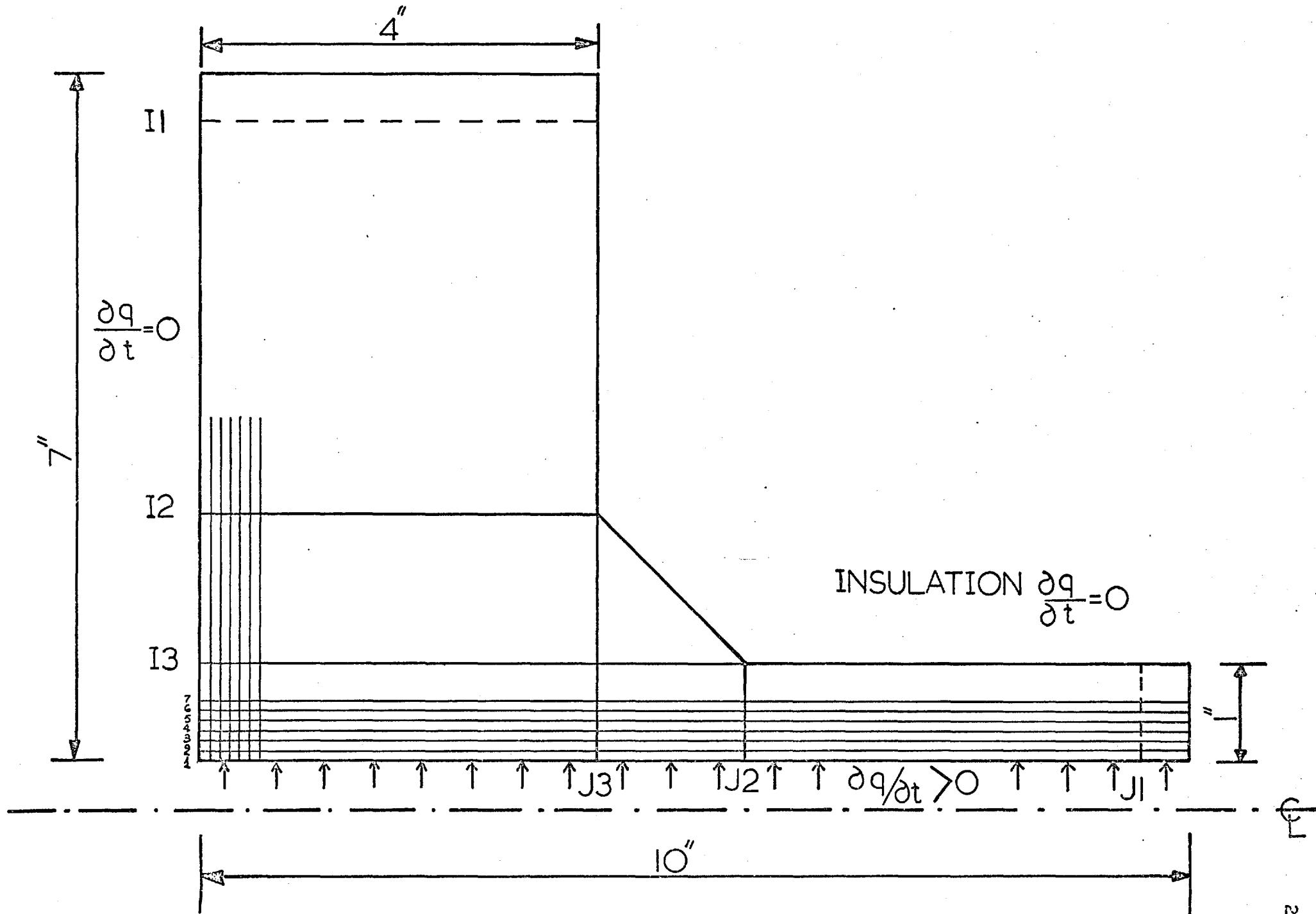


FIGURE 4.4.5. CASE A. MEAN TEMPERATURE VARIATION  $\Delta T_m$  BETWEEN NOZZLE AND VESSEL.

FIGURE 4.5.1 TEMPERATURE GRID FOR CASE B.



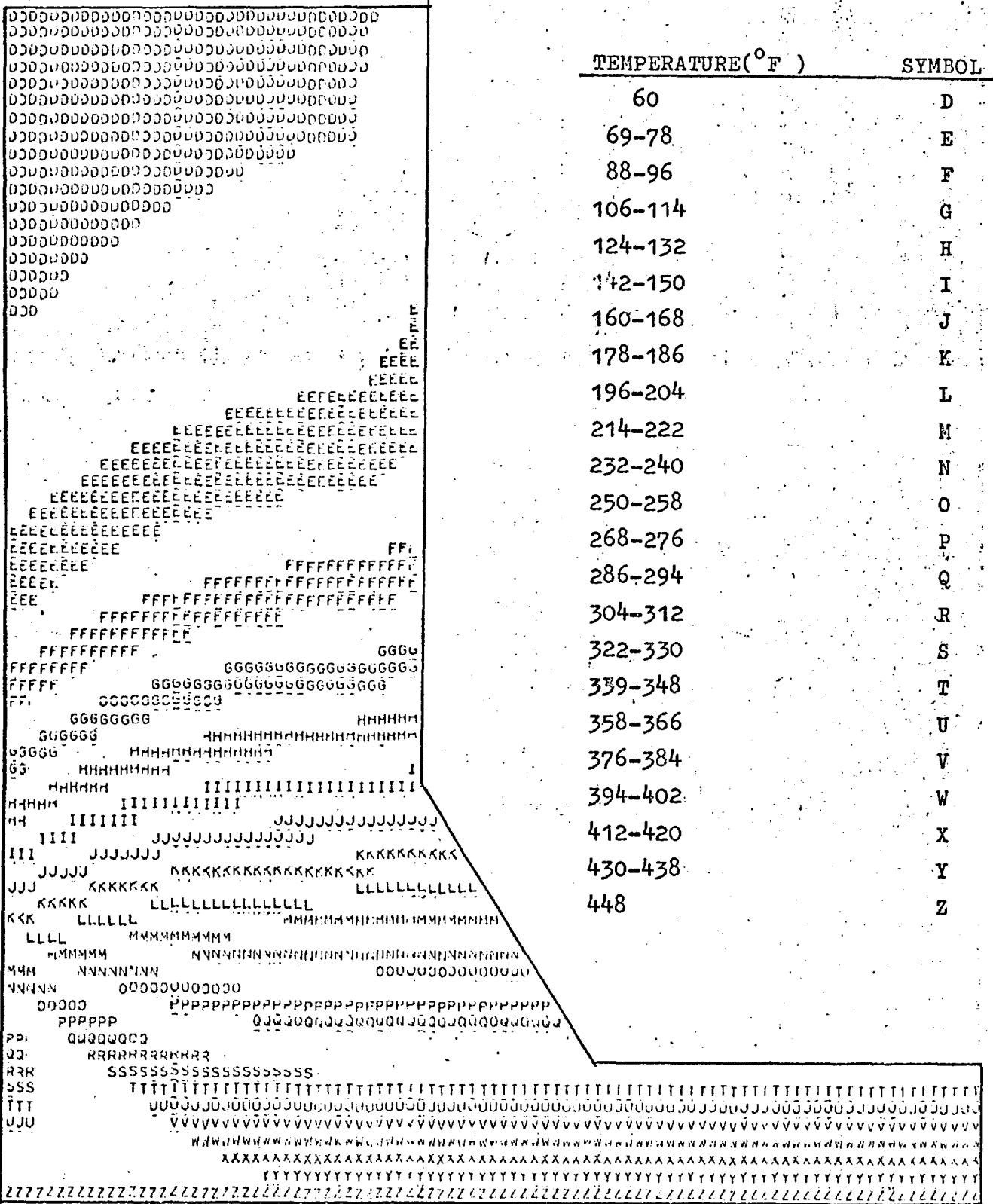


FIGURE 4.5.2(a).

CASE B. TEMPERATURE PROFILES FOR TIME = 10 minutes.

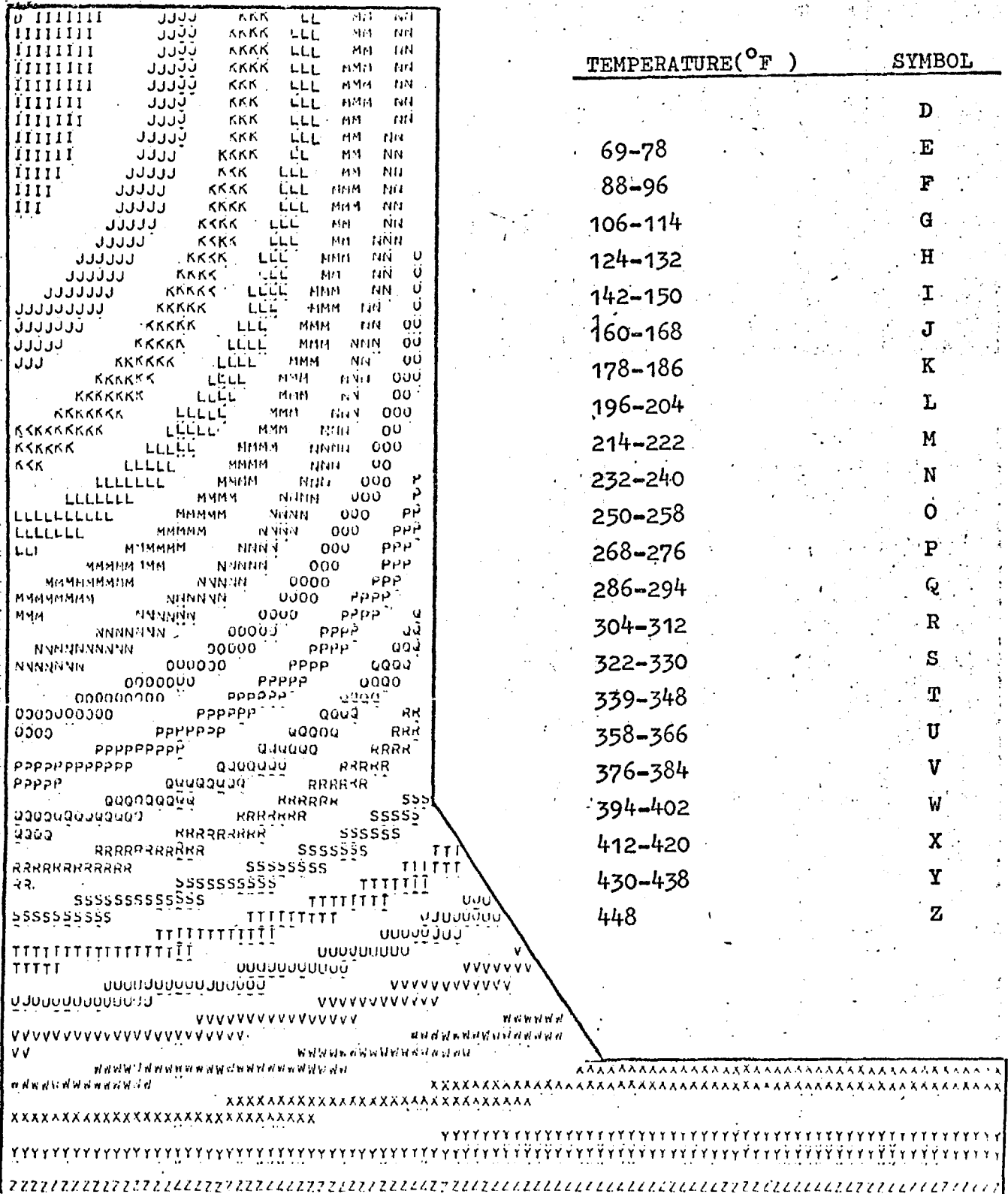


FIGURE 4.5.2 (b).

CASE B. TEMPERATURE PROFILES FOR TIME = 54 minutes.



TEMPERATURE PROFILES FOR CASE B. TEMPERATURES IN DEGREES °F

FIGURE 4.5.3(d)

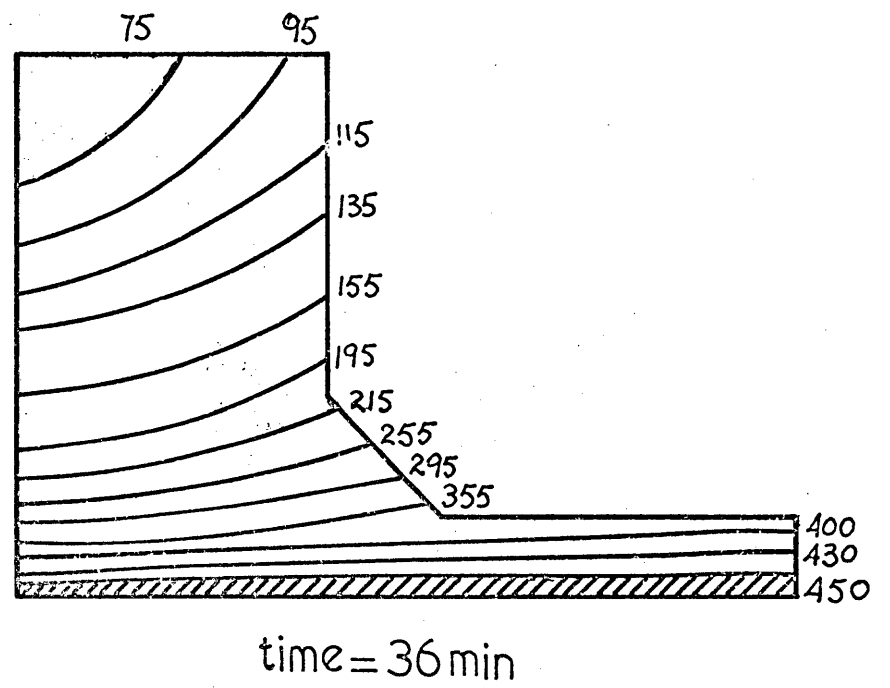
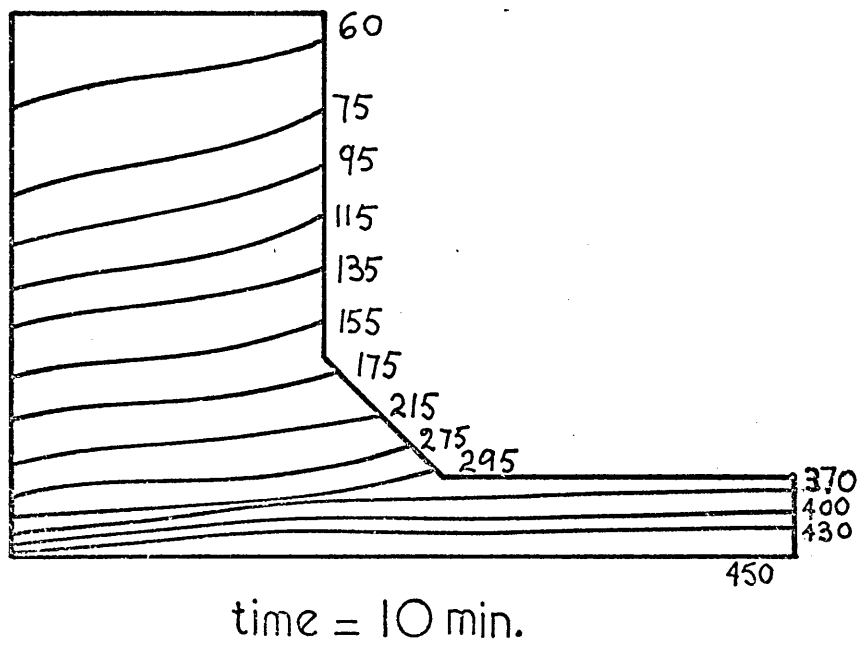
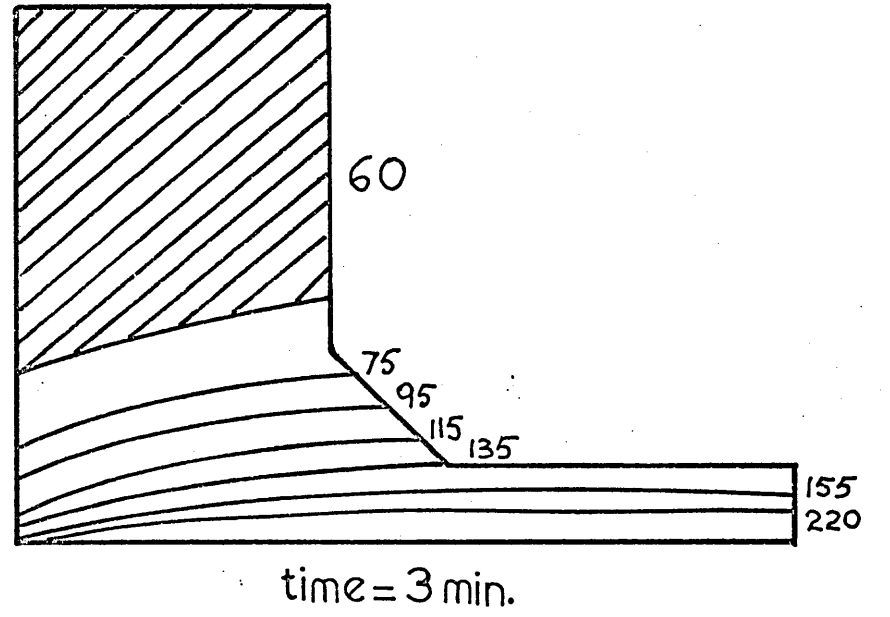
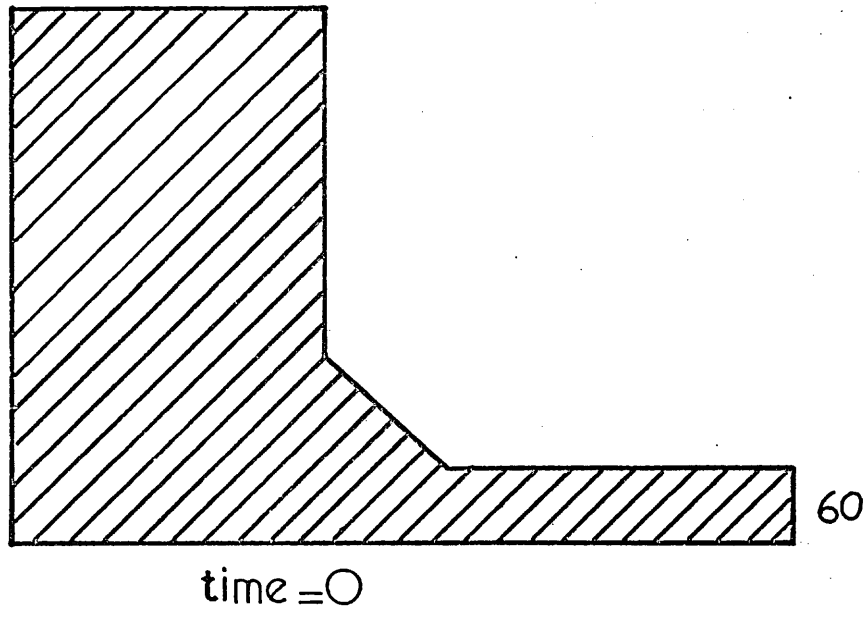
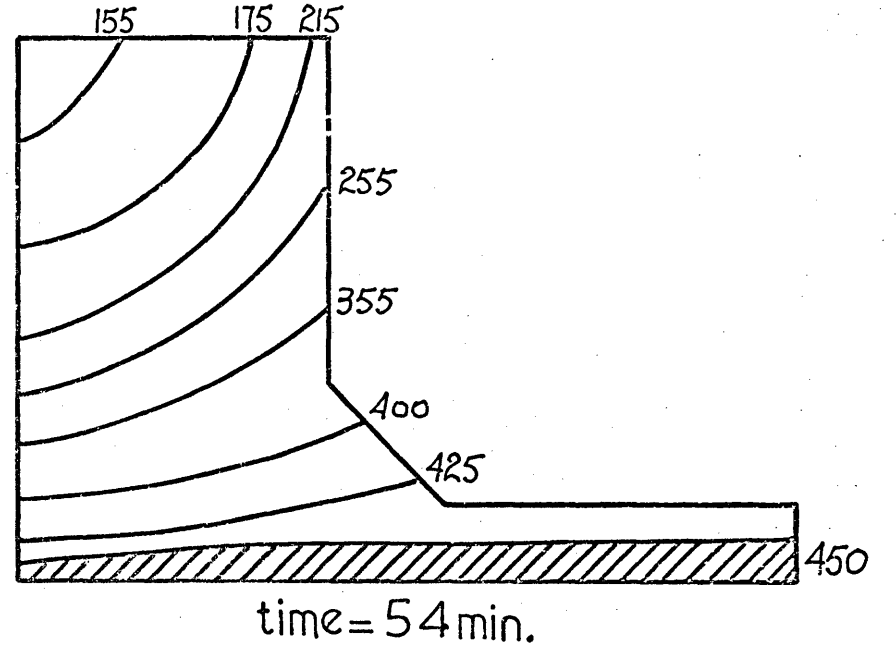
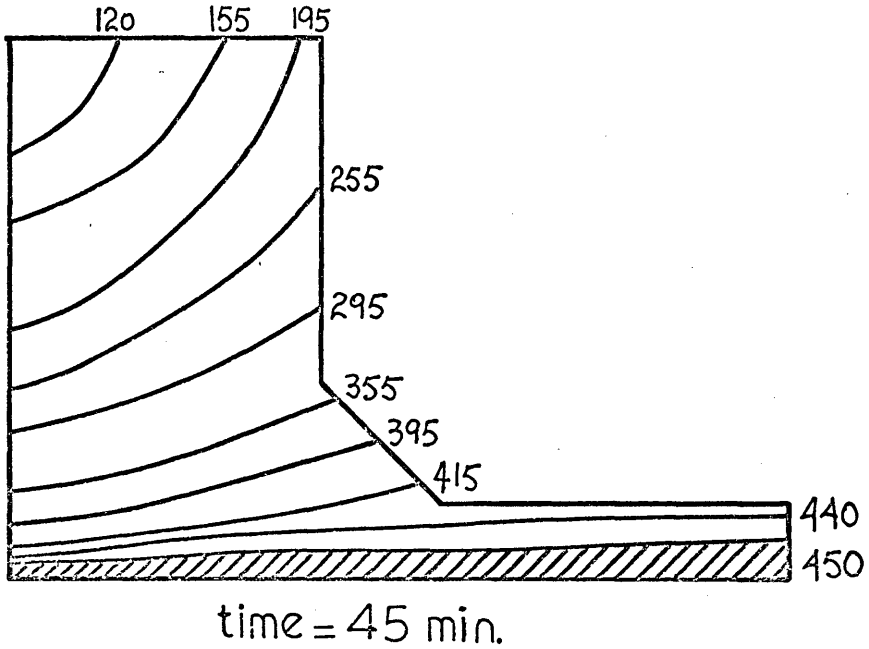
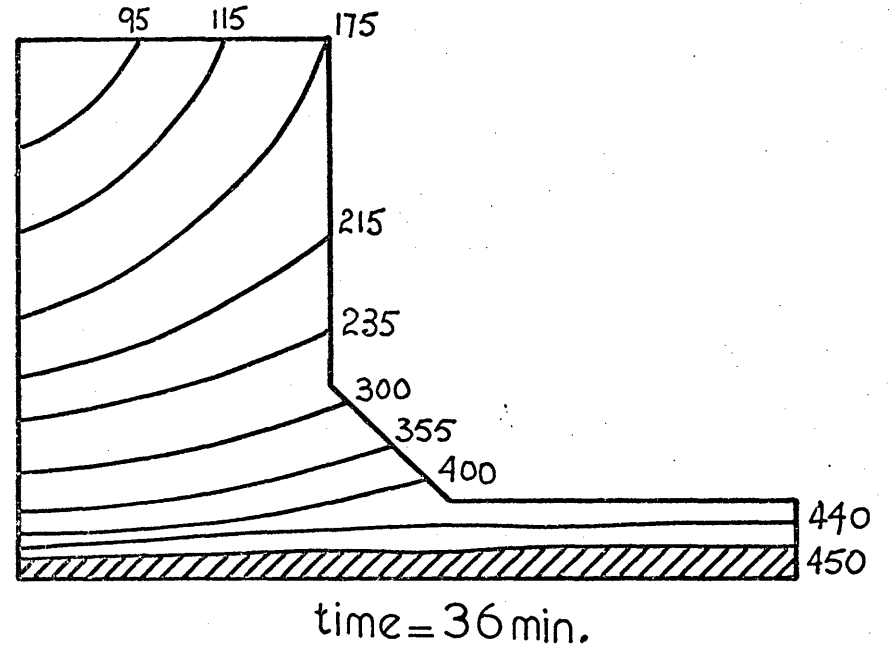
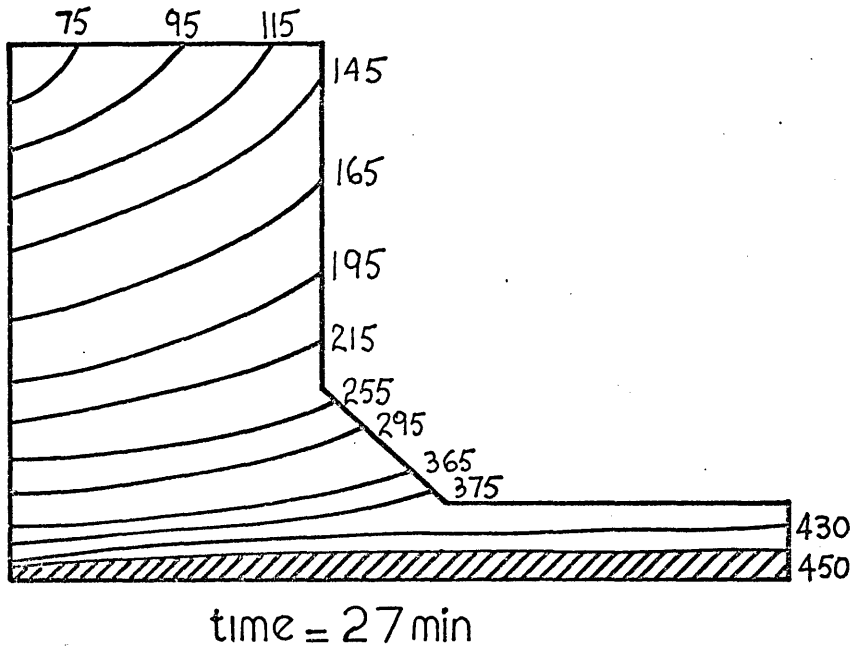


FIGURE 4.5.3 (b)



\* For definition of  $\Delta T_m$  see page 282

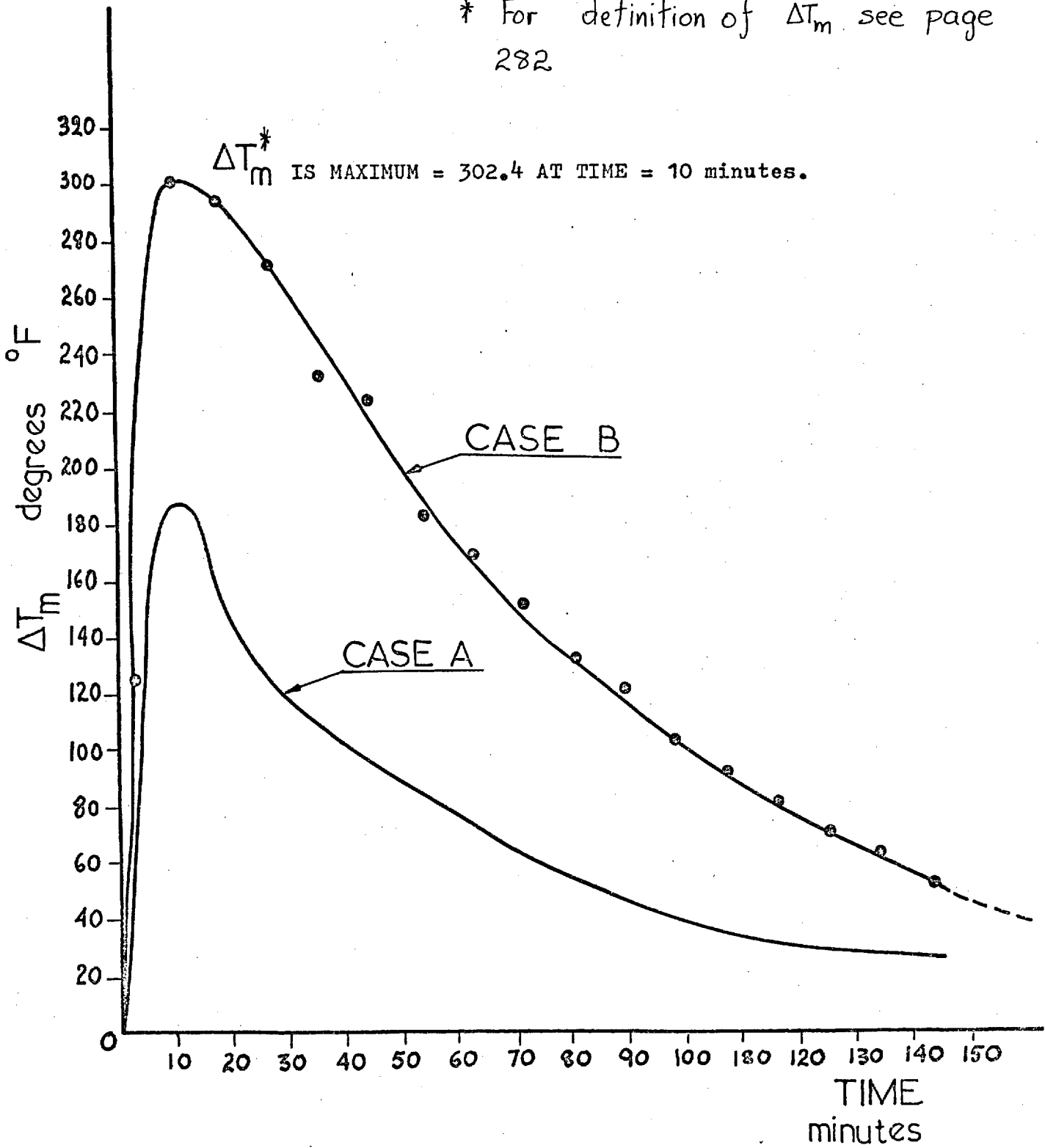


FIGURE 4.5.4 CASE B. MEAN TEMPERATURE VARIATION  $\Delta T_m$  BETWEEN NOZZLE AND VESSEL.

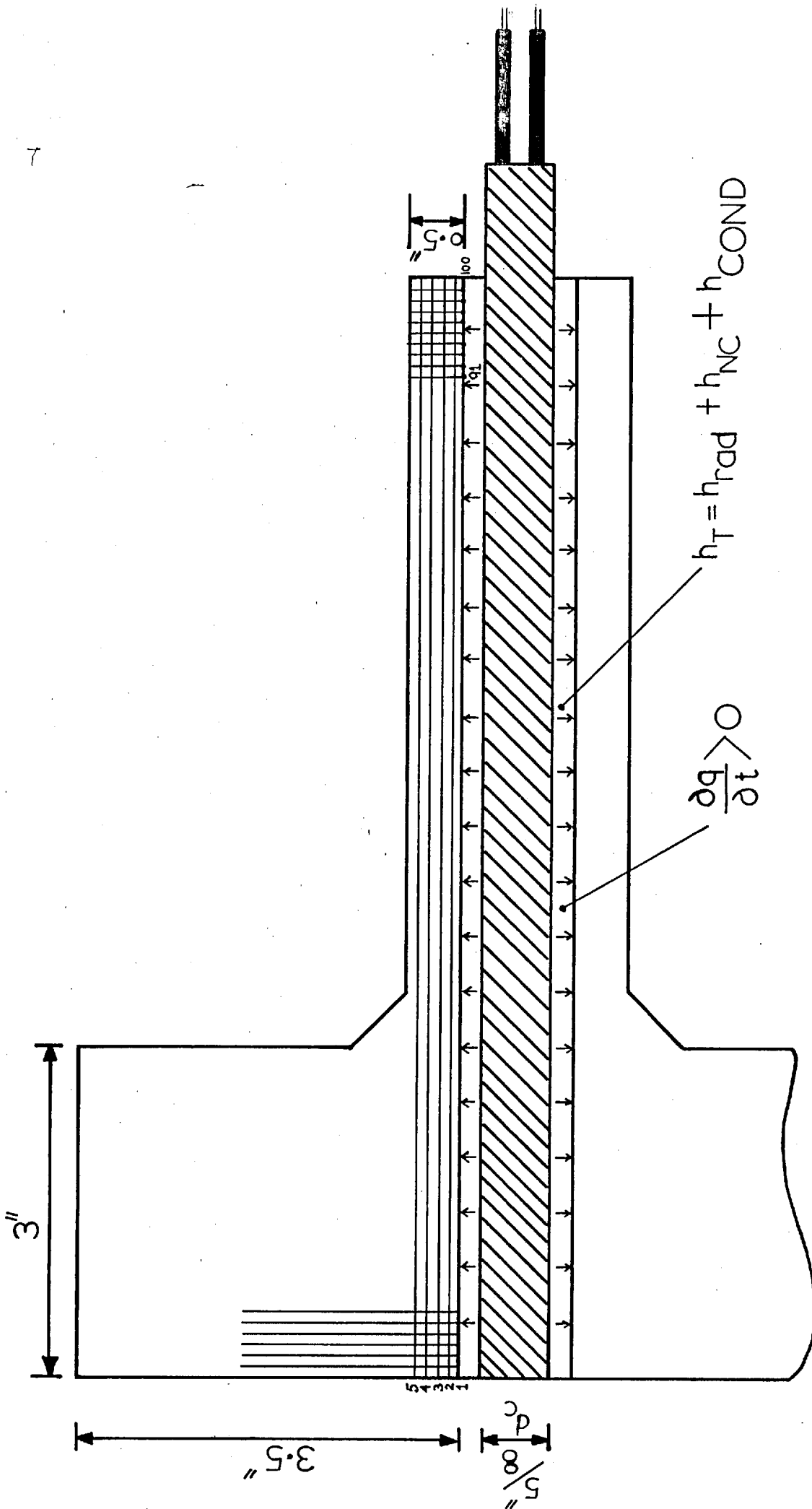


FIGURE 4.6.1 TEMPERATURE GRID FOR CASE C.

FIGURE 4.6.2(d)

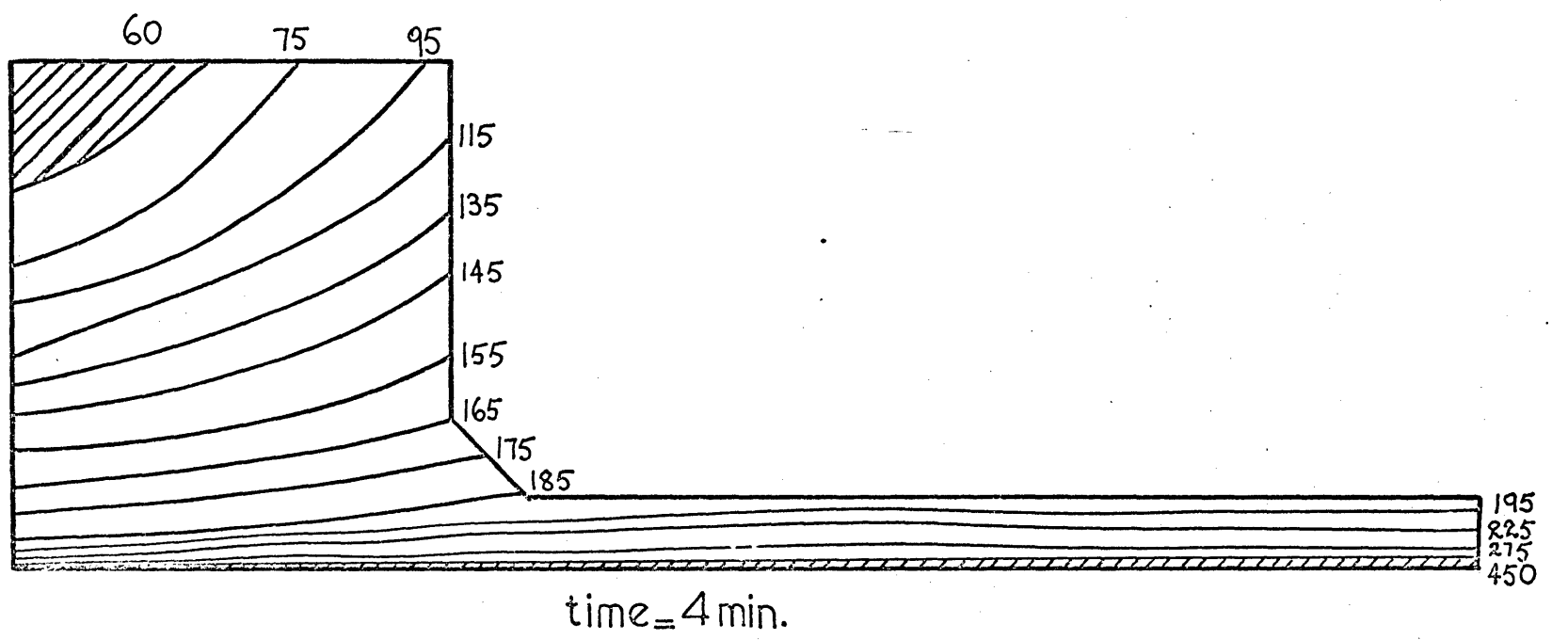
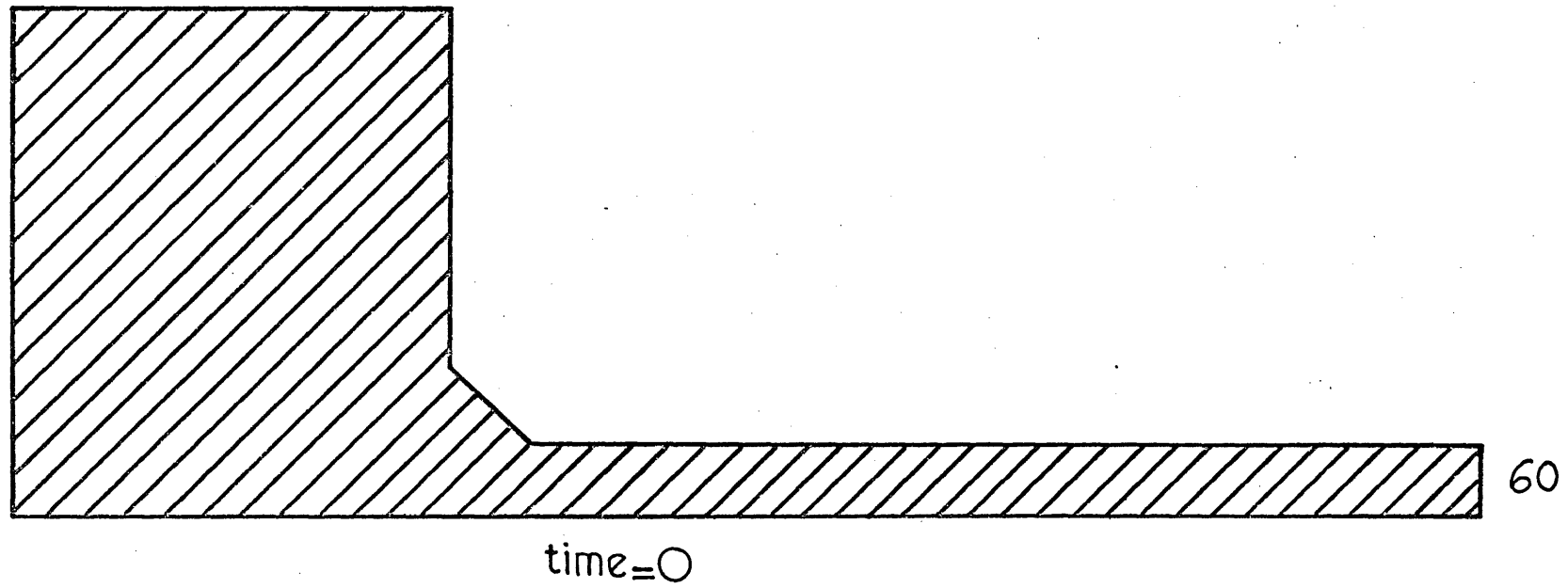


FIGURE 4.6.2(b)

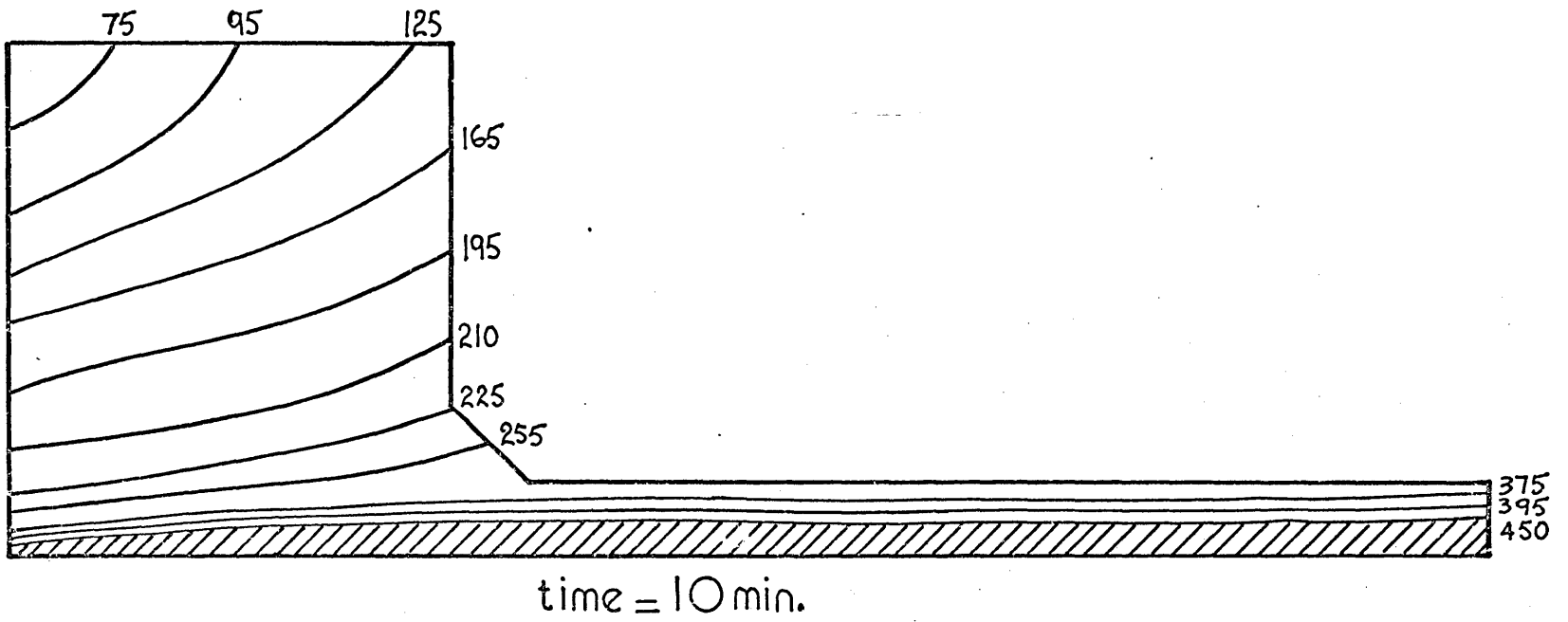
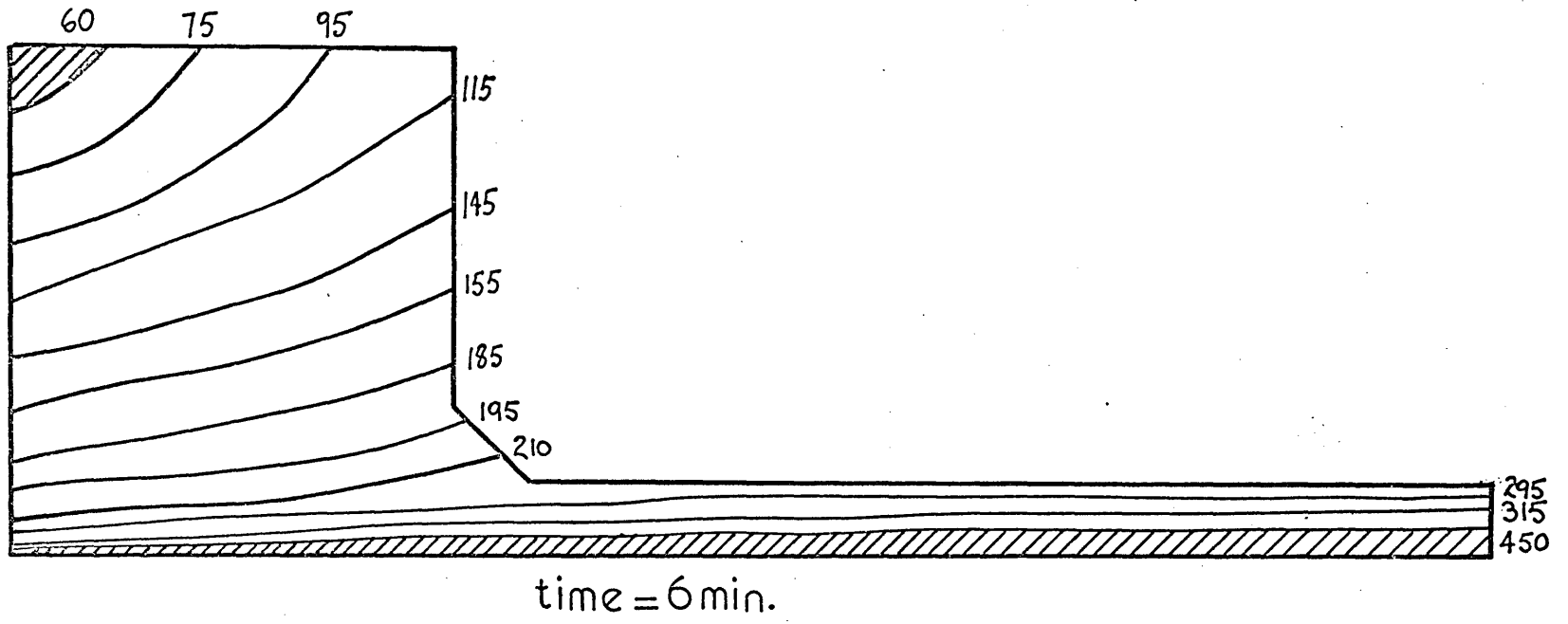
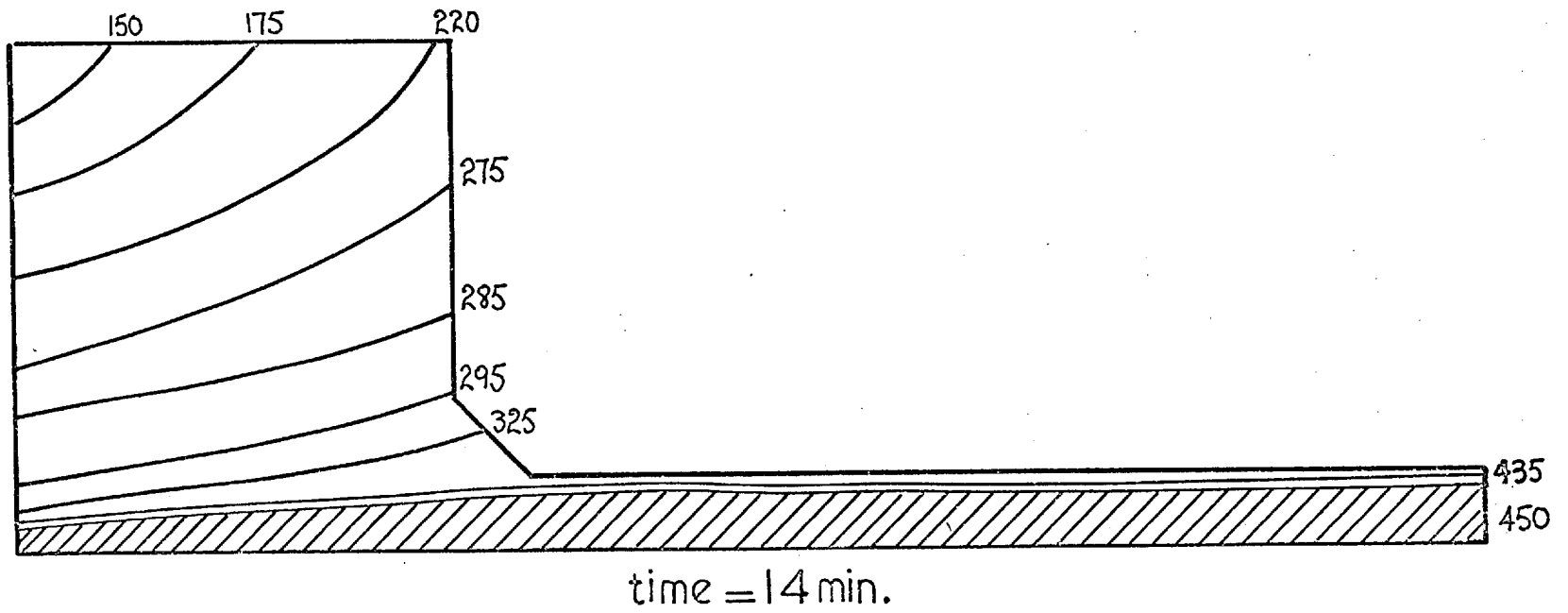
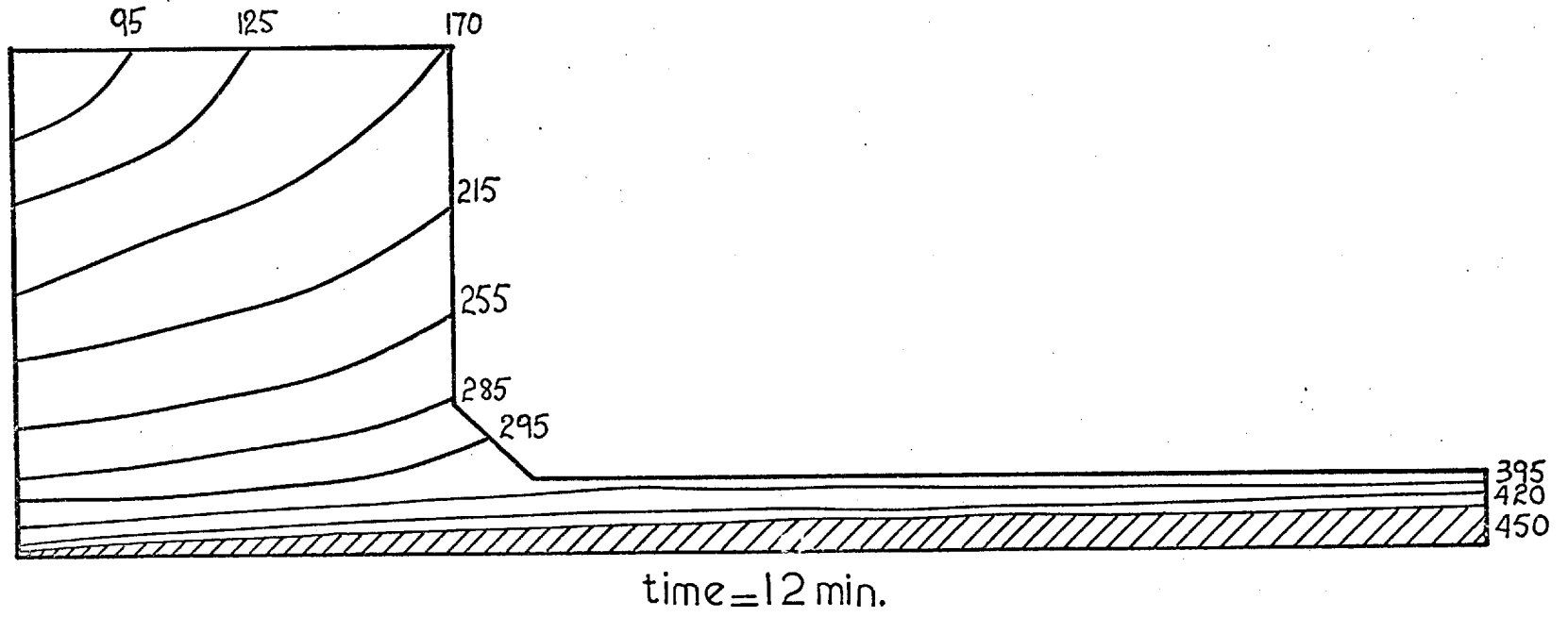


FIGURE 4.6.2(c)



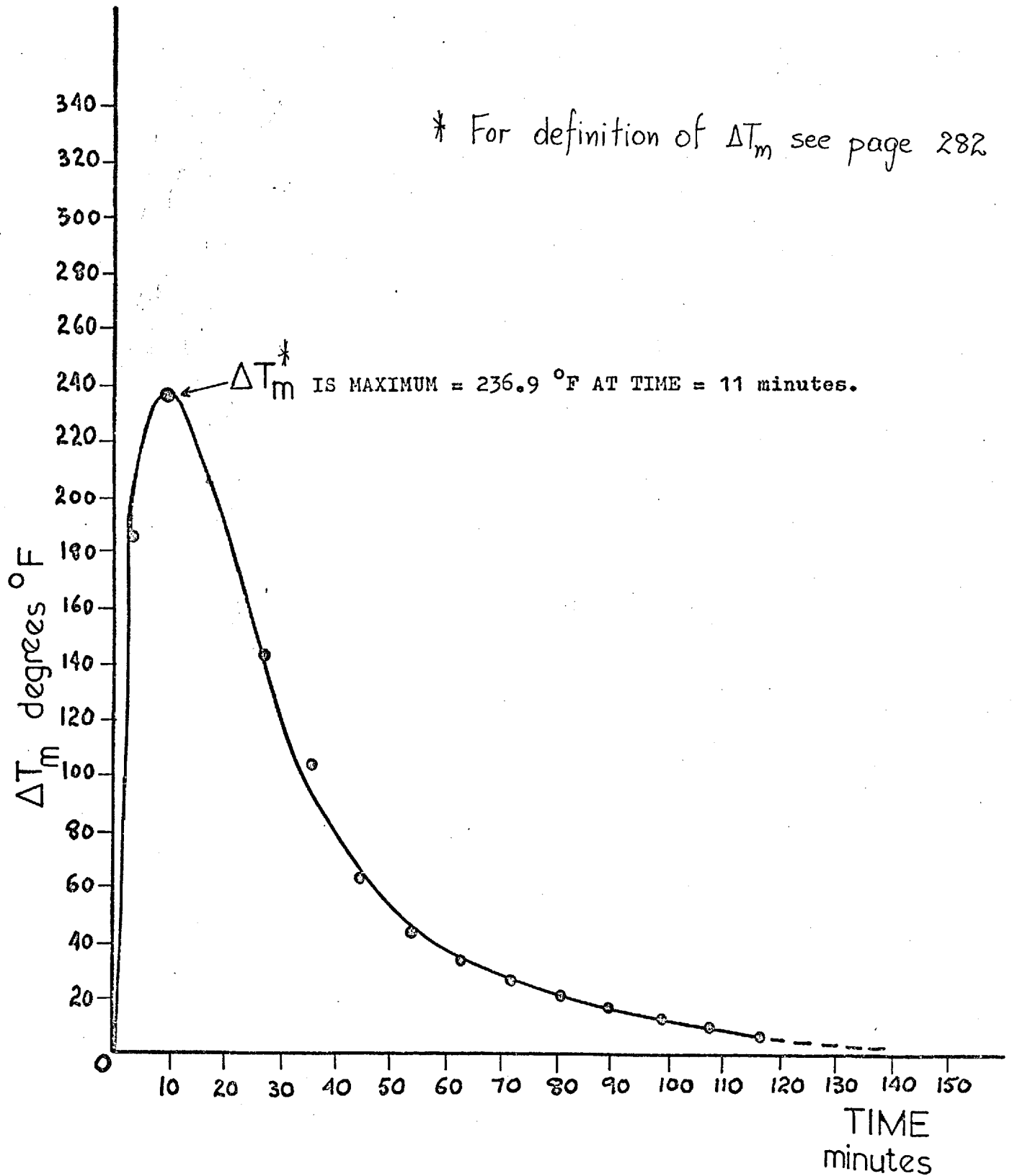


FIGURE 4.6.3 CASE C. MEAN TEMPERATURE VARIATION  
 $\Delta T_m$  BETWEEN NOZZLE AND VESSEL.



FIGURE 5.1.1

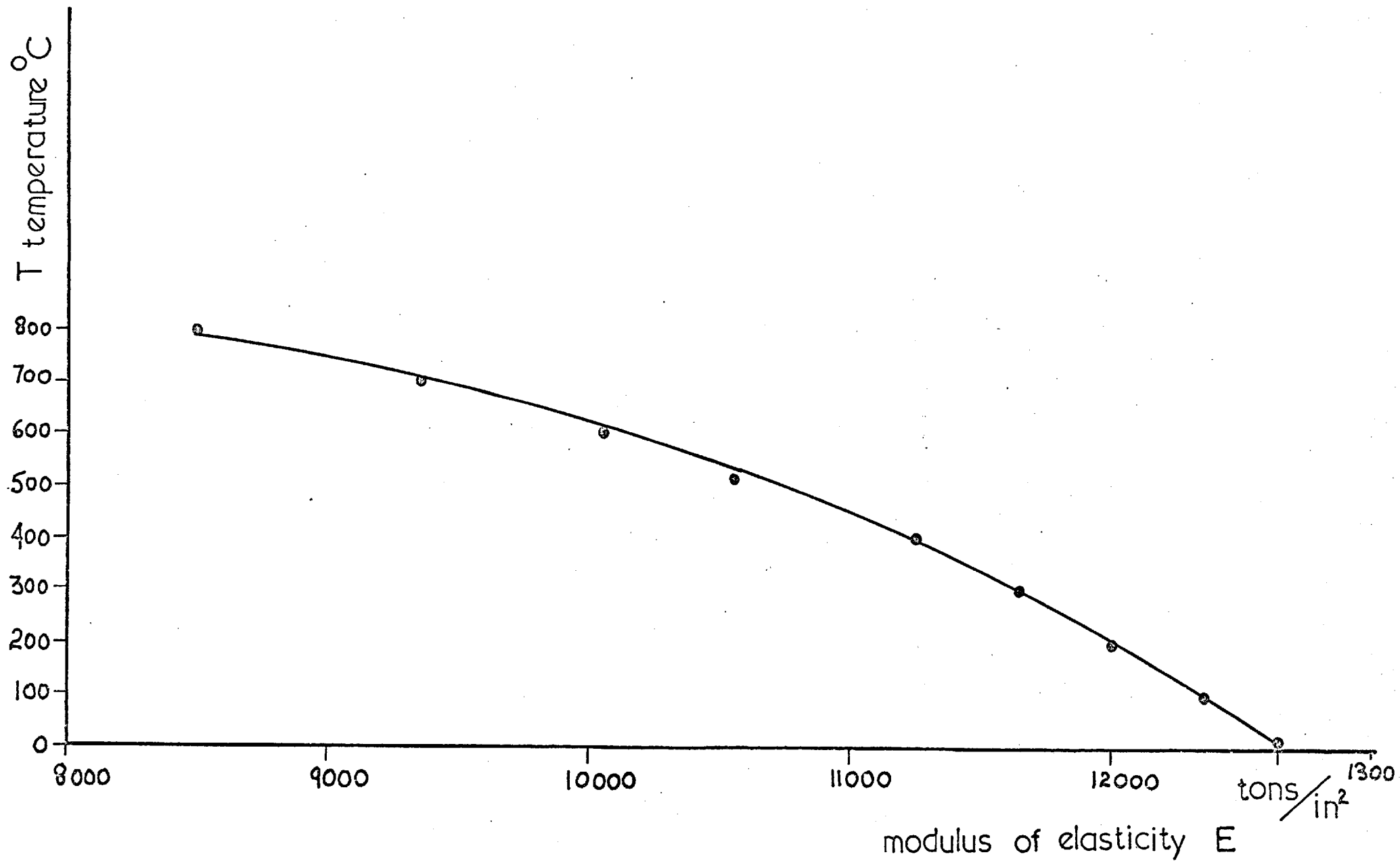


FIGURE 5.1.1

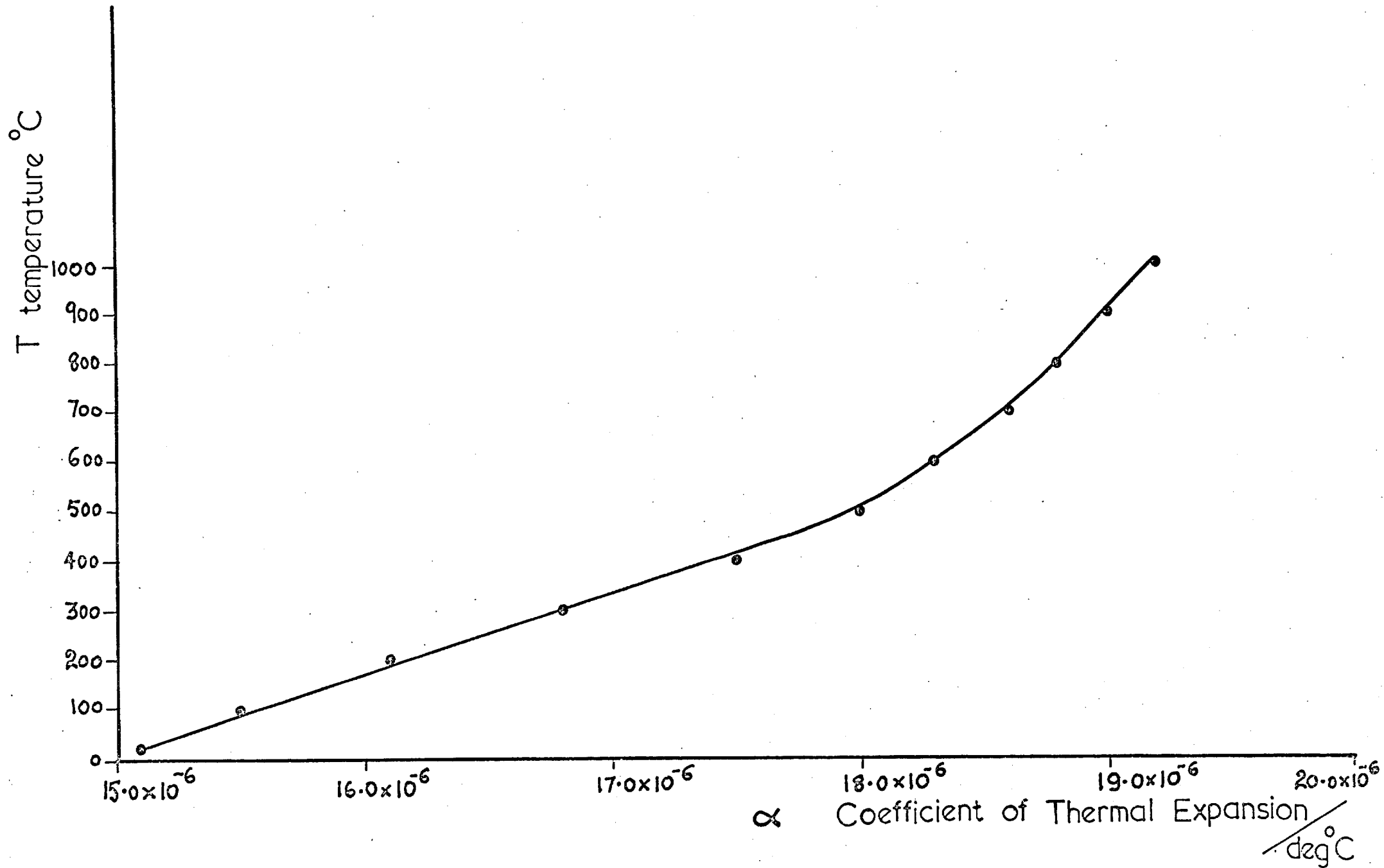


FIGURE 5.1.2

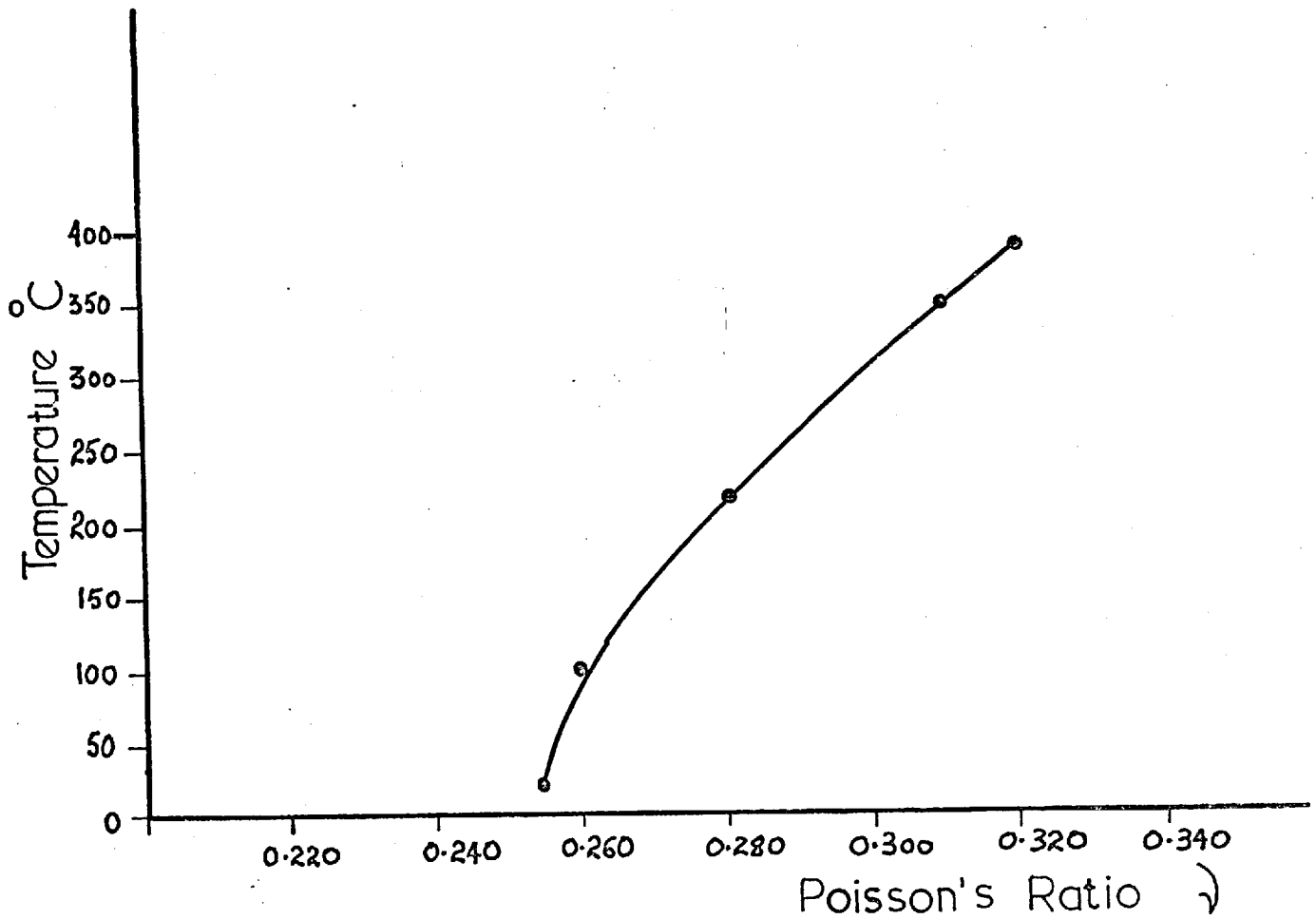


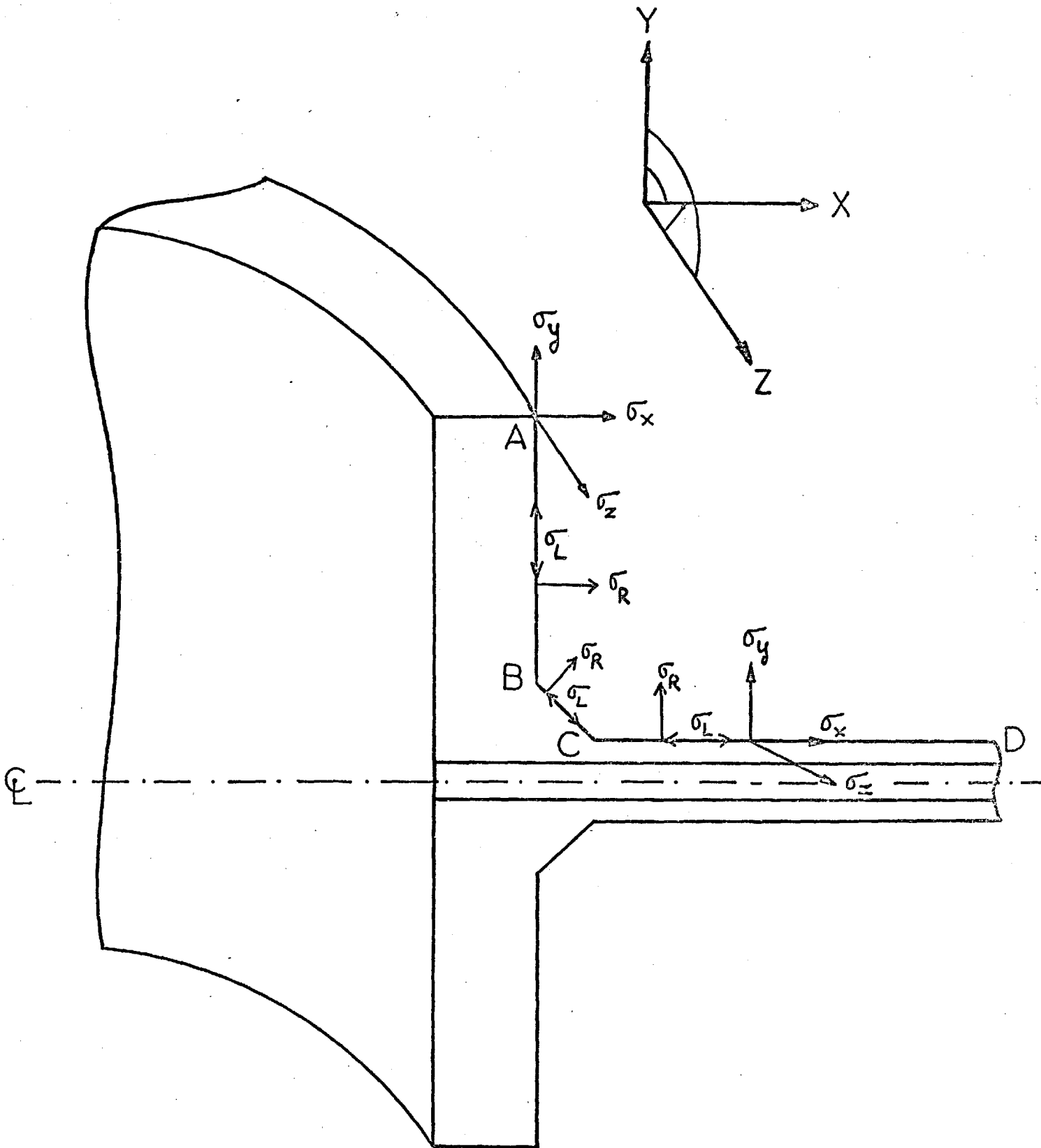
FIGURE 5.1.3

POISSON'S RATIO VERSUS TEMPERATURE.

STRESS NOTATION(See figure 5.1.4 in the next page)

In order to facilitate the comparison of the theoretical predictions with the experimental results on the outside of the vessel-junction-nozzle boundary, two stresses  $\sigma_L$  and  $\sigma_R$  are introduced into the system. Stress  $\sigma_L$  always lies along the boundary ABCD and  $\sigma_R$  is always perpendicular to the boundary ABCD at any point. Stress  $\sigma_L$  is in fact stress  $\sigma_y$  at the vessel part of the boundary (AB) and stress  $\sigma_x$  at the nozzle part (CD) and the stress component of  $\sigma_y$  and  $\sigma_x$  at the junction part BC. Similarly  $\sigma_R$  is in fact stress  $\sigma_x$  at the vessel part,  $\sigma_y$  at the nozzle part and the stress component of  $\sigma_y$  and  $\sigma_x$  at any point perpendicular to the junction part (BC).

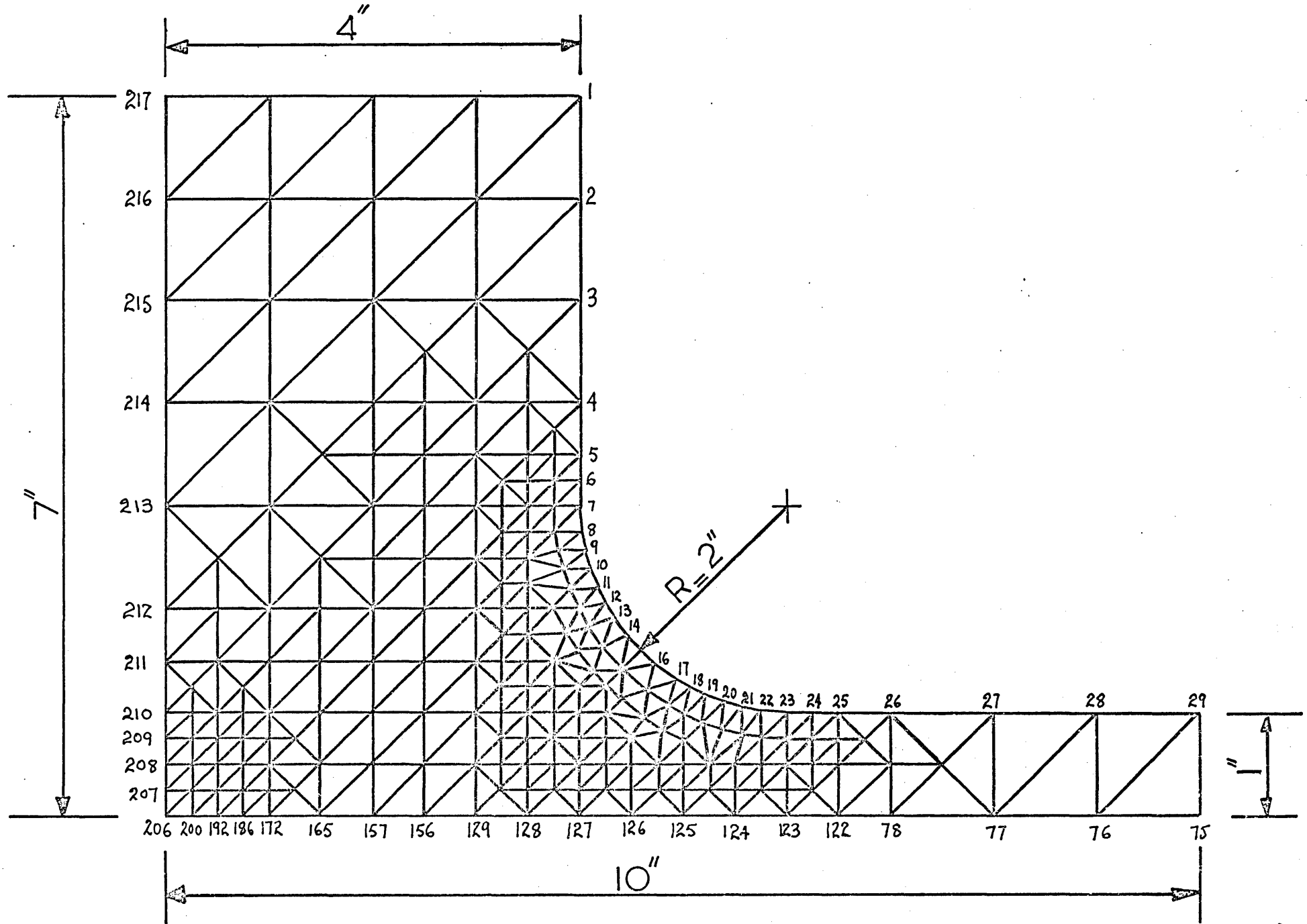
Therefore the introduction of  $\sigma_L$  and  $\sigma_R$ , which are in fact the stresses  $\sigma_y$  and  $\sigma_x$  (or their stress component for the junction part), makes the representation of the stress field at the outside boundary more uniform and the comparison with the experimental results more comprehensive.



NOTE: STRESS  $\sigma_z$  IS PERPENDICULAR TO THE PLANE OF THE PAPER ( z DIRECTION ).

FIGURE 5.1.4 DIRECTION OF STRESSES.

FIGURE 5.2.1



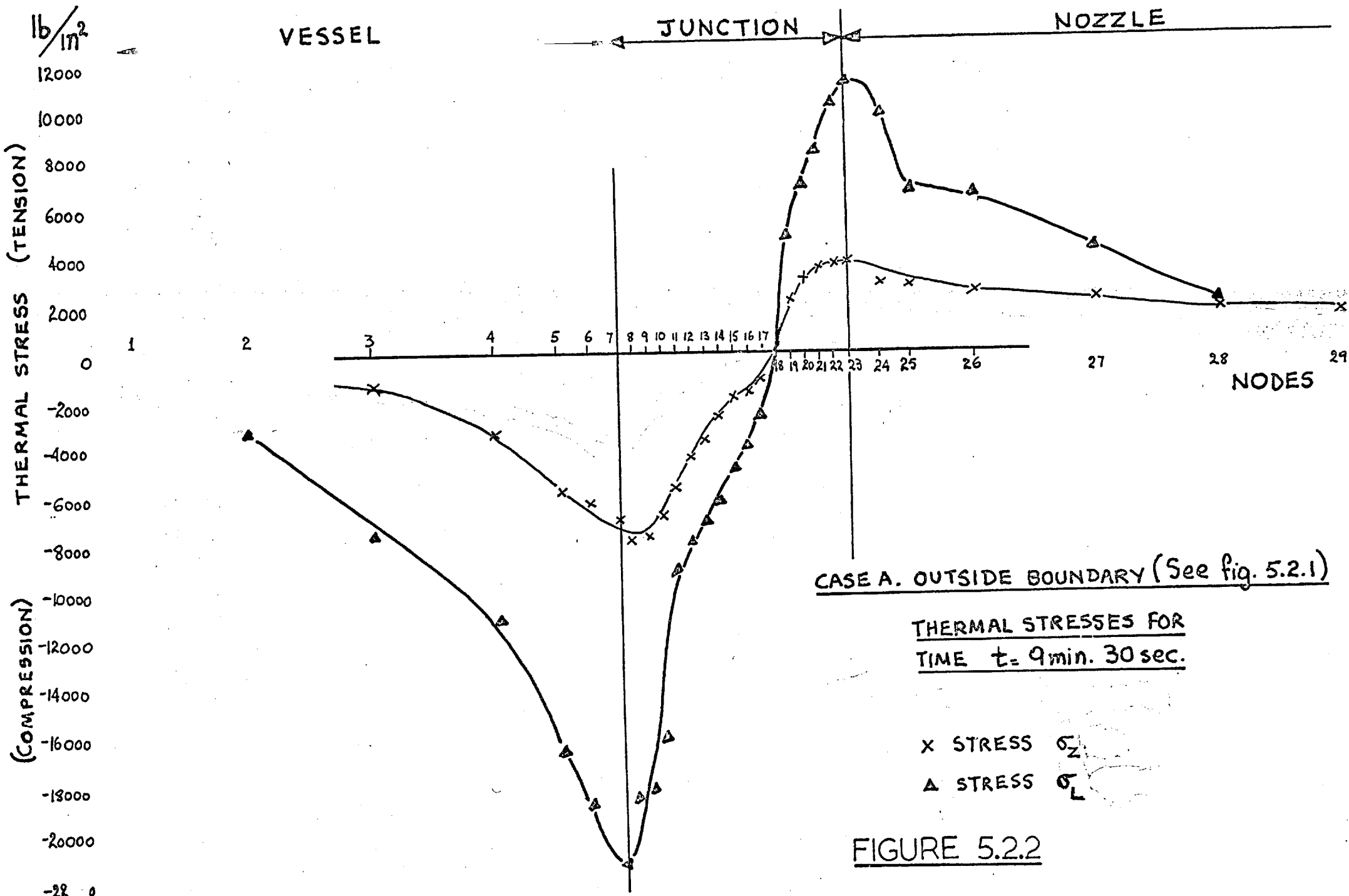


FIGURE 5.2.2

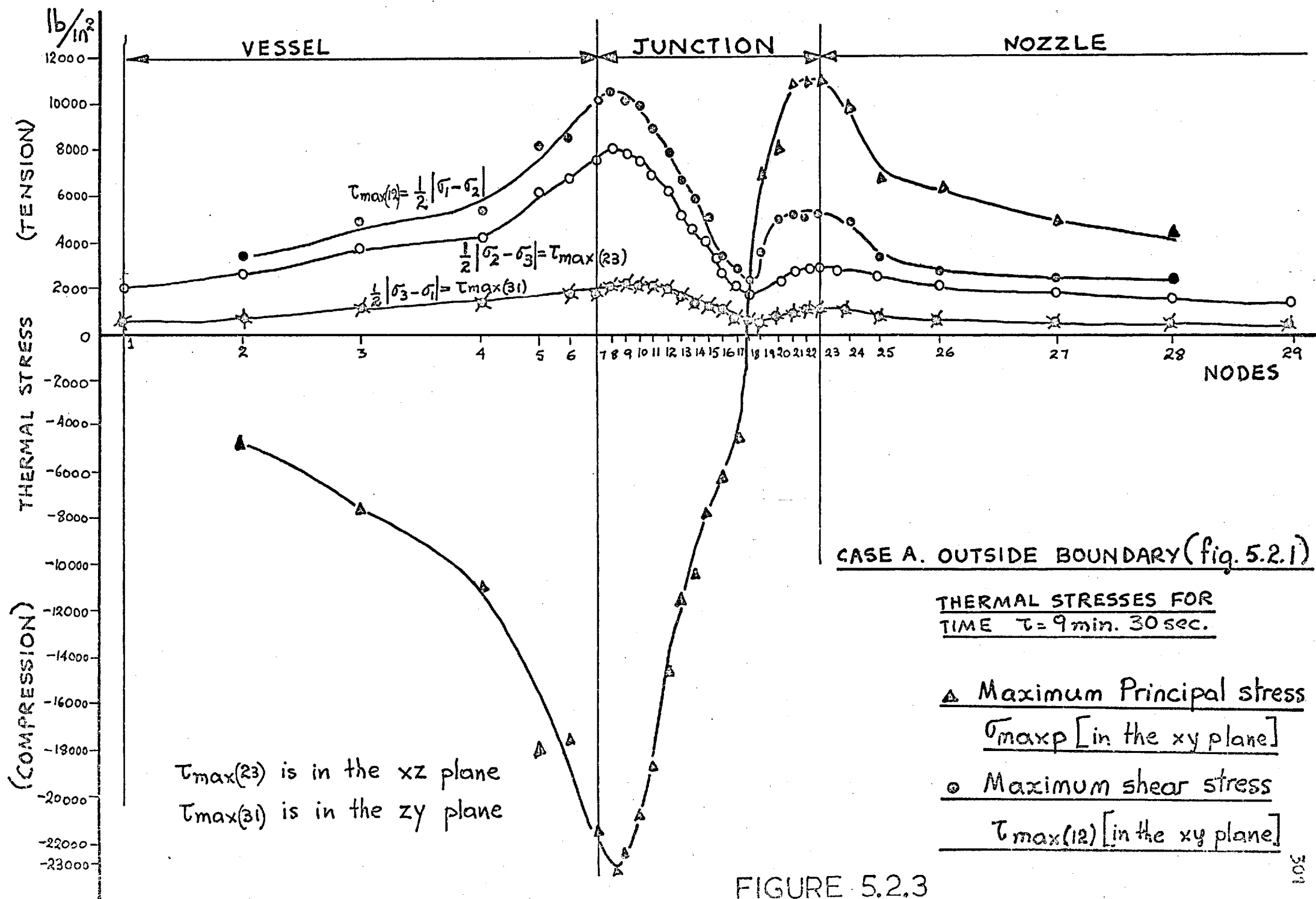
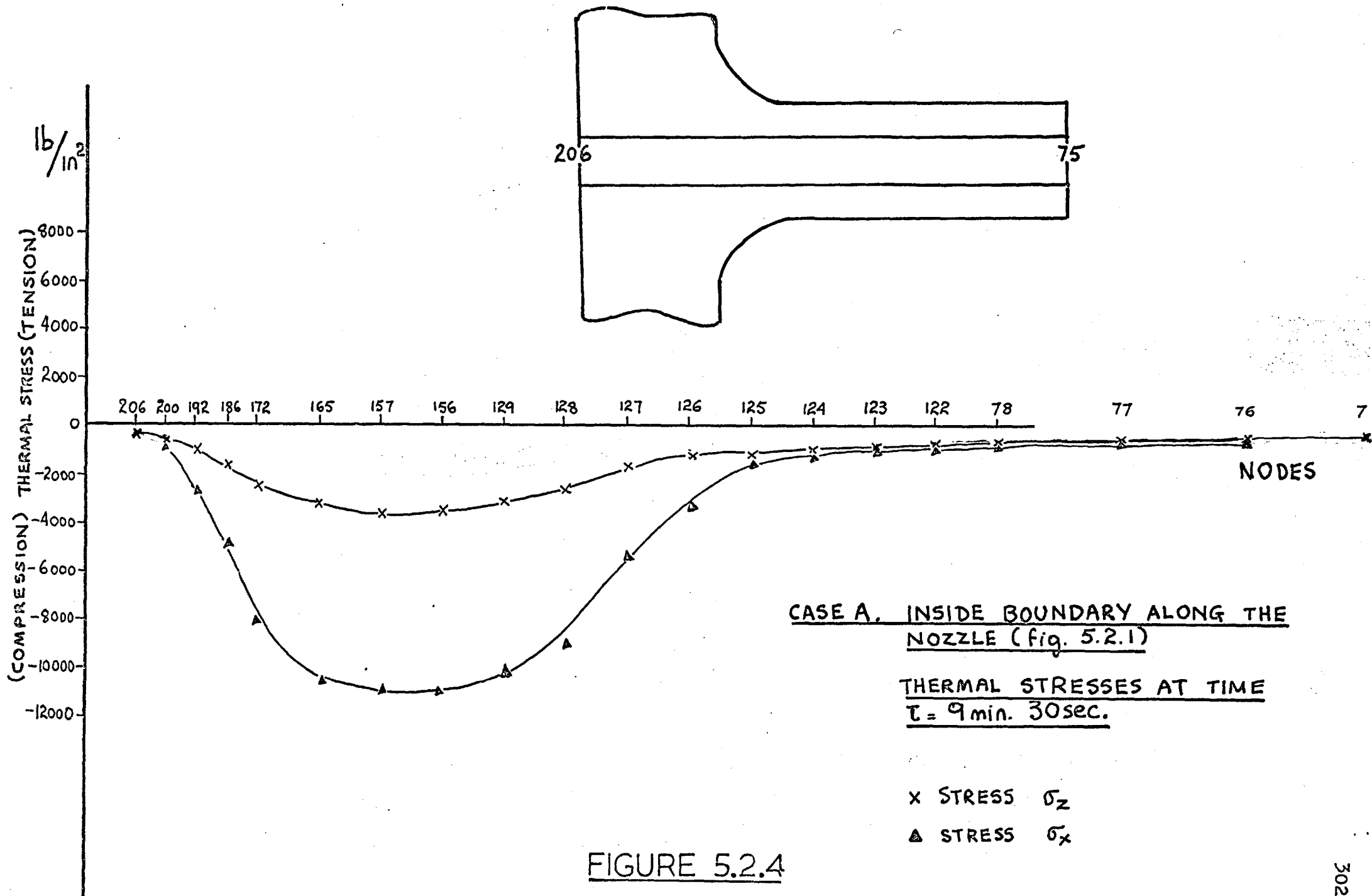
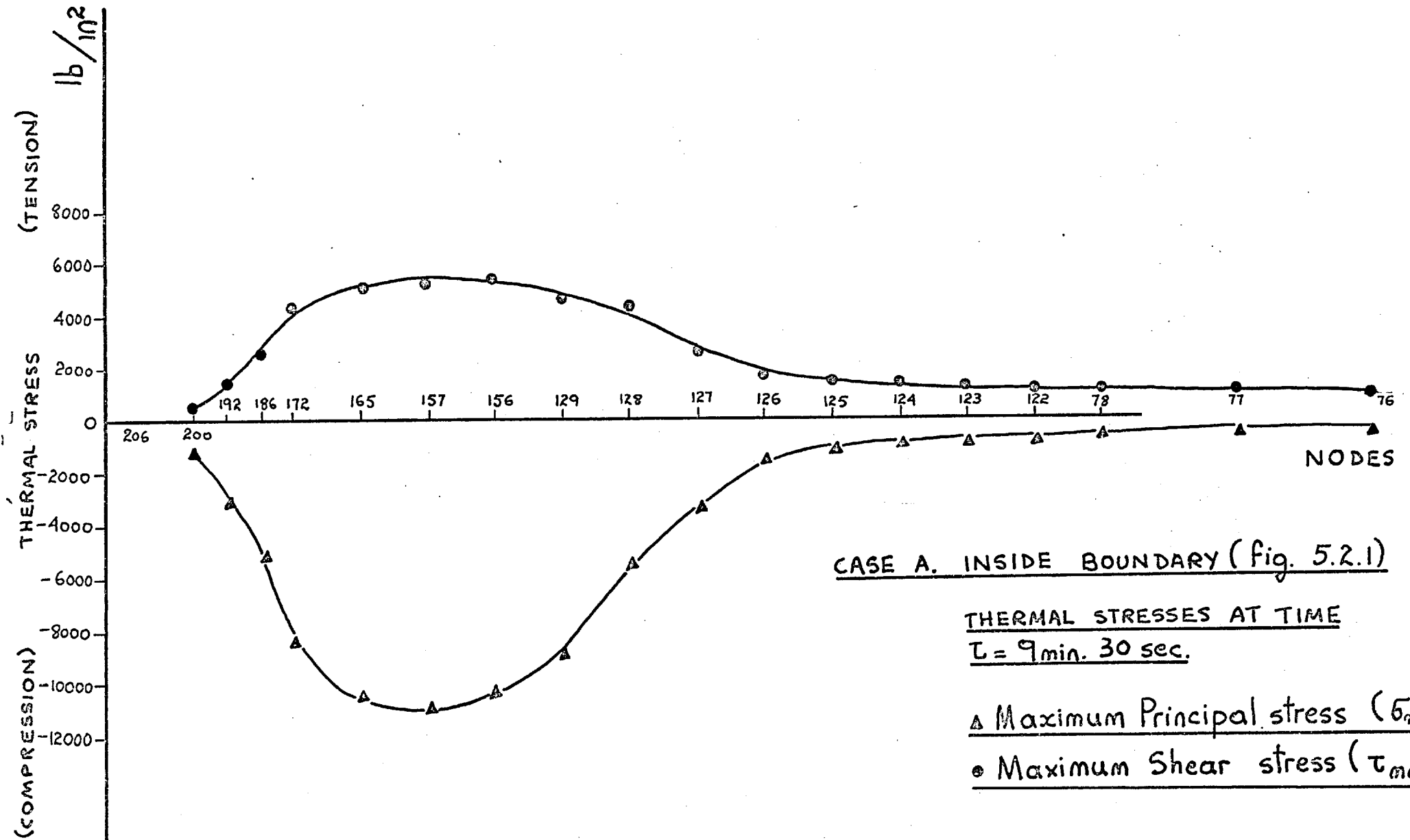


FIGURE 5.2.3







CASE A. INSIDE BOUNDARY (Fig. 5.2.1)

THERMAL STRESSES AT TIME  
 $T = 9 \text{ min. } 30 \text{ sec.}$

$\Delta$  Maximum Principal stress ( $\sigma_{\text{max}}$ )  
 $\bullet$  Maximum Shear stress ( $\tau_{\text{max}(12)}$ )

FIGURE 5.2.5

CASE B. FINITE ELEMENT MESH.

FIGURE 5.2.6

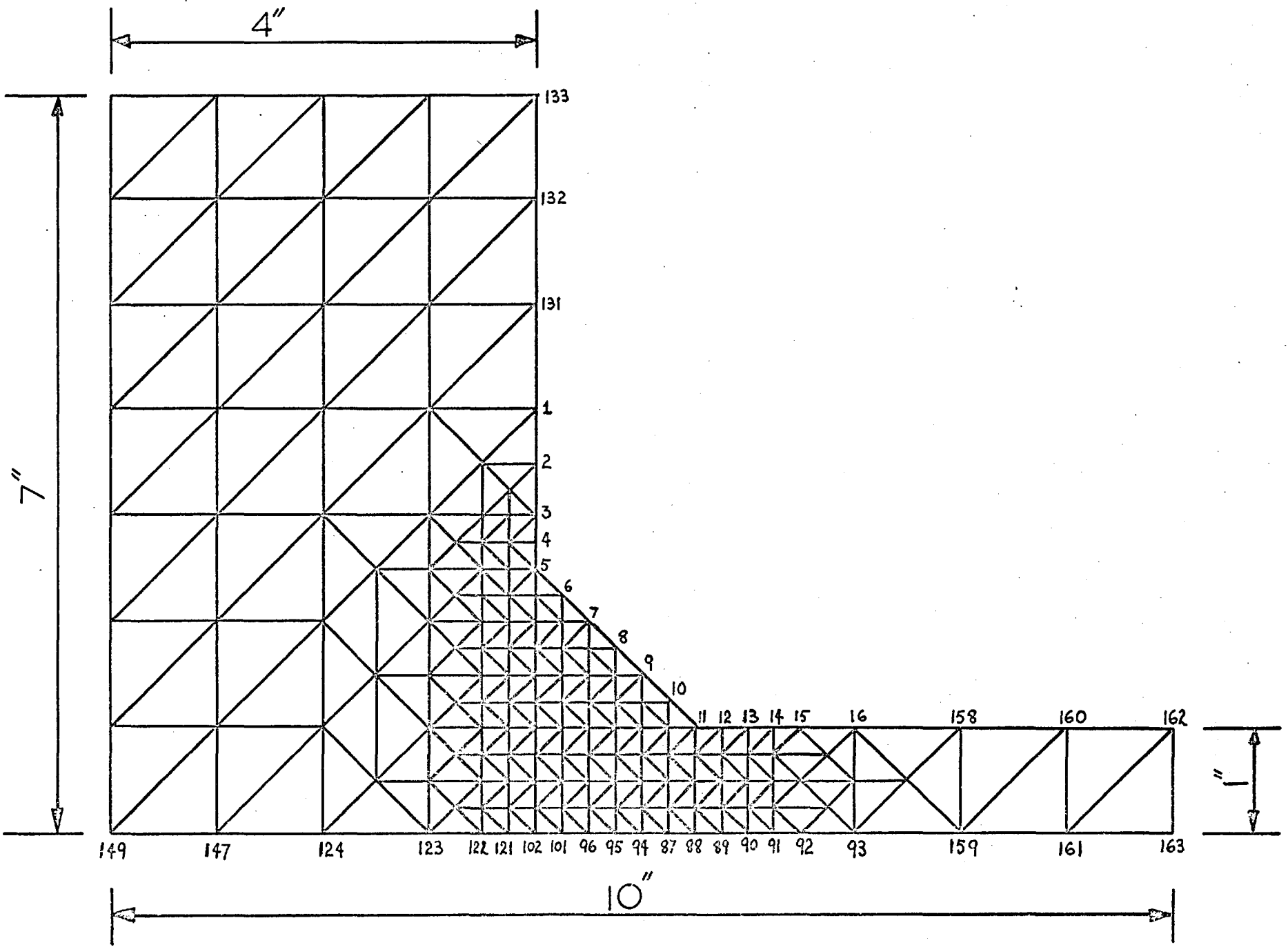
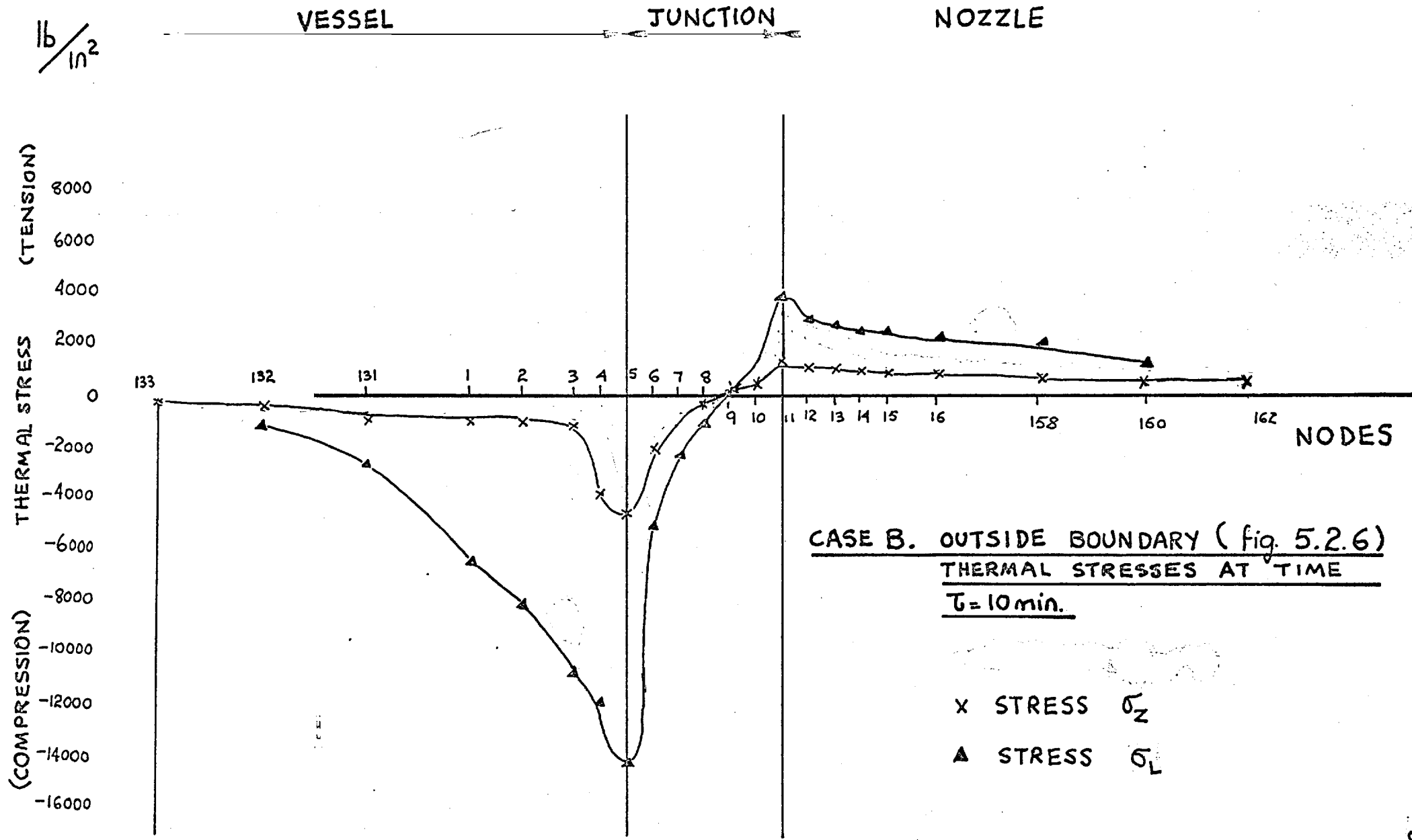


FIGURE 5.2.7



CASE B. OUTSIDE BOUNDARY (fig. 5.2.6)  
THERMAL STRESSES AT TIME  
 $\tau = 10 \text{ min.}$

X STRESS  $\sigma_z$   
 $\blacktriangle$  STRESS  $\sigma_L$

FIGURE 5.2.8

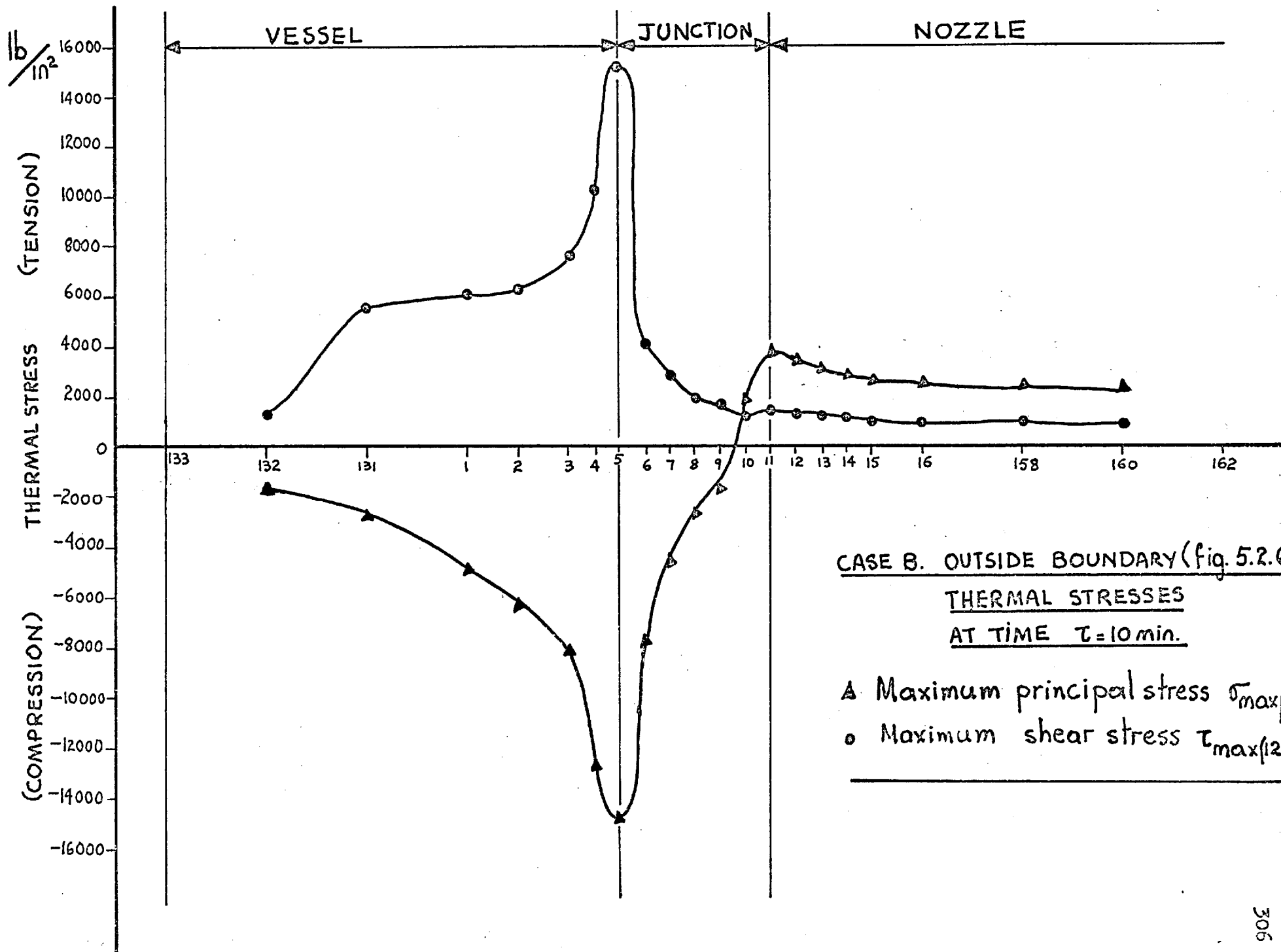


FIGURE 5.2.9

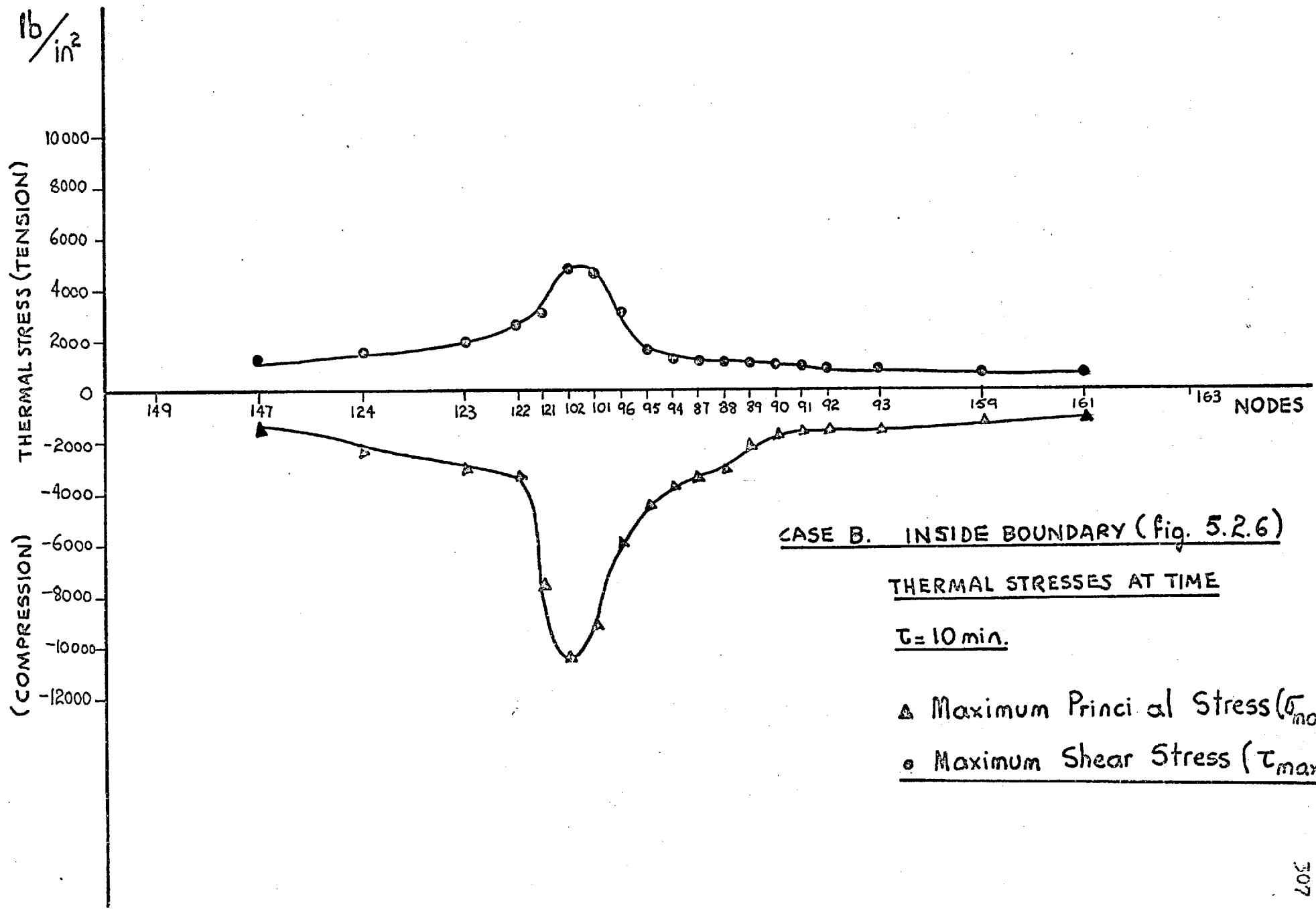
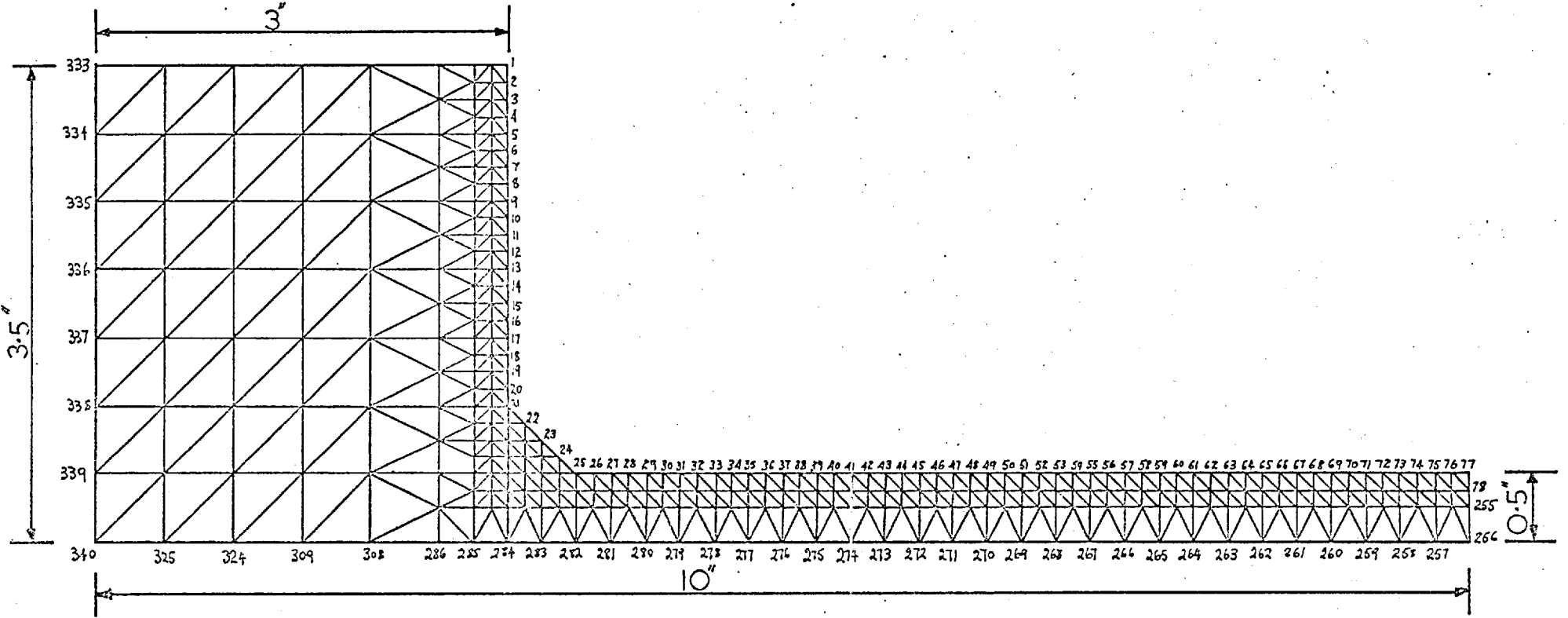
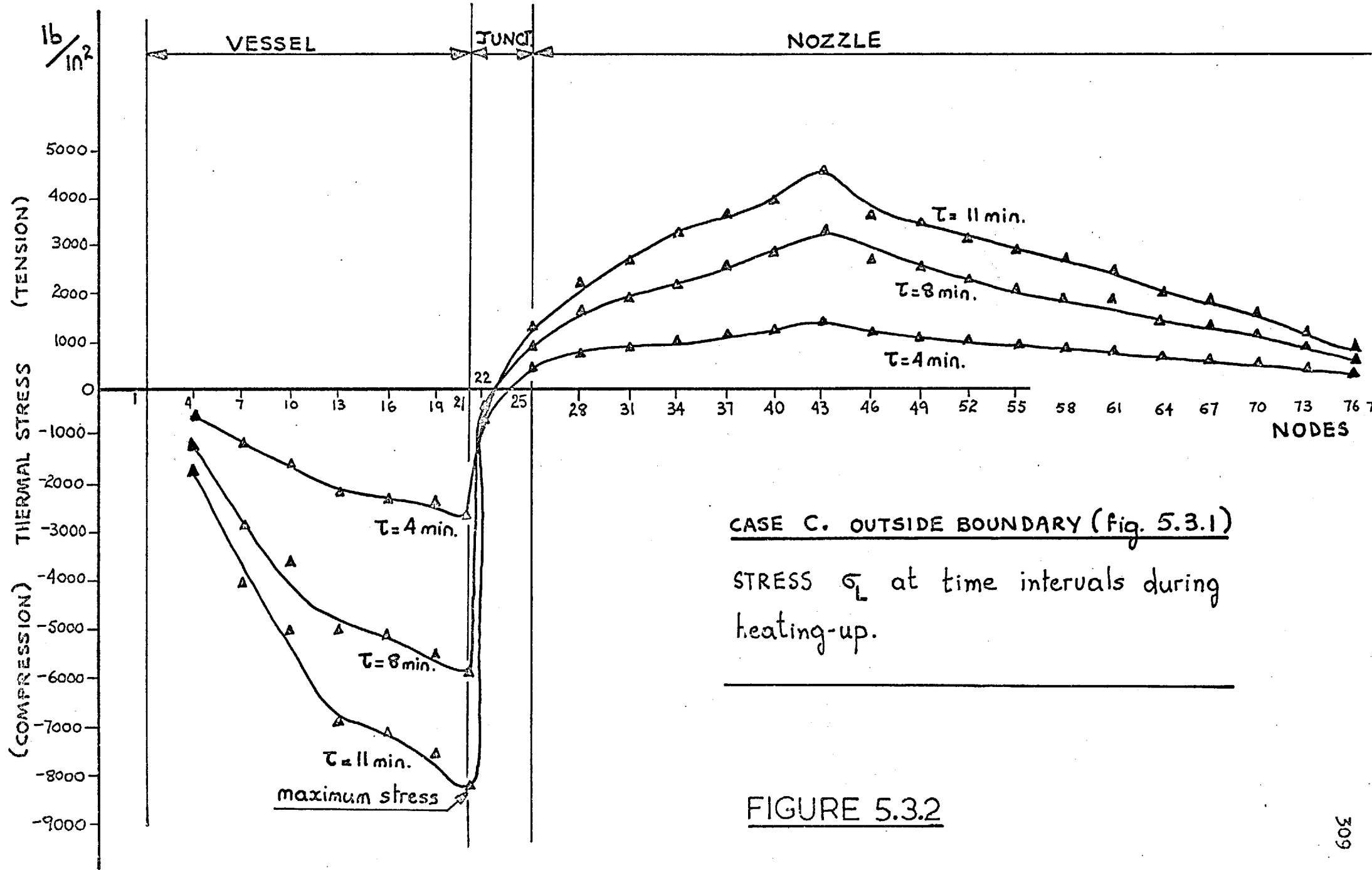


FIGURE 5.3.1 CASE C. FINITE ELEMENT MESH.

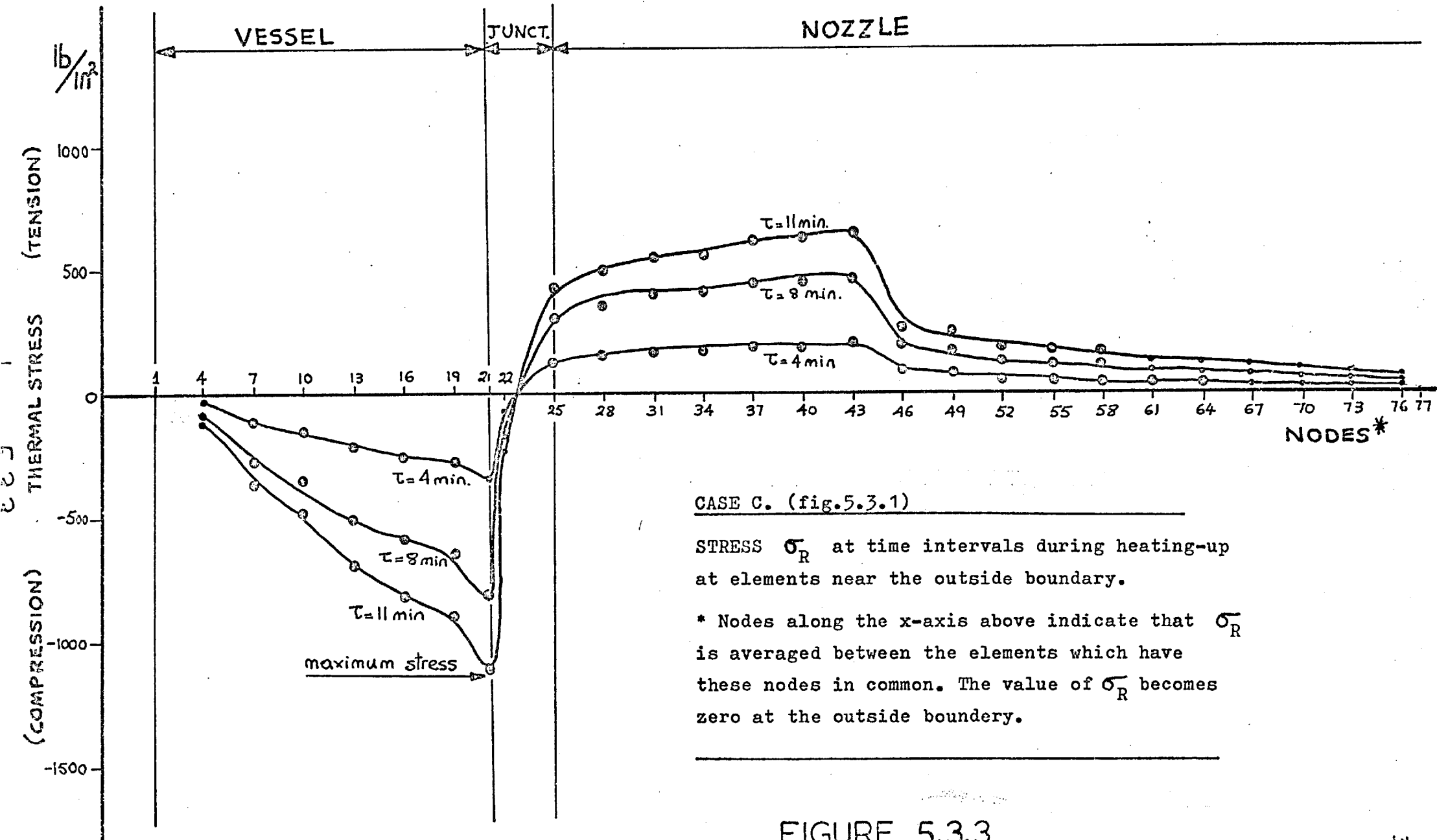




CASE C. OUTSIDE BOUNDARY (Fig. 5.3.1)  
 STRESS  $\sigma_L$  at time intervals during heating-up.

FIGURE 5.3.2



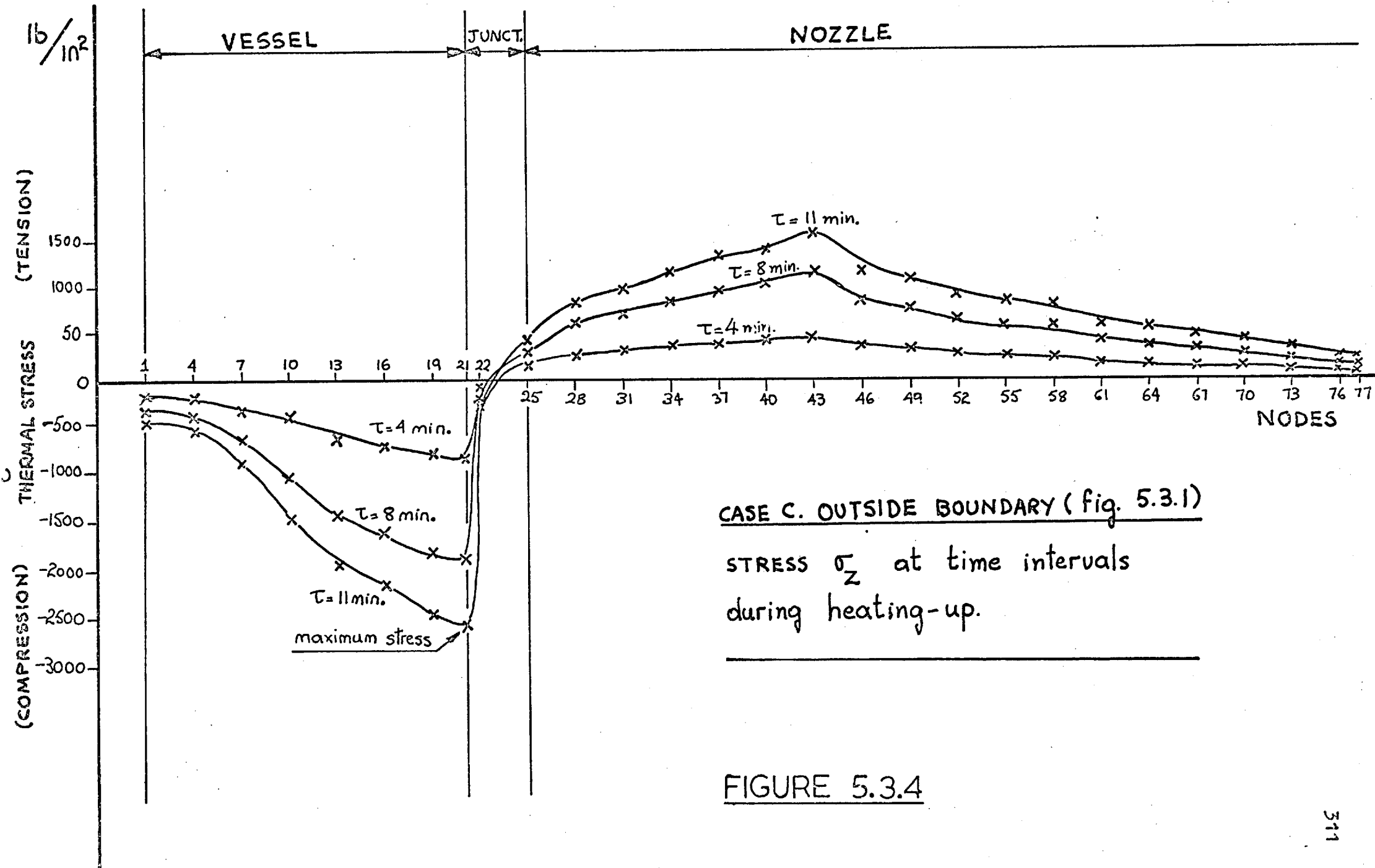


CASE C. (fig.5.3.1)

STRESS  $\sigma_R$  at time intervals during heating-up at elements near the outside boundary.

\* Nodes along the x-axis above indicate that  $\sigma_R$  is averaged between the elements which have these nodes in common. The value of  $\sigma_R$  becomes zero at the outside boundary.

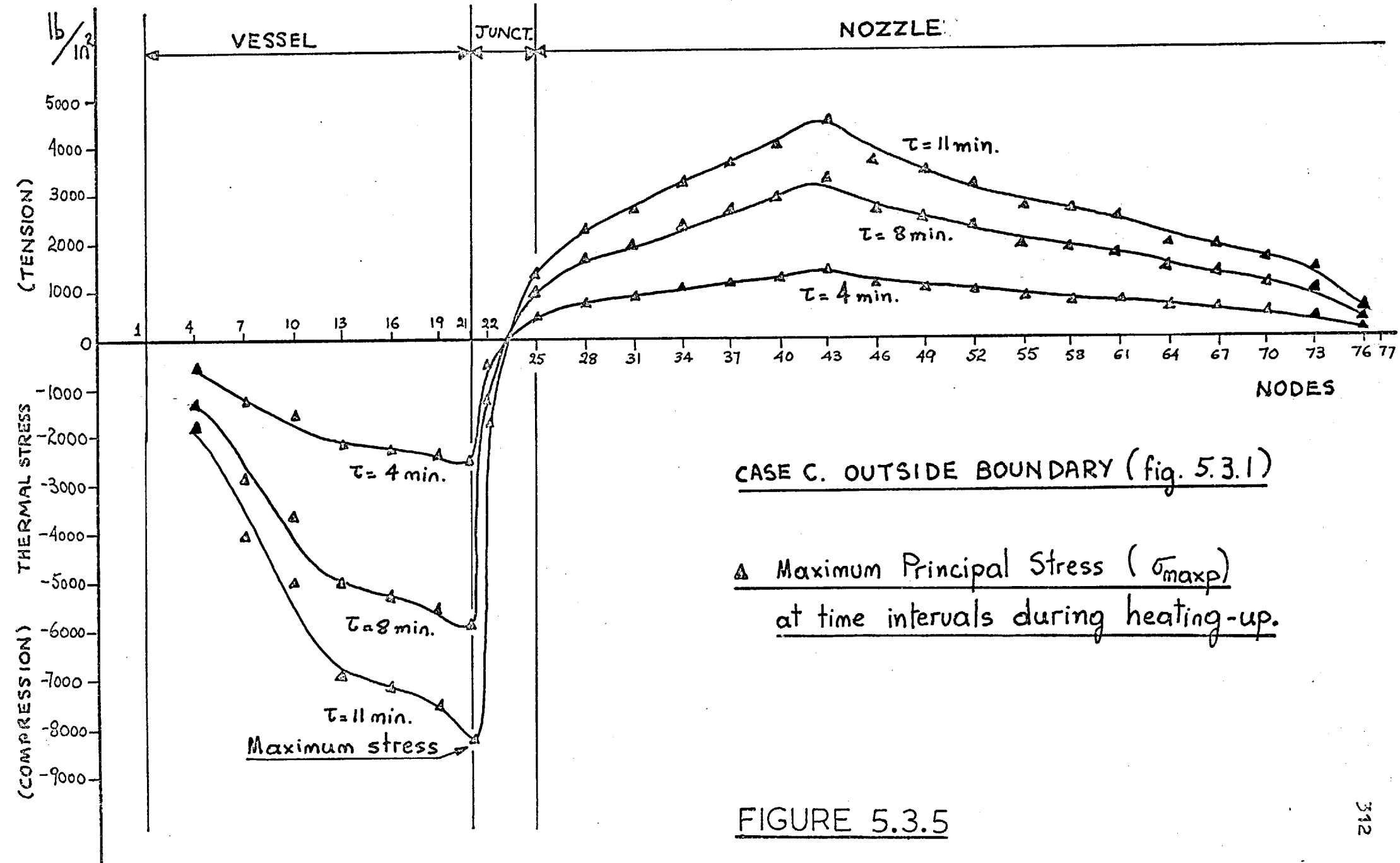
FIGURE 5.3.3

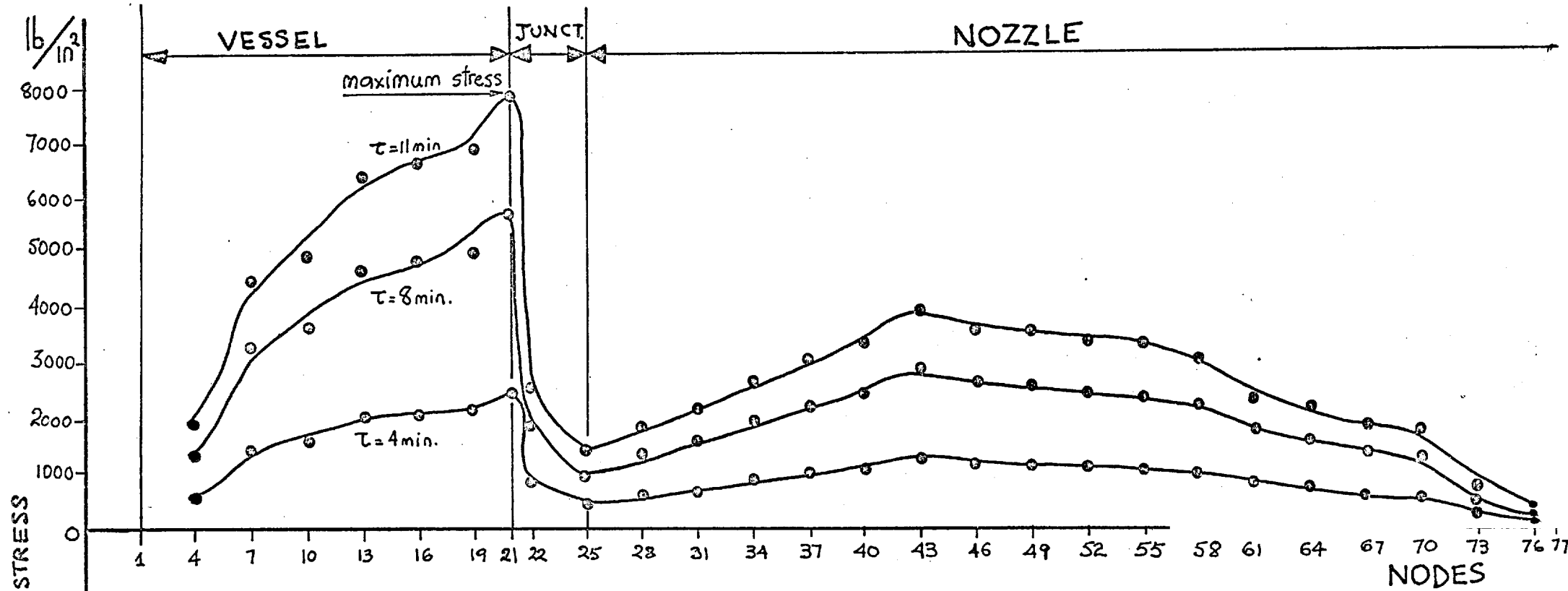


CASE C. OUTSIDE BOUNDARY (fig. 5.3.1)

STRESS  $\sigma_z$  at time intervals during heating-up.

FIGURE 5.3.4





CASE C. OUTSIDE BOUNDARY (fig. 5.3.1)

• Maximum shear stress  $\tau_{\max(12)}$  during heating-up.

FIGURE 5.3.6

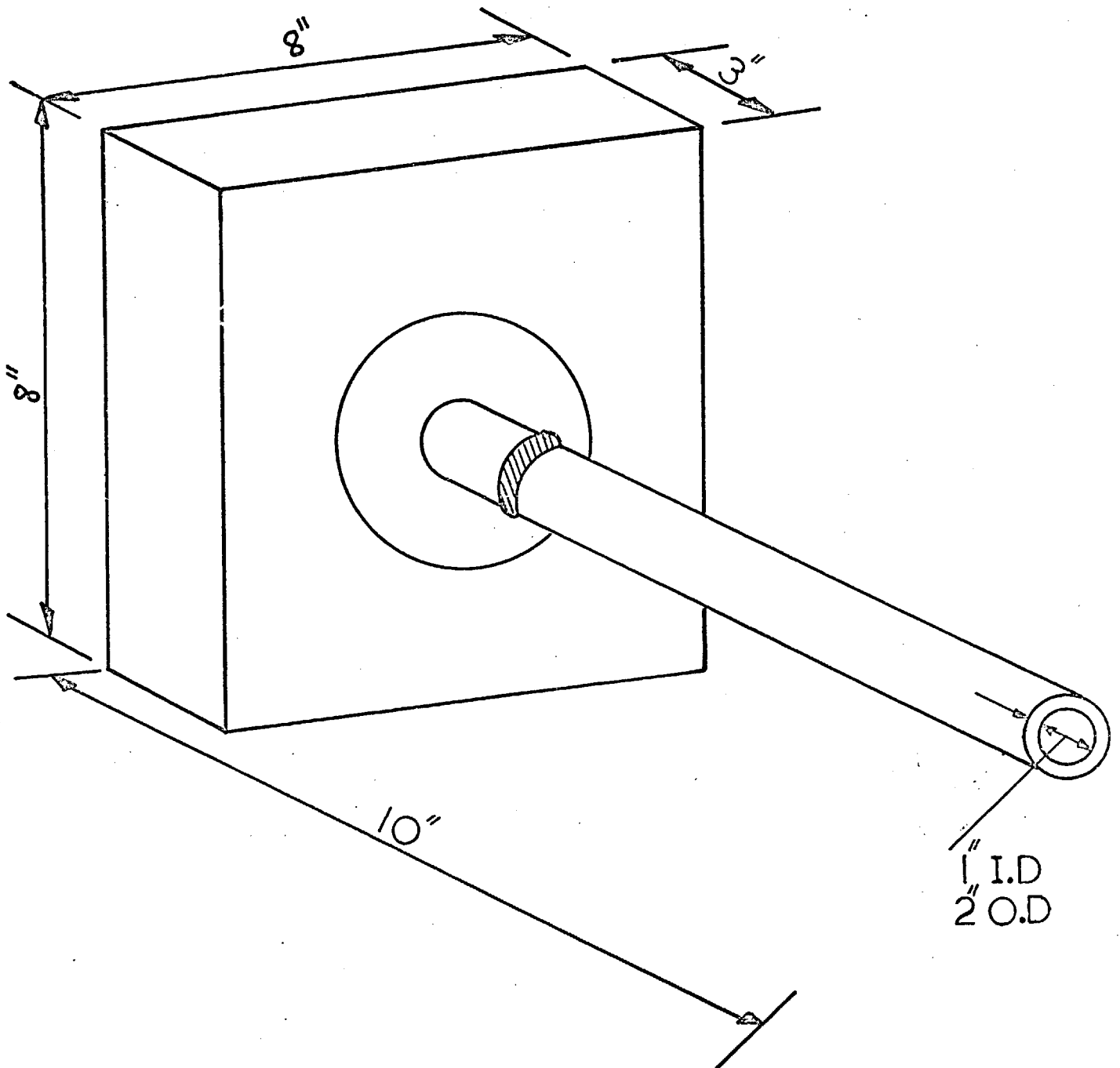
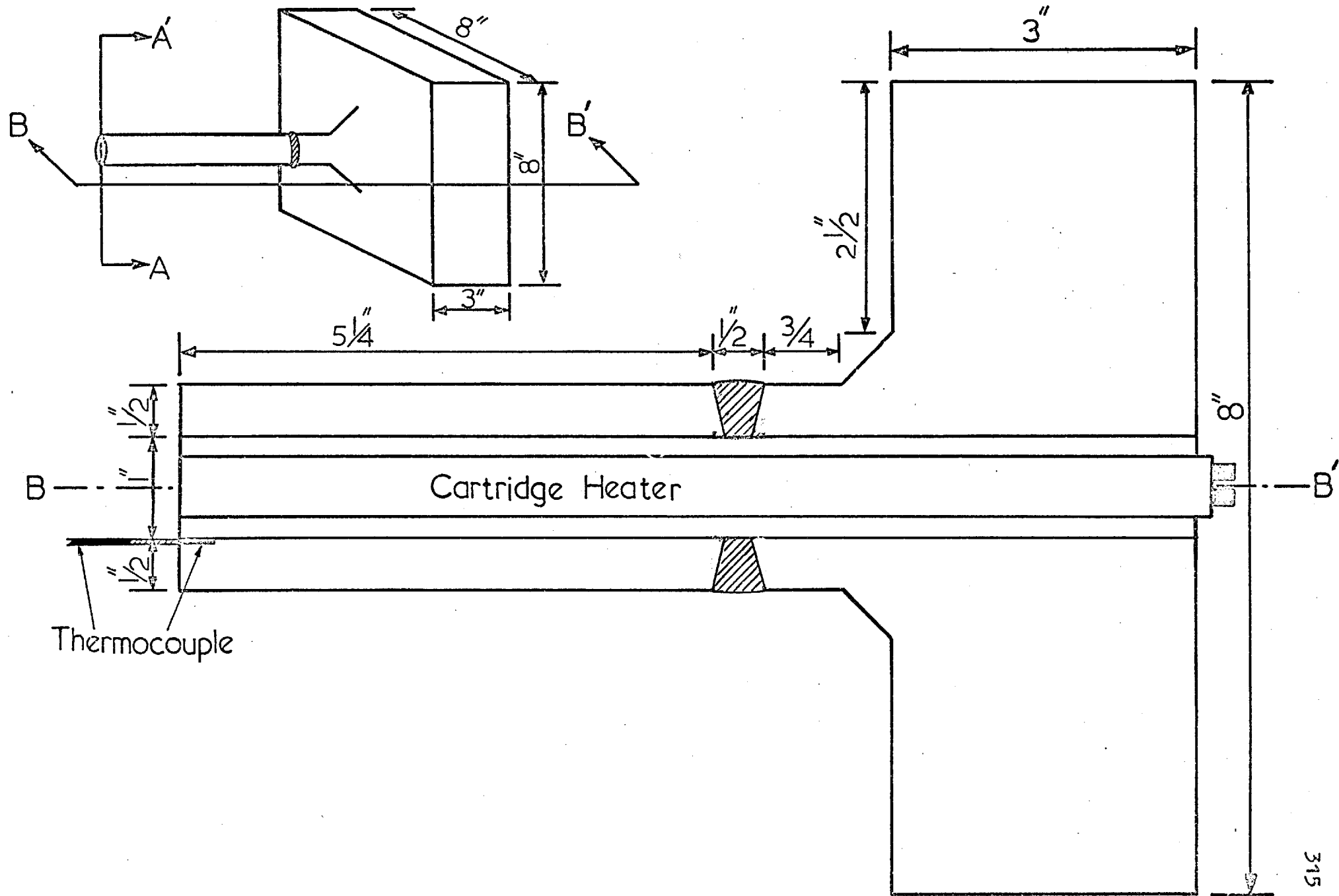
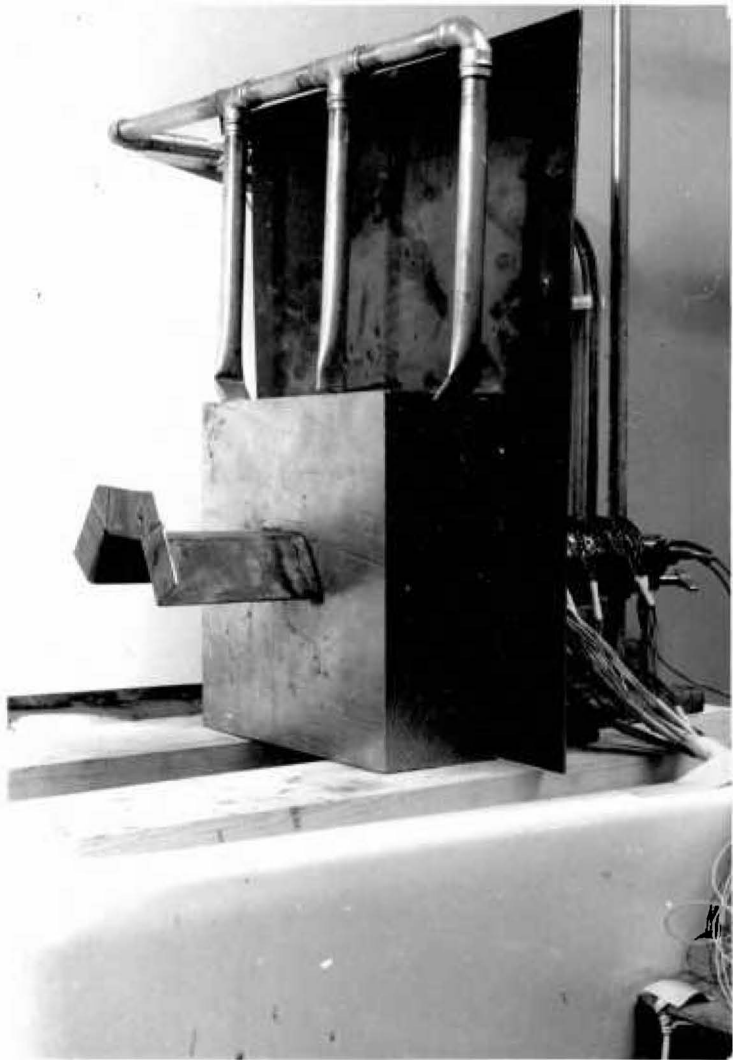


FIGURE 6.1.1. EXPERIMENTAL SPECIMEN.  
FULL DIMENSIONS SHOWN IN FIGURE 6.1.2

FIGURE 6.12 SPECIMEN

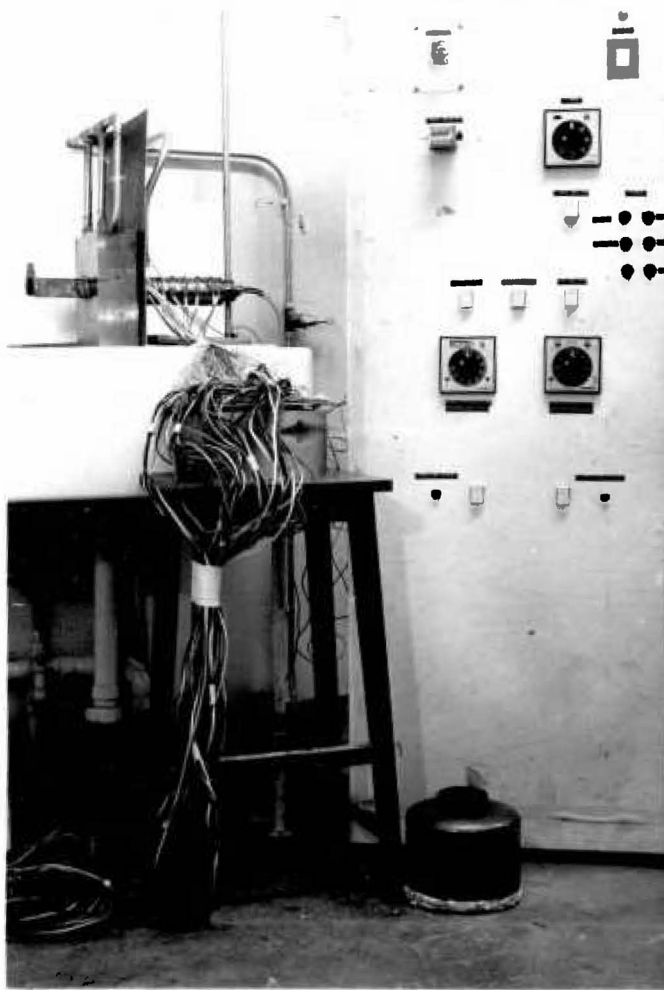




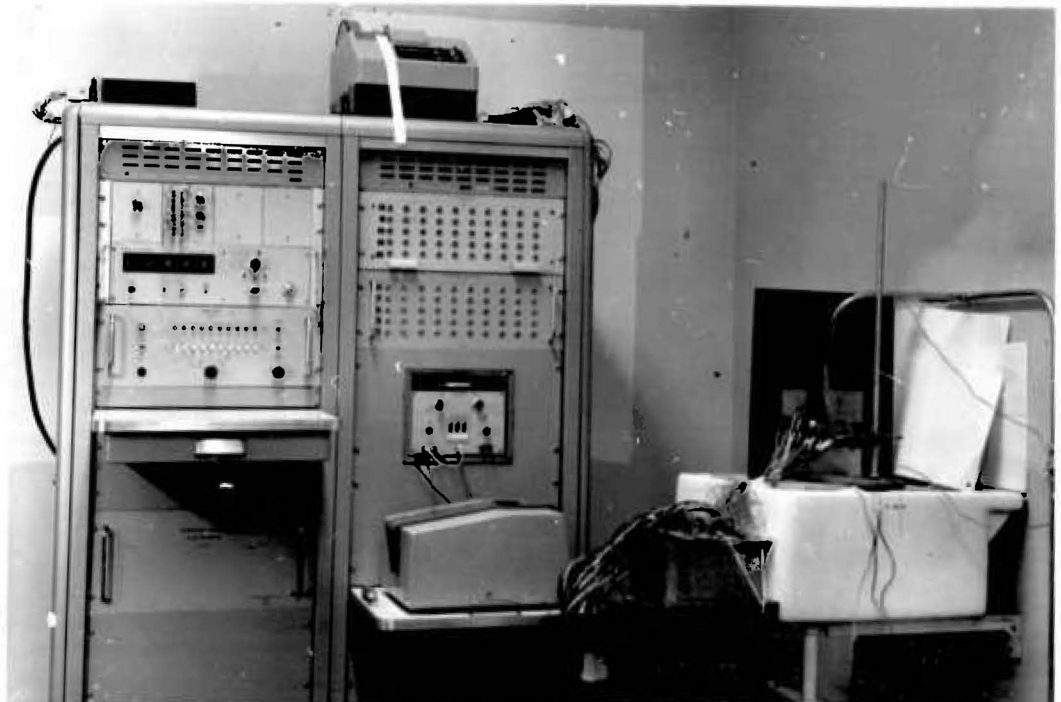
(a)



(b)

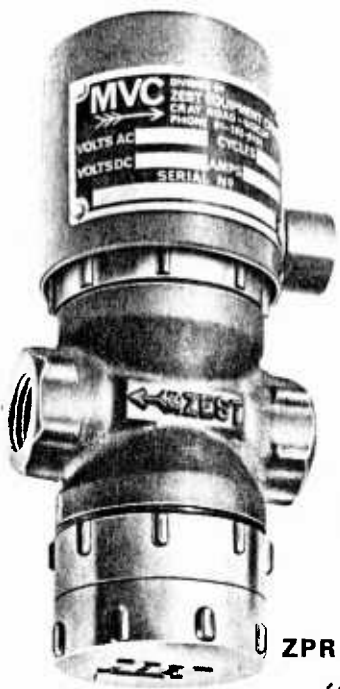


(a)



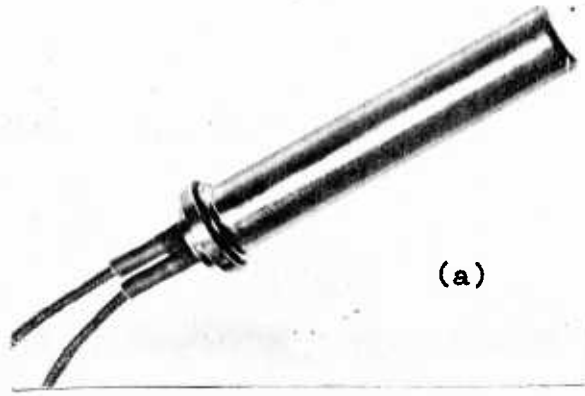
(b)





ZPR

(b)



(a)



(d)

STANDARD TYPE



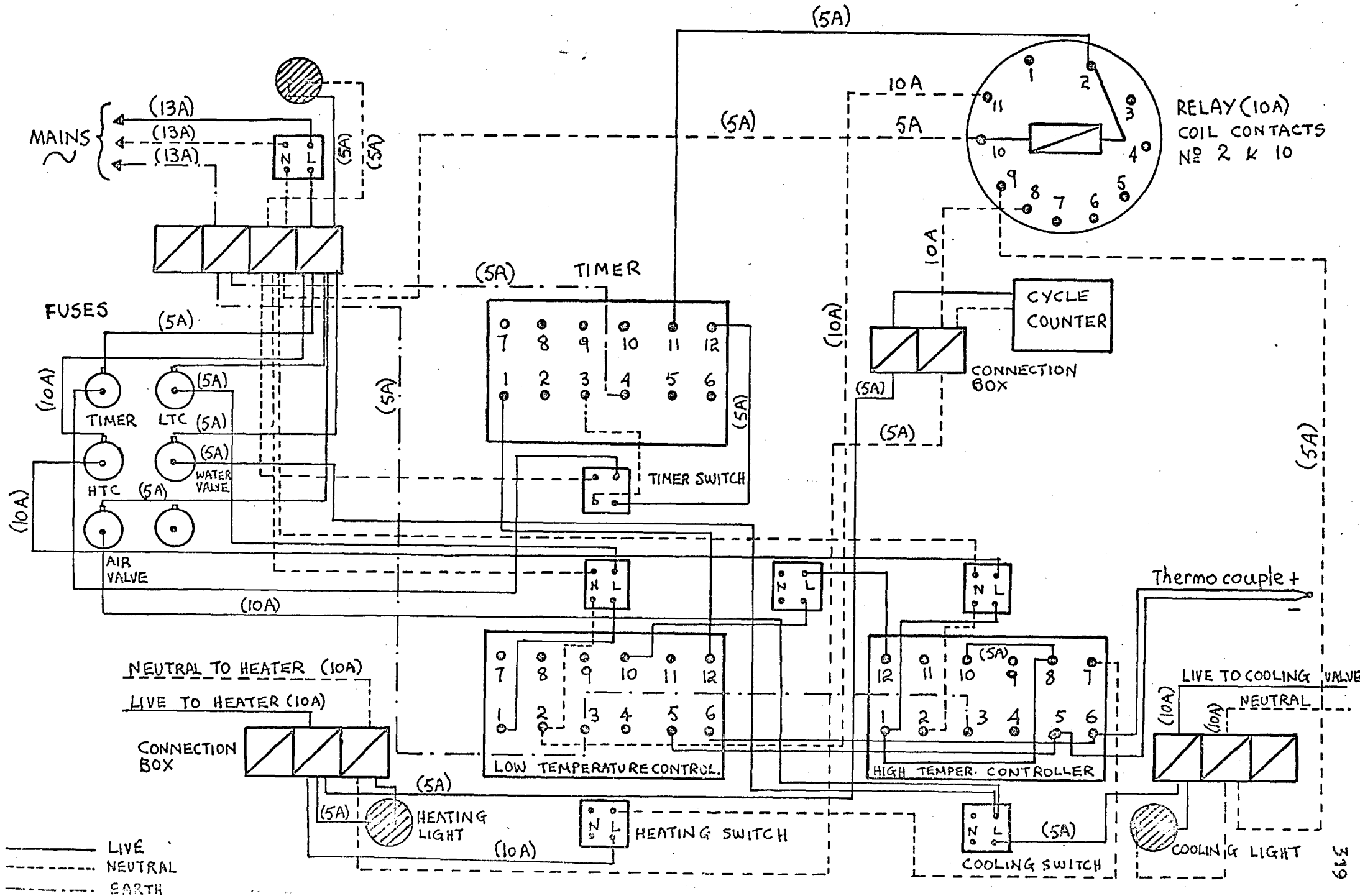
(c)



(e)

WITH DEVIATION METER

FIGURE 6.2.1



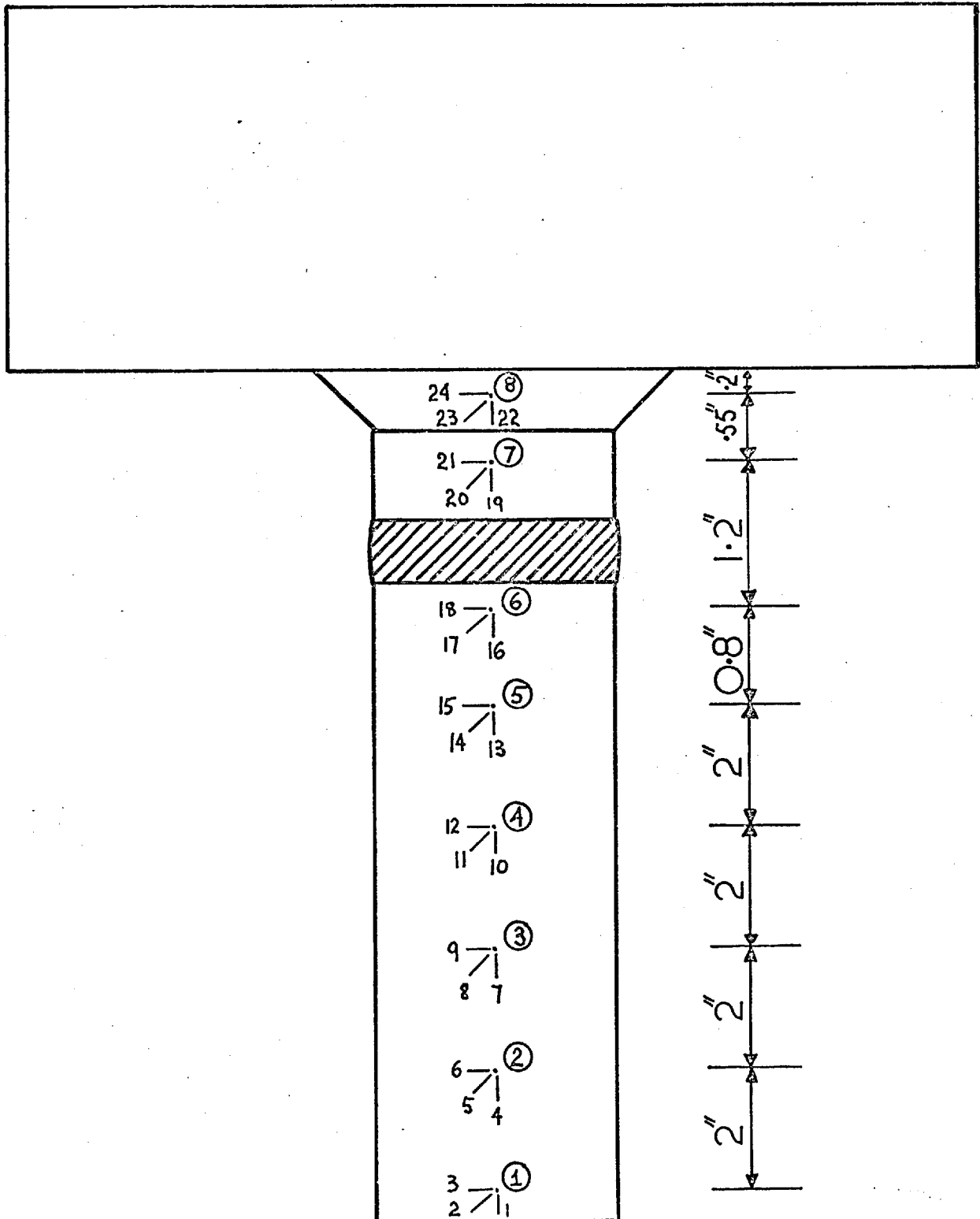


FIGURE 6.3.1(a) POSITIONS OF STRAIN GAUGE ROSETTES ON THE NOZZLE AND JUNCTION.

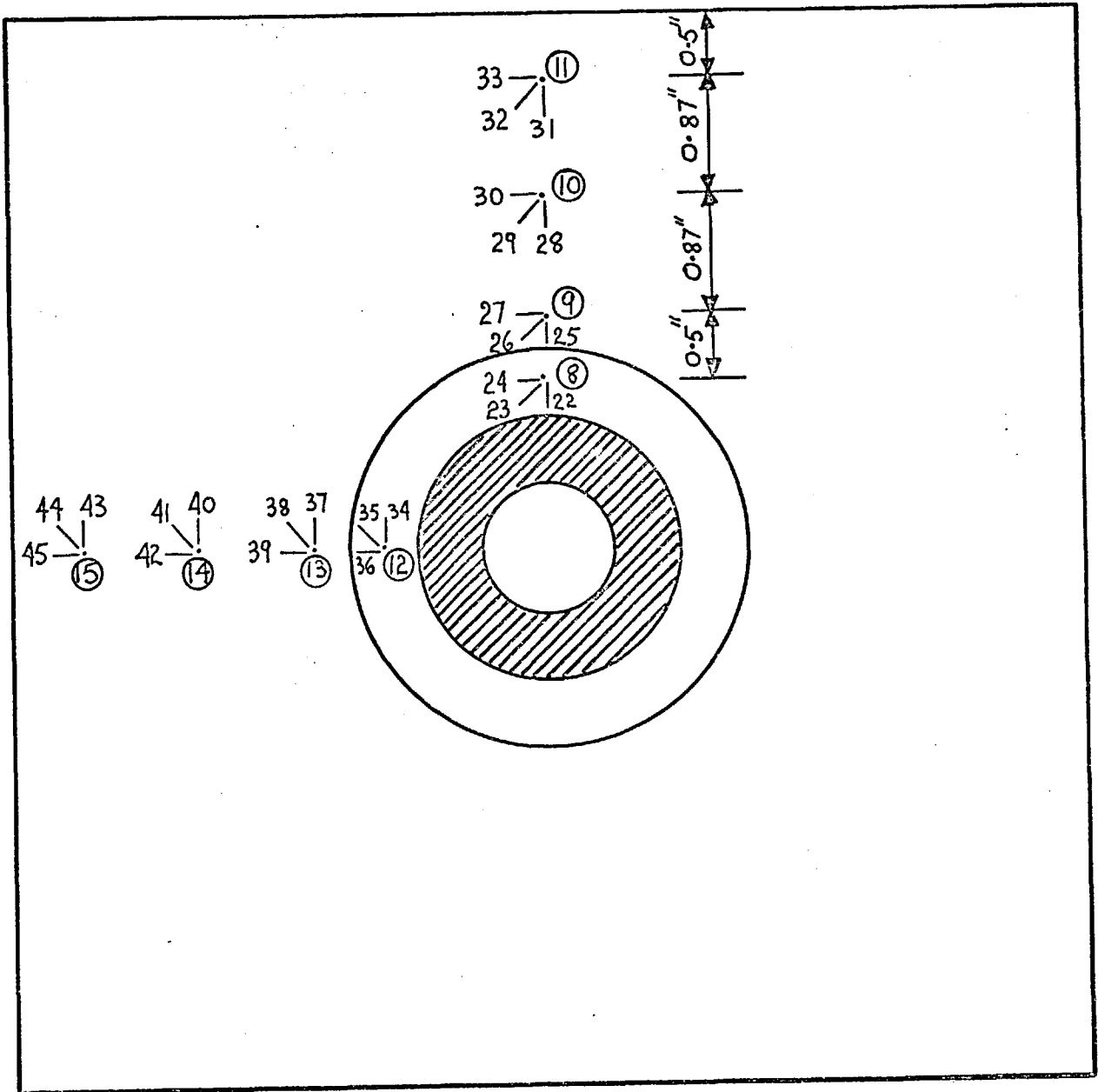
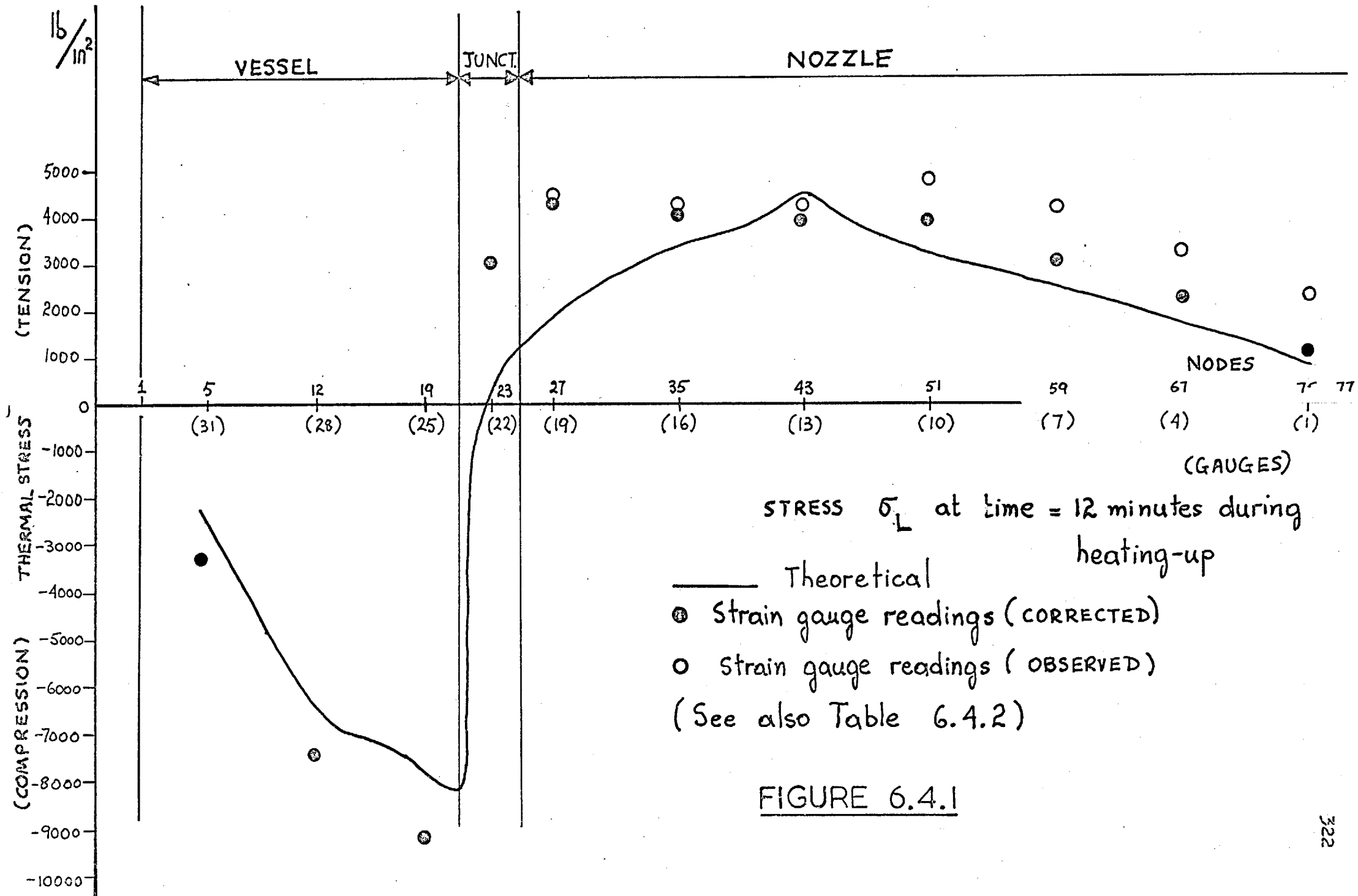
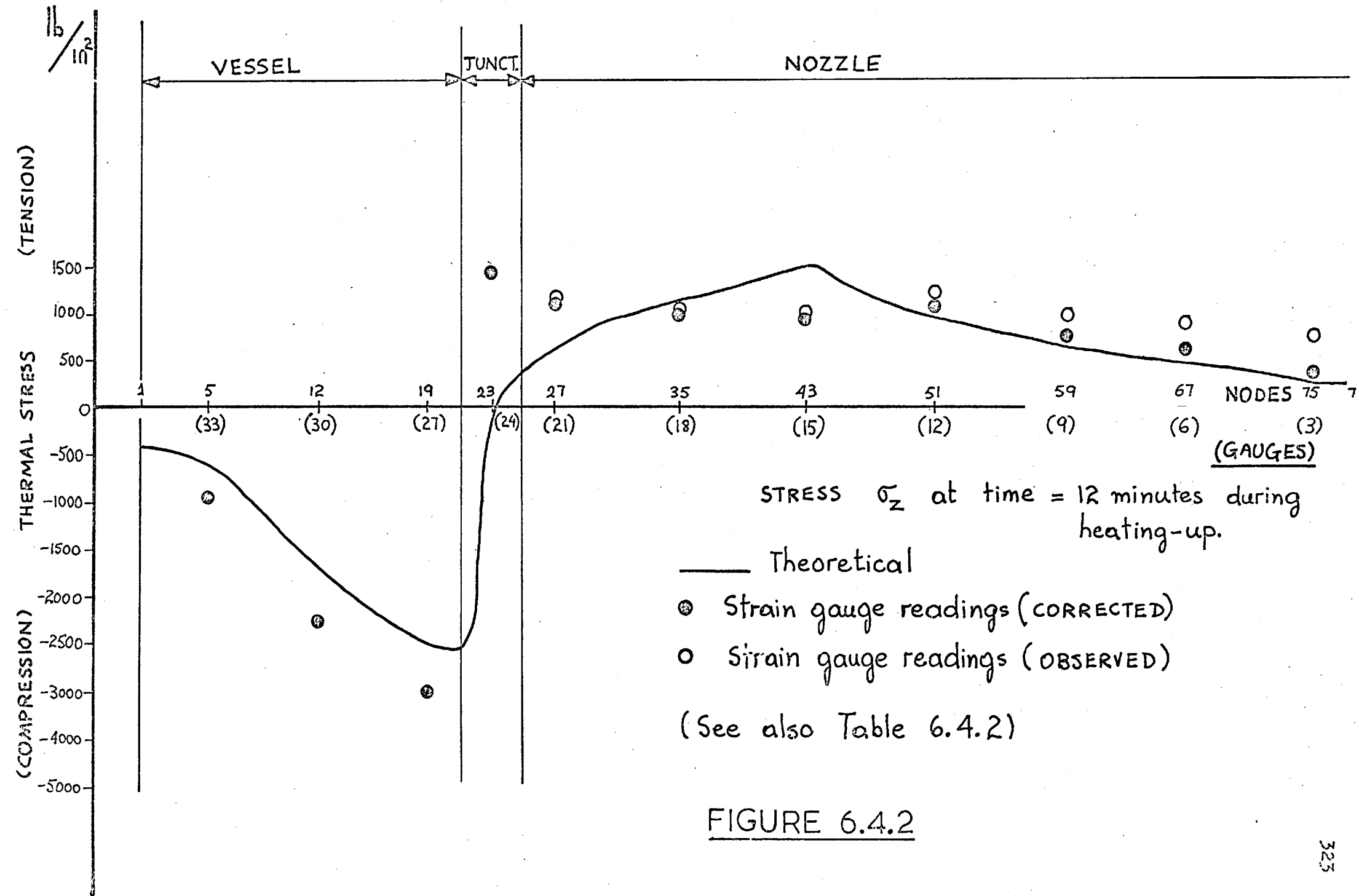
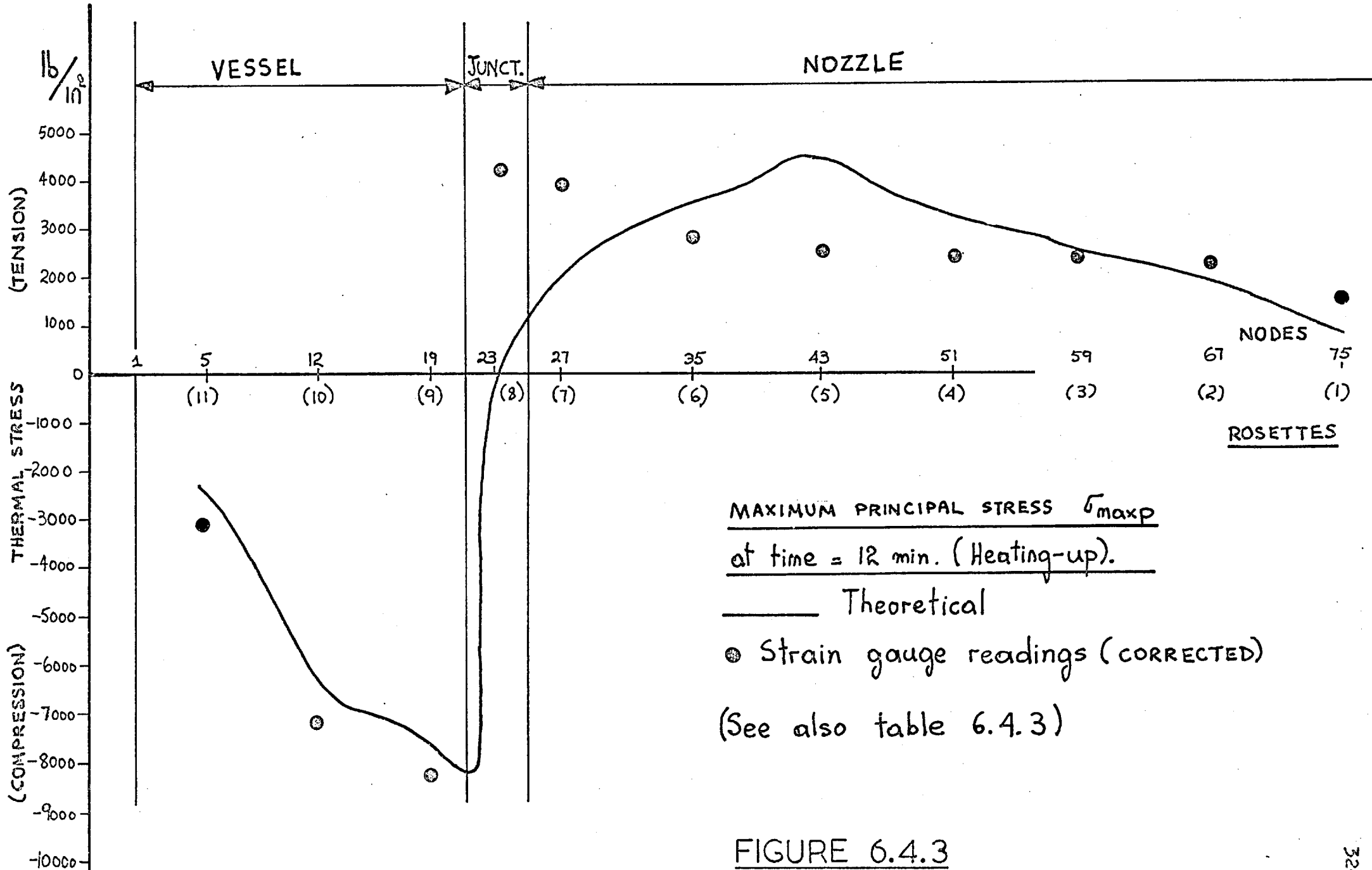


FIGURE 6.3.1(b) POSITIONS OF STRAIN GAUGE ROSETTES ON THE VESSEL.

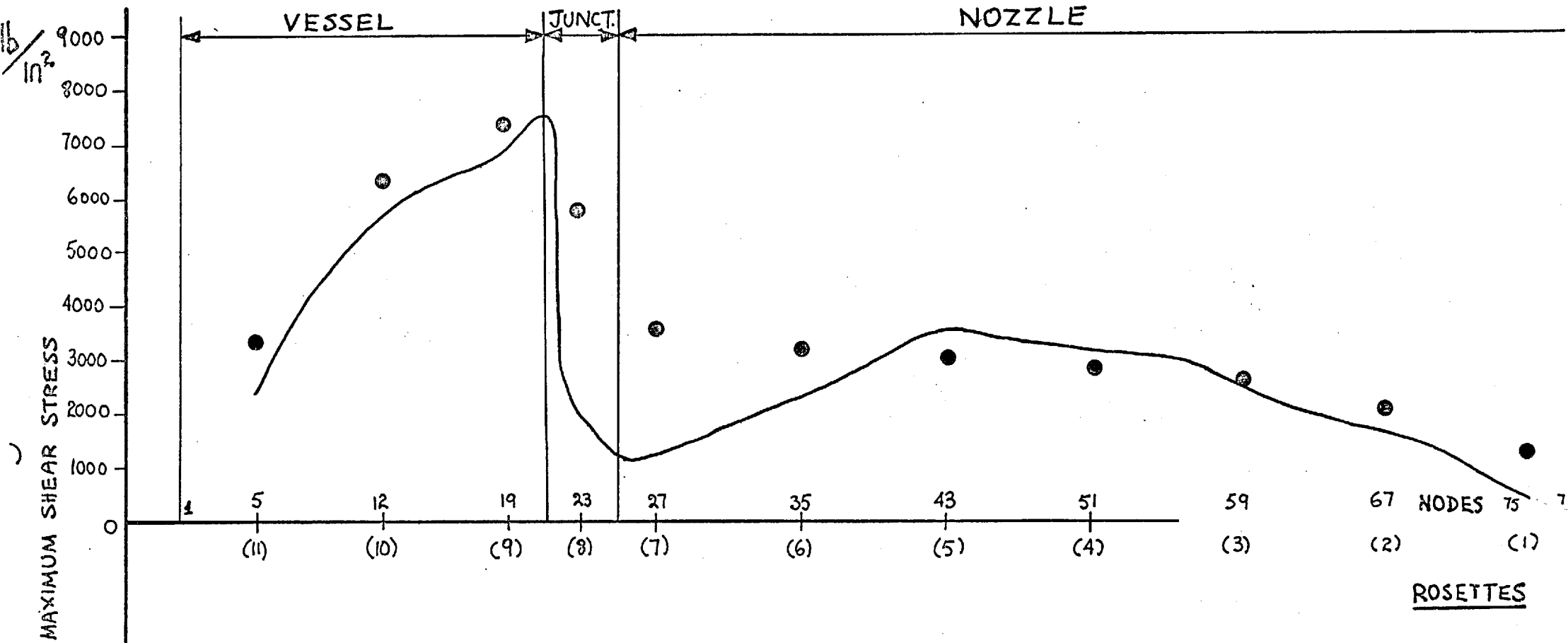






MAXIMUM PRINCIPAL STRESS  $\sigma_{maxp}$   
at time = 12 min. (Heating-up).  
 \_\_\_\_\_ Theoretical  
 ● Strain gauge readings (CORRECTED)  
 (See also table 6.4.3)

FIGURE 6.4.3



Maximum Shear Stress  $\tau_{\max(12)}$   
at time = 12 min. (heating-up)

— Theoretical  
 ● Strain gauge reading (CORRECTED)  
 (See also Table 6.4.3)

FIGURE 6.4.4



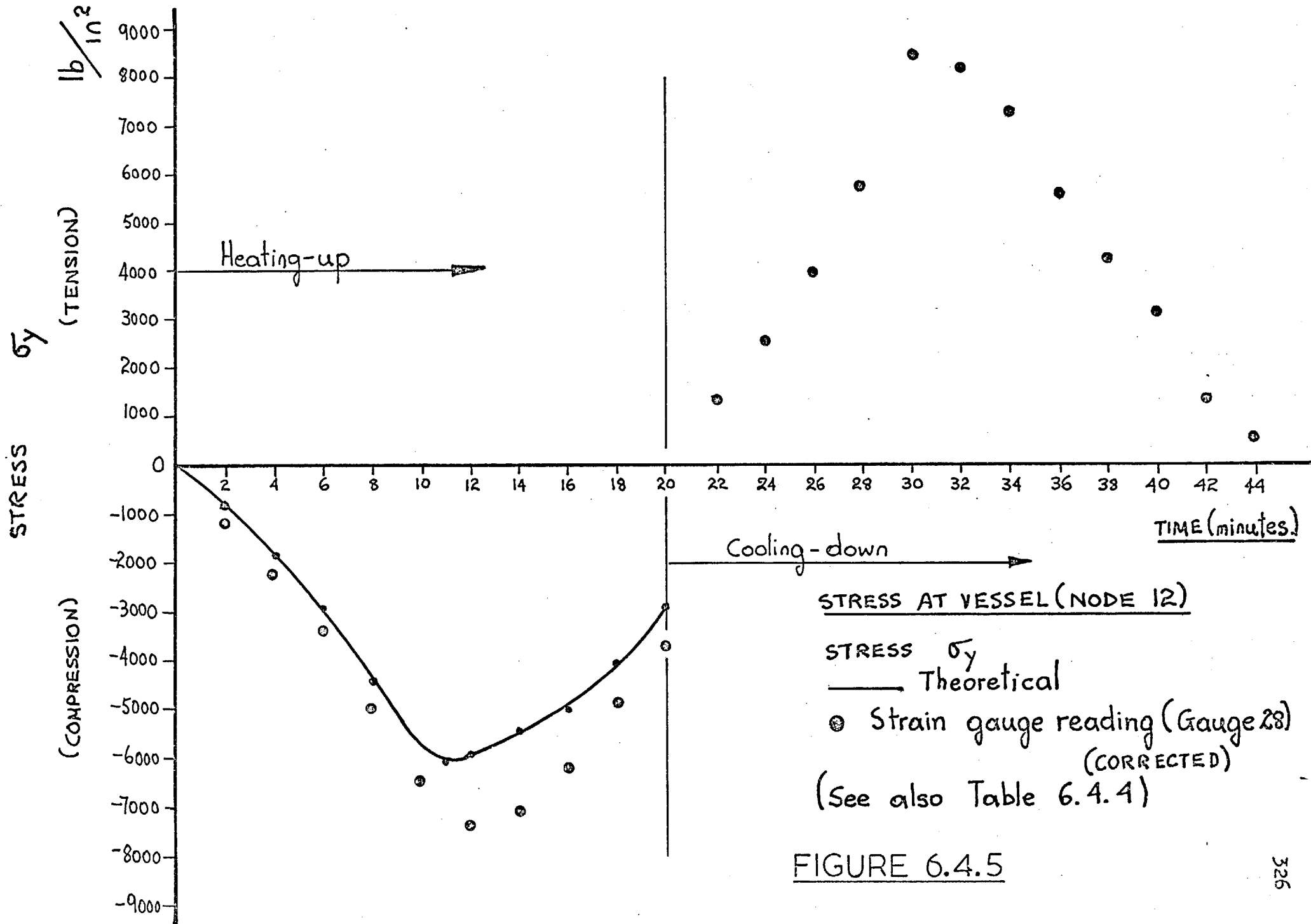


FIGURE 6.4.5

FIGURE 6.4.6

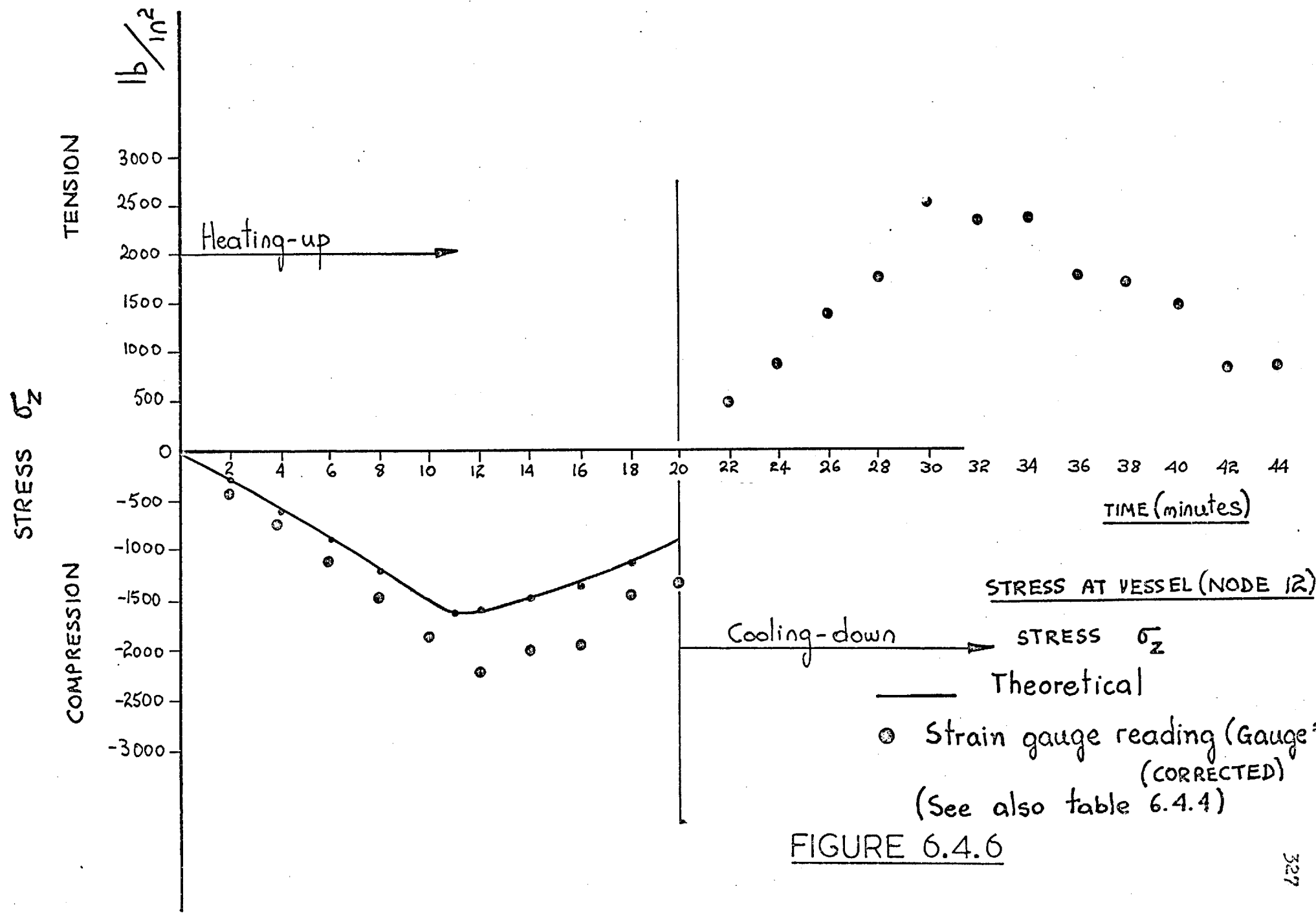


FIGURE 6.4.6

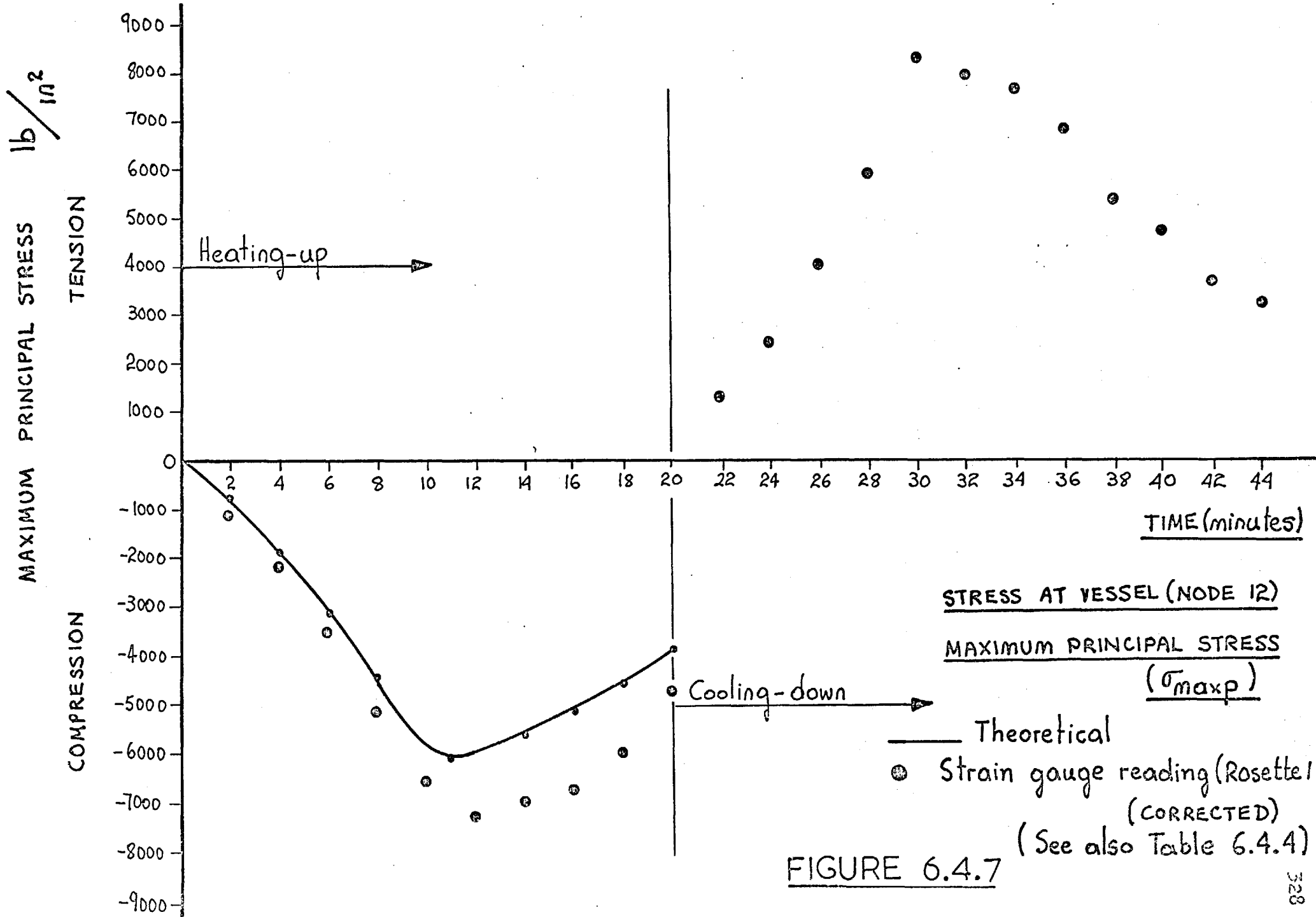
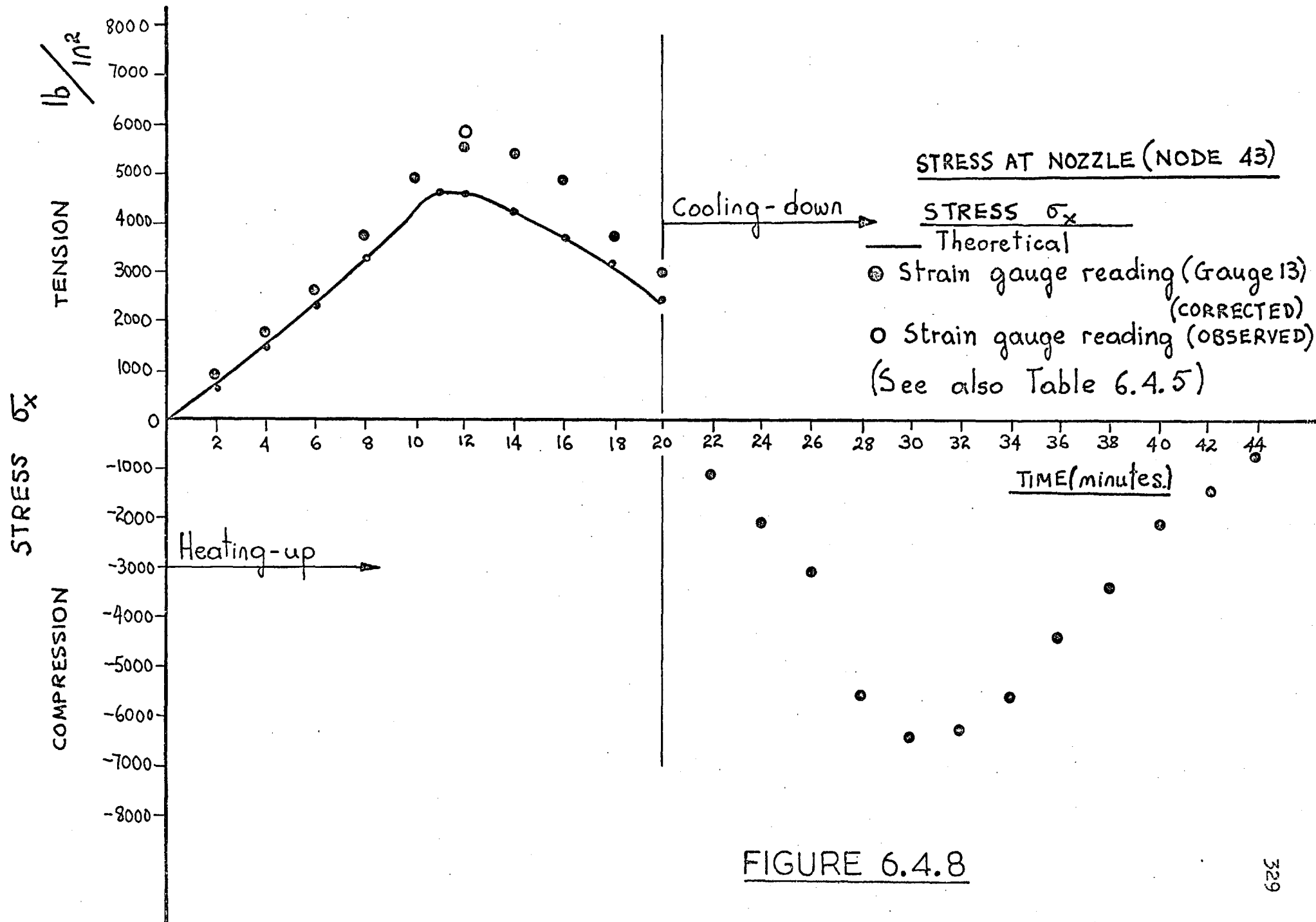


FIGURE 6.4.7



**FIGURE 6.4.8**

FC 9

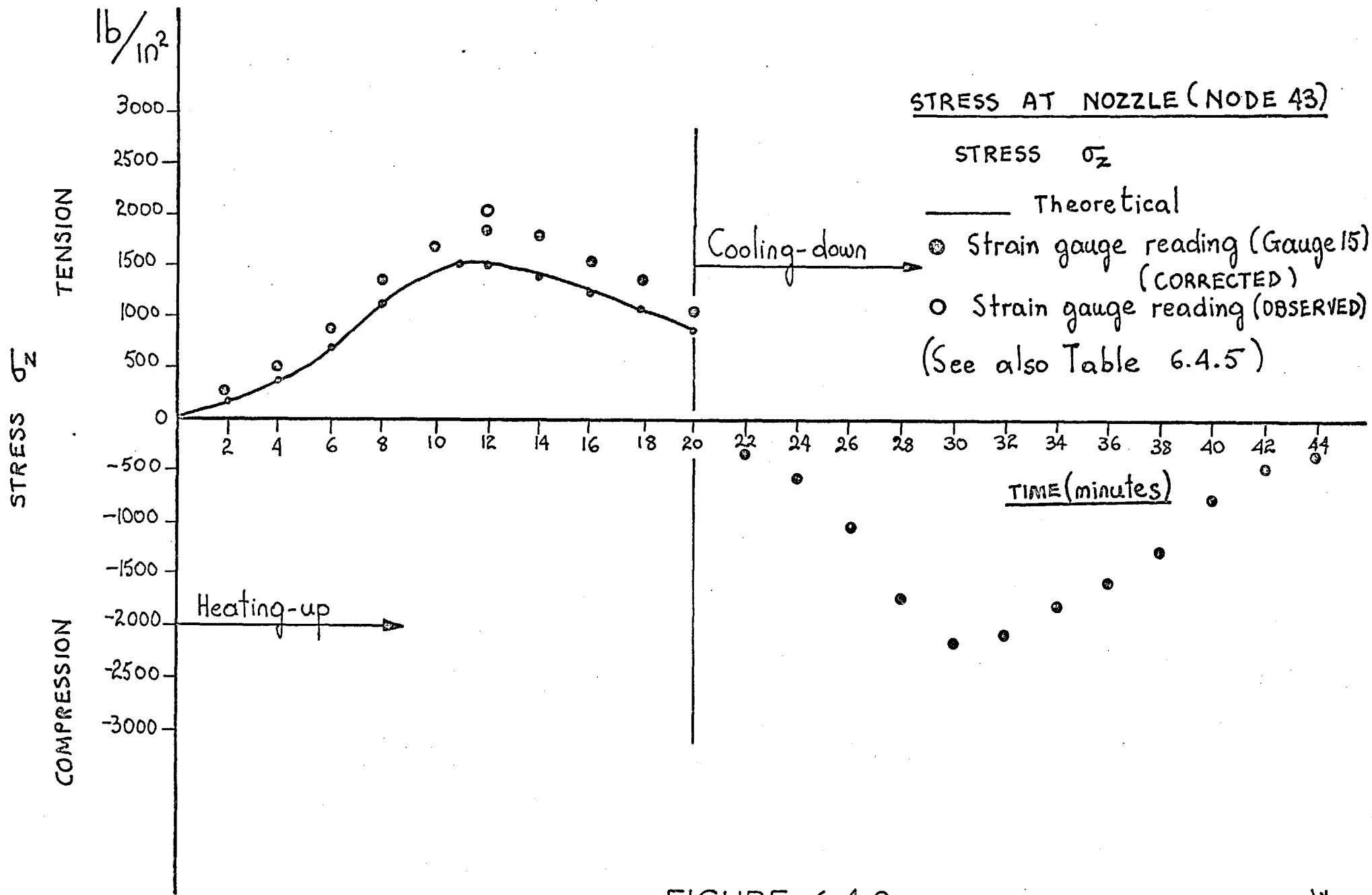


FIGURE 6.4.9

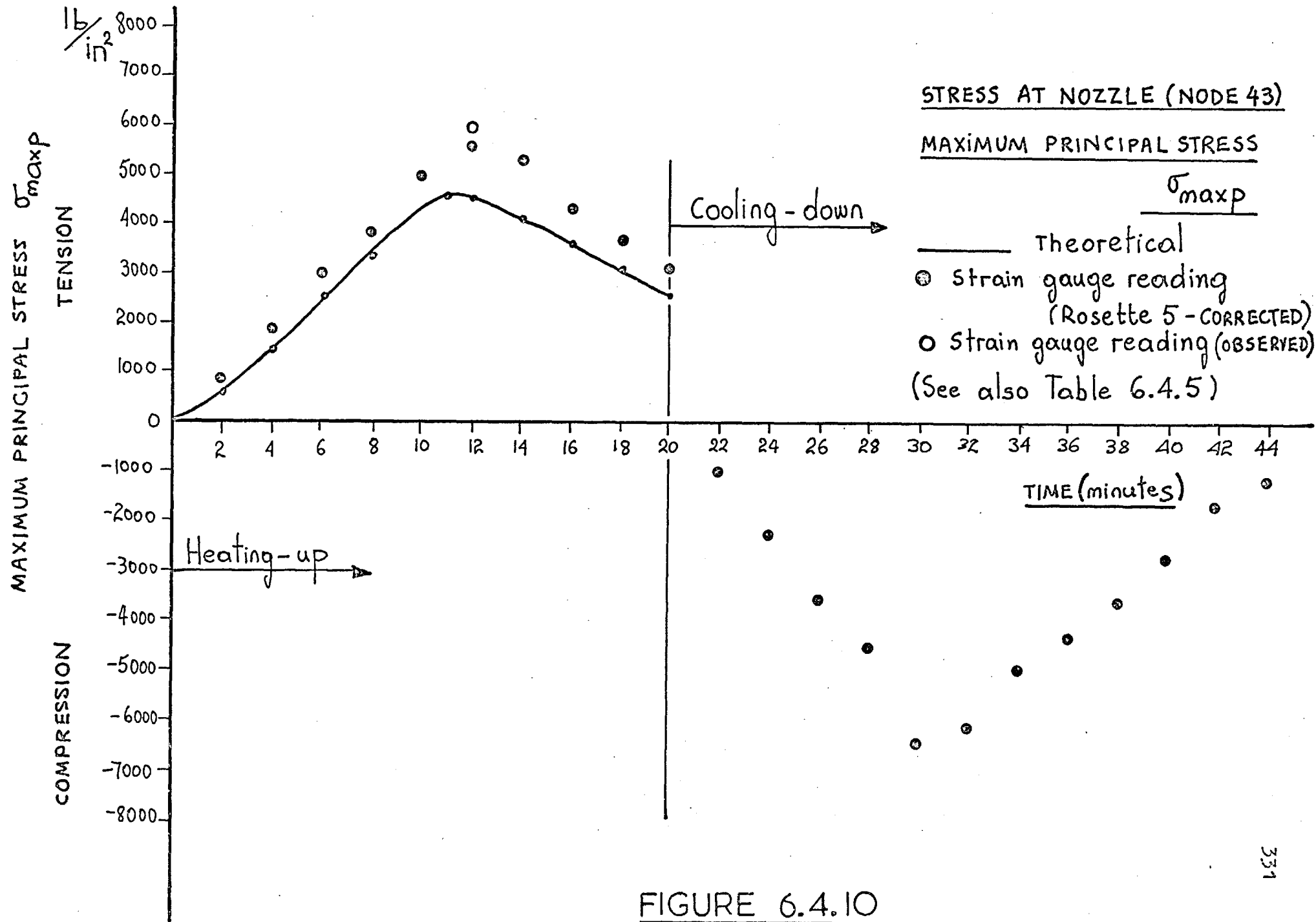
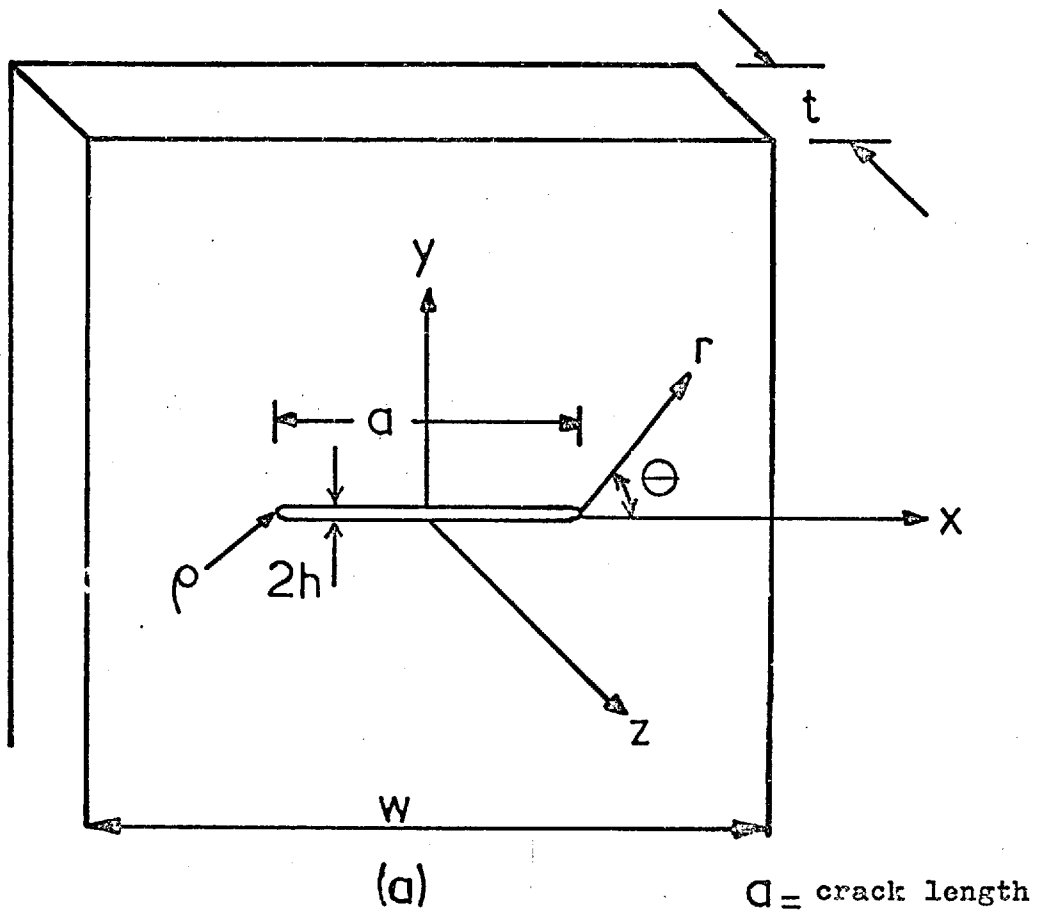
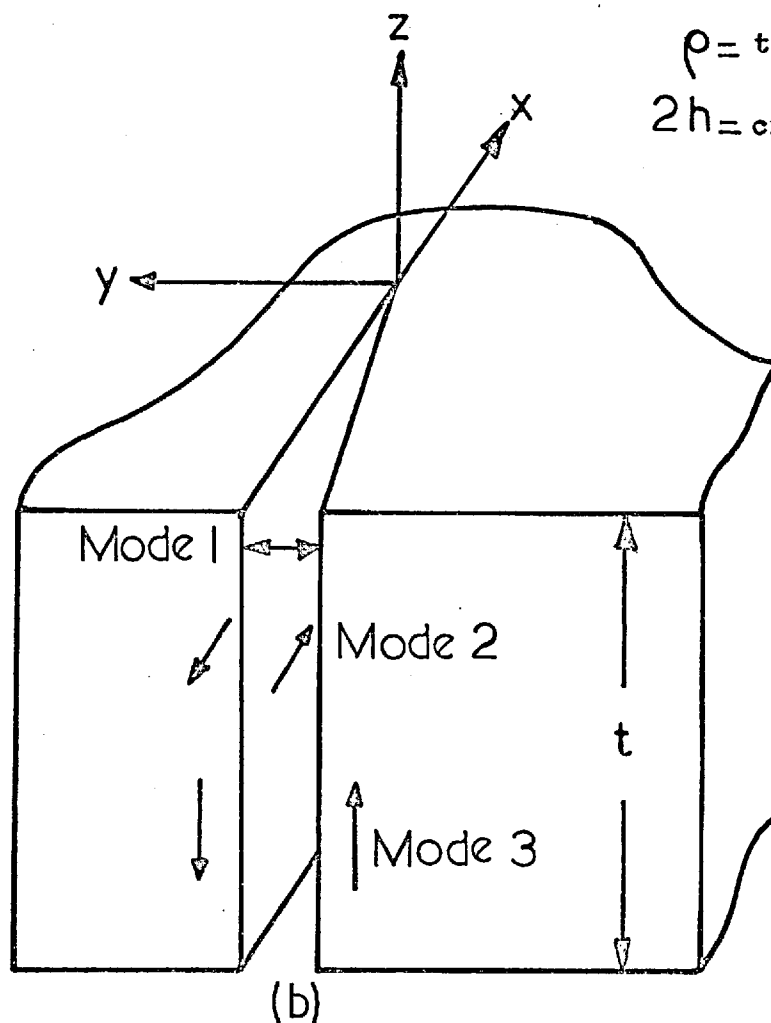


FIGURE 6.4.10



(a)

 $a =$  crack length $\rho =$  tip radius $2h =$  crack height

(b)

FIGURE 7.2.1 CO-ORDINATE SYSTEM FOR CRACK

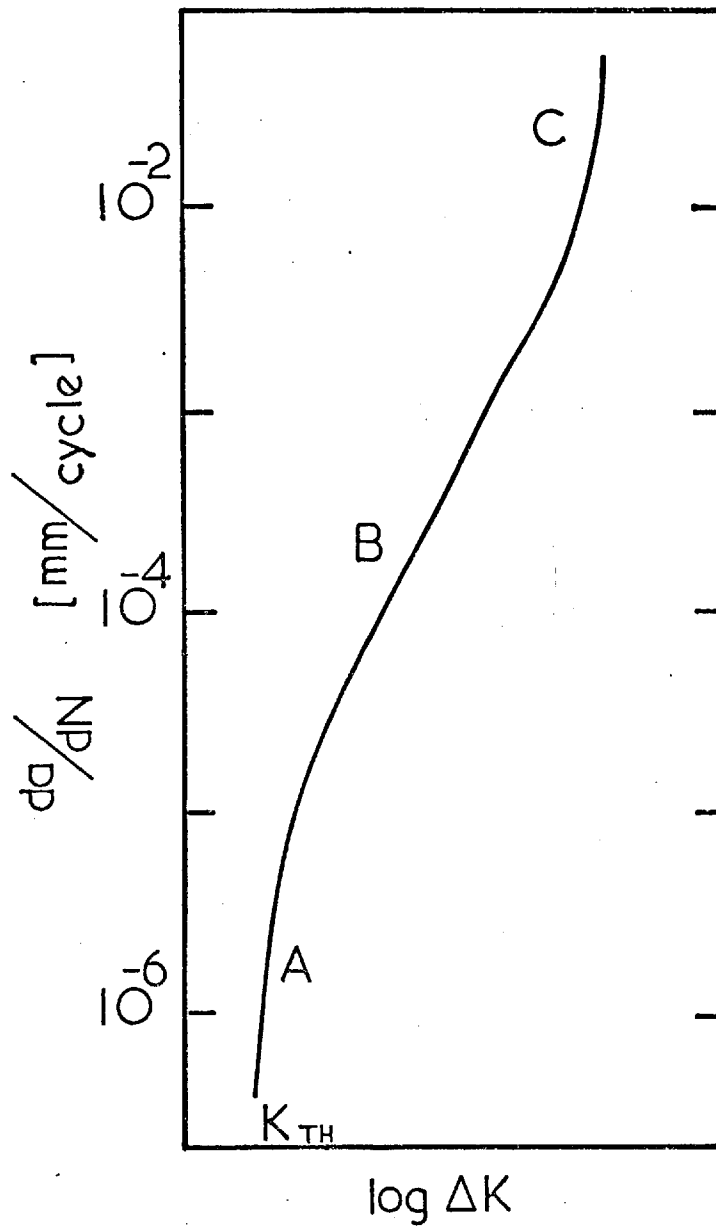


FIGURE 7.2.2 IDEALISED VARIATION OF FATIGUE CRACK GROWTH RATE( $da/dN$ ) WITH ALTERNATING STRESS INTENSITY  $\Delta K$  (R.7-11).



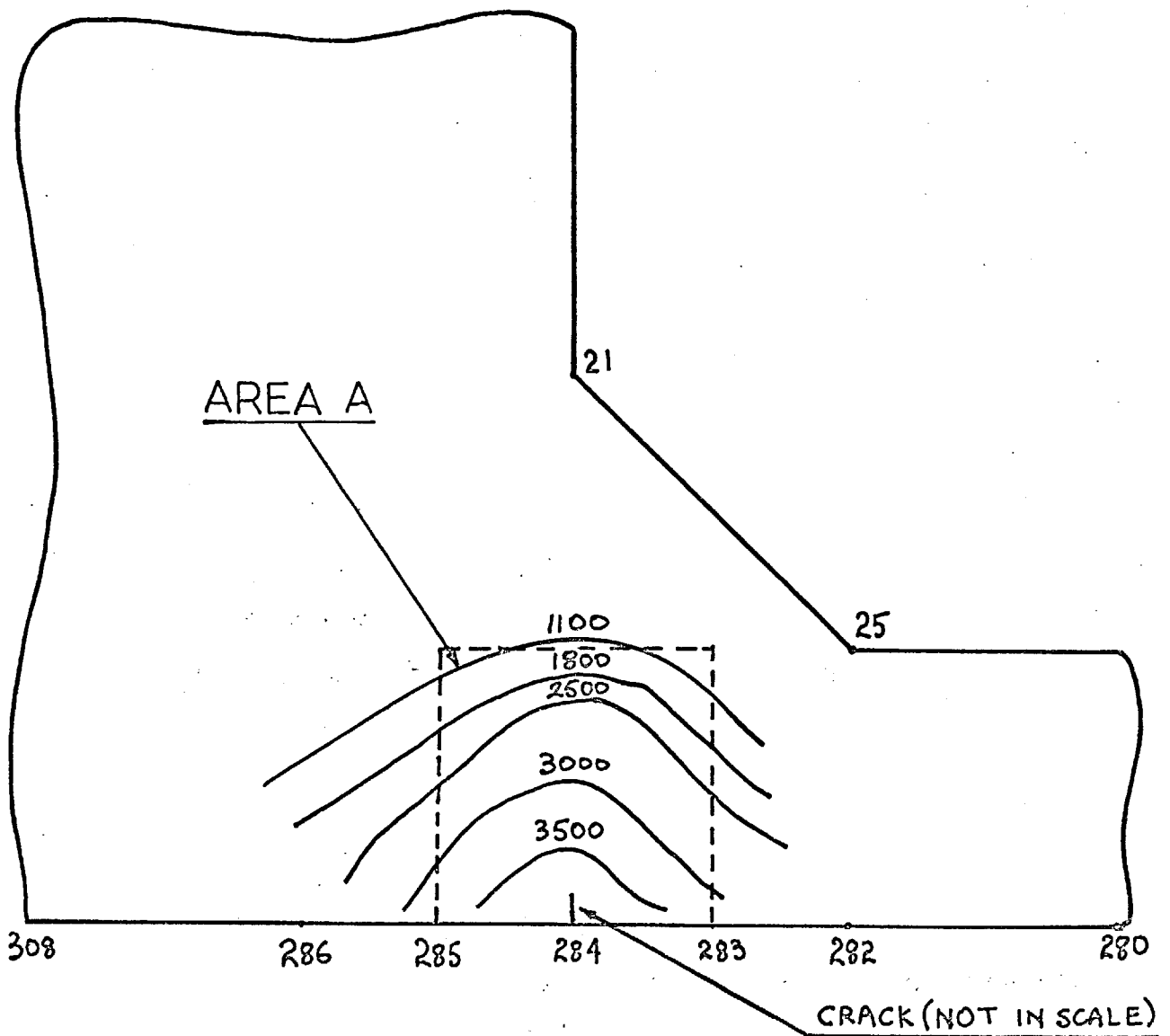
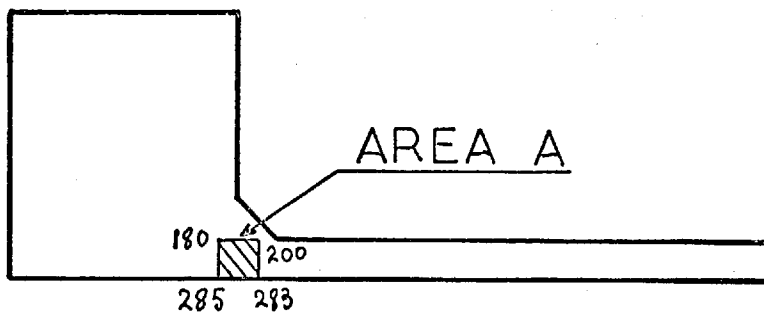
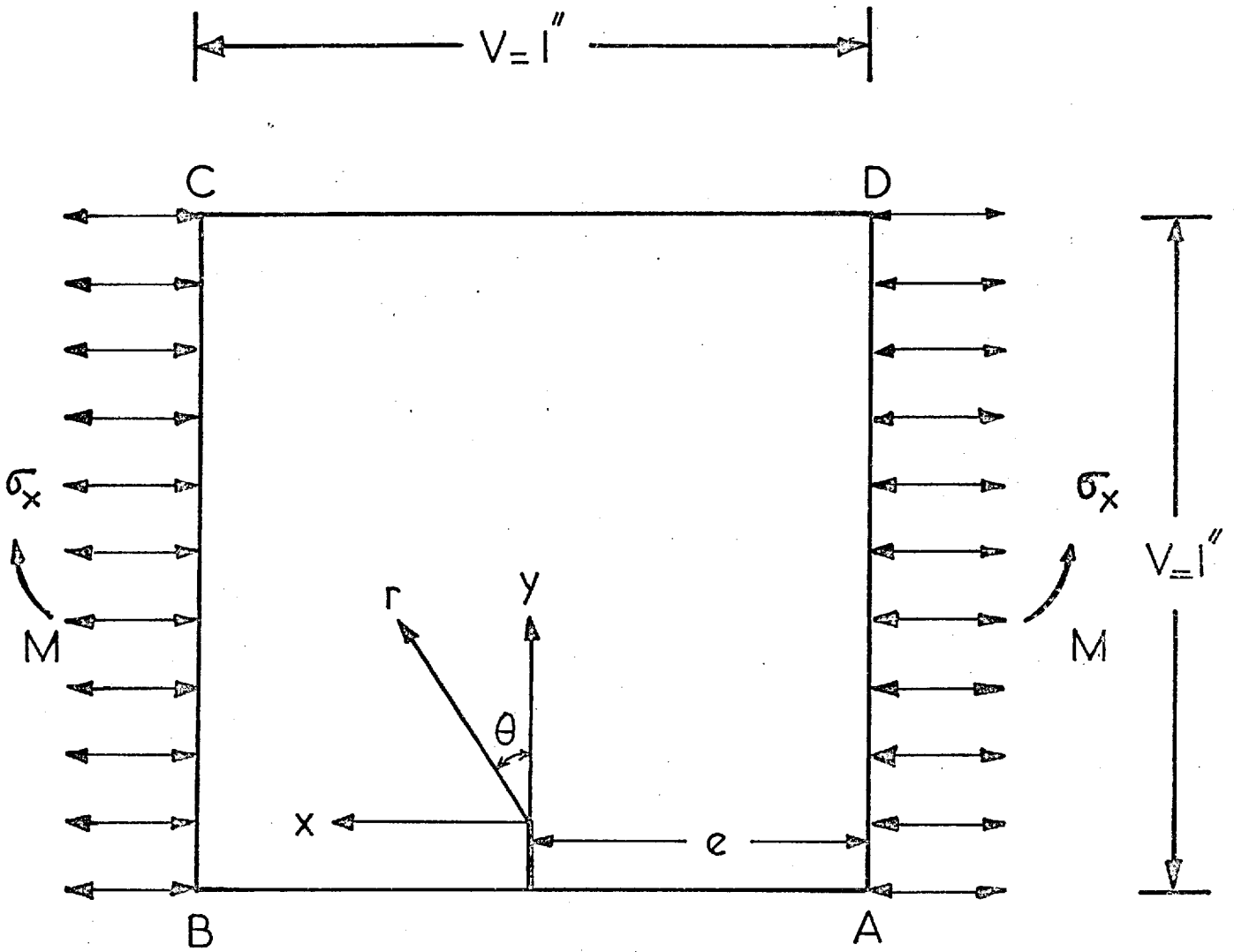


FIGURE 7.3.1.1. MAXIMUM PRINCIPAL STRESSES IN AREA A OF CASE C.  
(NUMBERS ALONG THE BOUNDARIES INDICATE NODES)



$a$  = CRACK LENGTH ( NOT IN SCALE ) = 0.04 in.

$r, \theta$  = CO-ORDINATES FOR THE TIP OF THE CRACK

FIGURE 7.3.2.1 AREA A WHERE CRACK IS CONSIDERED FOR CASE C.

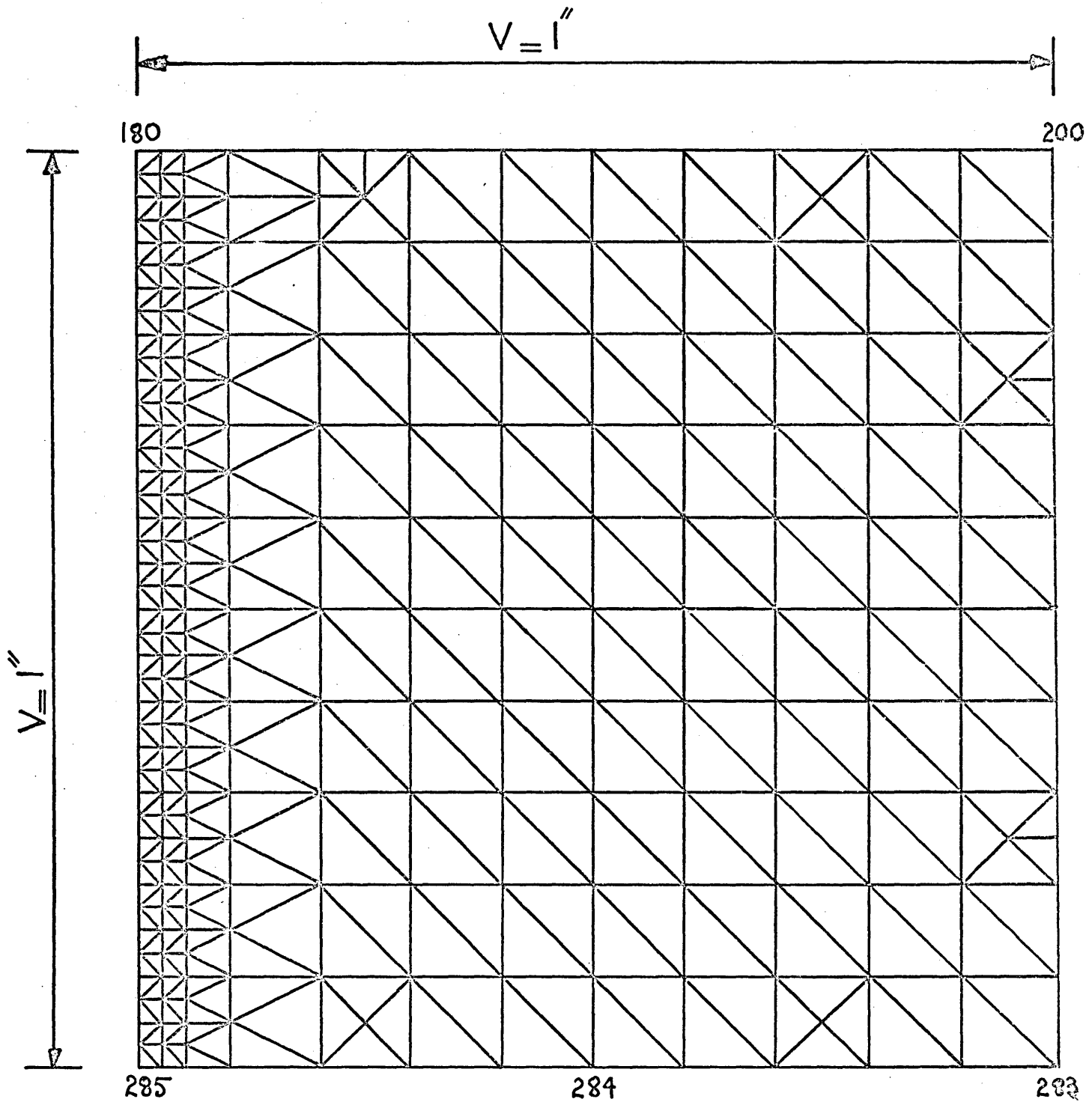
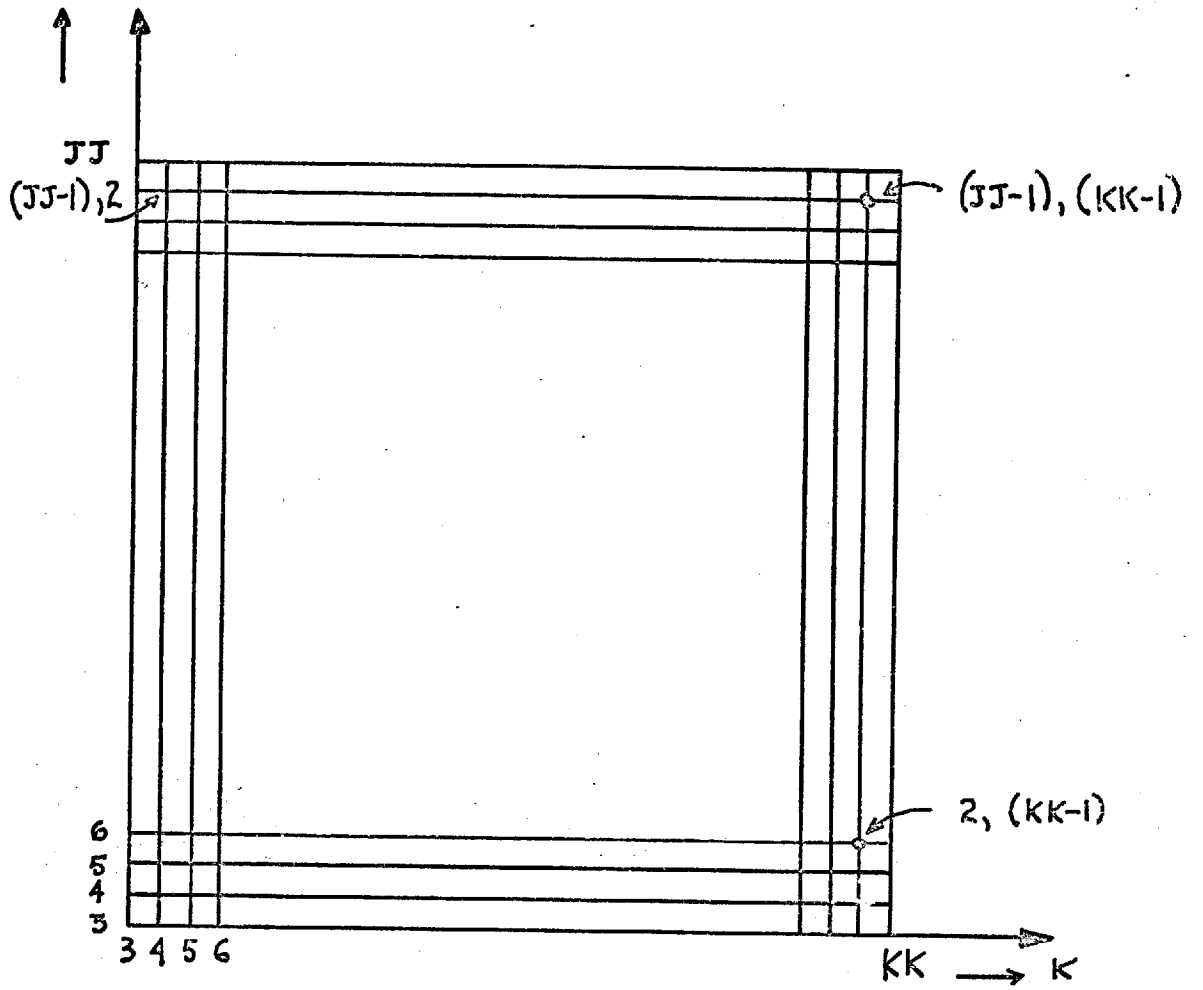
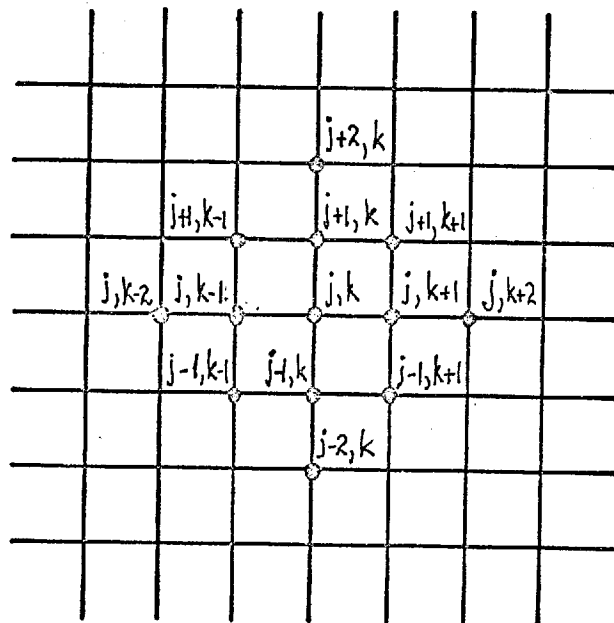


FIGURE 7.3.2.2 FINITE ELEMENT MESH FOR AREA A OF CASE C.  
NUMBER OF ELEMENTS = 430  
NUMBER OF NODES = 256



Grid for the determination of stress function  $\chi$



Cell for the finite difference solution of  $\nabla^4 \chi = 0$

FIGURE 7.3.2.3

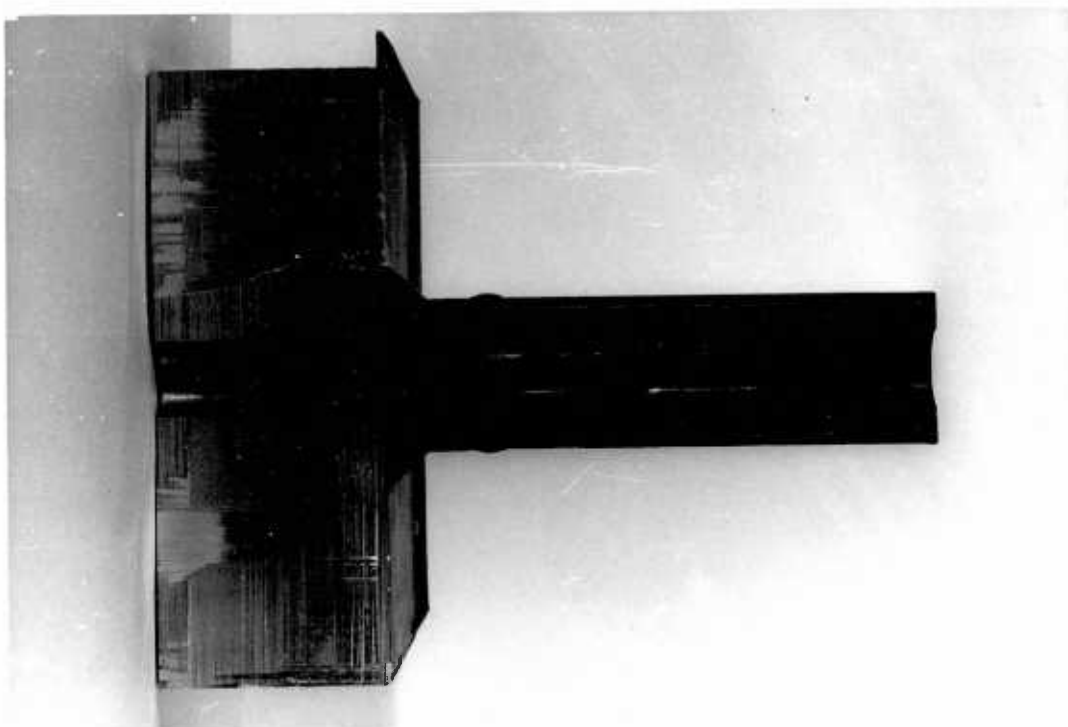
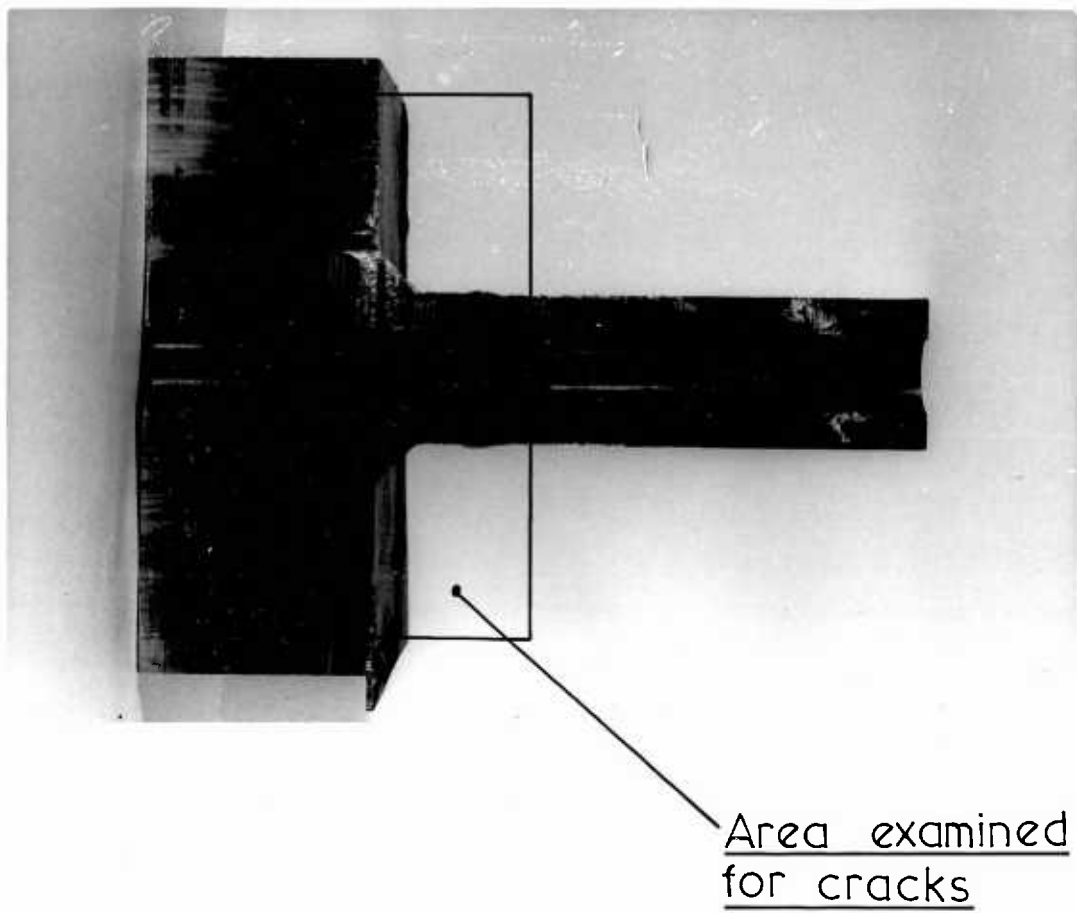


FIGURE 7.1.4